

0018a<sup>T</sup> OCCURRENCE AND PROPERTIES OF IRON AND TITANIUM OXIDES IN  
SOILS ALONG THE EASTERN SEABOARD  
OF SOUTH AFRICA

by

200 YF ROBERT WILLIAM FITZPATRICK . -

M.Sc. Agric. (Natal)

N Thesis (Ph.D; Soil Science and Agrometeorology) - University of Natal, Pietermaritzburg, 1978

Submitted in partial fulfilment  
of the requirements for  
the degree of

DOCTOR OF PHILOSOPHY

in the

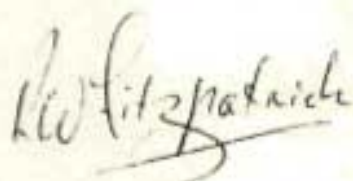
Department of Soil Science and Agrometeorology  
University of Natal

PIETERMARITZBURG

OCTOBER, 1978

- DECLARATION -

I hereby certify that this research  
is the result of my own original  
investigation, except as  
acknowledged herein.

A handwritten signature in dark ink, appearing to read 'R. W. Fitzpatrick', with a stylized, cursive script.

R. W. FITZPATRICK

## - CONTENTS -

CHAPTER	PAGE NO.
DECLARATION .. .. .	(i)
LIST OF FIGURES AND MAPS .. .. .	(vi)
LIST OF TABLES .. .. .	(ix)
LIST OF PLATES .. .. .	(xi)
ACKNOWLEDGEMENTS .. .. .	(xvii)
ABSTRACT .. .. .	(xviii)
GENERAL INTRODUCTION .. .. .	1
1 DISTRIBUTION, COMPOSITION AND CRYSTALLINITY OF GOETHITES .. .. .	7
1.1 <u>Introduction</u> .. .. .	7
1.2 <u>Materials</u> .. .. .	8
1.2.1 Natural samples .. .. .	8
1.2.2 Synthetic samples .. .. .	9
1.3 <u>Methods</u> .. .. .	9
1.3.1 Sample pretreatment .. .. .	9
1.3.2 Effect of 5 M NaOH pretreatment .. .. .	11
1.3.3 Chemical extraction .. .. .	11
1.3.4 X-ray diffraction .. .. .	12
1.3.5 Infrared spectroscopy .. .. .	12
1.3.6 Thin sections .. .. .	12
1.3.7 Electron microscopy .. .. .	12
1.4 <u>Results and discussion</u> .. .. .	13
1.4.1 Goethite formed in weathering limestone .. .. .	15
1.4.2 Geodes .. .. .	22
1.4.3 Ferricretes .. .. .	25
1.4.4 Concretions .. .. .	37
1.4.5 Crusts .. .. .	40
1.4.6 Pipestems .. .. .	42
1.4.7 Ferruginous bauxite .. .. .	45
1.4.8 Saprolites .. .. .	52
1.4.9 Sesquioxidic soil clays and gleys .. .. .	54
1.5 <u>Overall discussion</u> .. .. .	63
1.6 <u>Conclusions</u> .. .. .	72
2 THE DISTRIBUTION AND NATURE OF SECONDARY MAGNETIC MINERALS .. .. .	75
2.1 <u>Introduction</u> .. .. .	75

- CONTENTS -  
(Contd.)

<u>CHAPTER</u>	<u>PAGE NO.</u>
2.2 <u>Materials</u> .. .. .	77
2.2.1 Natural samples .. .. .	77
2.2.2 Synthetic samples .. .. .	79
2.3 <u>Methods</u> .. .. .	80
2.3.1 Sample pretreatment .. .. .	80
2.3.2 Magnetic susceptibility .. .. .	81
2.3.3 X-ray diffraction (XRD) .. .. .	81
2.3.4 Chemical extractions .. .. .	81
2.3.5 Total chemical analysis .. .. .	82
2.3.6 Electron microscopy .. .. .	82
2.3.7 Thin sections .. .. .	82
2.4 <u>Results and discussion</u> .. .. .	83
2.4.1 Distribution and mode of occurrence .. .. .	83
2.4.1.1 Magnetic bands .. .. .	83
2.4.1.2 Magnetic concretions .. .. .	84
2.4.1.3 Magnetic opaque single grain particles .. .. .	87
2.4.1.4 Magnetic clay-size fraction .. .. .	88
2.4.1.5 Magnetic bulk topsoil samples, attributed to heating .. .. .	88
2.4.2 X-ray diffraction analysis .. .. .	90
2.4.2.1 Oxidation of magnetite and Ti-magnetite.. .. .	94
2.4.2.2 Crystallinity.. .. .	98
2.4.3 Magnetic susceptibility analysis .. .. .	99
2.4.4 Chemical analysis .. .. .	103
2.4.4.1 Total chemical analysis .. .. .	103
2.4.4.2 Selective dissolution analysis .. .. .	105
2.4.5 Optical examination .. .. .	108
2.4.5.1 Morphology of magnetic bands and concretions .. .. .	108
2.4.5.2 Weathering of magnetic opaque single grains in ferruginous bauxites and soils derived from basic igneous rocks .. .. .	112
2.5 <u>Conclusions</u> .. .. .	116



- CONTENTS -  
(Contd.)

CHAPTER	PAGE NO.
3 SOIL MINERALS IN THE $\text{Fe}_2\text{O}_3 - \text{TiO}_2 - \text{H}_2\text{O}$ SYSTEM WITH SPECIAL REFERENCE TO SYNTHETIC PREPARATIONS AT NEAR AMBIENT CONDITIONS .. .. .	119
3.1 <u>Introduction</u> .. .. .	119
3.2 <u>Materials and methods</u> .. .. .	121
3.2.1 Synthetic Fe-Ti oxides .. .. .	121
3.2.2 Soil samples and clay analysis .. .. .	122
3.3 <u>Results and discussion</u> .. .. .	124
3.3.1 Comparison of synthetic and natural Ti oxides .. .. .	124
3.3.2 Freshly prepared Fe-Ti oxides.. .. .	128
3.3.3 The effect of aging Fe-Ti oxides at room temperature .. .. .	132
3.3.4 The effect of aging Fe-Ti oxides at pH 12 and 70 °C for 70 days.. .. .	134
3.3.5 The effect of aging Fe-Ti oxides at pH 5,5 and 70 °C for 70 days.. .. .	134
3.3.5.1 Composition range $0 < \text{Ti}/\text{Ti}+\text{Fe} \leq 0,20$	134
3.3.5.2 Composition range 0,20 $< \text{Ti}/\text{Ti}+\text{Fe} \leq 0,70$ .. .. .	140
3.3.5.3 Composition range 0,70 $\leq \text{Ti}/\text{Ti}+\text{Fe} < 1,0$ .. .. .	143
3.4 <u>Conclusions</u> .. .. .	145
4 FORMS OF PEDOGENIC IRON AND TITANIUM AND THEIR DISTRIBUTION IN RELATION TO CLIMATE AND TOPOGRAPHY	147
4.1 <u>Introduction</u> .. .. .	147
4.2 <u>Results and discussion</u> .. .. .	148
4.2.1 "Primary Fe and Ti" .. .. .	148
4.2.2 Secondary layer silicate Fe and Ti .. .. .	150
4.2.3 Organic Fe and Ti .. .. .	151
4.2.4 Oxidic Fe and Ti .. .. .	151
4.2.4.1 Protoferrihydrite and ferrihydrite	151
4.2.4.2 Pseudorutile, anatase and rutile	159
4.2.4.3 Goethite .. .. .	161
4.2.4.4 Haematite and its transformation to goethite .. .. .	161
4.2.4.5 Maghaemite and its transformation to goethite .. .. .	168
4.2.4.6 Lepidocrocite.. .. .	168
4.3 <u>Conclusion</u> .. .. .	173

- CONTENTS -  
(Contd.)

<u>APPENDIX</u>	<u>PAGE NO.</u>
1     PROFILE DESCRIPTIONS AND SAMPLE INFORMATION OF REPRESENTATIVE SOILS AND FERRUGINOUS BAUXITE     ..	175
2     PREPARATION AND CHARACTERISATION OF SYNTHETIC OXIDES     ..     ..     ..     ..     ..     ..	184
(i) Goethite, aluminous goethite and mixed Fe-Ti oxides prepared from chloride salts aged at pH13     ..     ..     ..	184
(ii) Haematite     ..     ..     ..     ..     ..	189
3     X-RAY DIFFRACTION ANALYSIS     ..     ..     ..     ..	190
REFERENCES     ..     ..     ..     ..     ..	192

-----oo0oo-----

## - LIST OF FIGURES AND MAPS -

FIGURE NO.		PAGE NO.
1	Generalised soil map of study area .. .. .	2
2	Generalised sketch showing landscape from coast to high Drakensberg .. .. .	3
1.1	Map showing sampling sites of various goethite containing materials, distribution of ferricretes and ferruginous bauxites in study area .. .. .	10
1.2	Relationship between shift in the d(111) goethite peak and Al content of goethite .. .. .	14
1.3	X-ray diffraction patterns of (a) synthetic goethite, (b) synthetic Al-goethite (6 mole % AlOOH), (c <sub>1</sub> ) and (c) goethite flake (cf. Plate 1.1 A) formed in weathering limestone (No. 262) (c <sub>1</sub> ) fitted flush into an X-ray aluminium sample holder and (c) after being finely ground to a powder and in randomly orientated form, (d) ferruginous bauxite (No. 62 c) pretreated with 5 M NaOH at 90 °C for 2 hours .. .. .	16
1.4	Infrared spectra of (a) synthetic goethite (b) synthetic Al-goethite (6 mole % AlOOH), (c) goethite flake (cf. Plate 1.1 A) formed in weathering limestone (No. 262) and (d) ferruginous bauxite (No. 62 c) pretreated with 5 M NaOH at 90 °C for 2 hours .. .. .	17
1.5	Histogram indicating the relative proportions of Al-substitution in goethite, calculated from the d(111) line shift for 183 samples .. .. .	64
1.6	Relationship between width at half height ( $^{\circ}2\theta$ ) and mole % AlOOH in goethite, using the d(111) line for 183 samples .. .. .	65
1.7	Relationship between width at half height ( $^{\circ}2\theta$ ) and shift in the d(110) line of goethite for 200 samples .. .. .	66
1.8	Relationship between d(111) and d(110) of goethite for 183 samples .. .. .	71
2.1	Map showing sampling sites of various magnetic materials, distribution and abundance of maghaemitic concretions .. .. .	78
2.2	Relationship between width of half height ( $^{\circ}2\theta$ ) and shift in the d(220) line of magnetite and maghaemite for 63 magnetic samples .. .. .	93
2.3	Relationship between magnetic susceptibility ( $\chi$ ) and colour for 31 non-ferromagnetic sesquioxidic soil clay (<2 $\mu$ m) samples .. .. .	102
2.4	Ferrous iron and titanium contents of synthetic and selected representative natural samples from sample collection .. .. .	104



- LIST OF FIGURES AND MAPS -  
(Contd.)

FIGURE NO.		PAGE NO.
3.1	X-ray diffraction patterns from synthetic Fe-Ti oxides	125
3.2	Relationship between $Ti_O/Ti_T$ and MCD ( $\text{\AA}$ ) for anatase 101 (calculated from the WHH of the anatase 101 X-ray reflection) .. .. .	127
3.3	Relationship between $Ti_O/Ti_T$ and $NH_4$ -oxalate extraction time (hours) .. .. .	129
3.4	Negative and positive charge variation with pH in relation to composition of freshly prepared Fe-Ti oxides .. .. .	131
3.5	Negative and positive charge variation with pH in relation to composition of Fe-Ti oxides aged at 70 °C and pH 5,5 for 70 days .. .. .	131
3.6	Variation in specific magnetic susceptibility ( $\chi$ ) with the composition of freshly prepared and aged (70 °C at pH 5,5 for 70 days) Fe-Ti oxides ..	133
3.7	Relationship between ammonium oxalate extractable Ti and Fe to total Ti and Fe ( $M_O/M_T$ ) and the composition of Fe-Ti oxides aged at 70 °C and pH 5,5 for 70 days .. .. .	133
3.8	X-ray diffraction patterns of synthetic Fe-Ti oxides aged at 70 °C and pH 5,5 for 70 days and from Indonesian pseudorutile .. .. .	136
3.9	Infrared spectra of synthetic Fe-Ti oxides aged at 70 °C and pH 5,5 for 70 days. .. .. .	137
3.10	X-ray diffraction patterns of synthetic Fe-Al oxides and Fe-Zr oxides aged at 70 °C and pH 5,5 for 70 days .. .. .	139
3.11	Variation in unit cell parameters ( $a_O$ and $c_O$ ) for pseudorutile in the composition range $0,20 \leq Ti/Ti+Fe \leq 0,70$ (prepared from Fe-Ti oxides aged at 70 °C and pH 5,5 for 70 days) .. .. .	142
3.12	X-ray diffraction data evaluation (cm relative intensity and width at half height) in relation to composition ( $Ti/Ti+Fe$ %) of the crystalline species present in the titano-ferric system after aging <i>in vitro</i> for 70 days at 70 °C (pH 5,5) and heating in air at 250 °C for 1 day and 14 days .. .. .	144
4.1	Map showing sampling sites of various ferrihydrite and haematite containing materials, and distribution of ferricrete containing haematite .. .. .	152



## - LIST OF FIGURES AND MAPS -

(Contd.)

FIGURE NO.		PAGE NO.
4.2	X-ray powder diffraction patterns of (a) gel-like precipitate from Cedarville, (b) crusts from Sani Pass and (c) thin crusts from Palm Beach .. ..	154
4.3	X-ray powder diffraction patterns of natural untreated ferrihydrites from various localities ..	156
4.4	X-ray powder diffraction patterns of natural and synthetic ferrihydrites before and after various aging treatments <i>in vitro</i> .. .. .	158
4.5	X-ray powder diffraction patterns of haematites from various sources .. .. .	164
4.6	IR spectra of haematites from various sources ..	165
4.7	Map showing sampling sites of various lepidocrocite containing materials, and distribution of the Highland Montane region where high amounts of lepidocrocite are found in "slope gley" soils .. .. .	170
4.8	X-ray powder diffraction patterns of the (020) reflections for synthetic and various types of lepidocrocite containing materials .. ..	172
App. 2.1	NH <sub>4</sub> -oxalate-pH3, extractable (ox) Fe or M (Ti and Al) expressed as a percentage of the total (HCl) Fe or M present in synthetic gels. A. Fe extracted from ferric and mixed gels. B. Ti and Al extracted from mixed gels. Where: (a) Pure ferric gel: (i) prepared using TiCl <sub>4</sub> (5, 10 and 20 % in Ti/Ti+Fe; (ii) prepared using TiCl <sub>3</sub> (5 and 10 % in Ti/Ti+Fe); (iii) prepared using AlCl <sub>3</sub> (5 and 10 % in Al/Al+Fe) .. .. .	188
1	Generalised soil map of study area (scale - 1:1 000 000	See folder at back cover
1.1	Map showing sampling sites of various goethite containing materials, distribution of ferricretes and ferruginous bauxites in study area (scale - 1:1 000 000)	

-----oo0oo-----

TABLE NO.	PAGE NO.
1.1 Sample location, description, and chemical and mineralogical composition of goethite containing materials formed in weathering limestone (lw). ..	18
1.2 Sample location, description, and chemical and mineralogical composition of geode samples (geo). ..	23
1.3 Sample location, description, and chemical and mineralogical composition of ferricretes (hp) ..	27
1.4 Sample location, description, and chemical and mineralogical composition of ferruginous concretions (cn) .. .. .	38
1.5 Sample location, description, and chemical and mineralogical composition of ferruginous crusts (cr)	41
1.6 Sample location, description, and chemical and mineralogical composition of ferruginous pipestems (ps)	43
1.7 Sample location, description, and chemical and mineralogical composition of ferruginous bauxite (ba) .. .. .	46
1.8 Sample location, description, and chemical and mineralogical composition of saprolites (so) ..	53
1.9 Sample location, description and chemical and mineralogical composition of clays from sesquioxidic soils (cl) and gleys (G) .. .. .	55
1.10 Comparison of XRD (this thesis) and Mössbauer (Golden, 1978) data for 2 Transvaal sesquioxidic soils .. .. .	59
2.1 Amounts (mass %) of magnetic and non-magnetic concretions from 5 horizons of 4 different soils	85
2.2 Sample location, description and mineralogical composition of magnetic samples .. .. .	91
2.3 Variation of XRD data for the (311) and (220) lines for magnetite after refluxing synthetic magnetite for 3 months. .. .. .	96
2.4 Magnetic susceptibility values of selected ferromagnetic samples after treatment with $\text{NH}_4$ -oxalate-pH3, CBD and 0,2M oxalic acid at 90 °C for 1h .. .. .	101
2.5 A comparison of Fe, Ti and Mn extracted from selected magnetic samples by 0,2M-ammonium oxalate-oxalic acid -pH3 ( $\text{Fe}_\text{O}$ and $\text{Ti}_\text{O}$ ), CBD ( $\text{Fe}_\text{d}$ , $\text{Ti}_\text{d}$ and $\text{Mn}_\text{d}$ ), $\text{HCl}$ ( $\text{Fe}_\text{HCl}$ , $\text{Ti}_\text{HCl}$ and $\text{Mn}_\text{HCl}$ ) and 0,2M oxalic acid at 90 °C for 1h .. .. .	106

- LIST OF TABLES -  
(Contd.)

<u>TABLE NO.</u>		<u>PAGE NO.</u>
3.1	Sample collection and Ti and Fe extracted from subsoil clays by acid ammonium oxalate ( $Ti_o$ and $Fe_o$ ), CBD ( $Fe_d$ ) and total Ti ( $Ti_t$ ) .. ..	123
3.2	Munsell colours of freshly prepared Fe/Ti coprecipitates and after aging at 70 °C (pH 5,5) for 70 days .. .. .	130
3.3	X-ray diffraction and infrared absorption data for goethites in the aged synthetic Fe-Ti oxides of composition $0 < Ti/Ti+Fe < 0,10$	138
3.4	Comparison between the three sharpest XRD lines for pseudorutile in the synthetic Fe-Ti oxides of composition $0,20 < Ti/Ti+Fe < 0,70$ , Indonesian pseudorutile and ASTM 19-635 Data reported for pseudorutile .. .. .	141
4.1	Relative abundance of Fe and Ti compounds in soils along the eastern seaboard of South Africa ..	149
4.2	Sample location, description and XRD data for haematites from various sources .. ..	162

-----oo0oo-----



## - LIST OF PLATES -

(Certain captions have been summarized)

<u>PLATE</u>		<u>PAGE NO.</u>
1.1	A. Photograph of a cross section of altered limestone (No. 262) from Umzimkulu Lime Co. quarry, Port Shepstone .. .. .	19
	B - D. Scanning electron micrographs (SEM) of uppermost surface (a) of the goethite flake showing the irregular, porous, spongy surface texture and globular goethite at progressively increasing magnifications B(x 32), C(x 120) and D (x 800) ..	19
1.2	A. SEM view of brown upperside surface (a in Plate 1.1 A) of goethite flake showing further detail of globular morphology at higher magnification (x 1600) ..	20
	B. SEM view of yellow, lowerside surface (b in Plate 1.1 A) of goethite flake (x 1600) and C, higher magnification of the latter (x 3 200) indicating a less spongy surface texture and a less pronounced globular goethite morphology than on the upperside surface (a) ..	20
	D - E. Transmission electron micrographs of the <2 $\mu$ m fraction of part of the goethite flake shown in Plate 1.1 A .. .. .	20
1.3	A. Photograph of fossil ferruginized ammonites derived from Cretaceous bedrock at Uloa, ---- ..	24
	B. Photograph of a hard, shiny pyritized goethite/nodule (No. 177) from a layer within a deep profile in a railway cutting at Uloa .. .. .	24
	C. Photograph of exposed surface ferricrete (No. 206) on plateau above Steelpoort River valley 8 km west of Stoffberg, ---- .. .. .	24
	D. Fragment of vesicular ferricrete (No. 195 b) derived from granite, collected near Piet Retief, ---- ..	24
	E. Fragment of vesicular ferricrete underlying a yellow apedal horizon of Glencoe soil from the Steelpoort River valley, ---- .. .. .	24
	F. Concretionary ferricrete (No. 35) (hard plinthite horizon) underlying "bleached" E-horizon of Wasbank soil, ---- .. .. .	24
1.4	A - C. Profile of vesicular ferricrete underlying the A horizon of a Klipfontein soil in a quarry near Belfast (No. 205), ---- .. .. .	31
	D. SEM of void from the upper layer (x 320) ---- ..	31
	E. A close-up SEM view of rectangular particle (arrow in D) ---- .. .. .	31



## - LIST OF PLATES -

(Contd.)

PLATE		PAGE NO.
1.5	A. Vesicular ferricrete outcrop, 15 km east of Newcastle along road to Utrecht (No. 250) ..	32
	B. Close-up view of hard upper part (0-40 cm) of A, ----- .. .. .	32
	C - E. SEM of void in B at progressively increasing magnification, C (x 160), D (x 320) and E (x 800) ..	32
1.6	A. Close-up view of vesicular ferricrete underlying humic A-horizon of Nomanci soil associated with the Early Cainozoic "African" cyclic erosion surface and developed from Table Mountain sandstone at Cibini (No. 181 b) .. .. .	33
	B - D. SEM of void in Cibini ferricrete (A), at progressively increasing magnifications B (x 160), C (x 320) and D (x 800), ----- .. .. .	33
1.7	A. Angular, plate-like fragments of ferricrete concentrated in the stoneline of a Farningham soil exposed in a road cutting 15 km west of Umzimkulu along the road to Franklin (No. 72).. .. .	36
	B. Fragment of "snuff-box shale" ferricrete from hardpan ferricrete material below the A-horizon of a Klipfontein soil near Albert Falls (No. 171), ..	36
	C. Angular, ferruginous concretions from Rensburg soil near Albert Falls (No. 39) separated into three broad textural classes, ----- .. .. .	36
	D. Thin, friable ferruginous crust between underlying gleyed clayey foot-slope or colluvial material and overlying friable material (soft plinthite) ----- below E horizon of Longlands soil, exposed on river bank near Pietermaritzburg (No. 179).. ..	36
	E. Fragment with soft, yellowish-red, weakly cemented, sandy ferruginous crust between cream coloured friable, partly leached aeolianite in Clansthal soil from insized cliff overhanging sea near Richards Bay (No. 183).. .. .	36
1.8	A. Typical relict, large, hard, hollow pipestems in a freely drained Clansthal soil near Umhlanga Rocks (No. 52), ----- .. .. .	44
	B - D. Thin friable pipestems of more recent origin in Warrington and Dundee soils from Palm Beach (B; No. 193) and Pietermaritzburg (C; No. 200) respectively, ----- .. .. .	44
	C. Small, fairly hard, yellow-brown pipestems surrounded by orange coloured haloes of clay containing lepidocrocite in gleyed soil matrix from the B23 horizon of an Ouwerf soil near Loteni (No. 142) ..	44

(Contd.)

PLATE		PAGE NO.
	E. SEM of fracture surface and tubular cavity in pipistem (x 800) from Loteni,----- .. ..	44
1.9	A. An exposure of a Farmhill soil derived from dolerite in a railway cutting near Sweetwaters, Pietermaritzburg, showing a layer of nodules, fragments and blocks of ferruginous bauxite (No. 62) .. .. .	47
	B - C. Typical ferruginous bauxite nodules fractured in half before photographing, with porous weathered dolerite centres or cores and dense, shiny, high iron outer shells (rinds) from Sweetwaters profile and near Umzimkulu (No. 63 c) .. .. .	47
	D. Portion of a weathered dolerite boulder-block fractured in half to show the core of unweathered dolerite and abrupt transition to surrounding layers of weathered dolerite (ferruginous bauxite) from Sweetwaters profile. .. .. .	47
	E - F. Light micrographs (thin sections) illustrating changes during weathering of dolerite to ferruginous bauxite in D. .. .. .	47
1.10	A - C. SEM of fracture surface of ferruginous bauxite from Sweetwaters (No. 62 c) at progressively increasing magnifications A (x 160), B (x 800) and C (x 1 600) ----- .. .. .	49
1.11	A - D. Transmission electron micrographs of clay size material dispersed ultrasonically after gently grinding a small portion of ferruginous bauxite from Sweetwaters (62 b),----- .. .. .	50
1.12	TEM of untreated (A and B) and CBD treated (C) clays from Ruston soil (12M Av).. .. .	61
2.1	A. Photograph of a magnetic band in the C horizon of a Farningham soil in a road cutting 10km north of Ixopo (No. 199) .. .. .	109
	B. Large rounded magnetic fragment or nodule from a stoneline in a Griffin soil, B22 horizon (No. 103) exposed in a road cutting 3km south of Richmond, fractured in half before photographing. ..	109
	C. Thin section light micrograph of magnetic band. ..	109
	D - E. SEM of fracture surface and cavity of magnetic band from sample No. 199 at progressively increasing magnifications,----- .. .. .	109
	F. TEM of clay-size fraction (<2 $\mu$ m) dispersed ultrasonically after gently grinding a portion of magnetic band from sample No. 199 .. ..	109
2.2	A. Photograph of hard, shiny magnetic concretions from a Farningham soil, B21 horizon near Howick (No. 42)	111
	B. SEM of fracture surface and cavity of a concretion from sample No. 42 .. .. .	111



## - LIST OF PLATES -

(Contd.)

PLATE		PAGE NO.
	C. TEM of clay-size fraction (<2 $\mu$ m) dispersed ultrasonically (10 min. at 20 K Hz in distilled water) after gently grinding several magnetic concretions from sample No. 42a. .. ..	111
	D. TEM of clay-size fraction from No. 42a (cf. C above) after 1 x 1h treatment with CBD. .. ..	111
2.3	A. Thin section light micrograph of dolerite core in a ferruginous bauxite boulder-block from a Farmhill soil exposed in a railway cutting near Sweetwaters, Pietermaritzburg (No. 62a). .. ..	113
	B. SEM of the "fracture surface" of an unweathered opaque magnetic grain isolate from crushed dolerite from sample No. 62a. .. ..	113
	C. Thin section light micrograph of ferruginous bauxite (No. 62b) adjacent to dolerite core. .. ..	113
	D - F. SEM of a large opaque magnetic grain in a void in the ferruginous bauxite (No. 62b) adjacent to the dolerite core, at progressively increasing magnifications. .. ..	113
2.4	A - E. SEM of magnetic opaque "single grain" isolates from the Farmhill soil (No. 88Gf), C horizon (on Mikes Pass, south aspect), of the ~62 - 500 $\mu$ m fraction at progressively increasing magnifications. ..	115
3.1	Electron micrographs of goethite prepared from Fe - Ti oxides with 20% in Ti/Ti + Fe aged at 60 °C and pH13 for 30 days and dialyzed against distilled water.	135
4.1	A. Photograph of drainage ditch near Cedarville (No. 13) showing a strong brown (7.5 YR 5/8) sludge-like or gel-like precipitate (i.e. "ochreous deposit") presently being deposited from spring water issuing from a crack in the side of the ditch. .. ..	153
	B and C. TEM of ensheathed filaments of "iron-oxidizing" bacterium mainly <i>Sphaerotilus</i> encrusted with protoferrihydrite from sample No. 13, at increasing magnification. .. ..	153
	D. TEM of protoferrihydrite from sheath structure at high magnification showing typical small spherical-like particles. .. ..	153
4.2	A. Photograph of drainage ditch near Palm Beach (No. 232) showing thin dark reddish-brown (5 YR 5/4) friable crusts "caked" on the side-wall of the ditch (arrowed), and on the left hand side of the geological hammer a more recent brown gel-like precipitate has been deposited and has a shiny, surface appearance.	155
	B. TEM of ferrihydrite from sample No. 232. .. ..	155

## - LIST OF PLATES -

(Contd.)

PLATE		PAGE NO.
	C. TEM of ferrihydrite from sample No. 234. .. ..	155
	D. Photograph of dark, rusty friable ferrihydrite-rich crusts weakly cementing unweathered gravel (basalt and TMS) to the surfaces of larger round basalt fragments from a lithosolic alluvium soil that has been cut by streams near the Sani Pass hotel (No. 234). .. ..	155
4.3	A. Profile of an Ouwerf soil exposed in a road cutting 5 km north of Impendle showing a layer of hard, thin plate-like goethite-rich crusts (arrowed) and a 5 to 10 cm wide band of lepidocrocite-rich orange clay above and below the thin crusts. ..	169
	B. Close-up view of goethite-rich crusts from A and a "thin iron-pan" sampled by the writer at Profile No. W4 during the field excursion of the North of England Soils Discussion Group meeting at High Force, U.K. 1975. Both samples have a thin (~ 1.0 mm thick) covering of lepidocrocite on their lower surfaces. ..	169
	C. Fragment or geode with large (2 to 6 mm) lepidocrocite-rich crystals (dark areas) cemented together by a goethite-rich matrix, from a stoneline in a Clovelly soil, north-east of Dullstroom. .. ..	169
	D. Ferruginous geode fragment from saprolite below a Farningham soil east of Ermelo photographed after fracture to show hollow centre (arrow) with loose "pinkish" crystals of lepidocrocite. The outer red and yellow layering is composed of crystalline haematite and goethite, respectively. .. ..	169
	E. TEM of large lath-shaped crystalline lepidocrocite crystals with serrated edges from ferruginous geode fragment (cf. D). .. ..	169
F -	G. TEM of clay-size material dispersed ultrasonically from orange coloured clay band showing typical elongated plates of lepidocrocite, serrated on two opposite edges. In G smaller lepidocrocite crystals are adsorbed on basal planes of silicate flakes. ..	169
App. 1.1	A. Mass-movement terraces (terraces) — Afro-alpine region near Sani Pass ----- .. ..	176
	B. Compact layer at depth of 110-125 cm in Blinkklip (humic phase) soil (No. 106) above Sani Flats in Lesotho .. ..	176
	C. Profile of Milford soil (No. 266) near Naudesnek-----	176
	D. Fragment of basalt from Milford soil B23 horizon (No. 266) ----- .. ..	176
App. 2.1	Electron micrographs of goethite prepared from:	
	A. precipitated ferric oxide gel. pH13 aged for 30 hours;	185
	B. coprecipitated alumino-ferric oxide gel (5% in Al/Al + Fe) pH13, aged for 30 hours; .. ..	185
	C. precipitated ferric oxide gel, pH13, aged for 30 days.	185



## - LIST OF PLATES -

(Contd.)

<u>PLATE</u>		<u>PAGE NO.</u>
App. 2.2	Electron micrographs of goethite prepared from Fe-Ti oxide gels, pH13, aged for 30 days (60 °C) and dialized against distilled water with:	
A.	5% in Ti/Ti+Fe; .. .. .	187
B.	5% in Ti/Ti+Fe and oxalate treated; .. ..	187
C.	10% in Ti/Ti+Fe; .. .. .	187
D.	10% in Ti/Ti+Fe and oxalate treated; .. ..	187
E.	20% in Ti/Ti+Fe; .. .. .	187
F.	20% in Ti/Ti+Fe and oxalate treated. .. ..	187
App. 3.1	Device used for preparing disorientated powdered samples for X-ray diffraction measurement----- ..	191

-----oo0oo-----

## ACKNOWLEDGEMENTS

I wish to express my sincere gratitude to :

Professor J. le Roux, Associate Professor in the Department of Soil Science and Agrometeorology, and Supervisor of this project for his continued interest during this investigation and for his critical appraisal of the draft manuscript. I wish to express my gratitude to him for much encouragement over the past ten years;

Professor U. Schwertmann, Director of the Institute für Bodenkunde, Technische Universität, München for his encouragement and advice while he was on study leave for 8 months at Natal University in the Department of Soil Science and Agrometeorology. It was my privilege to work with him, and the access to his wide knowledge of iron oxides has been of inestimable value;

Professor M.E. Sumner, formerly Head of the Department of Soil Science and Agrometeorology, University of Natal, for his interest, valuable guidance and encouragement over a number of years prior to, and during part of this investigation;

Dr. M.C.F. du Plessis and Dr. C.N. MacVicar, Director and Deputy Director respectively, of the Soil and Irrigation Research Institute, and the Department of Agricultural Technical Services for allowing the writer to study part-time under the auspices of the University of Natal and for permission to use the results of research projects for thesis purposes;

Individuals of various Departments at the University of Natal for technical assistance rendered during this investigation;

Mrs. M.G. Gilliland and Mr. V.H. Bandu of the Electron Microscope Unit, Dr. E. Kyle (infrared analysis) and Mr. W.E. Helfer (magnetic susceptibility analysis) of the Department of Chemistry,

Mr. P. Seyambu (thin sections) of the Department of Geology, Messrs. B. Martin and R. Poonsamy (photographic facilities) of the Department of Geography, and to colleagues and staff of the Department of Soil Science and Agrometeorology;

Messrs. M. Dhani and J. Schoonraad, Department of Agricultural Technical Services, for assistance with the reproduction of the Plates and the thesis;

Messrs. K. Maurer and B.H. Armitage of the Town and Regional Planning Commission for their assistance in the art-work on Fig. 2;

Ms. P. Waugh of the Soil and Irrigation Research Institute for her invaluable technical help, willing assistance in the preparation of maps and diagrams and for typing parts of the thesis;

Mrs. D. Judkins and Mrs. A.J. Humphreys for kindly typing the thesis;

Alison, my wife, for her encouragement and help throughout the investigation and for typing the initial draft.



## ABSTRACT

The object of this work was to study the interrelationships between the various forms of Fe and Ti oxides, their pedogenic environment, composition, and crystallinity in soils and related materials along the eastern seaboard of South Africa. For this purpose it was necessary (i) to construct a generalised soil map of the area (scale 1 : 1 000 000) in order to relate mineralogical data to pedogenic information, (ii) to conduct detailed laboratory examinations on a wide range of samples from the study area, and (iii) to prepare various synthetic oxides in order to interpret more accurately pedogenic results.

Chapter 1 is concerned with distribution, composition and crystallinity of goethites. Over 200 goethite containing samples from a variety of diverse environments along the eastern seaboard of South Africa were described in detail and examined mainly by X-ray powder diffraction (XRD), and by one or more of the following methods: IR, thin section, electron optical (SEM and TEM) and chemical extraction analysis. The distribution of goethite-rich ferricretes and ferruginous bauxites is shown in a map at a scale of 1 : 1 000 000.

Aluminium-substituted goethite ranging from 0 to about 32 mole %  $\text{AlOOH}$  was identified mainly by XRD line shift and chemical extraction in one or other form (i.e. in weathering limestone, geodes, ferricretes, concretions, crusts, pipestems, ferruginous bauxites, saprolites, sesquioxidic soil clays, vughs in gleys and mottles in plinthite) in virtually every soil zone and major soil type in the area. These various accumulations of goethite, formed in different climatic and weathering conditions, were grouped according to their amount of Al-substitution and crystallinity (as determined by XRD line broadening). Al-substitution in goethite formed in weathering limestone (i.e. high pH) and in geodes (i.e. pure system) was generally low, although the goethite occurring in the latter was the more crystalline. Goethite formed in acid freely drained environments was generally high in Al-substitution (15 to 32 mole %  $\text{AlOOH}$ ) and increased in the following order: saprolites and freely drained dystrophic sesquioxidic soil clays < ferruginous bauxites < dystrophic Avalon and Glencoe soil clays. Goethite formed in more poorly drained sites (i.e. under redox conditions) and in organic-rich environments was generally lower in Al-substitution (3-15 mole %  $\text{AlOOH}$ ) and could be arranged in the following order: pipestems and crusts < ferricretes concretions, gleys and high base status soil clays (e.g. sesquioxidic



mesotrophic soils and possibly organic-rich Afro-alpine soils).

This study revealed that the degree of Al-substitution and crystallinity of goethites may reflect the environment in which it has formed and serve as an indicator of the direction of pedogenic processes.

Chapter 2 deals with the distribution and nature of secondary magnetic compounds. In the study area 5 types of magnetic materials (maghaemite-rich) were identified according to origin, morphology, mineralogy and composition: (i) bands in saprolite (highly ferromagnetic with strong XRD superstructure lines), (ii) concretions (ferromagnetic with XRD superstructure lines), (iii) opaque single grains [highly ferromagnetic, high  $d(220)$  spacings, high Fe(II) and Ti(IV) contents, no XRD superstructure lines] (iv) clay-size fractions [weakly ferromagnetic, low  $d(220)$  spacings, no superstructure lines] and (v) bulk surface horizons of soils attributed mainly to heating by ground fire (ferromagnetic).

Field and laboratory (magnetic susceptibility, XRD, chemical, light microscope and electronoptical) data indicated that all five types occur mainly in freely drained soils in the Mistbelt and Highland Montane regions and that they show a definite soil-climate-terrain zonality. In these regions the yellow-brown apedal horizons of the Griffin and Clovelly soils contain lower amounts of magnetic minerals in the clay-sized fractions, concretions, and opaque single grain particles than in the red apedal horizons (decreasing in the C horizon) suggesting that maghaemite is transformed via solution to goethite.

Poorly crystalline maghaemite (i.e.  $MCD \leq 300 \text{ \AA}$ ) was selectively removed by  $1 \times \frac{1}{2}$  h extraction with CBD, whereas treatment with oxalic acid (0.2M,  $90^\circ\text{C}$  for 1 h) selectively extracted higher amounts of crystalline magnetic material from the opaque single grains than in the concretions and bands.

Evidence for three modes (i.e. via solution, topotactic and heating by ground fire) of magnetic mineral (i.e. relatively pure maghaemite, Ti- and Al-substituted maghaemite and cation deficient Ti-magnetite) formation in a considerable range of magnetic materials from various sources is discussed.



Chapter 3 deals with soil minerals in the  $F_2O_3$ - $TiO_2$ - $H_2O$  system with special reference to synthetic preparations at near ambient conditions. In order to establish a working model for pedogenic titanium and titanoferric oxides, a series of mixed iron and titanium oxide coprecipitates ranging in composition between  $0 < Ti/Ti+Fe < 1$  was synthesized by precipitating Fe and Ti nitrate with  $NH_3$  and aging under varying conditions of pH, temperature and time. XRD, IR spectroscopy, magnetic susceptibility, charge distribution, electron optical and selective chemical dissolution methods were used to characterize both the freshly prepared and aged Fe-Ti oxides.

The freshly prepared Fe-Ti oxides consist of an Fe-rich (Ti-ferrihydrite) phase ( $Ti/Ti+Fe \leq 0,70$ ) having pH dependent positive charge and a Ti-rich X-ray amorphous phase ( $Ti/Ti+Fe > 0,70$ ) with permanent and pH dependent negative charge. Both phases are completely soluble in acid  $NH_4$ -oxalate (2 h extraction in the dark) whereas the dissolution of poorly crystalline anatase is related to its mean crystallite dimension as calculated from the width at half height of the anatase (101), reflection for crystallites  $< 50 \text{ \AA}$ .  $NH_4$ -oxalate soluble Ti was therefore considered as having been derived from these phases in soils. It was particularly high in the clay fractions of soils developed under the cool montane climate of the Afro-alpine zone and lower in soils of warmer subtropical regions which contains mainly anatase, rutile and pseudorutile.

On aging at  $70^\circ C$  and pH 5,5 for 70 days three main crystalline phases were detected depending on the  $Ti/Ti+Fe$  ratio: (i) Goethite and haematite in the composition range  $0 < Ti/Ti+Fe \leq 0,20$ . Low amounts of Ti ( $< 5 \text{ mole } \%$ ) inhibits haematite and results in goethite formation of higher crystallinity as compared with the Ti free system (determined by line broadening). As  $Ti/Ti+Fe$  increases the  $2,450 \text{ \AA}$  reflection of goethite shifts to  $2,445 \text{ \AA}$  and the vibrations at  $890$  and  $795 \text{ cm}^{-1}$  shift to lower frequencies ( $875$  and  $780 \text{ cm}^{-1}$ ) possibly indicating Ti incorporation and formation of Fe-O-Ti bonds. (ii) Pseudorutile in the range  $0,20 \leq Ti/Ti+Fe \leq 0,70$ . As  $Ti/Ti+Fe$  increases there is a marked decrease in the unit cell parameters ( $a_0$  and  $c_0$ ). The IR spectra exhibit broad absorption bands which vary in shape with composition changes. (iii) Ferriferous anatase and anatase in the range  $0,70 \leq Ti/Ti+Fe < 1,0$ . As  $Ti/Ti+Fe$  decreases XRD and IR spectroscopy show structural modifications in the anatase structure.

The origin of pseudorutile has long been attributed to topotactic



alteration of ilmenite. These experiments show that a wide range of Fe-Ti oxides may form by removal of Fe and Ti from primary Ti-bearing silicates or oxides followed by coprecipitation and crystallization in the weathering solution.

Chapter 4 gives an overall assessment of the distribution and formation of the various pedogenic forms and types of Fe and Ti and their association with each other with special reference to climate and topography.

From combined soil survey and detailed mineralogical investigations of various materials from divergent soil-terrain-climate regions in the study area, several forms of pedogenic Fe and Ti have been identified: primary, secondary layer silicate, organic, and oxidic (protoferrihydrite, ferrihydrite, pseudorutile, anatase, rutile, goethite, haematite, maghaemite and lepidocrocite).

Goethite is the most widespread and common iron oxide in the soils, saprolites, ferruginous bauxites and ferricretes. There is a relationship between the magnitude of Al-substitution in the goethite structure, crystal size and mode of formation. In red soil materials (i.e. soil clays, saprolites, ferricretes, concretions), the goethite presence is usually masked by differentially disordered Al-substituted (mostly) haematite.

Maghaemite (Ti- and Al-substituted), pseudorutile and anatase occur mainly in freely drained soils in the Mistbelt and Highland Montane regions whereas lepidocrocite is found in "slope gley" soils in the cooler Montane and Highland Montane regions. Protoferrihydrite and ferrihydrite has been identified by XRD in gel-like precipitates and thin crusts respectively, mainly in drainage ditches throughout the study area. Generally, relatively higher amounts of pyrophosphate (i.e. organic complexed Fe and Ti) and  $\text{NH}_4$ -oxalate- $\text{pH}3$  (ferrihydrite and amorphous Ti) extractable Fe and Ti occur in Afro-alpine soils than in soils from the other soil-terrain-climate regions. Various types of ferrihydrite, goethite, haematite, maghaemite and lepidocrocite have been identified in the study area according to their mineralogical properties (i.e. amount of isomorphous substitution and crystallinity) and origin. Secondary silicate Fe is found mainly in black clays where Fe is incorporated in the smectite structure.

Several examples illustrating the relationship between soil colour, iron oxide form (transformation from ferrihydrite, haematite and maghaemite to goethite) and soil climate (as determined by altitude, aspect and topography) are given to show the distribution of red materials (haematite and maghaemite) in contrast to the yellow brown materials (goethite).

-----oo0oo-----



## GENERAL INTRODUCTION

For the past six years the writer has been associated with the various phases of a land type\* survey along the eastern seaboard of South Africa (see inset locality map, Fig. 1). The total area is approximately 117 000 sq. km and extends from long.  $29^{\circ}$  E. to  $33^{\circ}$  E. and from lat.  $25^{\circ}$  S. to  $31^{\circ}$  S. The western boundary is defined by the Lesotho border and the Southeastern Transvaal district boundary and the eastern boundary is the Indian Ocean coast and Swaziland border; whereas the southern and northern boundaries are Transkei (except for Umzimkulu) and Swaziland/Mozambique borders, respectively. Surface features of the area show remarkable diversity (see Fig. 2). Within 200 km the scenery ranges from impressive mountains at an altitude over 3 000 m through striking plateaux (e.g. Highveld), Upland Regions, Basin Plainlands, incised river valleys and Coastal Hinterland to Coastal Lowlands (Turner, 1973). The area is complex, having great variety of parent rock, and marked differences in climate and vegetation over short distances (Fig. 2). It is outside the scope of this discussion to give a comprehensive account of these various soil forming factors. The following excellent references deal with the physiography (Turner, 1973), geomorphology (King, 1967), geology (du Toit, 1954; Haughton, 1969), vegetation (Acocks, 1953; Edwards, 1967) and bioclimate (Phillips, 1973) of the area, respectively.

The interaction between these factors has resulted in the development of a varied but repetitive pattern of a large number of different kinds of soils in this area (Fig. 1). Moreover, a major characteristic of these soils is the abundance of Fe and/or Ti compounds in one or other form either in the clay, silt or sand fractions or as concretions and ferricretes. The interest aroused from field observations strongly induced the writer to undertake the present study.

The origin and distribution of pedogenic iron and titanium compounds are better understood when viewed in the light of certain generalised soil

---

\* A land type denotes land over which soil pattern, terrain form and macroclimate each exhibit a marked degree of uniformity. Land type maps (scale 1 : 250 000) and inventories are obtainable from the Government Printer, Pretoria and Director of Agricultural Information, Department of Agricultural Technical Services, Pretoria respectively.



# GENERALISED SOIL MAP OF STUDY AREA

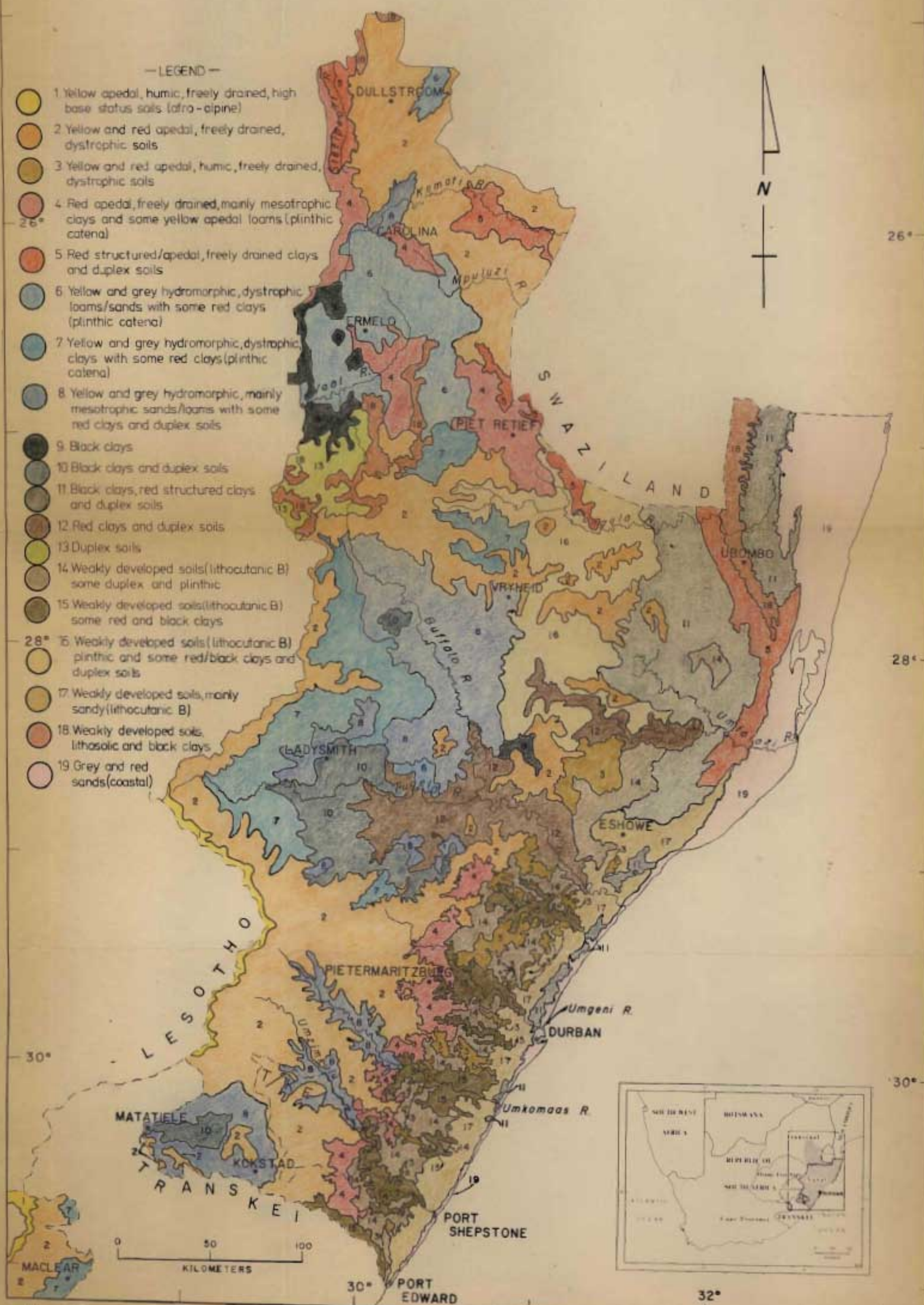


Fig. 1.



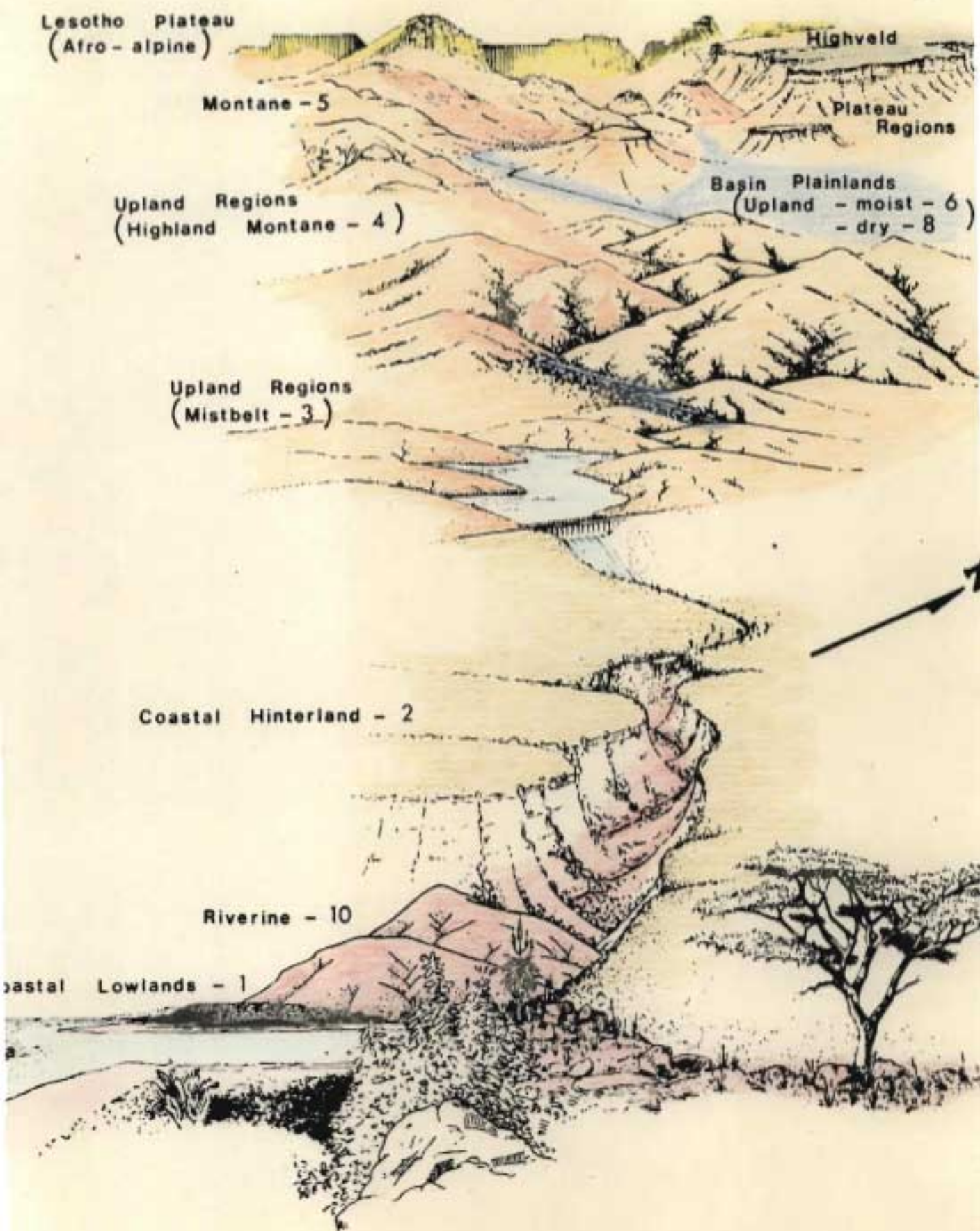


Fig. 2 Generalised sketch showing landscape from coast to high Drakensberg.

Numbers refer to Bioclimatic regions (Phillips, 1973)



patterns. For this reason a generalised small-scale soil map (Fig. 1)\* has been prepared, based to a large degree on information about the area gathered during the land type survey by the writer. The maps by de Villiers (1962), van der Eyk, MacVicar and de Villiers (1969), and Beater (1957, 1959 and 1962) were used as a source of information where no new data were available. This map provides no more than a basis for relating sample sites and for discussion. For this reason, much attention is given in the 19 soil mapping units (see legend in Fig. 1) to soil colour, soil catenary sequences, plinthite and weakly developed groups of soils.

The South African soil classification system (MacVicar, de Villiers, Loxton *et al.*, 1977) use several criteria (e.g. soil colour, plinthic character and gley) which intimately involve the presence or absence of various forms of iron oxides\*\*. Furthermore, this system, unlike for example Soil Taxonomy (Soil Survey Staff, 1975), regards ferricrete as a diagnostic horizon (hard plinthite) and consequently it serves to distinguish between soils at a high level of classification (i.e. soil form). Iron oxides (and Ti-oxides) not only play an important role as a cementing agent and in affecting soil structure but also in plant nutrition by acting as sorption sites for anions (e.g. phosphate) and cations (e.g. essential trace elements).

Despite the fact that the presence, appearance and behaviour of iron compounds are used as important criteria in classifying soils and in studying their genesis, they are also some of the least understood aspects. Very little information is at present available on the distribution and nature of the Fe and Ti compounds to be found in soils along the eastern seaboard of South Africa. The main reason for this lack of knowledge is perhaps due to the difficulties encountered by several workers (e.g. de Villiers and van Rooyen, 1967; Fouche and Fölscher, 1975) in identifying these extremely fine-grained oxide minerals. Physical separation of poorly crystalline oxides in the clay fraction of soils is very difficult, because they are intimately "mixed" with clay minerals and organic matter. In consequence most soil mineralogists in South Africa have not conducted detailed studies on these minerals or have

---

\* Drawn at a scale of 1 : 1 million (see map in folder in back cover)

\*\* The term oxides in this thesis includes all compounds in the system  $\text{Fe}_2\text{O}_3 \cdot \text{H}_2\text{O}$  and  $\text{TiO}_2 \cdot \text{H}_2\text{O}$  respectively.



preferred to speculate on their occurrence and composition, thus there is a noticeable lack of precise information. For these reasons as well as the developing awareness of the important role these oxides play in soil physico-chemical reactions, it seemed pertinent to investigate them in greater detail.

From the pattern of iron oxide distribution, valuable information on present-day and former climates may also be deduced. According to Schwertmann, Fischer and Taylor (1974) a definite zonal and intrazonal distribution of the various iron oxides seem to exist in soils:

Goethite	:	Soils of cool and temperate humid climates
	:	Tropical soils
	:	Hydromorphic soils in subtropical climates
Haematite	:	Tropical and subtropical soils
	:	Soils of mediterranean climates
Lepidocrocite	:	Non-calcareous, hydromorphic soils of temperate climates (pseudogleys)
Maghaemite	:	Tropical and subtropical soils
Ferrihydrite	:	Acid soils of cool and temperate climates rich in organic matter.

Several workers (Norrish and Taylor, 1961; Norrish, 1975; Davey, Russell and Wilson, 1975; Beneslavsky, 1957; Fitzpatrick and le Roux, 1976; Perinet and Lafont, 1972; Schwertmann, Fitzpatrick and le Roux, 1977) have indicated that pedogenic Fe (and Ti) oxides differ in composition and crystallinity from the so called "pure end-members" mainly as a result of isomorphous substitution of foreign elements (mainly Al) for Fe in their structures. Norrish and Taylor (1961) suggested that since Al-substitution shortens unit cell dimensions, the aluminium probably reduces crystal size or crystallinity, increases surface area and hence surface reactivity (e.g. phosphate fixing capacity). Recent studies by Golden, Bigham and Weed (1977) on synthetic goethites indicate that the reactivity and bonding of anions on goethite surfaces are not only related to surface phenomena, but are also strongly influenced by certain structural phenomena resulting from the isomorphous substitution of Al. Furthermore, the presence of cations, (or anions) may inhibit or promote the formation of some Fe (Schwertmann and Taylor, 1977) or Ti oxides. Therefore it is important to determine (i) how far the Fe (and Ti) oxides deviate from that of the pure end-member composition, (ii) the range



and preference of substitution of iron by other elements (e.g. Al, Ti and Si), (iii) the influence of isomorphous substitution on crystallinity, and (iv) the influence of environment on composition and crystallinity.

It has become increasingly clear (see Schwertmann and Taylor, 1977) that to fully understand the formation, properties and transformation of pedogenic iron oxides, studies cannot be undertaken solely on natural materials, but should involve laboratory synthesis experiments as well. Synthesis experiments conducted as closely as possible to near pedogenic conditions may serve as a basis for determining the composition and structure of pedogenic oxides and also to some degree elucidate possible conditions of their occurrence. Unlike Fe and Al systems, related synthetic studies involving Ti and in particular mixed Fe-Ti systems are seriously lacking. For this reason, data is required on Ti and mixed Fe-Ti systems *in vitro* in order to monitor the "natural system" and determine the mineralogical composition of pedogenic Ti and Fe-Ti oxides more precisely.

The objectives of this study are to determine the distribution and mode of occurrence of various forms of pedogenic iron and titanium compounds in the study area, and their properties and association with each other.

## CHAPTER 1

## DISTRIBUTION, COMPOSITION AND CRYSTALLINITY OF GOETHITES

1.1 Introduction

Goethite is by far the dominant and most widespread form of pedogenic iron oxide (Schwertmann and Taylor, 1977) and is the main yellow-brown pigment in soils and saprolites. Consequently it may originate and persist in a wide variety of diverse environments, ranging from temperate to subtropical regions (Schwertmann, Fischer and Taylor, 1974). Furthermore, it has been reported in nature to occur in association with haematite (Schwertmann, 1971), maghaemite (Taylor and Schwertmann, 1974a) and lepidocrocite (Schwertmann and Fitzpatrick, 1977; Iwasa, 1965).

Diverse environmental conditions along the eastern seaboard of South Africa (Fig. 2) which have given rise to a great variety of sesquioxidic soils (Fig. 1) together with a wide range of pedogenic iron-rich accumulations (e.g. ferricretes, concretions, ferruginous bauxites etc.) provide an excellent opportunity to study the mineralochemical characteristics of goethites, in different pedogenic environments and from a single area. In view of this widespread occurrence of goethite in soils, and its important role in fertility studies, it is somewhat surprising that little specific attention has been paid to its occurrence, properties and function in South African soils. The heavy minerals (de Villiers, 1962; Verster, 1964), layer phyllosilicates (van der Merwe and Heysteck, 1955; de Villiers and Jackson, 1967; le Roux, 1973; Fey, 1974; Fitzpatrick and le Roux, 1977) and amorphous alumino-silicates (van Reeuwijk and de Villiers, 1970; Fey and le Roux, 1976; 1977) have attracted, by comparison, more interest and study.

Correns and Engelhardt (1941) presented evidence (reduction in unit cell size) for the isomorphous substitution of Al for Fe in "sedimentary" goethites and Beneslavsky (1957) observed similar goethite in ferruginous bauxite. Several workers (Norrish and Taylor, 1961; Davey, Russell and Wilson, 1975) have reported that soil goethite may also contain structurally incorporated Al. According to Norrish and Taylor this could account for the finely divided nature of soil goethites and also contribute significantly to the surface reactivity in soils. There is also some evidence that V and Mo (Taylor and Giles, 1970; Norrish, 1975), Ni (Roorda and Queneau, 1973;



Norrish, 1975) and Ti (see Chapter 3) could also replace Fe in the goethite structure but in lesser amounts. Although the high stability of goethite in soils has been attributed mainly to its inherent structural and thermodynamic stability (Schwertmann and Taylor, 1977), isomorphous substitution of foreign elements for Fe may also account for this stability, possibly by releasing lattice strain.

With exception of Kühnel, Roorda and Steensma (1975) and Nahon *et al.* (1977) very little work has been done in relating range of crystallinity and Al-substitution in goethite, respectively, to different kinds of pedogenic conditions responsible for goethite crystallization. No information on this aspect is available in South Africa.

For these reasons, a detailed study of goethites from a variety of weathering environments and soil climates is important, and could enable one not only to elucidate the genesis of pedogenic materials more clearly, but also provide a basis for fertility studies. The objectives of this chapter are, therefore, to (i) determine the variability in the mineralochemical composition of goethite as a function of pedogeochemical environment, with particular reference to isomorphous substitution of Al and, (ii) determine to what degree Al-substitution is a function of goethite crystallinity.

## 1.2 Materials

### 1.2.1 Natural samples

Over 200 samples suspected of containing goethite (i.e. as suggested by yellow-brown colours ranging mainly between 7,5 YR to 10 YR) were collected from a wide range of pedogenic materials. For the purpose of this study these samples were grouped according to their morphology and origin, as follows: (1) goethite formed in weathering limestone and hence referred to as "limestone weathering" (lw); (2) geodes (geo); (3) ferricretes (hp)\*; (4) concretions (cn)\*; (5) crusts (cr); (6) pipestems (ps); (7) ferruginous bauxites (ba)\*; (8) saprolites (so)\*; (9) soil clays (cl)\*; (10) gleys (G, bg) or "underclays". Where necessary, further subsamples from each group were taken by isolating or subdividing certain characteristic features such as conspicuous colour or texture zones in materials. Concretions were collected

---

\* Symbols used according to abbreviations given by MacVicar, de Villiers, Loxton *et al.* (1977) p. 139-141.

by hand-picking or by wet-sieving to remove adhering soil material. Magnetic concretions were separated with the aid of a hand-magnet, and yellow-brown and red concretions separated by hand-picking.

Sampling sites of various kinds of goethite containing materials, as well as the distribution of ferricretes and ferruginous bauxites, are shown in Fig. 1.1. Pertinent site information relating to each sample or specimen collected is given in Tables 1.1 to 1.9. The soils selected for study are found in a wide range of environments with vegetative cover ranging from Afro-alpine grassland at an altitude over 3 000 m to thornveld (open *Acacia* savanna) in dry valleys and to coastal forest (Fig. 2). The soil samples used were taken from diagnostic horizons (MacVicar, de Villiers, Loxton *et al.* 1977). Representative profile descriptions and other information of soils and ferruginous bauxite are given in Appendix 1.

#### 1.2.2 Synthetic samples

In order to provide an adequate range for comparison with natural samples, synthetic goethite and aluminous goethite samples were also prepared (see Appendix 2).

### 1.3 Methods

#### 1.3.1 Sample pretreatment

The relatively low goethite content in certain of the samples, together with the coincidence of some of the broad X-ray diffraction lines of goethite with those of other minerals, meant that certain physical and chemical pretreatments were necessary. The concentration techniques used depended on the nature of the sample:

- (i) Cemented (indurated) iron-rich samples (e.g. ferricrete, concretions, geodes and some pipestems, "limestone weathering" and crust samples). Goethite in these materials was considered to be "naturally" concentrated and XRD measurements (Appendix 3) could be made without prior chemical pretreatment. Samples (fragments) were finely ground by hand in an agate mortar to pass a 300 mesh sieve and used as such, for study.
- (ii) Weakly cemented, friable iron-rich samples with high amounts of quartz (e.g. in crusts, pipestems, saprolites, gleys). Samples were first lightly



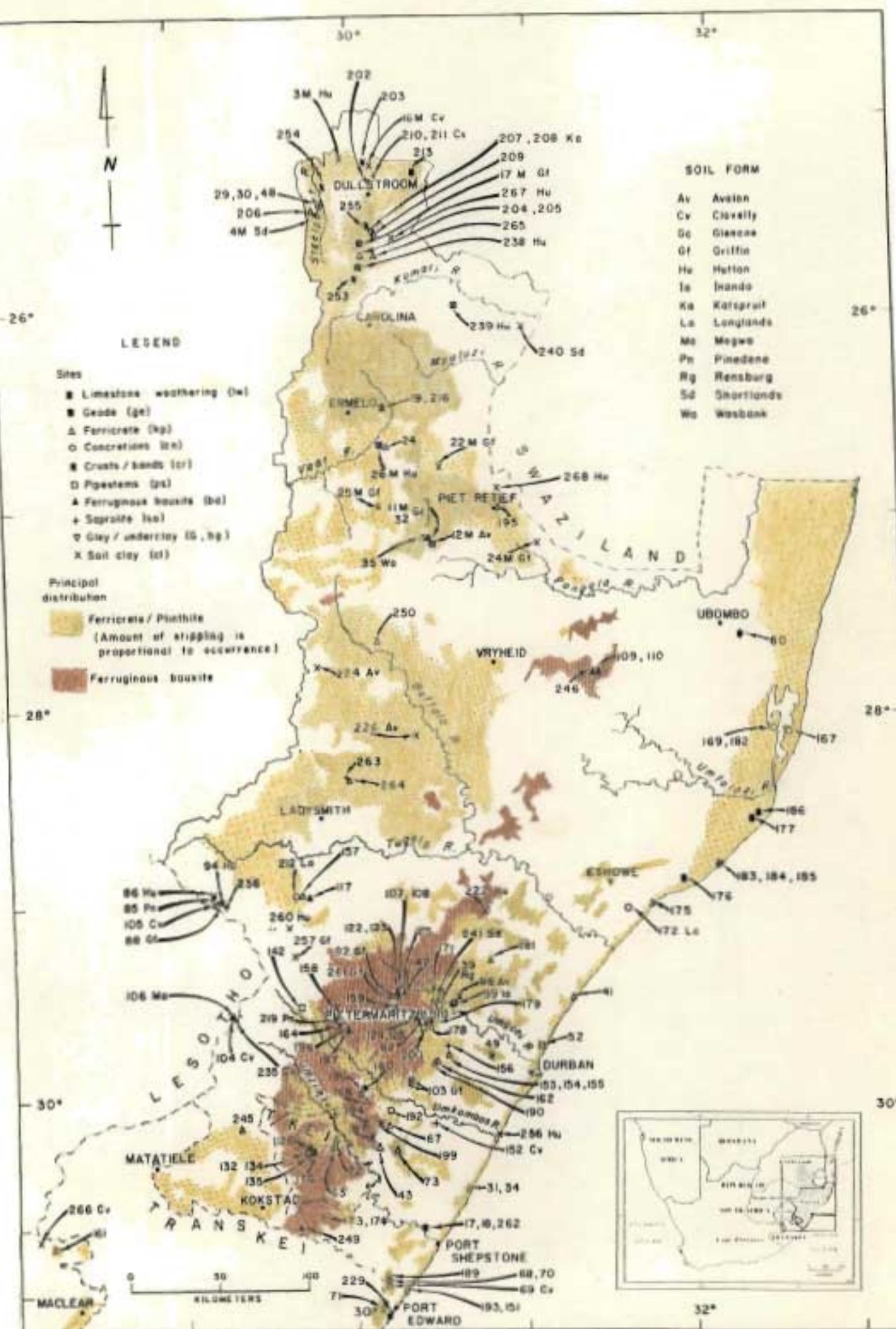


Fig. 1.1 : Map showing sampling sites of various goethite containing materials, distribution of ferricretes and ferruginous bauxites.



ground by hand in an agate mortar to break up large fragments and lumps (heavy grinding was avoided wherever possible so as not to pulverize quartz particles). Clay-size ( $< 2 \mu\text{m}$ ) fractions were separated for study after ultrasonic disaggregation (10 to 15 min treatment) by sieving and repeated settling in dilute aqueous suspension.

(iii) Materials where kaolinite and/or gibbsite predominate (i.e. 50 to 90%) (e.g. soil clays, ferruginous bauxites and some saprolites). Samples were weakly ground, soaked overnight in water or 0,0003 M NaOH and then treated ultrasonically for 10-20 minutes. The clay ( $< 2 \mu\text{m}$ ) fraction was separated from all soil samples as well as the fine ( $< 0,2 \mu\text{m}$ ) fractions from selected samples by centrifugation (Jackson, 1968). Strongly ferromagnetic particles (e.g. magnetite and Ti-magnetite) were separated from the dispersed bauxite sample suspensions by three successive extractions with a small horseshoe-magnet). The dispersed soil clay and bauxite samples were then either freeze-dried or dried on a water bath and lightly ground to a powder using an agate mortar.

All soil clays and bauxites (except for Fe-rich rinds on bauxite nodules) were pretreated with 5 M NaOH for one hour at  $90^{\circ}\text{C}$  (method similar to Norrish and Taylor, 1961) in order to selectively dissolve kaolinite and gibbsite. Residues were weighed.

### 1.3.2 Effect of 5 M NaOH pretreatment

A sequence of 5 M NaOH pretreatments were carried out to investigate the relative ability of goethite to transform to haematite as a function of sample type. For this purpose four kinds of goethite containing materials were selected on the basis of their purity and degrees of line broadening. Treatments with 5 M NaOH were as follows: (i) heated in teflon dish on water bath for 1 hour, (ii) heated in screwtop teflon bottles submerged in water bath at  $90^{\circ}\text{C}$  for 1 hour, (iii) same as (ii) for 3 hours, and (iv) boiled in nickel beaker on hot plate for 1 hour.

### 1.3.3 Chemical extractions

Selected representative samples (50 to 100 mg) before and after pretreatment (as in 1.3.1) were extracted with (i) 10 ml of 0,2 M acid (pH 3) ammonium oxalate in the dark (Schwertmann, 1964) on an end-over-end shaker for two hours, (ii) two successive 15 minute treatments with citrate-bicarbonate dithionite (CBD) (Mehra and Jackson, 1960), (iii) 10 ml 0,1 M



Na-pyrophosphate (pH 9) for 12 hours on an end-over-end shaker, and (iv) 5 ml boiling 5 M HCl for 5 - 10 minutes (strongly cemented samples only). After centrifugation in a Sorvall ultracentrifuge at 10 000 X g for 10 minutes or sedimentation [e.g. (iv)] the extracts were analyzed for Fe, Mn and Al by atomic absorption and Ti by the Tiron method (Pruden and King, 1969).

#### 1.3.4 X-ray diffraction

XRD analysis, using a Phillips P.W. 1050/70 instrument with  $\text{CoK}\alpha$  radiation and a graphite monochromator, was conducted on all pretreated samples (1.3.1) in randomly orientated form (pressing samples in aluminium and/or PVC holders against a filter paper surface, see Appendix 3). Patterns were run from  $23^\circ 2\theta$  to  $46^\circ 2\theta$  at a scan rate of  $\frac{1}{4}^\circ$  per min. The spacings and widths at half height (WHH) of the (110), (130) and (111) goethite peaks were determined (Appendix 3). Lead nitrate was added to some selected samples as an internal standard for the measurement of the (111) spacing of goethite (Norrish and Taylor, 1961). Semiquantitative estimations of goethite and other minerals were made from peak heights of the XRD patterns using standard minerals (i.e. relative estimations done visually).

#### 1.3.5 Infrared spectroscopy

I R absorption spectra of selected samples were obtained from KBr disks using a Perkin Elmer Model 457 grating infrared spectrophotometer.

#### 1.3.6 Thin sections

Optical observations were made on thin sections of a coherent dolerite and adjacent resin-impregnated highly weathered ferruginous bauxite.

#### 1.3.7 Electron microscopy

The external morphology of selected samples (mainly on limestone weathering samples, ferruginous bauxites, pipestems and ferricretes) were investigated with the aid of a Hitachi SSM-2 scanning electron microscope (SEM). Thin fragments, flakes and chips were cemented to 15 mm diameter brass stubs with silver cement, and then sputter coated with a thin film of gold-palladium.

Transmission electron optical observations (TEM) using a Hitachi Hu-11E instrument were made on selected samples. Samples were first dispersed ultrasonically in distilled water and spotted onto collodion or

carbon (for large crystals) coated 200 mesh per inch copper grids.

#### 1.4 Results and discussion

In Tables 1.1 to 1.9 the wide range of goethite containing materials are described, together with their chemical and mineralogical composition. Aluminium, iron, manganese, titanium, nickel and cobalt were only determined in CBD and HCl extracts of selected representative samples. In all the samples, goethite was successfully identified by XRD. In every case the strongest line (110) was observed; but in some soil materials both the (111) and (130) spacings were too broad and where haematite or lepidocrocite were present, the (130) and (111) spacings respectively could not be measured. In accordance with Norrish and Taylor (1961) these d-spacings did not alter after treatment with 5 M NaOH.

The d(111) and d(130) spacings obtained for pure synthetic goethite (i.e. Appendix 2) are 2,452 and 2,698 Å respectively, which are slightly larger than those given by the ASTM card index, but agree fairly well with the work of Thiel (1963), Jonas and Solymar (1970) and Golden (1978). The relationship between the Al content extracted by CBD and HCl (e.g. ferri-cretes) from selected natural samples after pretreatment with 5 M NaOH and the shift in the d(111) spacing is in good agreement with the line joining d(111) of goethite and diasporite (Fig. 1.2). Furthermore, the data for synthetic Al-substituted samples (i.e. 6 and 10 mole % AlOOH) aged at 90°C also coincide fairly well with this line. The line, using data of Thiel (1963) which is based on synthetic products aged hydrothermally, seems to yield higher values for Al-substitution (Fig. 1.2). For these reasons the line joining d(111) and d(130) of goethite and diasporite was used for determining the degree of Al-substitution in the samples (Tables 1.1 to 1.9) from the following equations:  $d(111) = 2,452 - 0,001377 (\text{Al mole \%})$  and  $d(130) = 2,698 - 0,00146 (\text{Al mole \%})$ . In view of the various experimental calibration curves which exist in the literature (Thiel, 1963; Jonas and Solymar, 1970; Golden, 1978) for estimating the AlOOH content in goethites from line shift [i.e. equations relating d(hkl) and Al-substitution] the actual d-spacings for each sample have also been recorded in Tables 1.1 to 1.9. In general the sharper the peak (i.e. low WHH values) the more accurate the peak spacing can be measured.

XRD patterns and IR spectra of some synthetic (pure goethite and aluminous goethite) and natural (goethite formed in weathering limestone



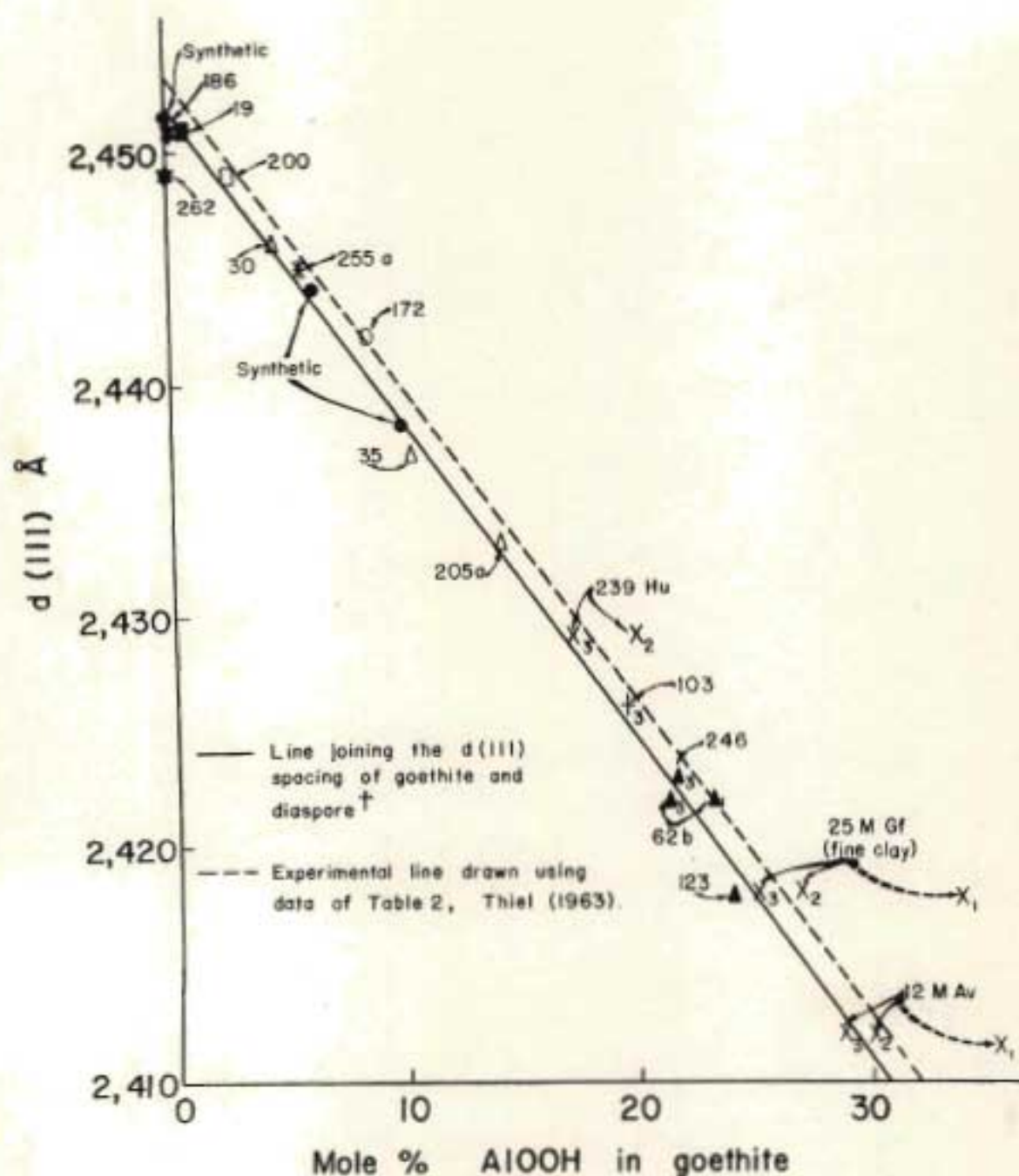


Fig. 1.2 Relationship between shift in the d(III) goethite peak and Al content of goethite; where: ● = synthetic goethite (App. 2), ★ = limestone weathering, ■ = geode, Δ = ferricrete, O = concretions, \* = crusts, □ = pipestems, ▲ = ferruginous bauxite, † = saprolite and X = soil clay; X<sub>1</sub> and ▲ = untreated samples (— indicates that d-spacing could not be measured accurately and was therefore estimated to be similar to X<sub>2</sub>), X<sub>2</sub> = treatment with 5 M NaOH on water bath for 1 hour, X<sub>3</sub>, †<sub>3</sub> and ▲<sub>3</sub> = treatment with 5 M NaOH at 90°C for 1 hour, and † d(III) = 2,452 - 0,001377 (AlOOH mole %) )

and ferruginous bauxite) samples of different aluminium content are presented in Figs. 1.3 and 1.4 respectively. In agreement with Norrish and Taylor (1961), Beneslavsky (1957), Thiel (1963) and Davey *et al.* (1975) there is a decrease in the (130) ( $2,696 \text{ \AA}$ ) and (111) ( $2,451 \text{ \AA}$ ) spacings of goethite with increasing Al-substitution (Fig. 1.3). None of these workers report a similar relationship for the strongest goethite line (110) at  $4,186 \text{ \AA}$ . It was decided also to determine this spacing, especially in view of the wide range of materials being investigated. Apart from the large number of oxide (e.g. haematite and maghaemite) and silicate (e.g. vermiculite minerals which coincide with the goethite IR absorption band at  $890 \text{ cm}^{-1}$  (even after 5 M NaOH treatment) a definite shift may still be detected in certain samples (Fig. 1.4). According to the relationship of Jonas and Solyman (1970) the shift in the  $890 \text{ cm}^{-1}$  band to  $929 \text{ cm}^{-1}$  for the ferruginous bauxite sample corresponds to a substitution of Al for Fe in goethite of 20 mole % which agrees with both chemical and XRD [shift in the (111) spacing] data (Table 1.7).

#### 1.4.1 Goethite formed in weathering limestone

Ferruginous veins in limestone deposits at Marble Delta near Port Shepstone (Plate 1.1 A) and fossil ferruginized coral reefs and mollusca (Plate 1.3 A) from weathered Cretaceous deposits were examined (Table 1.1) in order to provide data on the formation of goethite in a limestone environment. The fossil faunas (including ferruginous ammonites, see Plate 1.3 A c) at Uloa have been studied by King (1970) and Frankel (1966a). They merely indicate a  $\text{CaCO}_3$ -rich marine environment with probably a rather muddy, but not extremely anaerobic, bottom condition. Pieces of silicious fossil-wood, rich in veins of iron were sampled in Cretaceous Beds at Mzamba (No. 229). All these materials occur at various localities along the coastal (marine) margin (Fig. 1.1) and are described briefly in Table 1.1.

An untreated flake from a ferruginous vein in limestone at Marble Delta (Plate 1.1 A a-b) was examined by SEM and XRD (flake fitted into X-ray sample holder). In addition, an untreated crushed sample ( $< 62 \text{ \mu m}$ ) of this material was also analyzed by TEM, IR and XRD methods. Plate 1.1 B shows an SEM view of the brown upper surface of the flake (Plate 1.1 A a) under low magnification and indicates a homogeneous, irregular, porous or spongy surface texture. Higher magnification (Plate 1.1 C and D, and Plate 1.2 A) and the lowerside surface (Plate 1.2 B and C) reveals that



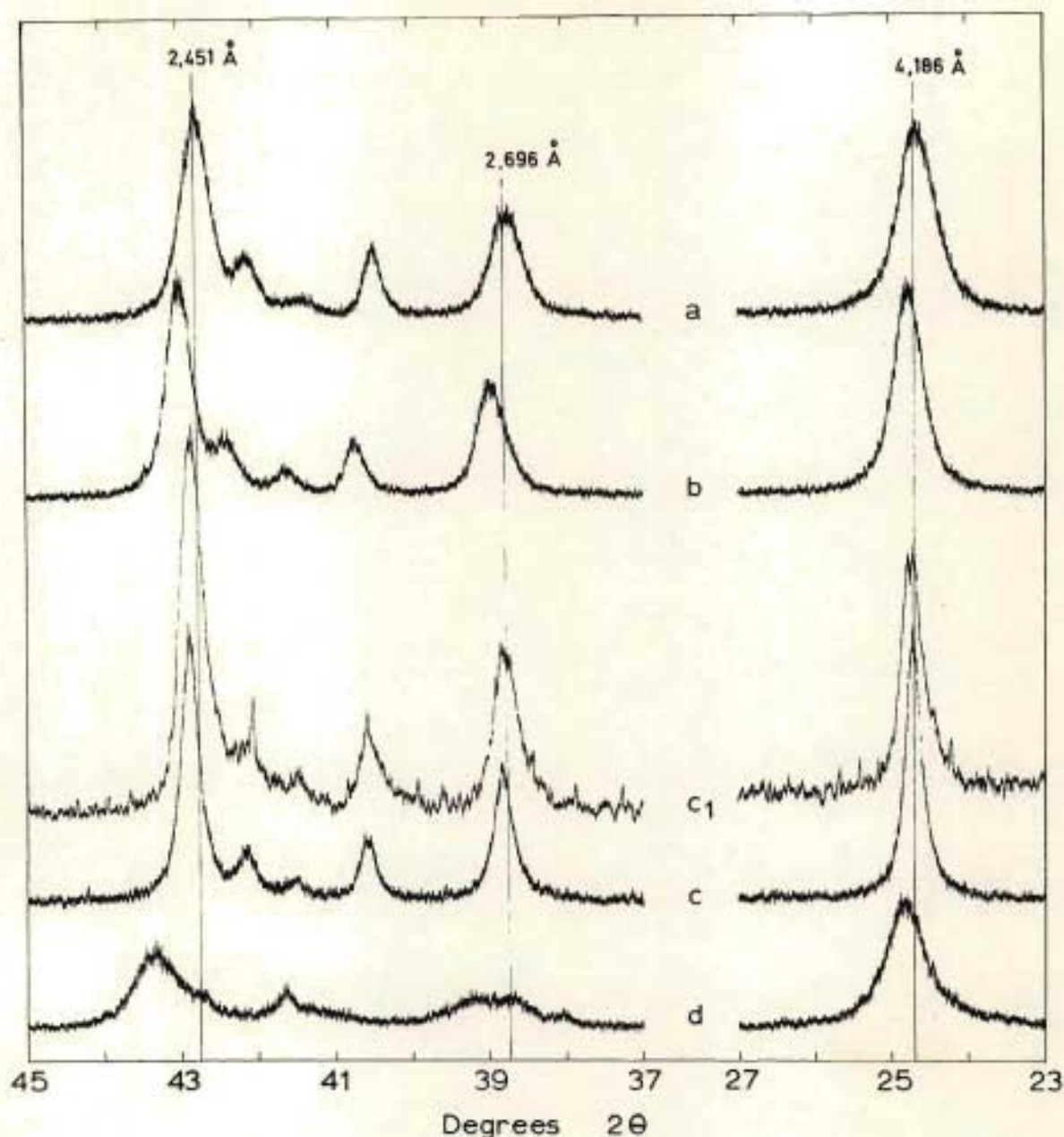


Fig. 1.3: X-ray diffraction patterns of (a) synthetic goethite, (b) synthetic Al-goethite (6 mole %  $\text{AlOOH}$ ), (c<sub>1</sub>) and (c) goethite flake (c.f. Plate 1.1 A) formed in weathering limestone (No. 262) (c<sub>1</sub>) fitted flush into an X-ray aluminium sample holder and (c) after being finely ground to a powder and in randomly orientated form, (d) ferruginous bauxite (No. 62 c) pretreated with 5 M NaOH at  $90^{\circ}\text{C}$  for 2 hours

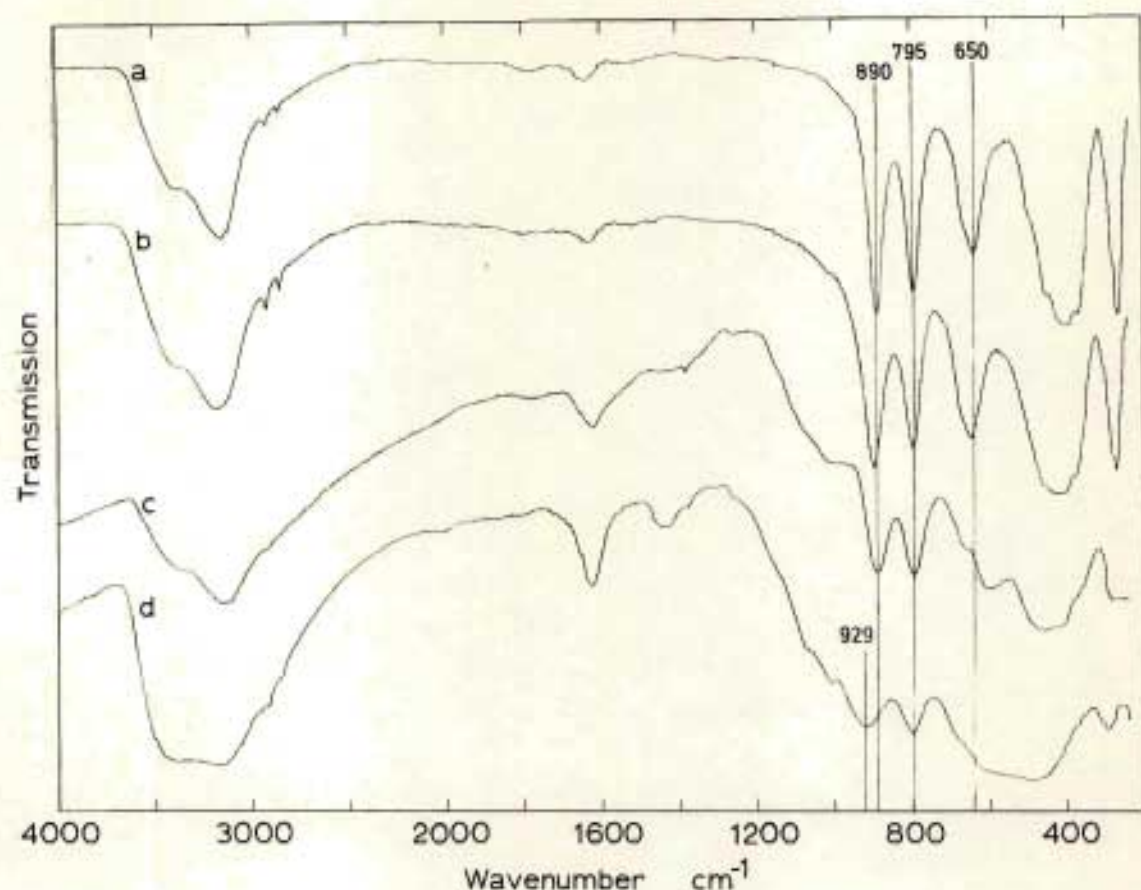


Fig. 1.4: Infrared spectra of (a) synthetic goethite, (b) synthetic Al-goethite (6 mole % AlOOH), (c) goethite flake (c.f. Plate 1.1 A) formed in weathering limestone (No. 262), and (d) ferruginous bauxite (No. 62 c) pretreated with 5 M NaOH at 90°C for 2 hours

both have a knobbly or globular-like surface morphology. XRD of the upper surface (Fig. 1.3 c) shows the presence of goethite only, with the (110) line at 4,186 Å (strongest line) suppressed and the (111) line at 2,451 Å enhanced indicating preferential orientation of goethite crystals on the "globular surface". Furthermore, the goethite crystals on this surface show somewhat greater line broadening than for the whole crushed sample (Table 1.1, Fig. 1.3). Trace c on Figs. 1.3 and 1.4 gives XRD and IR patterns, respectively of the untreated powder sample (portion of the flake crushed) and are similar to the patterns of pure synthetic goethite (trace a in Figs. 1.3 and 1.4). However, although no Al was detected in both CBD and HCl extracts (after pretreatment with 5 M NaOH)



Table 1.1 Sample location, description, and chemical and mineralogical composition of goethite containing materials formed in weathering limestone (lw)

Subsample No. (Fig. 1.1)	Soil zone (Fig. 1)	Locality	Subsample description	Munsell colour (powder)	Chemical composition <sup>4</sup>				Mineralogy <sup>5</sup>			d (110)		d (130)		d (111)			
					Fe <sub>d</sub> %	Fe <sub>HCl</sub> %	Fe <sub>o</sub> %	Fe <sub>HCl</sub> %	Go	Qz	He	Å	WHH (°2θ)	Å	mole % AlOOH <sup>6</sup>	WHH (°2θ)	Å	mole % AlOOH <sup>6</sup>	WHH (°2θ)
262	15	Port Shepstone <sup>1</sup>	Flake (2-3mm) Pl. 1.1A crushed	10 YR <sup>5</sup> / <sub>8</sub>	37,2	46,8	0,15	0,003	D	-	-	4,177	0,12	2,694	3,4	0,16	2,449	2,2	0,13
	15	Port Shepstone <sup>2</sup>	Flake (2-3mm) yellow-brown surface, b in Pl. 1.1A <sup>3</sup>	10 YR <sup>5</sup> / <sub>8</sub>	n.d.	n.d.	n.d.	n.d.	D	-	-	4,177	0,22	2,694	3,4	0,26	2,450	1,5	0,24
17a	15	Port Shepstone <sup>1</sup>	Soft yellow veins	10 YR <sup>5</sup> / <sub>8</sub>	41,7	51,3	0,16	0,003	D	-	-	4,180	0,19	2,690	6,2	0,10	2,446	4,4	0,08
18b	15	Port Shepstone <sup>1</sup>	Hard brown veins	10 YR <sup>5</sup> / <sub>8</sub>	39,7	47,9	0,17	0,004	D	-	-	4,185	0,16	2,693	4,1	0,08	2,448	2,9	0,06
60	11	Mkuzi <sup>2</sup>	Soft yellow zones	7,5 YR <sup>5</sup> / <sub>8</sub>	25,5	46,8	0,20	0,004	D	A	-	4,178	0,63	2,694	3,4	0,50	2,449	2,2	0,41
176	19	Mtunzini <sup>2</sup>	Soft yellow zones (< 62µ)	10 YR <sup>6</sup> / <sub>8</sub>	n.d.	n.d.	n.d.	n.d.	D	A	-	4,177	0,46	n.d.	n.d.	n.d.	2,446	4,4	0,46
229	19	Mzamba <sup>2</sup>	Soft yellow micro-zones in pieces of fossil-wood	10 YR <sup>6</sup> / <sub>8</sub>	n.d.	n.d.	n.d.	n.d.	D	SD	-	4,178	0,36	2,692	4,8	0,36	2,451	0,7	0,36
186	19	Uloa <sup>2</sup>	Very hard ferruginous amonite (Pl.1.3 Ac)	5 YR <sup>4</sup> / <sub>8</sub>	n.d.	n.d.	n.d.	n.d.	D	T	A	4,192	0,23	2,704 <sup>7</sup>	-3,4 <sup>7</sup>	0,36 <sup>7</sup>	2,451	0,7	0,30

<sup>1</sup> Basement Complex crystalline limestone deposits at Marble Delta area, Umzinkulu Lime Co. quarry (weathering of dark brown coloured, highly ferruginous dolomite)

<sup>2</sup> Cretaceous deposits where coral reefs and mollusca have had their calcium carbonate replaced by goethite (c.f. King, 1970)

<sup>3</sup> XRD data (c.f. trace c, on Fig. 1.3) was obtained by placing flake into an X-ray aluminium sample holder (frame) and exposing the flushly fitted surface directly to X-ray

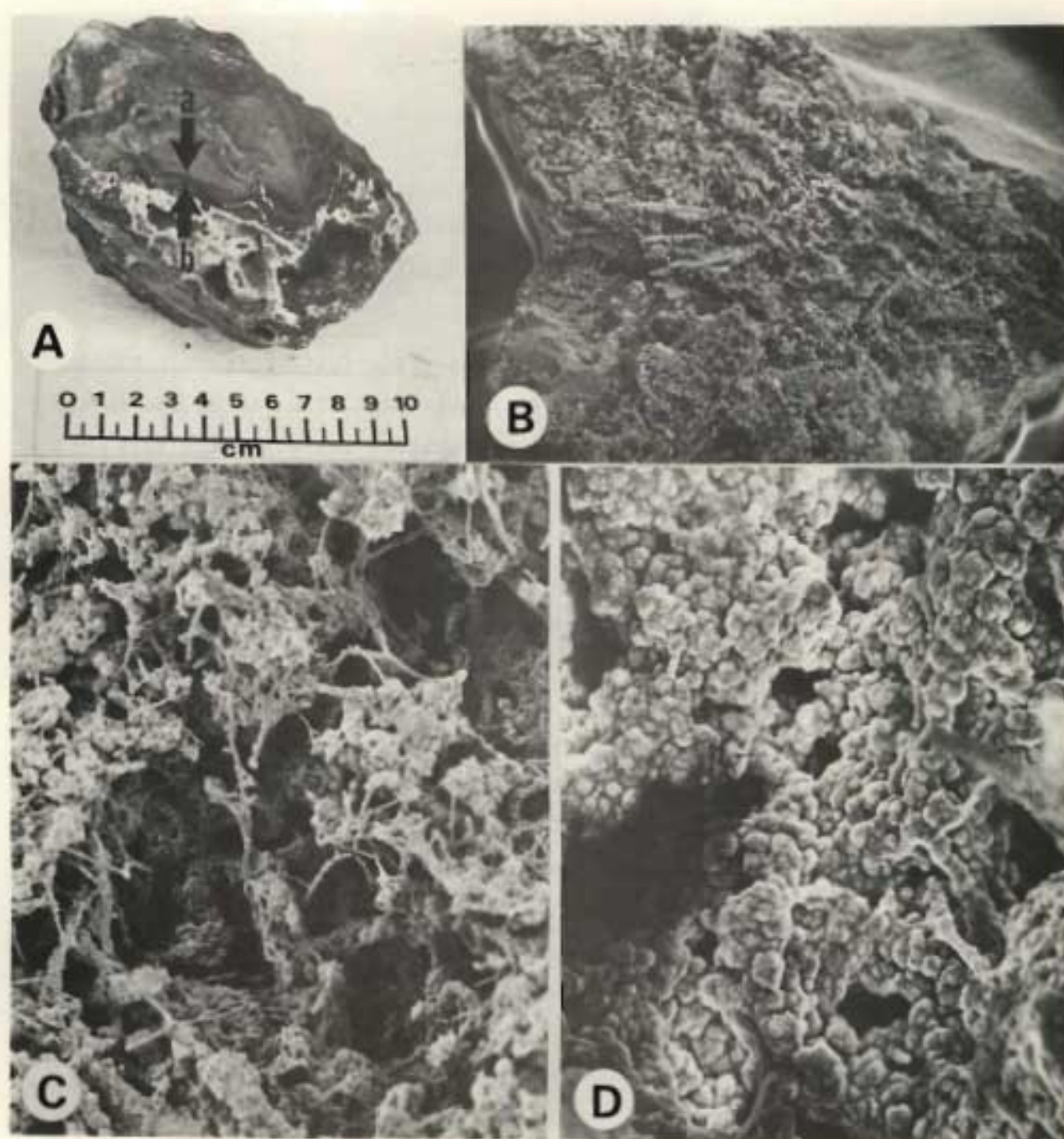
<sup>4</sup> Fe<sub>d</sub> = CBD extractable Fe; Fe<sub>HCl</sub> = HCl extractable Fe and Fe<sub>o</sub> = NH<sub>4</sub>-oxalate (pH3) extractable Fe; n.d. = not determined

<sup>5</sup> Go = goethite; Qz = quartz; He = haematite

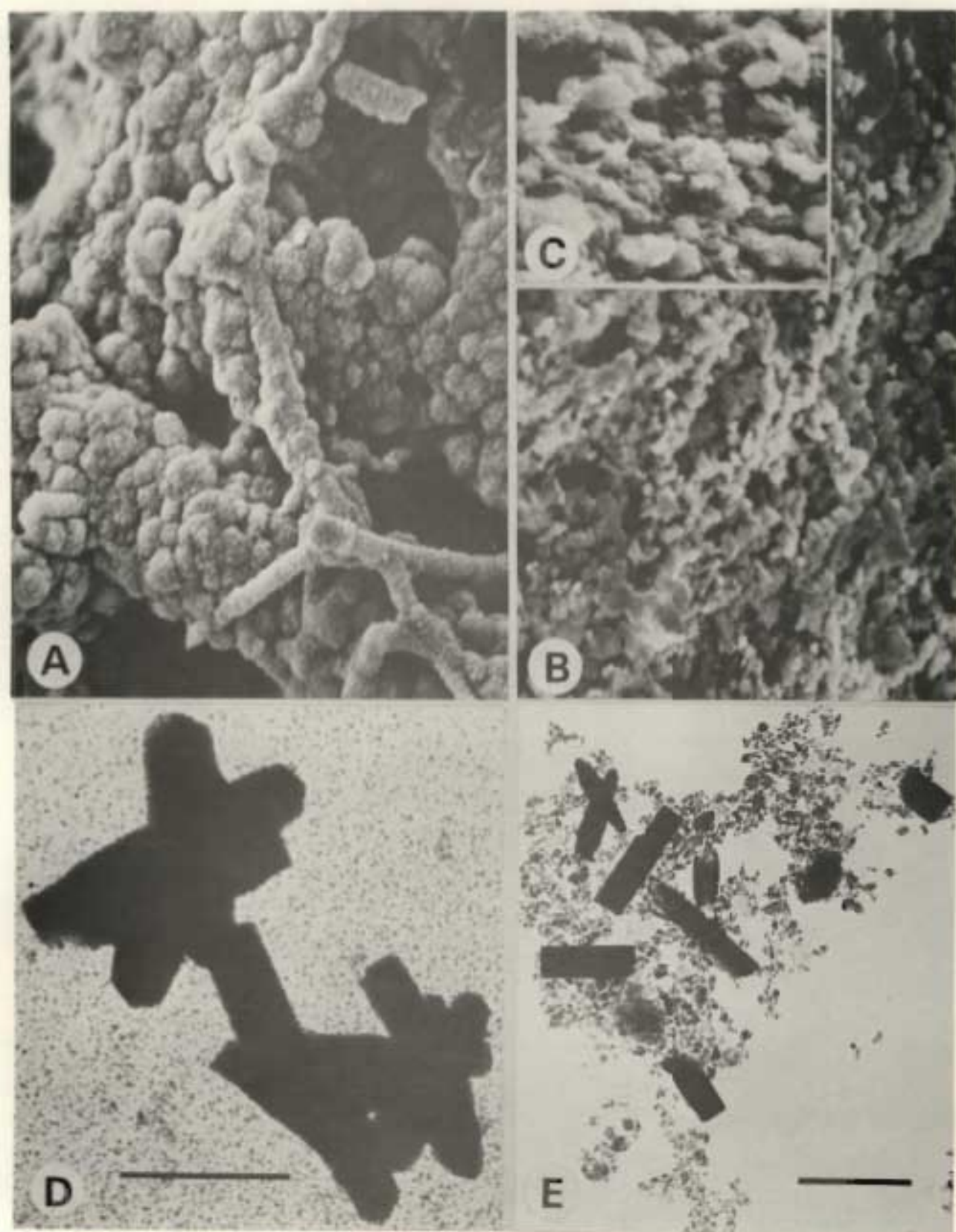
XRD: D = dominant; CD = co-dominant; SD = sub-dominant (15-30%); A = accessory (5-15%); T = trace (0-5%); - = not detected

<sup>6</sup> Determined from the linear relationship between the d(111) and d(130) spacings of goethite and diasporite (Fig. 1.2)

<sup>7</sup> Haematite interference







there is nevertheless a slight shift in all the measured d-spacings to higher angles (Figs. 1.2 and Table 1.1). The reason for the slight shift to lower d-spacings and the globular surface morphology is not evident, but it could be speculated that Ca and/or Mg carbonate may have played a role, possibly in the nucleation of goethite. Sample No. 262 was digested in 5 M HCl and gave the following composition (in percent): Fe = 46,8; Ti = 0,03; Ca = 0,05; Mg = 0,04; Mn = 0,47 and P = 0,33. Small amounts of these elements together with Si (not measured) could have been incorporated into the goethite structure explaining this unexpected d-spacing shift in the absence of Al.

Comparing the globular morphology shown by Eswaran (1971) (his Fig. 1 c) and Eswaran and De Coninck (1971) (their Figs. 10 a & b) with the similar morphology of goethite (confirmed by XRD) shown in Plates 1.1 and 1.2, it seems possible that they were viewing goethite and not "amorphous Fe" as suggested. Furthermore, it is noteworthy that Norrish (1975) shows an SEM of a soil goethite grain (his Fig. 4) with very similar globular morphology.

Transmission electron micrographs of the  $< 2 \mu\text{m}$  fraction from sample No. 262 reveals considerable variation of goethite crystal shapes and sizes (Plate 1.2 D & E) and confirms the relatively low WHH values given in Table 1.1. There is a close similarity between these large twinned and acicular (some broken fragments) goethite crystals shown in Plate 1.2 D & E respectively and aged synthetic goethites prepared at high pH (Atkinson, Posner and Quirk 1968; Cornell, Posner and Quirk, 1974; see also Appendix 2).

The low  $\text{Fe}_\text{O}/\text{Fe}_\text{HCl}$  ratios for a few representative samples also indicate that the iron oxides are crystalline (Table 1.1). XRD confirmed that goethite is the only iron oxide present, except in the ferruginous ammonite sample (No. 186) which contained some haematite (Table 1.1). In synthetic laboratory experiments, Schellmann (1959) concluded that adsorption of Ca and Mg ions on a freshly precipitated iron gel directs aging to haematite. Thus except for sample No. 186 the main possible mechanism for goethite formation is via siderite ( $\text{FeCO}_3$ ). The low degree of Al-substitution in the goethite structure (Table 1.1) also suggests a relatively "Al-free" environment.



#### 1.4.2 Geodes

Most of the geodes or "ironstone nodules" occur at various depths in layers (e.g. stonelines) within the soil mantle. In the literature (e.g. King, 1970) these are often considered to be erosional remnants of ferruginous horizons of former more extensive "lateritic" or highly weathered materials.

These geodes average 2 - 10 cm in diameter and are generally spherical to ellipsoidal in shape. When broken in half they are seen to consist of a hard, surface rind or crust of goethite (and/or haematite) 1 - 10 mm thick and may have either a hollow centre with inward pointing iron oxide grains or crystals (Nos. 19, 170 and 213) or a solid core of iron pyrites (FeS) (No. 177, see Plate 1.3 Ba).

King (1953 and 1970) considers the rounded ferruginous gravel layer with several pyritized nodules (Plate 1.3 B) between middle to late Cretaceous and fossiliferous Miocene beds at Uloa to be erosional remnants of ferruginous profiles from the Early Cainozoic surface. Similar relict layers of ironstone nodules or geodes with cores of pyrite crystals surrounded by hard rinds of goethite and haematite occur in deeply weathered soils derived from Middle Beaufort sandstone in the Drakensberg Highlands of Natal. The pyrite in these nodules is considered to be inherited (i.e. geological) and possibly formed by early marine diagenetic bacterial reduction. The progressive replacement of FeS with goethite and formation of the surface rinds is associated with soil development. Thus these geodes provide evidence not only of current soil conditions but also of past processes.

Optical, electron-optical and XRD observations on hand-picked iron oxide grains from the hollow centres of geode samples (Nos. 213 and 19, see Chapter 4) show highly crystalline lepidocrocite crystals with cubic morphology. This type of "macro-crystal" morphology strongly indicates that FeS has been completely pseudomorphed and suggests that these geodes could have formed from FeS weathering.

The geode subsamples are composed dominantly of quartz and very crystalline goethite (Table 1.2) which acts as a strong cementing agent. In most of the samples there is only a very slight shift in the (111)

1.2 Sample location, description, and chemical and mineralogical composition of goode samples (geo)

Sample No. (1.1)	Soil zone (Fig. 1)	Locality	Subsample description	Munsell colour (powder)	Chemical composition <sup>a</sup>				Mineralogy <sup>b</sup>				d (110)		d (120)			d (131)		
					Fe HCl %	Fe <sub>2</sub> O <sub>3</sub> %	Fe <sub>2</sub> O <sub>3</sub> Fe HCl	Go	Qz	FeS	He	Le	X	Wt% (°2θ)	X	mole % AlO <sub>2</sub> H <sup>+</sup>	Wt% (°2θ)	X	mole % AlO <sub>2</sub> H <sup>+</sup>	Wt% (°2θ)
72a	19	Ulos <sup>1</sup>	Surrounding hard brown layer (Pl. 1.3 Bb)	5 YR 4/6	47.1	0.12	0.003	D	A	-	-	T	4,190	0.19	2,705 <sup>5</sup>	-4.1 <sup>5</sup>	0.26	2,453	-0.7	0.30
		Ulos	FeS rich core (Pl. 1.3 Ba)	10 YR 4/4	-	-	-	SD	A	D	-	T	4,190	0.11	2,688 <sup>5</sup>	0.7 <sup>5</sup>	0.21	2,451	0.7	0.15
19	6	Ernele (in saprolite)	Yellow zone on surface of weathered fragment (Pl. 4.3 D)	10 YR 4/4- 7.5 YR 4/4	50.3	0.18	0.004	D	-	-	T	-	4,180	0.11	2,692	4.8	0.21	2,451	0.7	0.21
70a	2	Glengarry (in stoneline)	Hollow geode, outer hard crust	10 YR 5/6	43.2	0.13	0.003	D	A	-	-	-	4,185	0.23	2,693	4.1	0.33	2,451	0.7	0.32
b			Hollow geode, protruding tubes	10 YR 5/8	46.1	0.12	0.003	D	A	-	-	-	4,185	0.34	2,691	5.5	0.36	2,451	0.7	0.38
13b	6	Dollstroom (in stoneline)	Crust cementing large cubic lepidocrocite rich crystals (Pl. 4.3 C)	10 YR 5/8- 7.5 YR 5/8	42.5	0.20	0.005	D	A	-	-	T	4,180	0.16	2,696	2.1	0.21	2,451	0.7	0.21

King (1953; 1970)

<sup>a</sup>Fe HCl and Fe<sub>2</sub>O<sub>3</sub> as in Table 1.1

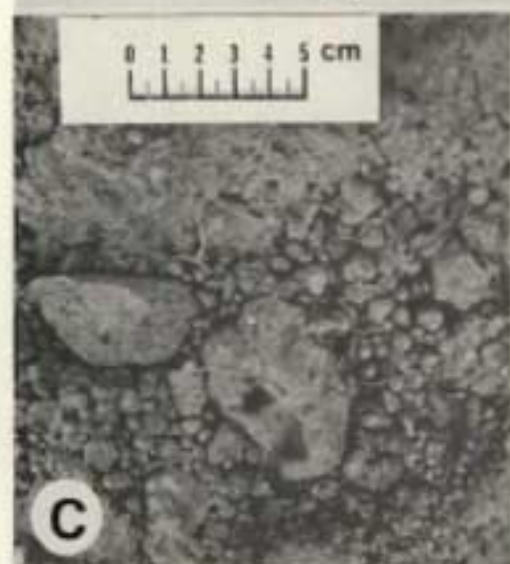
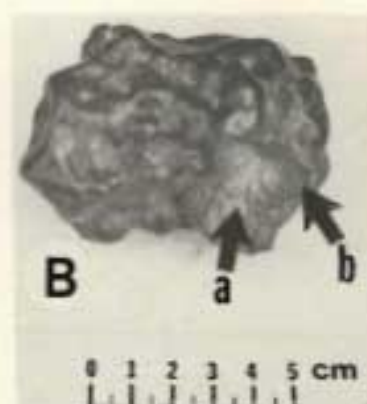
<sup>b</sup>D = Go, Qz and He as for Table 1.1; FeS = iron pyrites; Le = lepidocrocite.

SD, A, T and -, as for Table 1.1

for Table 1.1

ematite interference





goethite spacing, representing only 0,7 mole % AlOOH. Correspondingly there is small variation in the (110) spacings. However, the increase in the (111) and (130) spacings (i.e. negative AlOOH values) for sample No. 177a could be due to substitution of  $\text{Fe}^{2+}$  for  $\text{Fe}^{3+}$  in the goethite structure. The larger variation in the (130) spacings is not understood.

XRD line broadening (small WHH values; Table 1.2) suggest that the goethite is very crystalline. This is supported by the low  $\text{Fe}_\text{O}/\text{Fe}_\text{HCl}$  ratios (Table 1.2). These results strongly suggest that goethite formed from FeS weathering or in an FeS environment is relatively pure (i.e. Al-free) and crystalline.

#### 1.4.3 Ferricretes\*

The distribution and geographic relationships of ferricrete along the coastal region of Natal has been studied by Maud (1965;1968 a,b) and, Frankel and Bayliss (1966). Apart from this, reference is made by MacVicar (1962) de Villiers (1965), King (1967), and Loxton and van Straten (1973) when considering erosional surfaces or soil distribution patterns. However, little is known about the chemistry and mineralogy of these ferricretes and their "inland" distribution.

Using information collected by the writer\*\* and all other available information (Maud, 1965; 1968 a,b; van der Eyk, MacVicar and de Villiers, 1969) a map showing the distribution and density of occurrence of ferricrete was compiled first on working plans of various scales, then collated and drawn at a scale of 1:1 million\*\*\* (see Fig. 1.1, which has been reduced from a scale of 1:1 million). As indicated in Fig. 1.1 ferricrete occurs over widely scattered areas through a considerable soil (Fig. 1) and climatic range.

A feature of this area is not only the widespread occurrence of ferricrete but also its great variety i.e. vesicular, cellular, pisolitic, nodular, "snuffbox" patterned and platy (stoneline fragment) forms. This variety can be explained in terms of several factors, such as, derivation

---

\* Strongly indurated material containing predominantly Fe and varying amounts of Al and Si, together with widely varying amounts of included sand and rock fragments (i.e. ferriferous duricrust or hard plinthite)

\*\* During land type surveys

\*\*\* see map in back cover folder



from a variety of rock types (i.e. diabase, dolerite, sandstone, shale, granite and aeolianite), occurrence on various erosional surfaces (ranging from Recent to Early Cainozoic) and topographic positions (plateaux, valley sides, footslopes and valley bottom). Furthermore, they may either be exposed (e.g. outcrop) or found associated within a wide variety of soils (ranging from poorly to freely drained, and within various layers of coastal dune soils). The selected samples are reasonably representative of the range of types of ferricrete and soil in which they frequently occur (Table 1.3; Plates 1.3 - 1.7).

The topographic position combined with soil pattern (Fig. 1) may explain to some extent the distribution (Fig. 1.1) and some of the variability in the various morphological types of ferricrete. Its absence on the high Drakensberg in the Afro-alpine zone (see Fig. 2 and Fig. 1 soil zone 1), suggests that temperate environmental conditions do not favour ferricrete formation. Furthermore, in view of evidence of buried fossil permafrost horizons (Fitzpatrick, 1978; see also Appendix 1) it is likely that this area has suffered a temperate climate for a considerable period of time (i.e. since the Pleistocene and possibly even late Tertiary). It would appear therefore, that ferricrete only occurs in areas varying from a little above sea level to 2 280 m (7 500 ft), in a climate ranging from humid to arid, decreasing at progressively higher elevations. The latter phenomena may be due to lack of intensive weathering and/or an adequately "dry" season, which is apparently necessary for ferricrete formation. Furthermore, in soil zone 2 (Fig. 1) adjacent to the Afro-alpine zone (soil zone 1) only fragments of vesicular and platy ferricrete (i.e. remnants) occur in stonelines of deeply weathered soils (see Plate 1.7 A).

Most ferricrete areas shown in Fig. 1.1 have soil above the ferricrete, and generally the soils are genetically associated with specific types of ferricrete. For example, freely drained humic soils on the Table Mountain sediments Early Tertiary plateaux (soil zones 3 and 14; Fig. 1) are associated with reddish-brown vesicular ferricrete (Plate 1.6 A). According to Maud (1965) these sesquioxidic soils (e.g. Inanda soil) are derived by re-weathering of this ferricrete. However, MacVicar (1978) claims that there is no reason why the Table Mountain sediments should not give rise to these soils.

Where ferricrete occurs in bottomland positions in soil zones 7 and 8



Table 1.3 Sample location, description, and chemical and mineralogical composition of ferricretes (hp)

Subsample No. Fig. 1.1)	Soil zone (Fig. 1)	Locality	Soil series (depth cm)	Type and subsample description <sup>1</sup>	Munsell colour (powder)	Chemical composition <sup>2</sup>				Mineralogy <sup>3</sup>					d (110)		d (130)			d (111)		
						Fe <sub>d</sub> (Mnd) %	Fe <sub>HCl</sub> %	Fe <sub>o</sub> %	Fe <sub>o</sub> / Fe <sub>HCl</sub>	Ga	Qz	He	An	Gl Ka	X	W <sub>SH</sub> (°2θ)	X	mole % AlO <sub>3</sub> H <sub>2</sub> <sup>4</sup>	W <sub>SH</sub> (°2θ)	X	mole % AlO <sub>3</sub> H <sub>2</sub> <sup>4</sup>	W <sub>SH</sub> (°2θ)
206a	4	Steelpoort (plateau)	Outcrop	Pis. & vis., shiny hard con- cretions & brown matrix (Pl. 1.3 C)	10 YR 5/6	24,6 (0,11)	33,8	0,10	0,003	D	A	-	-	-	4,175	0,34	2,684	10,3	0,46	2,440	8,7	0,48
29	5	Steelpoort (valley side)	Glencoe (95-180)	Ves., hard brown parts (Pl. 1.3 E)	10 YR 5/8	22,5 (tr.)	31,5	0,23	0,007	D	SD	-	-	-	4,185	0,36	2,690	6,2	0,46	2,447	3,6	0,51
30	5	Steelpoort (valley side)	Glencoe (95-180)	Ves., soft, yellow parts (Pl. 1.3 E)	10 YR 6/8	30,0 (0,03)	29,7	0,11	0,004	D	SD	-	-	-	4,185	0,39	2,693	4,1	0,41	2,446	4,4	0,40
48	5	Steelpoort (valley side)	Glencoe (80-150)	Ves., very hard dark brown	10 YR 5/8	21,1 (tr.)	27,9	0,38	0,014	D	SD	-	-	-	4,183	0,40	2,686	8,9	0,32	2,442	7,3	0,36
195b	4	Piet Retief (crest)	Outcrop	Ves., hard yellow zones (Pl. 1.3 D)	10 YR 6/8	15,8 (tr.)	21,2	0,14	0,007	CD <sup>7</sup>	CD	-	-	-	4,177	0,36	2,684	10,3	0,56	2,438	10,2	0,56
35	7	Dirkiesdorp (valley bottom)	Washbank (35-60)	Pis., matrix and en (Pl. 1.3 F)	7,5 YR 5/6	15,4 (0,22)	18,6	0,21	0,011	D	CD	-	T	-	4,172	0,38	2,684	10,3	0,73	2,437	10,9	0,54
32a	7	Dirkiesdorp (crest)	Appam (70-180)	Mod., brown parts & rinda	10 YR 5/6	16,8 (0,47)	31,4	0,22	0,007	D	SD	-	-	-	4,178	0,66	2,686	8,9	0,83	2,445	5,1	0,76
b	7	Dirkiesdorp (crest)	Appam (70-180)	Mod., yellow parts	7,5 YR 5/8	16,0	20,2	0,12	0,006	D	SD	-	-	-	4,177	0,51	2,686	8,9	0,81	2,440	8,7	0,76
205a	2	Belfast (plateau)	Klipfontein (10-30)	Ves., brown parts (Pl. 1.4 B)	10 YR 5/8- 7,5 YR 5/6	17,3	25,6	0,13	0,005	D	SD	-	T	-	4,164	0,51	2,676	15,7	0,56	2,433	13,8	0,56
b	2	Belfast (plateau)	Klipfontein (35-90)	Ves., yellow-brown parts & crusts (Pl. 1.4 C)	10 YR 5/8	14,5	18,9	0,26	0,014	D	CD	-	T	-	4,180	0,55	2,686	7,5	0,71	2,448 <sup>5</sup>	2,9 <sup>5</sup>	0,53
250a	8	Newcastle/ Utrecht (crest)	Outcrop (0-40)	Ves., (Pl. 1.5 A, B)	10 YR 5/8	22,6	32,8	0,11	0,003	D	SD	-	T	-	4,177	0,34	2,686	8,9	0,43	2,443	6,6	0,36
181a	14	Cibini (plateau)	Nonanci (95-160)	Ves., soft yellow parts (Pl. 1.6 A)	10 YR 7/8	27,2	31,4	0,12	0,004	D	A	T	T	A	4,175	0,41	2,684	10,3	0,43	2,441	8,0	0,36
b	14	Cibini (plateau)	Nonanci (95-160)	Ves., hard brown parts (Pl. 1.6 A)	10 YR 5/8	28,1	37,2	0,14	0,004	D	A	T	T	T	4,180	0,21	2,688	7,5	0,31	2,444	5,8	0,29
c	14	Cibini (plateau)	Nonanci (95-160)	Ves., reddish-brown parts (Pl. 1.6 A)	2,5 YR 5/8	24,5	33,5	0,12	0,004	SD	SD	SD	T	SD	4,152	0,26	n.m. <sup>5</sup>	n.m. <sup>5</sup>	n.m. <sup>5</sup>	2,427	18,2	-0,41
72	8	Omzinkulu/ Franklin (midslope)	Farningham (90-100)	Angular, plate like frag- ments in sl (Pl. 1.7 A)	10 YR 5/8	21,7 (tr.)	35,4	0,18	0,005	D	T	T	T	-	4,190	0,23	2,695	2,7	0,25	2,451	0,7	0,35
171a	4	Albert Falls (crest)	Klipfontein (30-120)	"Snuffbox", hard brown rim (Pl. 1.7 B a)	2,5 YR 4/6	28,2	38,6	0,15	0,004	CD	T	CD	-	-	4,175	0,11	n.m. <sup>5</sup>	n.m. <sup>5</sup>	n.m. <sup>5</sup>	2,446	4,4	0,17
c	4	Albert Falls (crest)	Klipfontein (30-120)	"Snuffbox", soft, yellow interior (Pl. 1.7 B c)	7,5 YR 6/6-6/8	26,3	36,4	0,14	0,004	CD	CD	-	-	T	4,177	0,15	2,688	7,5	0,21	2,445	5,1	0,22
43	4	Highflats (crest)	Farningham (60-90)	Ves., dark brown parts	7,5 YR 5/6- 10 YR 5/6	19,2 (0,09)	38,4	0,19	0,005	D	SD	T	T	A	4,152	0,39	2,693	4,1	0,41	2,446	4,4	0,40
25	2	Howick/Loskop (midslope)	Farningham (120-180)	Pis., brown parts	7,5 YR 5/6	27,8 (0,58)	31,8	0,31	0,010	D	SD	T	T	-	4,177	0,56	2,688	7,5	0,71	2,442	7,3	0,51
24	4	Overvaal (midslope)	Farningham (80-120)	Pis., dark brown parts	7,5 YR 4/4	15,3 (1,1)	21,7	0,72	0,033	CD	CD	-	T	T	4,177	0,71	2,692	4,8	0,91	2,440	8,7	0,76
178	4	Cleland (crest)	Appam (75-95)	Ves., dark brown parts	7,5 YR 4/4	16,7 (1,4)	22,3	0,74	0,033	CD	CD	-	T	-	4,172	0,56	2,684	10,3	0,81	2,440	8,7	0,60
67	4	Ixopo (midslope)	Kroonstad	Massive, hard, purple fragments in stoneline	7,5 YR 4/4	23,6 (3,3)	36,6	0,27	0,007	D	A	T	T	-	4,169	0,76	2,697	1,4	0,51	2,453	-0,7	0,74
68	3	Port Edward (plateau)	Outcrop	Ves., hard, red parts	2,5 YR 4/8	23,2 (0,01)	34,7	0,13	0,004	D	A	A	T	-	4,172	0,23	n.m. <sup>5</sup>	n.m. <sup>5</sup>	n.m. <sup>5</sup>	2,442	7,3	0,31



Sample No. (g. 1.1)	Soil zone (Fig. 1)	Locality	Soil series (depth cm)	Type and subsample description <sup>1</sup>	Munsell colour (powder)	Chemical composition <sup>2</sup>				Mineralogy <sup>3</sup>					d (110)		d (130)			d (111)		
						Fe <sub>d</sub> (%)	FeHCl (%)	Fe <sub>0</sub> (%)	Fe <sub>2</sub> (%)	Go	Qz	He	An	Gl + Ka	$\bar{X}$	YHH (°20)	$\bar{X}$	mole % AlOON <sup>4</sup>	YHH (°20)	$\bar{X}$	mole % AlOON <sup>4</sup>	YHH (°20)
70	3	Fort Edward (plateau)	Outcrop	Ves., hard, maroon parts	7.5 YR 5/6- 10 YR 5/6	17.0 (0.11)	47.9	0.13	0.003	D A T T -					4.183	0.12	2.694	3.4	0.21	2.431	0.7	0.20
71	3	Fort Edward (crest, coastal)	Outcrop	Ves.- pis., brown matrix	5 YR 5/8	21.0 (tr.)	25.7	0.57	0.022	D A A T -					4.164	0.37	n.m. <sup>5</sup>	n.m. <sup>5</sup>	n.m. <sup>5</sup>	2.435	12.4	0.93
73	14	Highflats (crest)	Appan (40-60)	Pis., Mn-rich cn, hard brown parts	7.5 YR 5/6	23.2 (0.45)	31.3	0.41	0.013	D A T T T					4.193	0.71	2.698	0.7	1.03	2.449	2.2	~0.86
41a	19	Umhlali (midslope)	Glansthal (90-120)	Ves. to massive, purple red layer	10 YR 4/4	12.5 (4.3)	18.0	0.53	0.029	SD D T T T					4.177	0.46	2.698	0.7	0.75	n.m. <sup>6</sup>	n.m. <sup>6</sup>	n.m. <sup>6</sup>
31a	19	Umvalumi (crest)	Glansthal (60-85)	Ves. to massive, hard parts	7.5 YR 5/8	15.3 (tr.)	30.9	0.12	0.004	D A - T -					4.180	0.48	2.698	0.7	0.48	2.448	2.9	0.46
b	19	Umvalumi (crest)	Glansthal (60-85)	Ves. to massive, red surface layer	7.5 YR 5/8	26.7 (0.09)	33.3	0.23	0.007	D A T T -					4.185	0.46	2.692 <sup>5</sup>	4.6 <sup>5</sup>	0.48 <sup>5</sup>	2.448	2.9	0.46
175	19	Fairbreeze (midslope)	Glansthal (85-100)	Ves., red parts	2.5 YR 4/8	n.d.	n.d.	n.d.	n.d.	D CD A T -					4.169	0.18	n.m. <sup>5</sup>	n.m. <sup>5</sup>	n.m. <sup>5</sup>	2.436	11.6	0.41
243a	8	Swartberg (crest)	Hutton (120-180)	Pis., brown-red matrix	5 YR 5/8	n.d.	n.d.	n.d.	n.d.	D SD T - -					4.175	0.36	2.675 <sup>5</sup>	16.4 <sup>5</sup>	0.66 <sup>5</sup>	2.442	7.3	0.41
b	8	Swartberg (crest)	Hutton (120-180)	Pis., rind of Mn-rich cn	10 YR 5/8	n.d.	n.d.	n.d.	n.d.	D SD - - -					4.170	0.43	2.684	10.3	0.56	2.439	9.5	0.54
c	8	Swartberg (crest)	Hutton (120-180)	Pis., core of Mn-rich cn	10 YR 5/4	n.d.	n.d.	n.d.	n.d.	SD SD - - -					4.165	0.67	2.682	11.6	0.71	2.436	11.6	0.61
154a	14	Tala (bottom land)	Wasbank (35-130)	Pis., hard brown nodules	5 YR 6/8	n.d.	n.d.	n.d.	n.d.	D SD T - -					4.175	0.33	2.687	8.2	0.41	2.442	7.3	0.31
b	14	Tala (bottom land)	Wasbank (35-130)	Pis., matrix and cn	7.5 YR 5/8	n.d.	n.d.	n.d.	n.d.	D SD - - -					4.178	0.42	2.688	7.5	0.54	2.443	6.6	0.46
57a	7	Rosedale (footslope)	Wasbank (68-95)	Pis., hard, brown matrix & Mn-rich cn	10 YR 5/6-6/6	n.d.	n.d.	n.d.	n.d.	CD CD - - -					4.174	0.48	2.686	8.9	0.86	2.436	11.6	0.66
b		Rosedale (footslope)	Wasbank (68-95)	Pis., soft, yellow matrix	10 YR 6/8	n.d.	n.d.	n.d.	n.d.	CD CD - - -					4.169	0.36	2.678	14.4	0.91	2.435	12.4	0.53
59a	7	Midmar (footslope)	Appan (75-180)	Pis.- ves., hard, yellow- brown parts	10 YR 5/6	n.d.	n.d.	n.d.	n.d.	CD CD - - -					4.175	0.36	2.682	11.6	0.48	2.440	8.7	0.48
59b		Midmar (footslope)	Appan (75-180)	Pis.- ves., soft matrix plus Mn-rich cn	10 YR 5/4-5/6	n.d.	n.d.	n.d.	n.d.	CD CD - - -					4.169	0.51	2.682	11.6	0.78	2.439	9.5	0.66
61	2	Naudes Nek (crest)	Outcrop	Ves., dark brown parts	10 YR 5/8	n.d.	n.d.	n.d.	n.d.	CD CD T T -					4.176	0.58	2.682 <sup>5</sup>	11.6 <sup>5</sup>	0.67 <sup>5</sup>	2.442 <sup>5</sup>	7.3	0.67
62	4	Bopuvel (crest)	Klipfontein (20-180)	Ves. to pis., hard brown parts	10 YR 5/8	n.d.	n.d.	n.d.	n.d.	D A - - -					4.177	0.51	2.685	9.6	0.65	2.441	8.0	0.56
70	4	Bar Lee	Outcrop	Ves., hard, dark brown parts	10 YR 5/8	n.d.	n.d.	n.d.	n.d.	D A T - -					4.180	0.36	2.688 <sup>5</sup>	8.9 <sup>5</sup>	0.70 <sup>5</sup>	2.445	5.1	0.61
16a	2	MacKenzie (footslope)	Wasbank (35-85)	Pis., hard reddish-brown parts	5 YR 5/8	n.d.	n.d.	n.d.	n.d.	CD CD T T -					4.169	0.56	2.682	11.6	0.60	2.433	13.8	0.56
b	2	MacKenzie (footslope)	Wasbank (35-85)	Pis., hard brown-black Mn- rich parts	7.5 YR 5/6- 10 YR 5/6	n.d.	n.d.	n.d.	n.d.	CD CD T T -					4.172	0.56	2.685 <sup>5</sup>	9.6 <sup>5</sup>	0.86 <sup>5</sup>	2.432	14.5	0.66
4a	2	Hella-Hella (plateau)	Farningham (160-220)	Pis., - ves., hard, yellow- brown parts	10 YR 5/8	n.d.	n.d.	n.d.	n.d.	D SD - - -					4.174	0.51	2.684	10.3	0.51	2.440	8.7	0.55
b	2	Hella-Hella (plateau)	Farningham (160-220)	Pis. - ves., soft, yellow parts	10 YR 6/8	n.d.	n.d.	n.d.	n.d.	D SD - - -					4.175	0.46	2.684	10.3	0.61	2.441	8.0	0.61
9a	2	Dullstroom (plateau)	Outcrop	Ves., hard brown parts	10 YR 5/8	n.d.	n.d.	n.d.	n.d.	D SD - T -					4.177	0.46	2.687	8.2	0.61	2.445	5.1	0.57

1.3 (contd.)

Sample No. (Fig. 1)	Soil zone	Locality	Soil series (depth cm)	Type and subsample description <sup>1</sup>	Munsell colour (powder)	Chemical composition <sup>2</sup>				Mineralogy <sup>3</sup>				d (110)		d (130)			d (111)				
						Fe <sub>d</sub>	Fe <sub>HCl</sub>	Fe <sub>o</sub>	Fe <sub>o</sub> / Fe <sub>HCl</sub>	Co	Qz	He	An	Gl +	Ka	$\bar{x}$	WHH (°2 $\theta$ )	$\bar{x}$	% AlOCH <sup>4</sup>	WHH (°2 $\theta$ )	$\bar{x}$	% AlOCH <sup>4</sup>	WHH (°2 $\theta$ )
						g/g	g/g	g/g															
12	7	Estcourt	Washbank (60-80)	Pis., soft matrix & hard round cn	10 YR 5/8	n.d.	n.d.	n.d.	n.d.	D	SD	-	T	-	4,177	0,47	2,685	9,6	0,80	2,442	7,3	0,56	
14	8	Sundays River (plateau)	Outcrop	Ves., hard brown parts	10 YR 6/6	n.d.	n.d.	n.d.	n.d.	CD	CD	-	T	-	4,174	0,28	2,683	11,0	0,36	2,440	8,7	0,34	
14a	2	Wess (crest)	Farningham (95-120)	Frag. in sl., soft yellow- brown part	10 YR 5/8	n.d.	n.d.	n.d.	n.d.	D	A	-	T	-	4,169	0,44	2,683	11,0	0,58	2,441	8,0	0,52	
14b	2	Wess (crest)	Farningham (95-120)	Frag. in sl., hard brown part	10 YR 5/6	n.d.	n.d.	n.d.	n.d.	L <sup>5</sup>	A	-	-	-	4,180	0,38	2,694	3,4	0,46	2,445	5,1	0,44	
19	3	Port Edward (plateau)	Outcrop (0-290)	Ves., purple-red zones	2,5 YR 5/6	n.d.	n.d.	n.d.	n.d.	CD	A	CD	T	T	4,175	0,21	n.m. <sup>5</sup>	n.m. <sup>5</sup>	n.m. <sup>5</sup>	2,442	7,3	0,37	

pis. = pisolitic; ves. = vesicular; nod. = nodular; cn = concretions; sl = stoneline; frag. = fragment

Fe<sub>d</sub>, Fe<sub>HCl</sub> and Fe<sub>o</sub> as Table 1.1; n.d. not determined

XRD: D, CD, SD, A, T and -; Co, Qz and He as Table 1.1; where An = anatase;

Gl = gibbsite and Ka = kaolinite

as Table 1.1

haematite interference; n.m. = not measurable

quartz interference

contains feldspar (A)

contains maghaemite (A)



(Fig. 1), i.e. drier areas in the valleys and central parts of the study area, the soil profiles usually contain predominantly Mn-rich pisolitic ferricrete underlying an E-horizon (Plate 1.3 F).

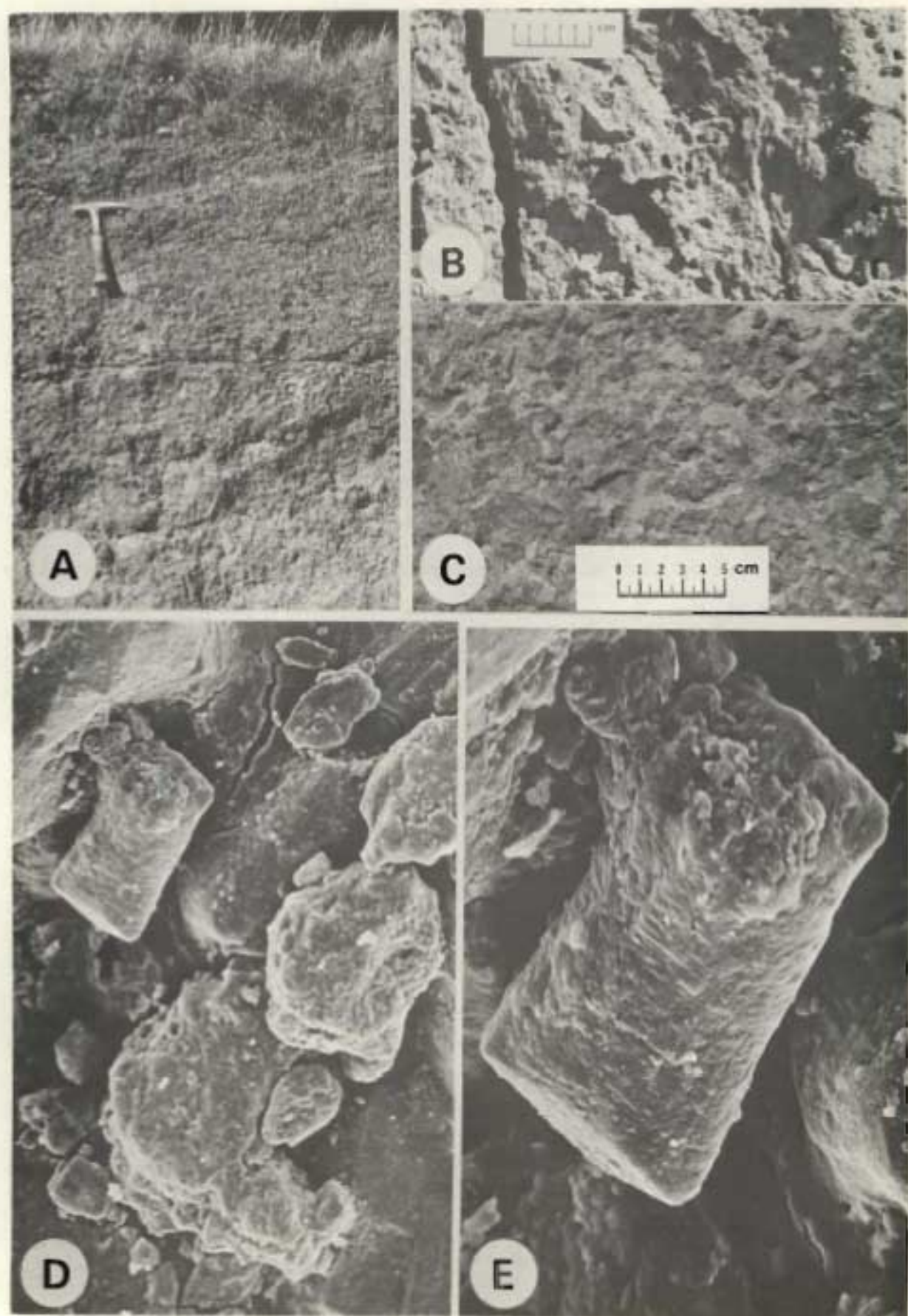
As shown in Fig. 1.1 the occurrence of ferricrete does not coincide with ferruginous bauxite. The lack of ferricrete in the "well drained" ferruginous bauxite landscapes is possibly due to both the absence of a seasonally oscillating ground water table and slow drainage conditions which are apparently necessary for ferricrete to form.

Although six "homogeneous" types of ferricretes have been recognized in the study area on the basis of their fabric, one type may contain inclusions of the other (e.g. Plate 1.3 C). However, the concretions incorporated in this predominantly vesicular ferricrete from the Steelpoort plateau (No. 206) are relatively lower in CBD extractable manganese than in the homogeneous pisolitic ferricretes (Table 1.3).

The pisolitic ferricretes examined are generally higher in Mn ( $Mn_d$ ; Table 1.3) because Mn is a mobile element under hydromorphic conditions and accumulates in depressions or along banks of rivers where these ferricretes are found. In general, these manganiferous samples (e.g. pisolitic ferricretes and Ixopo stoneline fragments) usually contain goethite as the only crystalline iron oxide (Table 1.3). In addition, these materials generally have higher X-ray line broadening than the other types of ferricretes [average WHH of (111) line is  $0,63$  against  $0,42^\circ 2\theta$  and average WHH of (110) line is  $0,51$  against  $0,36^\circ 2\theta$ ] suggesting that low crystallinity is related to high  $Mn_d$  contents. The presence of high amounts of Mn possibly interferes with the nucleation stage of goethite crystallization.

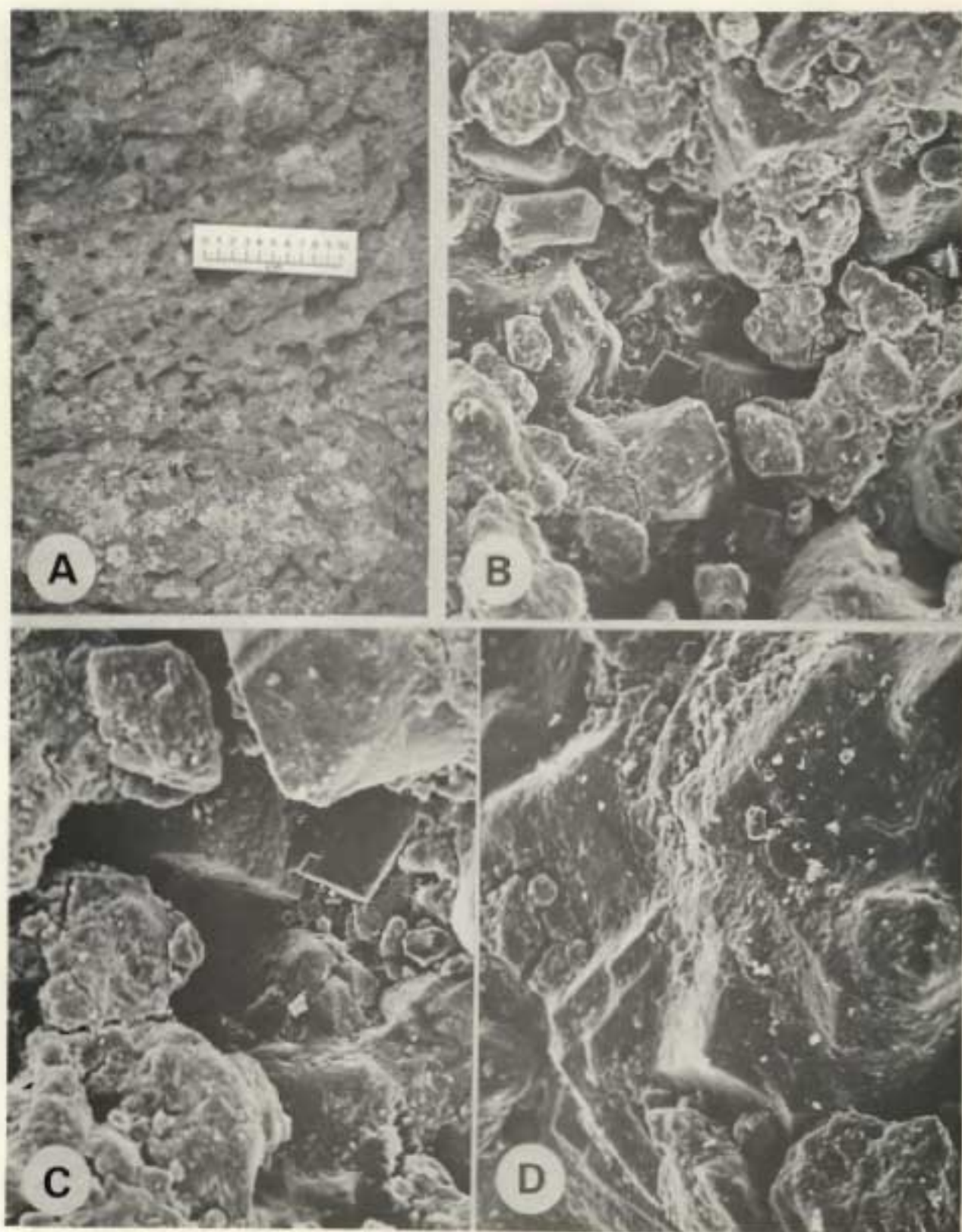
Vesicular ferricrete is best described as a brittle slag-like material. It varies considerably in colour (ranging from yellow-brown to maroon-red) and in the amount and sizes of the voids (Plates 1.3 to 1.6) and in fragments of rock (mainly quartz fragments) cemented together by iron oxides (Plate 1.3 C and D). There is little difference in goethite crystallinity (as shown by line broadening) and amounts of Al substituted in the goethite structure (Table 1.3) between the brown (29) and yellow (30) zones from the Steelpoort valley sample (Plate 1.3 E). However, in the Cibini sample (No. 181 a,b and c; Plate 1.6) higher amounts of Al are incorporated into the goethite structure in the reddish-brown parts (18,2 mole %  $AlOOH$ ) than in the yellow-brown parts (5,8 to 8,0 mole %  $AlOOH$ ). This demonstrates the complex nature of the













Cibini or Table Mountain sandstone derived ferricrete and that a wide range of Al-substitution can exist in close proximity. The high amount of Al-substitution suggests to some extent this material formed (partly) by weathering under relatively freely drained conditions (sections 1.4.7 and 1.4.8).

The distribution of trace elements (Ni, Co, and Ti) in CBD and HCl extracts for a selected range of various ferricretes was found to fluctuate widely. Both removal and enrichment of Co and Ni was found to occur. Generally in vesicular ferricretes Ni is enriched (especially in sample No. 161 derived from basalt with 1,1 % Ni and in the Cibini sample No. 181b derived mainly from Table Mountain sediments with 0,6 % Ni). The substitution of Ni for Fe in such goethites has been the subject of considerable speculation (Roorda and Queneau, 1973). In agreement with previous work (Fitzpatrick, 1974) Co is most abundant in pisolitic Mn-rich samples and ranges from 0,08 to 0,17 % (Sample No. 73). This Mn-Co association is in accordance with the data of Taylor and McKenzie (1966). In agreement with Frankel and Bayliss (1966) titanium is concentrated to some extent in both types of ferricretes. The average HCl extractable element content of the selected samples are:

Ferricretes	Fe	Mn	Co	Ni	Ti
	%	%	%	%	%
Vesicular-cellular (12 samples) ..	32,1	0,05	0,01	0,31	0,22
Pisolitic (8 samples) .. .. .	28,4	0,96	0,95	0,04	0,15

The deeper portion (35 - 90 cm) of the Belfast profile (No. 205) with reticulate yellow-brown veins and gleyed patches (Plate 1.4 A and C) contains relatively poorly crystalline goethite (according to WHH values) with lower Al-substitution (Table 1.3) than in the harder upper (10 - 30 cm) portion (Plate 1.4 A and B). This change in composition and crystallinity at varying depths is probably caused by formation under different hydrological and weathering regimes. The upper layer with better goethite crystallinity and higher Al-substitution possibly formed by *in situ* weathering and pseudomorphic alteration of primary ferromagnesian minerals (i.e. rapid removal of Si under well drained conditions) (see also section 1.4.7). Whereas in the poorly-drained lower zone the relatively lower

amount of Al-substitution is possibly due to mobilization of Fe under reducing conditions together with the solubilization of Al in the presence of organic matter under acid condition, followed by their separate precipitation and concentration as hydrated oxides under subsequent oxidizing conditions within this zone of oscillating groundwater.

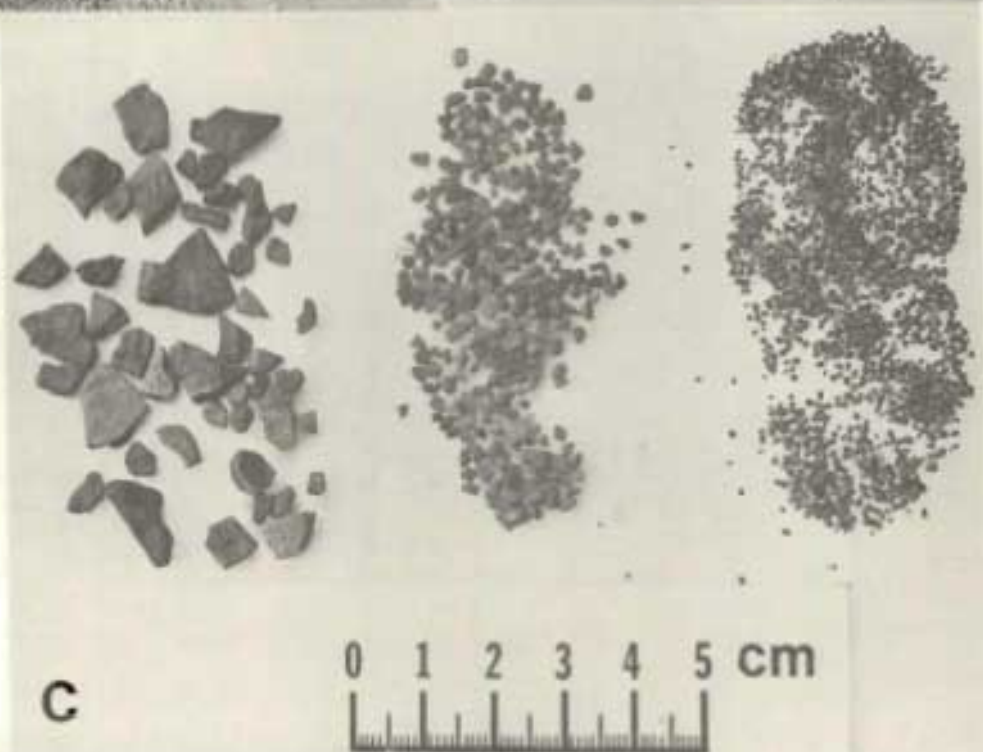
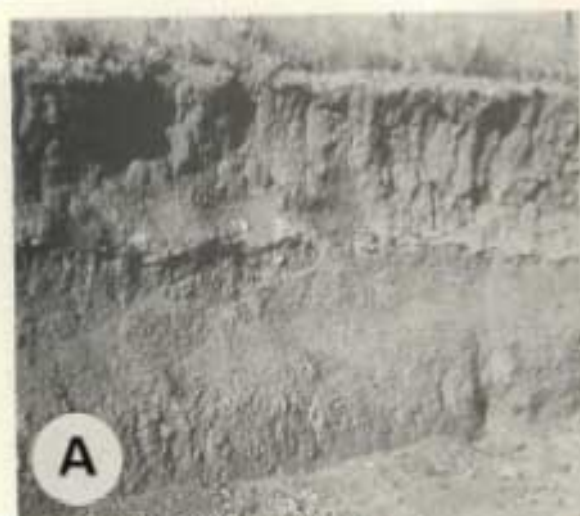
Clusters of euhedral and cubic-like quartz crystals (possibly cristobalite) are observed by SEM in voids of ferricrete from the upper part of the Newcastle profile (Plate 1.5 C and D). These particles are strongly cemented together and are coated by crystalline Al-goethite (Plate 1.5 E; Table 1.3). Similar groups of euhedral quartz crystals were observed by Kühnel *et al.* (1975) by SEM in a "strongly silicified laterite" from Indonesia. However, they report a "quasi amorphous" goethite matrix whereas in the Newcastle ferricrete well crystalline aluminous goethite is observed by XRD (Table 1.3). Eswaran and De Coninck (1971) reported on a void lined with similar smooth cubic crystals (their Figs. 6 a and b) and suggested that these were cristobalite.

A few cubic and polyhedral quartz particles were also observed in the lower portion of a cavity in the Cibini sample (Plate 1.6 B and C) whereas no cubic particles were detected in the Belfast sample (Plate 1.4). According to Stephens (1971) the presence of secondary quartz or cristobalite can possibly be attributed to particular processes of evaporation and transpiration under suitable climate and topographic conditions which cause an increase in concentration of silica. It is possible that such climate conditions prevailed at the Newcastle site for cristobalite to form.

Closer examination under high magnification of large particles (Plates 1.4 E, 1.5 E and 1.6 D) shows successive coatings or overgrowths of goethite (particularly in Plate 1.4 E) with finer particles on them. The fine particles also appear to be goethite since in plane reflected light they were seen to dissolve in 5 M HCl. This data suggests that most of the goethite, which is present as a dense compact matrix and as linings of voids and pores in these ferricretes, forms on impregnation (e.g. addition of  $\text{Fe}^{2+}$  from outside, i.e. from slope seepage etc.) on a frame-like network of mainly quartz and kaolinite particles.

The hard, dense compact nature of these ferricretes is probably associated with alternate wetting and drying conditions (i.e. fluctuating





water table). Moisture is required largely for the mobilization of Fe and crystal rearrangement whereas a dehydration step possibly prevents large separate crystals from forming (e.g. as observed in pure aqueous synthetic systems, see Appendix 1) and promotes more compact and dense crystal growth. Desiccation of the sesquioxidic coprecipitates possibly accounts for the cracks or "fissures" clearly visible in Plates 1.4 D, 1.5 E and 1.6 D. Furthermore, incorporation of some Al (5 - 10 mole %  $\text{AlOOH}$ ) into goethite crystals allows smaller crystals to form which possibly also promotes dense crystal growth.

The two subsamples from the Albert Falls snuffbox ferricrete (Plate 1.7 B) have well-crystalline, almost pure (i.e. low Al-substituted) goethite (Table 1.3) and in this respect closely resemble the geode samples. The laminated pattern morphology is formed from leaching out of Si and subsequent concentration of iron (as goethite and haematite) in the lower Eccra shales (i.e. fossilized by Fe-impregnation). Low ridges of almost intact snuffbox ferricrete occurs along the margins of some dissected foothills in the Albert Falls valley. Furthermore, numerous soil types in this area have high amounts of broken fragments of this material either scattered throughout the profiles or in stonelines (similar to Plate 1.7 A) presumably derived by progressive truncation.

#### 1.4.4 Concretions

Concretions\* are generally considered to be an important feature in soils and for this reason it is common to record their presence in profile descriptions. Various types of concretions are frequently encountered in these soils, ranging in size, shape, colour and magnetism. In fact from the coast to the foot of the high Drakensberg the occurrence of concretions is more the rule than the exception (i.e. concretions are absent in the Afro-alpine tract; soil unit 1 in Fig. 1). Hence they are present in a wide range of soil types, including Vertisols, hydromorphic plinthic soils and freely drained acid soils (Table 1.4). Certain soils in the region have diagnostic horizons which contain concretions comprising as much as over 30 - 40 per cent of the soil volume. Apart from studies on the distribution and chemical composition of coastal concretions by Beater (1940)

---

\* The term "concretion" as it is used here does not necessarily imply concentric layering (similar to Taylor and Schwertmann, 1974 a and c)



Table 1.4 Sample location, description, and chemical and mineralogical composition of ferrous concretions (cm)

Sample no.	Soil zone	Locality	Soil series	Subsample description	Munsell colour (powder)	Chemical composition <sup>1</sup>				Mineralogy <sup>3</sup>				d (110)		d (130)			d (111)		
						Fe <sub>d</sub>	Fe <sub>HCl</sub>	Fe <sub>o</sub>	Fe <sub>o</sub>	Go	Qz	He	Mn	Σ	Wt% (°2θ)	Σ	mole % AlOON <sup>4</sup>	Wt% (°2θ)	Σ	mole % AlOON <sup>4</sup>	Wt% (°2θ)
						(Mn) %	%	%	Fe <sub>HCl</sub>												
39 a	4	Albert Falls	Hensburg (10-40)	>2mm fraction, hard, brown, angular (Pl. 1.7 C)	7.5 YR 5/8-10 YR 5/8	11.7 (0.6)	35.5	0.70	0.020	D	A	T	-	4.174	0.61	2.686	8.9	0.76	2.442	7.3	0.68
b	4	Albert Falls	Hensburg (10-40)	1-2mm fraction, hard, brown, angular (Pl. 1.7 C)	7.5 YR 5/8-10 YR 5/8	24.7 (0.3)	36.7	0.90	0.020	D	A	T	-	4.169	0.51	2.685	9.6	0.73	2.443	7.3	0.60
03 a	2	Richmond	Griffin (30-50)	>2mm fraction, non-magnetic, hard, yellow-brown, mainly round	7.5 YR 5/8	19.8 (tr.)	20.1	1.00	0.030	D	A	T	-	4.142	0.79	2.672 <sup>2</sup>	18.5 <sup>3</sup>	1.26 <sup>3</sup>	2.418	24.7	1.26
b	2	Richmond	Griffin (30-50)	1-2mm fraction, non-magnetic, hard, yellow-brown, mainly round	7.5 YR 5/8	22.0 (tr.)	25.5	0.83	0.033	D	A	T	-	4.147	0.81	2.686 <sup>2</sup>	8.9 <sup>3</sup>	0.86 <sup>3</sup>	2.421	22.5	1.16
c	2	Richmond	Griffin (50-60)	>2mm fraction, magnetic, hard, reddish-brown, round to angular in stoneline	5 YR 4/4	20.4 (0.07)	51.3	0.09	0.002	CD	T	T	CD	4.177	0.20	2.690	6.2	0.26	2.446	4.4	0.31
92	4	Ikepe	Clovelly (35-55)	Hand-picked, hard, discus shaped (~1cm diameter)	2.5 YR 4/6	n.d.	n.d.	n.d.	n.d.	CD	CD	A	-	4.178	0.25	n.m. <sup>2</sup>	n.m. <sup>2</sup>	n.m. <sup>2</sup>	2.445	5.1	0.31
72	11	Gingindlovu	Washbank (0 - 3)	Small, reddish-brown, round, shiny, hard magnetic (Pl. 2.2 A)	5 YR 5/6	22.1	26.8	0.71	0.026	CD	T	A	CD	4.174	0.28	n.m. <sup>2</sup>	n.m. <sup>2</sup>	n.m. <sup>2</sup>	2.440	8.7	0.43
67 <sup>1</sup>	19	St Lucia (Dead Tree Bay)	Fernwood (0 - 3)	Hand-picked, hard, smooth irregular shaped, brown non-magnetic (0.5-2cm diam.)	10 YR 8/8	n.d.	n.d.	n.d.	n.d.	D	SD	-	-	4.178	0.17	2.691	5.5	0.18	2.445	5.1	0.22
82	19	St Lucia (False Bay)	Fernwood (0 - 3)	Hand-picked, hard, smooth oval shaped, brown non-magnetic (0.5-1cm diam.)	10 YR 8/8	15.6	21.5	0.08	0.004	D	SD	-	-	4.178	0.17	2.688	7.5	0.21	2.445	5.1	0.21

Sample kindly taken by Miss P. Kaugh

<sup>1</sup>Fe<sub>d</sub>, Fe<sub>HCl</sub>, Fe<sub>o</sub> as in Table 1.1.; n.d. = not determined

<sup>2</sup>CD, SD, A, T and -; Co, Qz, and He as in Table 1.1; where Mn = maghemite

Table 1.1

maghemite interference; n.m. = not measurable

and Frankel and Bayliss (1966) little work has been done on the relevance and mineralogy of concretions along the eastern seaboard of South Africa. Representative samples were collected from typical areas of occurrence (Fig. 1.1) and are described briefly in Table 1.4.

Concretions from profiles overlying both pisolitic manganese ferricretes (i.e. Wasbank soil, No. 35 and Appam soil, No. 73) and vesicular ferricretes (i.e. Glencoe soil, No. 29) contain goethite and haematite with markedly similar X-ray line broadening and d-spacing (i.e. degree of isomorphous substitution of Al for Fe) to that of the underlying ferricretes. This can be attributed to their respective similar mode of formation and illustrates the genetic association between the soil and underlying ferricrete.

Most of the angular concretions in the Rensburg soil (Plate 1.7 C) are similar in hardness, density, organization (layering) and mineralogy (Table 1.4) to concretionary fragments from snuffbox ferricrete (Plate 1.7 B) layers which occur upslope from these soils. It is reasonable to conclude therefore that these angular concretions are weathered fragments of these snuffbox ferricrete layers which have been transported by erosion (colluviation) and become rounded, especially with decreasing particle size (Plate 1.7 C).

The colour (i.e. yellowish-red hues of crushed samples) and XRD data (Table 1.4) indicate that most concretions contain predominantly goethite in association with variable proportions of haematite, in non-magnetic, and maghaemite in magnetic concretions. Several types of concretions (e.g. magnetic, non-magnetic, round, angular, yellow-brown or red) may occur together in one horizon or profile. Extensive field observations (see Chapter 2) indicate that magnetic concretions are strongly associated with well drained soils in the Mist Belt regions, but not in the Afro-alpine tract (Fig. 2). Furthermore, plinthic or hydromorphic soil zones (see Fig. 1.) generally contain fewer red coloured concretions and larger amounts of yellow ones especially in the A1 and B21 horizons. Most varieties of concretions examined had a hard yellow-brown surface zone or covering of iron oxide of varying thickness. Higher proportions of goethite were identified in these surface zones (with haematite and maghaemite rich interiors), but in some concretions it was not possible to separate the coating because of the very thin yellow-brown surface coating. This indicates that the haematite- or maghaemite-rich cores are goethite impreg-



nated or "goethitized" and are coated remnants of previous weathering.

Except for the round yellow-brown > 2 mm and 1 - 2 mm concretions from the freely drained Griffin profile (No. 103 a and b respectively), which contain goethite with over 20 mole %  $\text{AlOOH}$ , generally in most other soil concretions the degree of Al-substitution of goethite resembles that of ferricrete (see Tables 1.4 and 1.3) suggesting similar mode of formation. It is submitted that these hard non-magnetic yellow-brown concretions in the Griffin profile are probably formed by partial impregnation of iron (i.e. resistant coating of goethite) on ferruginous bauxite, saprolite or soil, since these latter materials contain goethite with a high degree of Al-substitution (see sections 1.4.7 to 1.4.9). In contrast, goethite in the strongly magnetic (maghaemite-rich) concretions (see Chapter 2) from the same Griffin profile and horizon are seen to have a much lower degree of isomorphous substitution of Al for Fe (Table 1.4), due to a different mode of formation, possibly by oxidation of a "Fe (II) - Fe (II) system" (Taylor and Schwertmann, 1974 b).

#### 1.4.5 Crusts

Thin ferruginous crusts are widespread (Fig. 1.1) and can be divided into roughly four types according to their accessory material as follows: (i) crusts on saprolites (see Plate 1.7 D); (ii) crusts formed in weathering limestone (e.g. Plate 1.7 E); (iii) crusts on the surface of maghaemite/magnetite bands (see Plate 2.1 A); and (iv) crusts adjacent to lepidocrocite-rich bands (Plate 4.3 A). Representative samples of each type are described briefly in Table 1.5.

In general, the soft to friable ferruginous crusts are considered to some extent to be more recently precipitated iron oxide (i.e. precursor) than in related harder older ferricrete or limestone weathering material. For example the soft crust consisting of parallel layers overlying weathered foot-slope colluvium (Plate 1.7 D) which formed by successive seepage of running water over a less permeable layer has high  $\text{Fe}_0/\text{Fe}_d$  ratios and relatively poorly crystalline goethite (as measured by XRD line broadening) (Table 1.5). In contrast, the harder crusts developed on saprolites on plateaux or on crests (i.e. Nos. 255 and 49) have lower  $\text{Fe}_0/\text{Fe}_d$  ratios and contain more crystalline goethite (lower line broadening) (Table 1.5). Furthermore, a soft and hard ferruginous weathering crust, derived from aeolianite near Richards Bay shows a similar pattern (Table 1.5). The first (Nos. 183 and 184) softer crust



Table 1.5 Sample location, description, and chemical and mineralogical composition of ferruginous crusts (cr) and bands (bn)

Subsample No. Fig. 1.1)	Soil zone (Fig. 1)	Locality	Soil series (depth cm)	Subsample description	Munsell colour (powder)	Chemical composition <sup>1</sup>			Mineralogy <sup>2</sup>					d (110)		d (130)			d (111)		
						Fe <sub>d</sub> %	Fe <sub>o</sub> %	Fe <sub>o</sub> /Fe <sub>d</sub>	Co	Qz	Ka	Mh	Le	X <sub>h</sub>	W <sub>h</sub> (°2θ)	X <sub>h</sub>	soil % AlO <sub>3</sub> H <sub>2</sub>	W <sub>h</sub> (°2θ)	X <sub>h</sub>	soil % AlO <sub>3</sub> H <sub>2</sub>	W <sub>h</sub> (°2θ)
179	4	Cleland	Longlands (55-60)	Friable 4-5 mm cr on weathered colluvium, so (Pl. 1.7D; arrowed)	10 YR 6/8	24.2	0.98	0.037	SD	SD	T	-	-	4.169	0.61	2.680	13.0	0.86	2.436	11.6	0.
183	19	Richards Bay	Clansthal (80-85)	<62 µm from soft parts (Pl. 1.7E)	7.5 YR 5/8	14.3	1.60	0.112	A	D	T	-	-	4.194	0.46	2.698	0.7	0.76	2.451	0.7	0.61
184	19	Richards Bay	Clansthal (80-85)	<62 µm from friable part (Pl. 1.7 E)	7.5 YR 5/6	17.1	1.12	0.065	A	D	T	-	-	4.194	0.71	2.698	0.7	0.66	2.451	0.7	0.71
185	19	Richards Bay	Clansthal (195-200)	<62 µm from hard parts	10 YR 6/8	25.8	0.81	0.031	SD	D	T	-	-	4.180	0.23	2.688	7.5	0.33	2.446	4.4	0.33
186	2	Hella Hella	Clovelly (75-80)	<62 µm from friable 2-4 mm, cr on weathering so	10 YR 5/8- 7.5 YR 5/8	n.d.	n.d.	n.d.	SD	A	A	-	-	4.183	0.71	2.692	4.8	0.78	2.446	4.4	0.61
187	2	Ikopo	Clovelly (90-120)	Friable, 3-5 mm cr on weathering shale above pallid zone	10 YR 5/8	n.d.	n.d.	n.d.	SD	A	A	-	-	4.177	0.73	2.686	8.9	0.96	2.441	8.0	0.71
49	3	Hillcrest	Inanda (195-210)	Friable, 3-5 mm cr on weathering granite in so	10 YR 6/8	33.7	0.13	0.004	SD	A	A	-	-	4.177	0.38	2.689	6.8	0.41	2.445	5.1	0.41
255a	2	Dullstroom	Clovelly (120-125)	Friable, 3-5 mm yellow cr in so	10 YR 6/6	24.2	0.17	0.007	D	A	A	-	-	4.177	0.31	2.686	8.9	0.36	2.443	5.1	0.28
b	2	Dullstroom	Clovelly (120-125)	Hard, 4-6 mm brown cr in so	10 YR 6/8	28.6	0.15	0.005	D	A	A	-	-	4.177	0.10	2.688	7.3	0.19	2.443	5.1	0.17
203a	2	Dullstroom	Trevelian (50-75)	Friable, 1-3 mm brown cr in weathering quartzite cracks (so)	10 YR 5/6- 7.5 YR 5/6	29.3	0.86	0.029	D	A	T	-	-	4.177	0.76	2.687	8.2	1.26	2.437	10.9	0.88
253	2	Weltevreden	Farningham (75-90)	Friable, 1-2 mm yellow-brown cr on (close to) Mt <sup>3</sup> /Mh band	10 YR 6/8	31.4	0.31	0.010	D	A	T	A	-	4.180	0.57	2.698	0.7	0.55	2.451	0.7	0.51
254	5	Stoffberg	Argent (130-170)	Friable, 3-6 mm red-brown cr on Ti-Mt/He band	10 YR 5/8	n.d.	n.d.	n.d.	SD	T	T	A	-	4.185	0.46	n.m. <sup>4</sup>	n.m. <sup>4</sup>	n.m. <sup>4</sup>	2.449	2.2	0.46
199a	4	Ikopo N.	Argent (90-95)	Friable, 3-10 mm yellow-brown cr 5cm below Mh/He band (Pl. 2.1 A)	10 YR 5/6	32.4	0.18	0.006	D	T	T	A	-	4.177	0.61	2.688	7.3	0.66	2.442	7.3	0.61
b	4	Ikopo N.	Argent (60-90)	Friable, 1-3 mm yellow-brown cr on (close to) Mh/He band (Pl. 2.1 A)	10 YR 5/6	29.6	0.32	0.010	D	T	T	A	-	4.197	0.61	2.700	-0.7	0.61	2.454	-1.2	0.61
20 site B in Fig. 4.7)	2	Loteni	Ouwerf (75-95)	Friable, 1-2 mm dark brown cr associated with orange clay bands	10 YR 5/8	25.5	0.17	0.007	D	A	T	-	T	n.d.	n.d.	2.686	8.9	0.36	2.441	8.0	0.36
126	2	Glengarry	Ouwerf (40-45)	Soft yellow-brown band (~4cm) with many pipestems	10 YR 5/8	42.6	0.14	0.003	D	A	A	-	T	4.187	0.61	2.695	2.7	0.31	2.453	-0.7	0.31
164	2	Gomane	Ouwerf (45-53)	Soft, yellow band (cr) in gleyed weathering so	10 YR 6/6	n.d.	n.d.	n.d.	D	T	A	-	T	4.180	0.71	2.686	8.9	0.75	2.440	8.7	0.46
219a	2	Impendla	Ouwerf (45-50)	Hard, brittle 3-5mm cr on gley cutanic [Pl. 4.3 A (arrowed) & B (larger cr)]	10 YR 6/8- 7.5 YR 5/8	35.6	0.31	0.009	D	A	T	-	T	4.177	0.44	2.689	6.8	0.56	2.443	6.6	0.52
b	2	Impendla	Ouwerf (42-54)	Soft, yellow clay bands above & below hard cr (arrowed) in Pl. 4.3 A	7.5 YR 6/8	24.2	0.96	0.040	SD	A	A	-	A	4.180	0.52	2.686	8.9	0.51	2.442	7.3	0.46
		Teesdale <sup>1</sup>	Iron pan Stagnopodzsol	Hard brittle 5 mm "thin Fe-pan" with root mat on upper surface & covering of lepidocrocite on lower surface [Pl. 4.3 B (smaller cr)]	10 YR 5/8	22.4	1.58	0.071	SD	A	T	-	A	4.177	0.43	2.695	2.7	0.66	n.m.	n.m.	n.m.

<sup>1</sup> Sample taken by the writer at Profile No. W4 (Hornung, 1977) during the field excursion of the North of England Soils Discussion Group meeting at High Force, U.K., 1975. <sup>2</sup> Fe<sub>d</sub> and Fe<sub>o</sub> as Table 1.1; n.d. = not determined. <sup>3</sup> D, SD, A, T and -; Co, Qz, Ka, Mh and Le as Tables 1.1 - 1.4. <sup>4</sup> as Table 1.1.

<sup>5</sup> Haematite interference; n.m. = not measurable. <sup>6</sup> Mn = Manganese.



formed between layers of weathering aeolianite (Plate 1.7 E) has less Fe, and less well-crystalline goethite. The other (No. 185) is harder, more yellow and contains a better crystalline goethite. The former has higher  $Fe_o/Fe_d$  ratio (0,112 against 0,031) and higher X-ray line broadening [WHH of the 010 line 0,61 against 0,33° 2 $\theta$ ] (Table 1.5).

The unusually high  $d(110)$ ,  $d(130)$  and  $d(111)$  spacings observed for goethite in the thin crust sample (No. 199) on the surface of and close to the maghaemite band (Plate 2.1 A) is possibly due to  $Fe^{2+}$  incorporation into the goethite structure ( $Fe^{2+} = 1,5\%$ ).

In all the crusts which contain some lepidocrocite (Table 1.5), the two  $FeOOH$  polymorphs are considered to be closely associated and to have formed simultaneously (Schwertmann and Fitzpatrick, 1978). An explanation for this is based on synthetic experiments by Schwertmann (1959) where increasing amounts of  $CO_2$  in a gas mixture produced higher amounts of goethite than lepidocrocite, (e.g. in better aerated interface sandy layers where crusts are developed). This is possibly due to goethite forming via siderite ( $FeCO_3$ ) rather than via green rust (Schwertmann and Taylor, 1977). In addition, the type of thin ferruginous crust that is formed in Ouerf soils near Impendla (see Plate 4.3 A and B) has somewhat similar morphological (Plate 4.3 B) and mineralogical (i.e. associated with lepidocrocite) features resembling that of a thin iron pan from a Stagnopodzol near High Force (North of England) (Table 1.5). This suggests a similar mode of formation, with Fe being reduced under anaerobic conditions (i.e. retarded drainage due to the impermeability of underlying gleys) and lepidocrocite and goethite forming on reoxidation (i.e. in better aerated zones such as more sandy layers adjacent to clayey layers).

#### 1.4.6 Pipestems

Three types of "fossilized" ferruginized pipestems or pedotubules (Brewer and Sleeman, 1963) occur throughout the region (Table 1.6) namely: (i) large, very hard, hollow, relict pipestems (Plate 1.8 A) occurring at various depths (up to 8 m) in deep red coastal soils (soil zone 19 in Fig. 1), (ii) thin friable pipestems of more recent origin with tubes or pipes filled with root material and occurring in hydromorphic vlei soils (Plate 1.8 B and D), (iii) small, fairly hard pipestems surrounded by orange haloes of clay containing lepidocrocite occurring in pseudogley soils in the Highland Montane region (Plate 1.8 C).

1.6 Sample location, description, and chemical and mineralogical composition of ferruginous pipestems (ps)

Sample no. (1.1) (Fig. 1)	Soil zone	Locality	Soil series	Subsample description	Munsell colour (powder)	Chemical composition <sup>2</sup>				Mineralogy <sup>3</sup>			d (110)		d (130)			d (111)		
						Fe <sub>d</sub>	Fe <sub>HCl</sub>	Fe <sub>o</sub>	Fe <sub>o</sub> /Fe <sub>HCl</sub>	Go	Qz	Le	g	wt% (°2θ)	g	mole % AlO <sub>3</sub> H <sub>2</sub> (°2θ)	wt% (°2θ)	g	mole % AlO <sub>3</sub> H <sub>2</sub> (°2θ)	wt% (°2θ)
						%	%	%												
2	19	Umhlanga Rocks	Clansthal	Relict large, very hard, hollow pipestems (Pl. 1.8 A)	10 YR 5/6	21,2	28,8	0,12	0,004	D	SD	-	4,183	0,19	2,695	2,7	0,26	2,450	1,5	0,24
3	19	Palm Beach	Warrington	Thin, friable pipestems of more recent origin (Pl. 1.8 B)	10 YR 5/6	15,2	22,5	0,11	0,005	D	SD	-	4,180	0,20	2,690	6,2	0,22	2,450	1,5	0,23
0	4	Pietermaritzburg	Dundee	Thin, friable pipestems of more recent origin (Pl. 1.8 D)	10 YR 5/8-7,5 YR 5/8	17,4	23,6	0,13	0,006	D	A	-	4,177	0,28	2,691	5,5	0,38	2,449	2,2	0,46
2 b	2	Loteni	Ouwerf	Single pipestem (large arrow in Pl. 1.8 C)	7,5 YR 6/8	26,7	28,5	1,10	0,039	D	A	T	4,182	0,96	2,692	4,8	1,06	2,445 <sup>5</sup>	5,1 <sup>5</sup>	0,71 <sup>5</sup>
2 a	2	Loteni	Ouwerf	Composite sample of several pipestems from gley cutanic horizon	7,5 YR 6/8	19,5	22,6	1,30	0,078	D	A	T	4,190	0,77	2,695	2,7	0,91	n.m. <sup>5</sup>	n.m. <sup>5</sup>	n.m. <sup>5</sup>
1	2	Glengarry <sup>1</sup>	Ouwerf	Composite sample of several pipestems from gley cutanic horizon	7,5 YR 5/8	18,5	24,9	1,19	0,048	D	A	T	4,178	0,86	2,692	4,8	0,86	2,451 <sup>5</sup>	0,7 <sup>5</sup>	~0,81 <sup>5</sup>
4	2	Glengarry <sup>1</sup>	Avoca	Composite sample of several pipestems from gley cutanic horizon	10 YR 5/8-7,5 YR 5/8	16,7	24,4	0,40	0,016	D	A	T	4,177	0,61	2,692	4,8	0,66	n.m. <sup>5</sup>	n.m. <sup>5</sup>	n.m. <sup>5</sup>

Samples from Schwertmann and Fitzpatrick (1977)

<sup>1</sup> Fe<sub>HCl</sub> and Fe<sub>o</sub> as for Table 1.1

Qz, and Le as for Table 1.2;

SD, A, T and - as for Table 1.1

Table 1.1

idocrocite interference;

- = not measureable



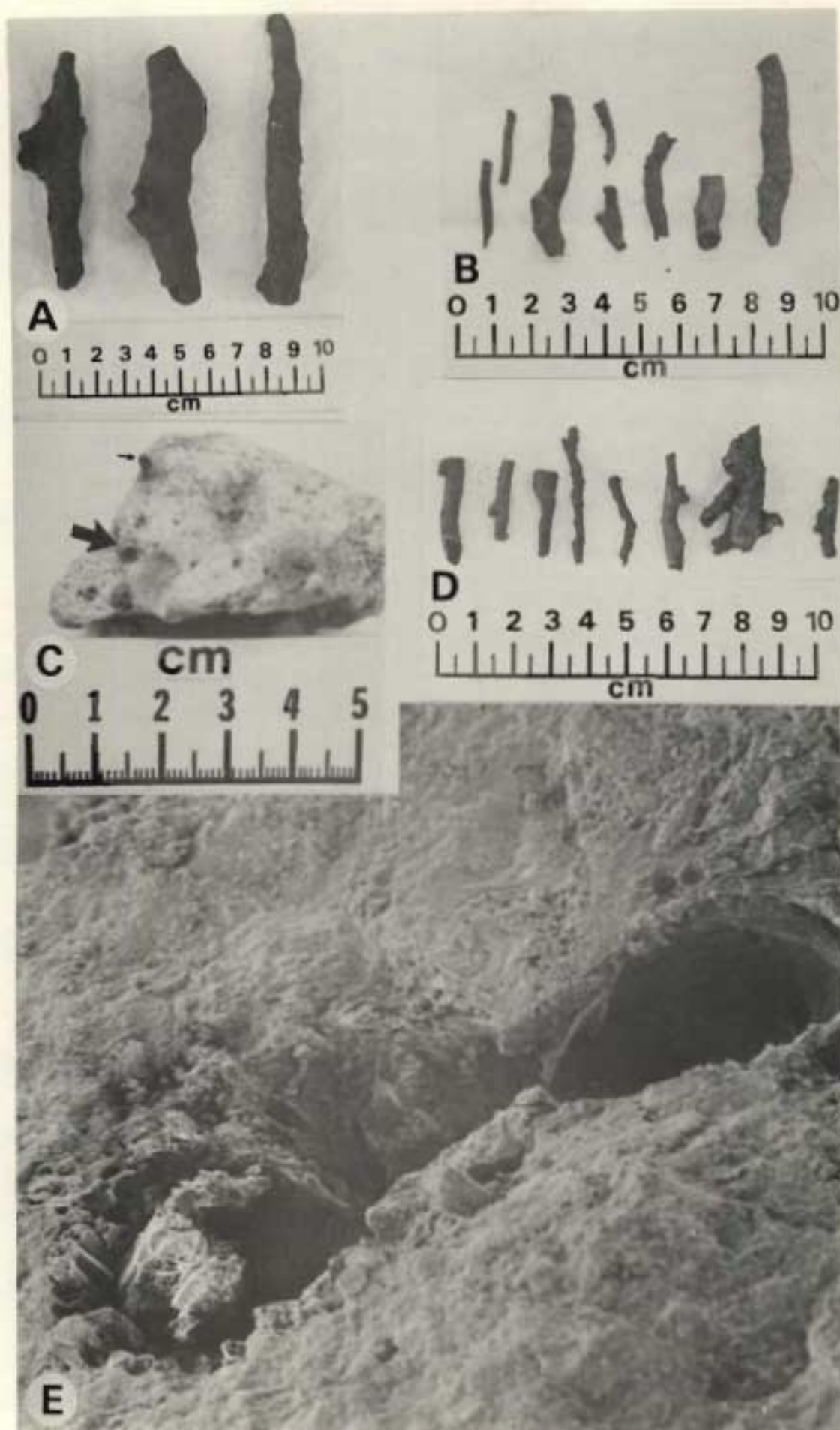
Plate 1.8: A - D. Photographs of ferruginous pipestems from various localities in Natal:

A. Typical relict, large, hard, hollow pipestems in a freely drained Clansthal soil near Umhlanga Rocks, N-coast (No. 52). These pipestems are scattered throughout the soil up to a depth of 8 m.

B and D. Thin friable pipestems of more recent origin in Warrington and Dundee soils from Palm Beach (B. No. 193) and Pietermaritzburg (C. No. 200) respectively with many of the narrow tubes or "pipes" partly filled with root material. Various shapes reminiscent of plant root patterns are evident.

C. Small, fairly hard, yellow-brown pipestems (arrowed) surrounded by orange coloured haloes of clay containing lepidocrocite (darker zones surrounding pipestems) in gleyed soil matrix from the B 23 horizon (gley cutanic) of an Ouwerf soil near Loteni (No. 142).

E. Scanning electron micrograph of fracture surface and tubular cavity in pipestem ( $\times 800$ ) from Loteni (large arrow in C. No. 142 b) showing fossilized, ferruginous internal fabric (e.g. epidermal cellular material).





The characteristic external form (i.e. branching pattern shown in Plate 1.8 A, B and D) and internal forms (i.e. partly filled with decayed root material; SEM view of hollow centre showing fossilized epidermal cellular material in Plate 1.8 E) presented here suggest that these materials originate from root systems. It is thought that Fe is precipitated preferentially within the rhizosphere and on the root epidermis either by oxidation of  $\text{Fe}^{2+}$  or in the presence of certain organic humates.

Failure to detect haematite and the prevalence of goethite in the pipestems examined, together with the presence of some lepidocrocite in certain samples (Table 1.6) suggests that the micro-conditions in the rhizosphere (i.e. pH,  $\text{PCO}_2$  and kinds of organic humates present) strongly favours the crystallization of goethite with a relatively low degree of Al-substitution over that of haematite (Table 1.6).

#### 1.4.7 Ferruginous bauxite

Ferruginous bauxite is found in scattered, plateau areas between 1 000 and 2 000 m elevation, roughly 50 to 100 km parallel to the coastline (Fig. 1.1)\*. All these areas receive about 1 000 mm or more of rainfall per year and have adequate grass (mostly) or forest cover to inhibit surface runoff and erosion. They occupy old land surfaces (possibly Tertiary) and are derived mainly from dolerites of various "textures". In localized areas ferruginous bauxites are derived from lidianite (e.g. Weza area), Middle Ecca sandstone (e.g. Pietermaritzburg escarpment) or Table Mountain sediments (e.g. in soil zones 3 and 16; Fig. 1) (Table 1.7). Apart from the Table Mountain sediment nodular bauxite which is relatively poor in Fe, the selected samples are representative of the range of types of ferruginous bauxite and their parent materials and are described† briefly in Table 1.7.

In a typical and fairly representative profile containing ferruginous bauxite at Sweetwaters near Pietermaritzburg (Plate 1.9 A) the lithological succession from bottom to top is: (i) unweathered dolerite, (ii) a red and/or yellow mottled to speckled kaolinitic zone (see section 1.4.8 below), (iii) ferruginous bauxite boulders‡ and/or nodules (Plate 1.9 A to D), and (iv) freely drained red or yellow kaolinitic soil (Balmoral or Farmhill soils).

---

\* Fey conducted detailed prospecting work on ferruginous bauxite in Natal and Transkei (private communication)

† see Appendix 1



Sample No. (Fig. 1.1)	Soil zone (Fig. 1)	Locality	Parent rock	Subsample description	Munsell colour (powder)	Chemical composition <sup>a</sup>				Mineralogy <sup>b</sup>								d (110) <sup>c</sup>		d (130) <sup>c</sup>			d (111) <sup>c</sup>		
						Fe <sub>d</sub> (Mn <sub>d</sub> ) %	FeHCl %	Fe <sub>o</sub> %	Fe <sub>o</sub> /FeHCl	Co	Cl	Qz	He	Mh	Mt	Il	Å	WtH (°2θ)	Å	mole % AlO <sub>2</sub> H <sup>+</sup>	WtH (°2θ)	Å	mole % AlO <sub>2</sub> H <sup>+</sup>	WtH (°2θ)	
2b	2	Sweetwaters (Pl. 1.9A&B)	Dolerite (fine gr.)	Speckled brown & white shell (2-5mm) adjacent to unweathered dolerite core (Pl. 1.9 D)	10 YR 6/6	11.9	16.6	0.25	0.015	CD	CD	T	-	T	T	T	4.144	0.41	2.664	24.0	1.06	2.422	21.8	0.51	
c		Sweetwaters	Dolerite (fine gr.)	Massive, surrounding uniform yellowish brown layer (Pl. 1.9D)	7.5 YR 6/8	16.1	18.6	0.07	0.004	CD	CD	T	-	T	T	T	4.147	0.41	2.664	24.0	0.43	2.418	24.7	0.38	
3a	2	Unzinkulu	Dolerite (med. gr.)	Brittle, weathered core of nodule (Pl. 1.9 C)	7.5 YR 5/8	12.8 (0.03)	19.1	0.07	0.004	CD	CD	T	-	T	T	T	4.154	0.33	2.670	19.9	0.86	2.418	24.7	0.38	
b		Unzinkulu	Dolerite (med. gr.)	Brittle interior between core & rim (Pl. 1.9 C)	7.5 YR 5/8	13.3 (0.11)	19.5	0.13	0.007	CD	CD	T	-	T	T	T	4.144	0.53	2.664	24.0	1.06	2.415	26.9	0.51	
e		Unzinkulu	Dolerite (med. gr.)	Hard rim surrounding nodule (Pl. 1.9 C)	10 YR 5/6	20.7 (0.35)	28.8	0.34	0.012	D	A	-	-	-	-	-	4.164	0.52	2.679	13.7	1.06	2.427	18.2	0.51	
0	2	Ngome	Dolerite (coarse gr.)	Brittle interior between core & rim (gabbroic)	5 YR 5/8	19.1	25.1	0.20	0.008	CD	CD	T	T	T	T	T	4.157	0.51	2.672	18.5	0.96	2.424	20.4	0.48	
9	2	Ngome	Dolerite (coarse gr.)	Hard, 5-10mm thick rim, surrounding nodule (gabbroic)	7.5 YR 5/8	23.1	39.5	0.25	0.006	D	T <sup>6</sup>	-	-	-	-	T	4.170	0.73	2.673	17.8	1.06	2.432	14.5	0.86	
1	2	Howick	Dolerite (fine gr.)	Brittle, massive, large joined weathered boulder	7.5 YR 5/8	17.2	19.5	0.13	0.007	CD	CD	T	T	T	T	T	4.149	0.44	2.664	24.0	0.48	2.418	24.7	0.47	
2	2	Howick	Dolerite (fine gr.)	Hard rim on large weathered boulders	7.5 YR 6/8- 10 YR 6/8	21.5	32.9	0.21	0.006	D	T	T	-	-	-	T	4.164	0.55	2.672	18.5	0.93	2.426	18.9	0.61	
3	2	Impendla	Dolerite (coarse gr.)	Brittle, massive, large joined weathered boulders	10 YR 6/6	16.0	18.5	0.15	0.008	CD	CD	T	T	T	T	T	4.157	0.51	2.665	23.3	0.81	2.419	24.0	0.46	
4	2	Hilton	Sandstone (fel- spathic)	Brittle, yellow-brown joined plates	10 YR 6/8	17.1	19.8	0.07	0.004	CD	CD	T	T	-	-	T	4.152	0.81	n.m. <sup>7</sup>	n.m. <sup>7</sup>	n.m. <sup>7</sup>	2.421	22.5	0.71	
	2	Hilton	Sandstone <sup>8</sup> (fel- spathic)	Brittle, reddish-brown, joined plates	7.5 YR 5/8	17.6	19.9	0.09	0.003	CD	CD	T	T	-	-	T	4.167	0.66	n.m. <sup>7</sup>	n.m. <sup>7</sup>	n.m. <sup>7</sup>	2.425	19.6	0.43	
	2	Loakop	Dolerite (med. gr.)	Brittle, massive weathered boulder fragment underlying ferricrete	7.5 YR 6/8- 10 YR 6/8	12.9	18.6	0.10	0.003	CD	CD	T	T	-	T	T	4.157	0.15	2.665	23.3	0.65	2.420	23.3	0.46	
a	10	Estcourt	Dolerite (fine gr.)	Brittle core of weathered boulder in saprolite underlying Viny soil	7.5 YR 5/8	n.d.	n.d.	n.d.	n.d.	CD	CD	T	T	-	T	T	4.160	0.57	2.662	25.3	1.26	2.418	24.7	0.68	
b		Estcourt	Dolerite	Brittle, layer surrounding weathered core of boulder in saprolite underlying Viny soil	7.5 YR 5/8	n.d.	n.d.	n.d.	n.d.	CD	CD	T	T	-	T	T	4.160	0.56	2.678	14.4	1.06	2.429	16.7	0.71	
	2	Wesa <sup>1</sup>	Midianite (fine gr.)	Composite of massive samples, reddish-brown v. fine gr.	7.5 YR 6/6	n.d.	n.d.	n.d.	n.d.	CD	CD	A	T	-	T	T	4.152	0.56	2.678	14.4	0.73	2.418	24.7	0.56	
	2	Wesa	Midianite (fine gr.)	Single fragment; pale reddish- brown v. fine gr.	10 YR 7/6	n.d.	n.d.	n.d.	n.d.	CD	CD	A	T	-	T	T	4.152	0.56	n.m. <sup>7</sup>	n.m. <sup>7</sup>	n.m. <sup>7</sup>	2.418	24.7	0.58	
	2	Ngome <sup>1</sup>	Dolerite (coarse gr.)	Composite of massive weathered samples	7.5 YR 5/6	n.d.	n.d.	n.d.	n.d.	CD	CD	T	T	T	T	T	4.160	0.50	2.672	18.5	1.06	2.423	21.1	0.53	
		Ngome	gabbroic	Magnetic fraction from com- posite samples	7.5 YR 5/6	n.d.	n.d.	n.d.	n.d.	D	SD	-	T	A	A	A	4.144	0.40	n.m. <sup>7</sup>	n.m. <sup>7</sup>	n.m. <sup>7</sup>	2.419	24.0	0.84	
		Ngome		< 66 µm fraction from com- posite samples	5 YR 4/6	n.d.	n.d.	n.d.	n.d.	CD	CD	T	T	T	T	T	4.157	0.71	n.m. <sup>7</sup>	n.m. <sup>7</sup>	n.m. <sup>7</sup>	2.424	20.4	0.76	

Samples kindly provided by Dr. M.V. Fey. <sup>2</sup> med. = medium & gr. = grained. <sup>3</sup> Middle Ecce Series (Karras System). <sup>4</sup> Fe<sub>d</sub>, FeHCl, Fe<sub>o</sub> and n.d. as for Table 1.1; Mn<sub>d</sub> = CD extractable Mn. D data before pretreatment with 5M NaOH; D, CD, SD, A, T and - : Go, Qz, He, Mh, as for Table 1.1 and 1.4; where Cl = gibbsite and Il = ilmenite. <sup>6</sup> Traces of boehmite. <sup>7</sup> XRD after pretreatment with 5 M NaOH. <sup>8</sup> as for Table 1.1. <sup>9</sup> Haemetite interference.

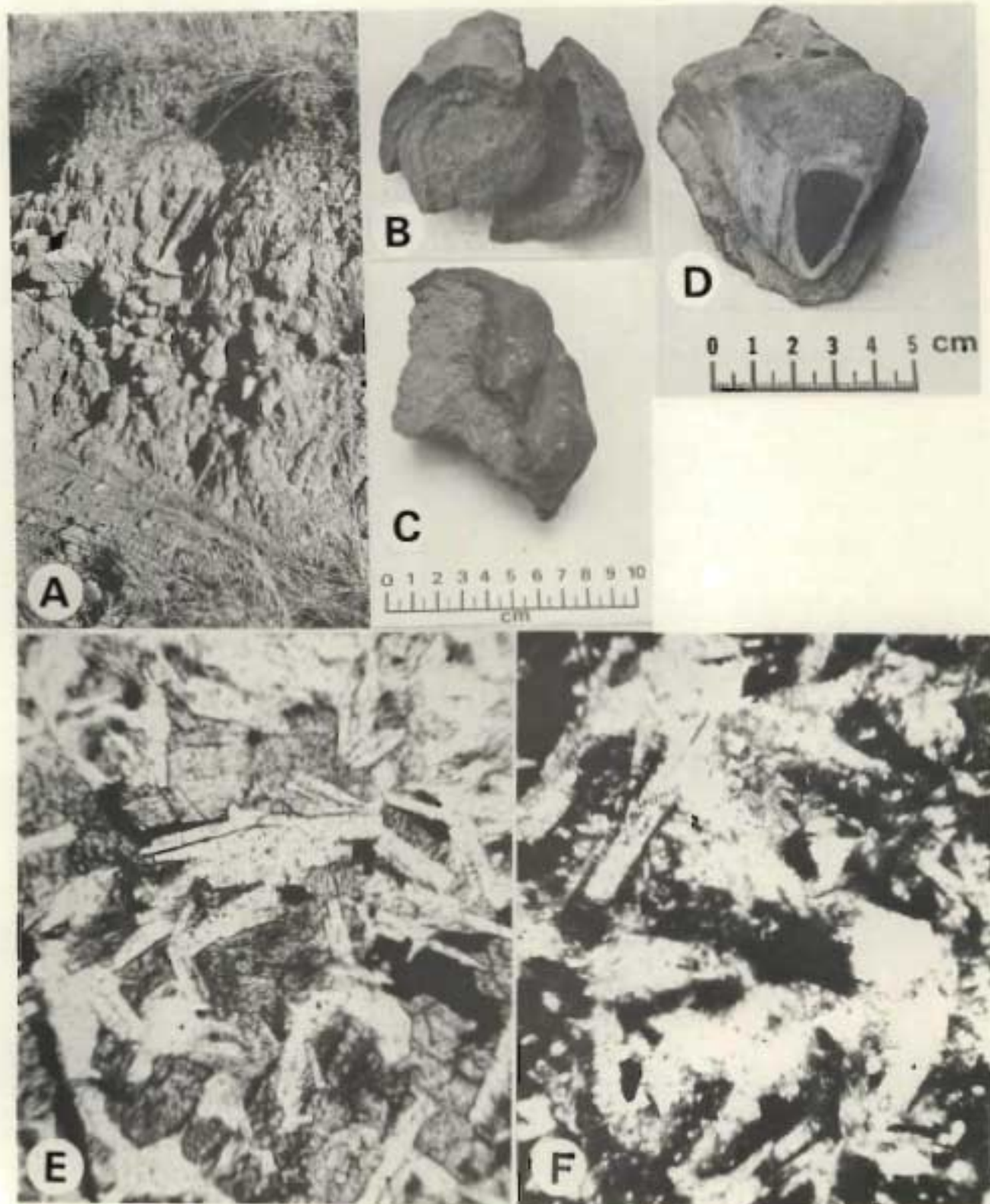


Plate 1.9: A. An exposure of a Farmhill soil derived from dolerite in a railway cutting near Sweetwaters, Pietermaritzburg, showing a layer of nodules, fragments and blocks of ferruginous bauxite (geological hammer rests on bauxitic layer) (No. 62).

B and C. Typical ferruginous bauxite nodules fractured in half before photographing, with porous weathered dolerite centres or cores and dense, shiny, high iron outer shells (rinds) from Sweetwaters profile (B, with thin rind, ranging from 1 - 4 mm) and near Umzimkulu, along the road to Franklin (C, No. 63 c, with thick rind, ranging from 5 - 10 mm). Boundary between the dark, hard rinds and brittle to friable lighter-coloured interior ferruginous bauxite is sharp, and is usually demarcated by a thin purplish-black layer or coating of Mn-oxide.

D. Portion of a weathered dolerite boulder-block fractured in half to show the core of unweathered dolerite and abrupt transition to surrounding layers (or shells) of weathered dolerite (ferruginous bauxite) from the Sweetwaters profile (No. 62 a and b).

E and F. Light micrographs illustrating changes during weathering of dolerite to ferruginous bauxite in D. In thin sections of parent rock, dolerite (E) and adjacent ferruginous bauxite (F) feldspars are replaced by gibbsite (light coloured, lath-shaped) and ferromagnesian minerals replaced by aluminous goethite (dark coloured). Note in E, magnetite and ilmenite appear black; Fe-silicates appear dark grey with speckles, and feldspars appear white to very light grey. Ordinary light x 65.





The mottled kaolinitic zone (lithomarge or saprolite) which represents the maximum extent of ground water fluctuation undergoes less intensive "lessivage" (leaching intensity; Millot, 1970) than ferruginous bauxite.

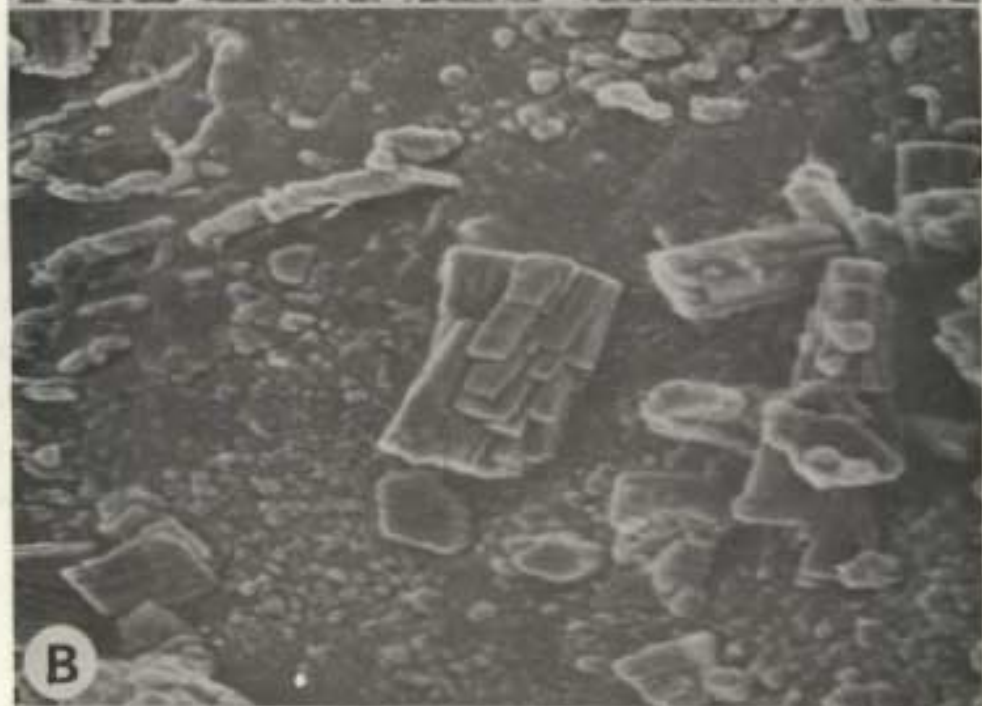
Most of the ferruginous bauxite in the study area has formed by *in situ* weathering of the original parent rock under particularly severe "lessivage" resulting in a brittle, yellow-brown porous massive residuum (Table 1.7). This is evident from the sharp front type of weathering (e.g. complete transition from rock to bauxite extends over a distance of less than two millimeters as shown in Plate 1.9 D) together with the preservation of parent rock cleavage planes (Plate 1.9 B) and crystal outlines. As seen from thin sections of parent rock (dolerite) and adjacent ferruginous bauxite (Plate 1.9 E and F) the original feldspar areas are pseudomorphously replaced by gibbsite (white to light grey areas) and the iron-silicates (augites and hornblende) by goethite (dark grey areas).

The SEM of fracture surfaces of ferruginous bauxite show large pores (Plate 1.10 A) with lath-shaped and "cruciform" feldspar grains replaced (pseudomorphed) by gibbsite (Plate 1.10 B and C respectively). The aluminous goethite crystals although fairly well formed and easily detectable by XRD (Fig. 1.3 d; Table 1.7) are generally much smaller as can be observed on some of the transmission electron micrographs (Plate 1.11 A to C). Plate 1.11 C and D show typical pseudo-hexagonal-like crystals of gibbsite and in Plate 1.11 C aggregates of finely grained crystalline aluminous goethite are evident. In all these ferruginous bauxite samples there was no evidence of halloysite using XRD methods. However, elongated tubular crystals, strongly resembling halloysite (similar to those identified by Torrent and Benayas, 1977) were observed (Plate 1.11 A and D) on some of the transmission electron micrographs.

As seen in Table 1.7, generally goethite in ferruginous bauxite samples contain roughly between 20 and 25 mole %  $\text{AlOOH}$  in solid solution. Beneslavsky (1957) found Al contents of about 20 mole % in USSR bauxites. Compared with soil clays of similar high levels of Al-substitution (Table 1.9) the goethite in ferruginous bauxite samples are relatively more crystalline (as determined from line broadening) (Table 1.7). This is possibly due to the formation of Al-goethite in bauxites under conditions where free drainage is permitted and Fe and Al coprecipitate close to their source (i.e. within weathered augite or hornblende crystals). Furthermore,

Plate 1.10: A - C. SEM of fracture surface of ferruginous bauxite from Sweetwaters (Nb62c) at progressively increasing magnifications A (x 160), B (x 800) and C (x 1 600) showing pores (A) lined with large lath-shaped feldspar grains which have been replaced (pseudomorphed) by gibbsite. B and C are detailed electron micrographs of pores showing that the lath-shaped and "cruciform" (clearly evident in C) morphology of feldspar is retained. The small globules or droplets and possibly the surrounding matrix comprises mainly finely grained aluminous goethite.





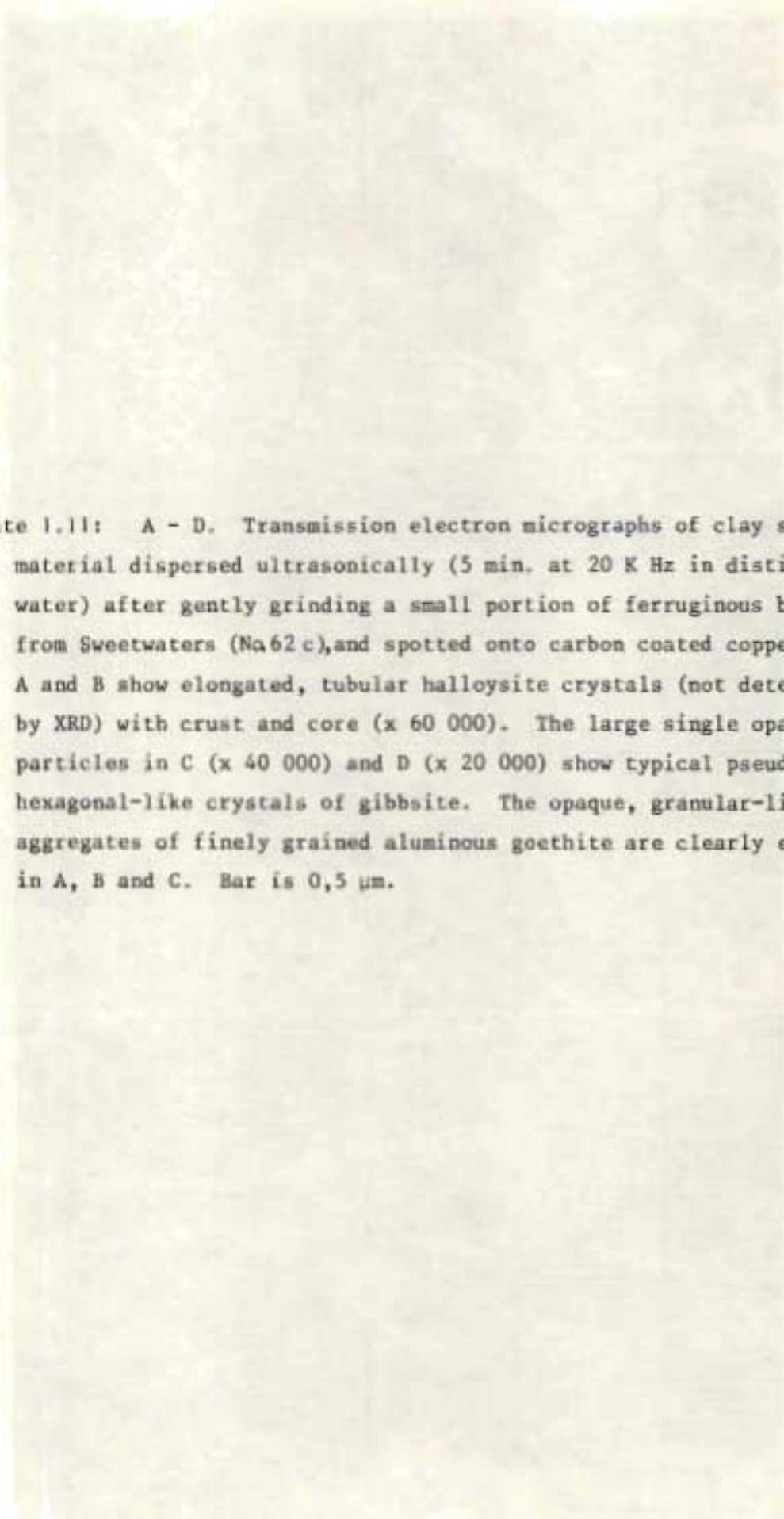
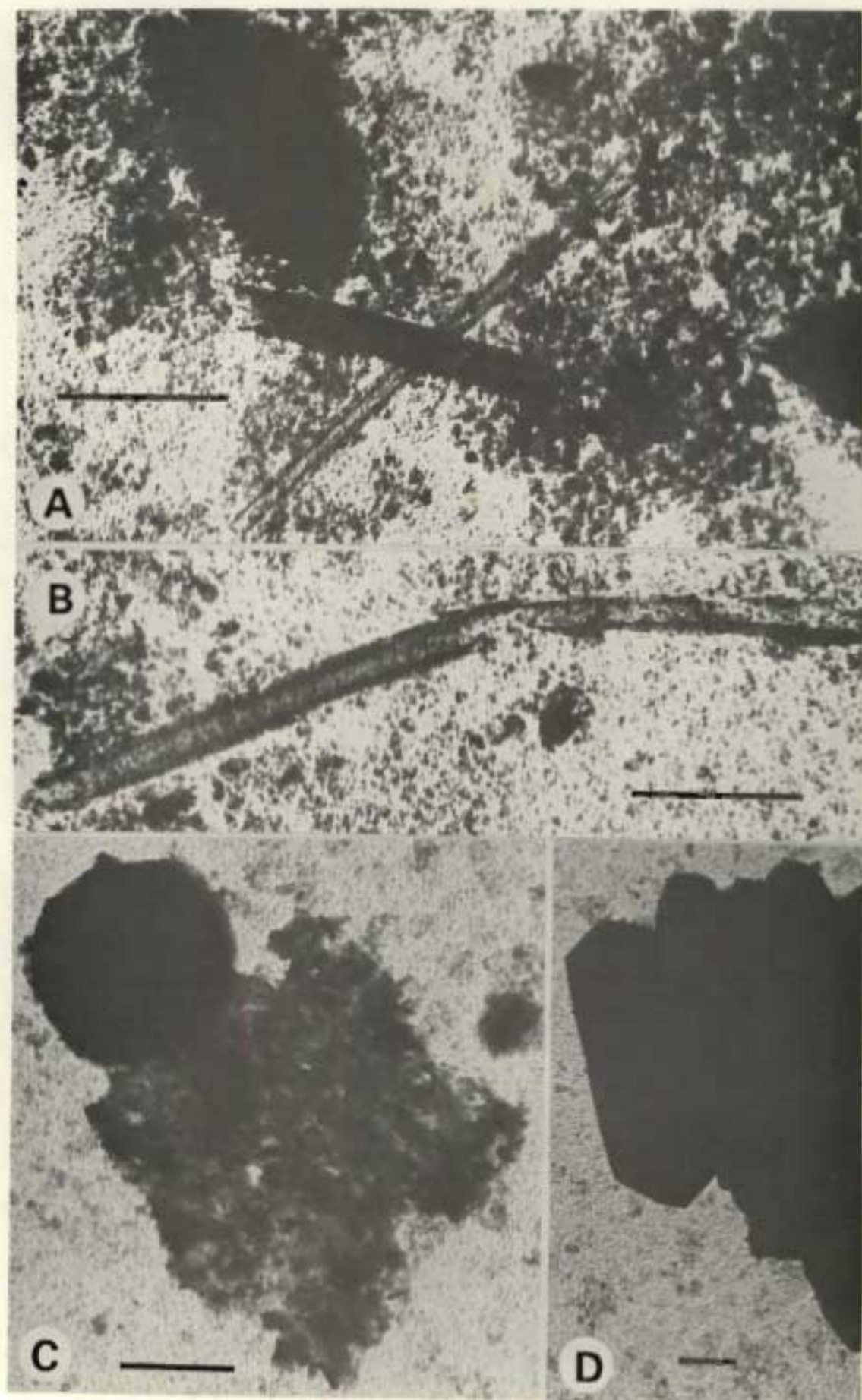


Plate 1.11: A - D. Transmission electron micrographs of clay size material dispersed ultrasonically (5 min. at 20 K Hz in distilled water) after gently grinding a small portion of ferruginous bauxite from Sweetwaters (Na62c), and spotted onto carbon coated copper grids. A and B show elongated, tubular halloysite crystals (not detected by XRD) with crust and core (x 60 000). The large single opaque particles in C (x 40 000) and D (x 20 000) show typical pseudo-hexagonal-like crystals of gibbsite. The opaque, granular-like aggregates of finely grained aluminous goethite are clearly evident in A, B and C. Bar is 0,5  $\mu$ m.





there is also very little movement between the Al and Fe as this mode of weathering (i.e. *in situ* bauxitization) consists essentially of the removal of Si, Ca and Mg (Keller, 1964; Millot, 1970).

Many of the highly weathered soils in the ferruginous bauxite zone (Figs. 1 and 1.1) may contain numerous ferruginous bauxite nodules ranging in size from 2 to 50 cm in diameter, and tend to concentrate mainly in stonelines (Plate 1.9 A). The nodules have a roughly round to oval shape with a shiny, wavy surface (Plate 1.9 B and C). The dense, hard outer crusts (rinds) ranging from 1 to 10 mm in thickness surround a much lighter brown coloured, brittle porous material, very much like that of typical ferruginous bauxite, sometimes with unweathered dolerite cores (Plate 1.9 B and C). The hard goethitic rinds act as a protective coating and were probably formed when fragments or boulders of ferruginous bauxite were moved (e.g. by colluviation) to a zone of intermittent water saturation where iron was deposited in the outer pores of the bauxite. It is further suggested that most of the iron was not derived from the "host" ferruginous bauxite but was supplied from adjacent sources. Hence the hard rinds and brittle interiors indicate a different mode of formation. X-ray and chemical analysis of the leached ferruginous bauxite interior and outer (rind) precipitation zones of several nodules examined (Table 1.7) show compositional differences. There is a relatively higher degree of Al-substitution in goethite of the leached interior zones (resembling that of ferruginous bauxite boulders and fragments) as compared to the rinds (Table 1.7). Furthermore, the Fe content ( $\text{Fe}_{\text{HCl}}$ ) of the outer rind is higher than that of the inner portions of the nodules, approximately 30 and 20 per cent, respectively (Table 1.7). Similarly, higher  $\text{Mn}_d$  values occur in the rind (Table 1.7).

It is suggested that the dense outer goethite rind is formed by the mobilization of ferrous iron, derived mainly from adjacent areas and partly from the "host" bauxite during periods of water logging, which penetrates and coprecipitates as an Al-goethite mass in the cracks and pores of the outer matrix of the "host" ferruginous bauxite material. Therefore, it is impossible to physically separate the "primary" (*in situ* weathered material) and "secondary" (reprecipitated material) Al-goethite in the rind. The incorporation of primary Al-goethite in the rinds may to some extent explain the relatively higher degree of Al-substitution measured in the rinds compared with that of ferricretes which are formed under hydromorphic



conditions. It is of interest to note that the only occurrences of boehmite were detected in rinds (Table 1.7) possibly due to secondary Al reprecipitation followed by a "drying" out stage.

The fact that these bauxites contain high amounts of goethite (average about 30 to 40%) with up to 25 mole %  $\text{AlOOH}$  in solid solution is significant to the economic viability of these materials. This is because the Al incorporated in the goethite structure is not recoverable by the normal Bayer process (i.e. treatment under strong alkaline conditions). For this reason the amount of Al substituted into the goethite (or haematite) structure is critical in determining the economic potential of this bauxite (Beneslavsky, 1957; Spencer, 1973).

#### 1.4.8 Saprolite

Regardless of geology most of the high rainfall and older land surfaces in the study area usually have a mantle of fairly deeply weathered rock. This weathered rock is considered to be saprolite because most of the textures and structures of the parent rock have been preserved but nearly all original minerals have been replaced during weathering. Although both saprolite and ferruginous bauxite are associated with well drained conditions and have formed by *in situ* weathering they differ in consistency and mineralochemical composition. Ferruginous bauxite is brittle ("biscuit-like" consistency) and is predominantly gibbsite and goethite with minor amounts of halloysite, ilmenite, anatase and titanomagnetite minerals (see section 1.4.7). In contrast, ferruginous saprolite is sufficiently soft to be easily removed with a spade and may erode fairly rapidly where the protective "upper" solum has been destroyed; and it is composed chiefly of kaolinite and halloysite minerals with various amounts of goethite, vermiculite, quartz, anatase, ilmenite and titanomagnetite minerals (Table 1.8). Hence, rough outlines of grain boundaries occur where coarse kaolinite replaces mica; finer kaolinite replaces feldspar, goethite replaces augites, pyroxenes and amphiboles, and where "unaltered" quartz grains are found. With few exceptions (notably No. 108) the powder colour is yellow (i.e. hues range between 7.5 YR and 10 YR) and the dominant crystalline iron oxide is aluminous goethite (Table 1.8). The amount of oxidic iron ( $\text{Fe}_d$ ) appears to be related to the kind of parent rock. For example, doleritic saprolite is highest in  $\text{Fe}_d$  whereas granite saprolite (high in micas and quartz) is lowest and shale saprolite intermediate (Table 1.8).

Table 1.8 Sample location, description, and chemical and mineralogical composition of saprolites (20)

Sample No. (Fig. 1.1)	Soil zone (Fig. 1)	Locality	Parent material	Soil series	Depth (cm)	Munsell colour (powder)	Chemical composition <sup>a</sup>			Mineralogy <sup>12</sup>					d (110) <sup>b</sup>		d (130) <sup>b</sup>			d (111) <sup>b</sup>		
							Fe <sub>d</sub> %	Fe <sub>o</sub> %	Fe <sub>o</sub> / Fe <sub>d</sub>	Go	Qz	Ka	Hc	An	$\lambda$	Wt% (°2θ)	$\lambda$	mole % AlO <sub>3</sub> H <sup>12</sup>	Wt% (°2θ)	$\lambda$	mole % AlO <sub>3</sub> H <sup>12</sup>	Wt% (°2θ)
107	2	Howick	dolerite <sup>1</sup>	Balmoral	195-250	10 YR 6/8- 10 YR 7/8	31,2	0,12	0,004	SD	-	D	-	T	4,169	0,63	2,672	18,5	0,66	2,430	16,0	0,66
108	2	Howick	dolerite <sup>1</sup>	Balmoral	195-250	2,5 YR 5/8	33,6	0,21	0,006	SD	-	D	A	T	4,177	0,96	n.m. <sup>12</sup>	n.m. <sup>12</sup>	n.m. <sup>12</sup>	2,432	14,5	0,61
197	2	Impendla	dolerite <sup>1</sup>	Balmoral	175-320	10 R 4/6	n.d.	n.d.	n.d.	SD	-	D	A	T	4,177	0,63	n.m. <sup>12</sup>	n.m. <sup>12</sup>	n.m. <sup>12</sup>	2,440	8,7	0,64
202	2	Dullstroom	shale <sup>3</sup>	Farmhill	180-210	7,5 YR 7/8	n.d.	n.d.	n.d.	SD	SD	D	-	T	4,174	0,56	2,678	14,4	0,56	2,430	16,0	0,48
210	2	Kederhorst	shale <sup>3</sup>	Clovelly	125-195	7,5 YR 6/8	n.d.	n.d.	n.d.	A	SD	D	T	T	4,177	0,43	2,680	13,0	0,51	2,434	13,1	0,36
88	2	Mikes Pass	basalt <sup>2</sup>	Farmhill	210+	7,5 YR 6/8	30,5	0,13	0,004	A	T	D	T	T	4,169	0,61	n.m. <sup>12</sup>	n.m. <sup>12</sup>	n.m. <sup>12</sup>	2,429	16,7	0,46
94	2	Mikes Pass	basalt <sup>2</sup>	Balmoral	180+	5 YR 5/8	24,4	0,15	0,006	A	T	D	T	T	4,162	0,81	n.m. <sup>12</sup>	n.m. <sup>12</sup>	n.m. <sup>12</sup>	2,424	20,3	0,61
103	2	Richmond	shale <sup>3</sup>	Griffin	220-330	10 YR 7/8	36,2	0,31	0,009	SD	SD	D	-	T	4,147	0,26	2,666	22,6	0,26	2,426	18,9	0,28
152	14	Platt	granite <sup>4</sup>	Oatdale	160-175	10 YR 7/8	14,6	0,41	0,028	SD	SD	D	-	T	4,177	0,36	2,691	5,5	0,51	2,441	8,0	0,47
194	2	Inopo	shale <sup>3</sup>	Farmhill	230-350	10 YR 7/8	n.d.	n.d.	n.d.	SD	SD	D	-	T	4,177	0,56	2,685	9,6	0,46	2,440	8,7	0,42
89	3	Port Edward	sandstone <sup>7</sup>	Inanda	120-140	7,5 YR 5/8	20,9	0,85	0,041	SD	SD	D	T	T	4,157	0,37	n.m. <sup>12</sup>	n.m. <sup>12</sup>	n.m. <sup>12</sup>	2,426	18,9	0,62
56	4	Tala	tillite <sup>6</sup>	Arrochar	175-190	10 YR 7/8	35,6	0,31	0,009	SD	SD	D	-	T	4,185	0,46	2,688	7,5	0,37	2,442	7,3	0,41
61	2	Sundays R.	sandstone <sup>8</sup>	Oatdale	130-150	10 YR 7/8	n.d.	n.d.	n.d.	SD	SD	D	-	T	4,170	0,51	2,686	8,9	0,48	2,440	8,7	0,48

intrusions in Ecca Series (Karoo System)  
 toruberg Series (Karoo System)  
 retoria Series (Transvaal System) (Smelterkop shales)  
 upper Ecca Series (Karoo System)  
 middle Ecca Series (Karoo System)  
 Wyke tillite (Karoo System)

<sup>7</sup> Table Mountain Series (Cape System)

<sup>8</sup> Basement Complex

<sup>9</sup> Determined after treatment with 5 M NaOH (90°C for 1 hr.)

n.d. = not determined

<sup>10</sup> XRD: D, SD, A, T, and -; Go, Qz, Ka, Hc and An as in Table 1.3

<sup>11</sup> as in Table 1.1

<sup>12</sup> haematite interference



Most of the 13 ferruginous saprolite samples examined (eight) contained goethite with between 15 and 20 mole %  $\text{AlOOH}$  substitution and five with between 6 and 9 mole %  $\text{AlOOH}$ . Hence, Al-substitution in saprolite samples are generally lower than in ferruginous bauxite samples possibly due to differences in hydrology or leaching intensity. The formation of kaolinite in mottled saprolite generally corresponds to more silicious stages which seem to coincide with the maximum extent of ground water fluctuation. In contrast ferruginous bauxite forms in a relatively better drained situation. However, crystallinity of Al-goethite (from XRD line broadening) as a function of degree of Al-substitution in saprolites and bauxites (Tables 1.8 and 1.7 respectively) seems to be similar (see also Figs. 1.6 and 1.7). The similar goethite crystallinity is possibly accounted for by the fact that similar space is made available for Al-goethite crystal growth by removal in solution of silica and alkali and alkaline earth metals during the *in situ* dissolution of ferromagnesian silicates.

#### 1.4.9 Sesquioxidic soil clays and gleys

Over most of the area the soils are strongly to slightly acid and are highly leached (van der Eyk, MacVicar and de Villiers 1969; Fitzpatrick, 1974). The most common soils on gentle to steep slopes in the Highland/Montane and Mistbelt areas (Fig. 2) are yellow and red apedal, freely drained, dystrophic soils (Fig. 1, map symbol No. 2). Of the other soil groups the yellow and grey hydromorphic soils usually with plinthite and ferricrete (Fig. 1, map symbol Nos. 6 - 8) occur on gentler slopes on sandstones and shales in Basin Plainland and Plateau (Highveld) regions (Fig. 2). The red mesotrophic clay soils (Fig. 1, map symbol Nos. 4 and 12) typically occur at lower altitudes and under somewhat drier conditions (Riverine) (Fig. 2), whereas the yellow-brown, humic soils (Fig. 1, map symbol No. 1) occur at high altitudes (above 2 280 m) in the Afro-alpine zone (Fig. 2). Humic soils on Table Mountain sediments (Fig. 1, map symbol Nos. 3 and 14) occur at moderate altitudes parallel to the coastline in the Coastal Hinterland (Fig. 2). Red and grey sands (Fig. 1, map symbol No. 19) occur near the shoreline in the Coastal Lowlands (Fig. 2).

Representative soil samples were taken from these soil zones throughout the area (Fig. 1.1), and have been arranged into four groups as set out in Table 1.9, as follows: Afro-alpine soils (pH ranges between 5.1 and 6.3); dystrophic red and yellow-brown freely drained soils (pH ranges between 4.1 and 5.2); dystrophic, yellow-brown hydromorphic (plinthic) soils (pH ranges



Table 1.9 Sample location, description, and chemical and mineralogical composition of clays from sesquioxidic soils (cl) and gleys (G)

Sample No. (Fig. 1.1)	Soil zone (Fig. 1)	Locality	Soil series	Diagnostic horizon <sup>1</sup>	H horizon	Depth (cm)	Russell colour of clay fraction (powder)	pH KCl	Chemical composition				Mineralogy <sup>2</sup>								d (110) <sup>3</sup>		d (111) <sup>3</sup>			
									Fe <sub>d</sub> <sup>1</sup>	Fe <sub>o</sub> <sup>1</sup>	Fe <sub>o</sub> <sup>1</sup> / Fe <sub>d</sub> <sup>1</sup>	Fe <sub>d</sub> <sup>1</sup>	Ka								Σ	VHM (°2θ)	Σ	mole % AlOOH <sup>4</sup>	VHM (°2θ)	
													Co	He	Mn	An	Qz	Ha	Chl	Ve						Gl
06 Cv (Ga)	1	Lesotho	Blinkklip (humic phase)	Yell. br. ap.	B21	55-65	10 YR 6/6	5.3	4.8	1.81	0.377	14.4	T	-	-	-	A	A	SD	D	-	4.178	1.05	n.m. <sup>5</sup>	n.m.	n.m.
				Yell. br. ap.	B3	110-125	10 YR 6/6	4.3	5.0	1.87	0.374	13.3	T	-	-	-	A	T	SD	D	-	4.177	1.06	n.m. <sup>5</sup>	n.m.	n.m.
15 Cv	1	Sani Pass	Makuya	Yell. br. ap.	B22	30-45	10 YR 6/6	5.1	4.5	1.90	0.422	15.6	T	-	-	-	A	A	SD	D	-	4.177	1.04	n.m. <sup>5</sup>	n.m.	n.m.
				Yell. br. ap.	B23	60-90	10 YR 6/6	5.4	6.0	1.58	0.263	11.5	A	-	-	-	A	T	SD	D	-	4.175	1.03	n.m. <sup>5</sup>	n.m.	n.m.
66 Ma (Cv)	1	Naudesnek	Milford	Yell. br. ap.	B22	70-85	10 YR 6/6	5.7	7.5	1.60	0.243	17.1	A	-	-	-	A	A	SD	D	-	4.172	0.96	n.m. <sup>5</sup>	n.m.	n.m.
05 Cv	1/2	Mikes Pass	Newport	Yell. br. ap.	B22	40-70	10 YR 6/6	4.4	10.3	2.09	0.203	19.4	A	-	-	T	T	SD	A	SD	-	4.169	0.86	2.424	20.3	0.86
85 Fu	2	Tarn	Ouverf	Yell. br. ap.	B22	25-40	10 YR 6/8	5.0	7.6	0.41	0.034	15.2	A	-	-	T	T	D	A	A	-	4.155	0.61	2.425	19.6	0.46
86 Hu	2	Tarn	Balmoral	Red. ap.	B22	35-45	7.5 YR 3/6	4.6	9.7	0.31	0.032	21.4	A	T	T	T	T	D	A	T	T	4.164	0.71	2.426	18.9	0.86
88 Gf	2	Mikes Pass S.	Farmhill	Yell. br. ap.	B21	12-25	10 YR 4/4	4.8	8.3	0.47	0.057	23.5	A	-	-	T	T	D	A	T	T	4.162	0.96	2.424	20.3	0.86
				Red. ap.	B22	35-45	7.5 YR 3/6	4.6	9.6	0.34	0.035	23.7	A	T	T	T	T	D	A	T	T	4.162	0.96	2.423	21.1	0.76
94 Hu	2	Mikes Pass N.	Balmoral	Red. ap.	B21	30-40	7.5 YR 3/6	4.5	8.5	0.26	0.031	20.0	A	T	T	T	T	D	A	T	-	4.164	0.86	2.425	19.6	0.86
				Red. ap.	B23	45-70	5 YR 5/8	4.5	8.9	0.23	0.028	23.1	A	T	T	T	T	D	A	T	-	4.149	0.71	2.425	19.6	0.76
06 Fu	2	Mikes Pass	Ouverf	Yell. br. ap.	B21	30-40	10 YR 5/8	4.5	8.7	0.34	0.039	26.1	A	-	-	T	T	D	A	A	-	4.172	0.41	2.439	9.5	0.56
				Underclay	bg	60-80	10 YR 6/6	4.4	10.0	0.40	0.040	24.1	A	-	-	T	T	D	A	A	-	4.177	0.66	2.436	11.6	0.86
37 Gf <sup>1</sup>	2	Highmoor	Farmhill	Yell. br. ap.	B21	22-60	7.5 YR 6/8	4.2	9.5	0.45	0.048	33.4	A	-	-	T	T	D	SD	T	T	4.164	1.03	2.426	18.9	0.85
				Red. ap.	B22	60-78	2.5 YR 5/8	4.1	13.1	0.50	0.030	41.7	SD	T	T	T	T	D	SD	T	T	4.160	0.76	2.432	14.5	0.85
58 Gf <sup>1</sup>	2	Dunbrook	Farmhill	Yell. br. ap.	B21	20-75	10 YR 6/6	4.3	7.6	0.08	0.011	37.6	A	-	-	T	T	D	SD	A	A	4.165	0.96	2.421	22.5	0.91
60 Hu <sup>1</sup>	2	Thahashlopa	Farningham	Orthic	A1	0-15	10 YR 9/6-9/4	4.0	8.6	0.54	0.063	34.2	A	-	-	T	T	D	SD	A	A	4.155	0.93	2.433	13.8	1.41
				Red. ap.	B22	45-60	7.5 YR 5/8	4.3	10.3	0.65	0.063	30.7	A	T	T	T	T	D	A	A	A	4.159	1.01	2.432	14.5	1.20
16M Cv	2	Dullstroom	Cleavelly	Yell. br. ap.	B22	25-62	7.5 YR 5/8	4.7	8.6	0.57	0.066	35.1	A	-	-	T	A	D	SD	A	A	4.159	0.66	2.423	21.1	0.71
17M Gf	2	Belfast	Farmhill	Yell. br. ap.	B21	30-50	10 YR 6/8	4.6	12.8	0.59	0.046	34.6	SD	-	-	T	T	D	SD	A	T	4.164	0.71	2.430	16.0	0.86
				Red. ap.	B22	50-120	5 YR 5/8	4.7	11.9	0.60	0.030	37.2	A	A	T	T	T	D	SD	A	T	4.162	0.61	2.432	14.5	0.71
38 Hu	2	Belfast	Farningham	Red. ap.	B22	45-75	5 YR 5/8	4.6	9.3	0.20	0.022	26.3	A	T	T	T	T	D	A	A	A	4.169	0.66	2.428	17.4	0.76
12M Gf	6	Piet Retief	Griffin	Yell. br. ap.	B21	35-70	10 YR 6/8	4.7	8.3	0.17	0.020	29.7	A	-	-	T	A	D	A	A	T	4.150	0.56	2.428	17.4	0.78
				Red. ap.	B22	85-130	2.5 YR 4/8	4.5	11.9	0.27	0.023	28.3	A	A	T	T	A	D	A	A	T	4.147	0.53	2.429	16.7	0.76
3M Hu	2	Drasikraal	Balmoral	Orthic	A1	0-30	5 YR 6/8	4.5	4.9	0.16	0.033	29.2	T	A	T	T	T	D	T	T	T	n.m. <sup>5</sup>	n.m.	n.m. <sup>5</sup>	n.m.	n.m.
				Red. ap.	B22	40-90	2.5 YR 5/8	4.5	5.3	0.10	0.019	27.9	T	A	T	T	T	D	T	T	T	n.m. <sup>5</sup>	n.m.	n.m. <sup>5</sup>	n.m.	n.m.
3 Gf	2	Richmond	Griffin	Yell. br. ap.	B21	35-45	10 YR 6/6-5/6	4.4	10.4	0.39	0.038	31.5	A	-	-	T	T	D	SD	A	A	4.157	0.86	2.423	21.1	1.86
				Red. ap.	B22	50-70	5 YR 5/8	4.8	10.4	0.37	0.036	30.2	A	T	T	T	T	D	SD	A	A	4.164	1.06	2.421	22.5	1.06
9 Ia	3	Windy Hill	Inanda	Red. ap.	B22	75-90	5 YR 5/8	5.2	11.1	0.21	0.019	24.2	T	A	T	T	A	D	SD	A	A	n.m.	n.m.	n.m.	n.m.	n.m.
2 Hu	2	Howick	Farningham	Orthic	A1	0-25	10 YR 5/4-5/6	4.3	9.7	0.45	0.046	29.1	A	-	-	T	T	D	SD	A	T	4.172	0.96	2.437	10.9	1.51
				Yell. br. ap.	B21	25-40	7.5 YR 5/6	4.5	12.5	0.12	0.010	34.3	A	-	-	T	T	D	SD	A	T	4.170	1.06	2.429	16.7	1.66
				Red. ap.	B3	60-85	5 YR 5/8	4.7	16.3	0.22	0.013	39.4	T	A	T	T	T	D	SD	A	T	n.m. <sup>5</sup>	n.m.	n.m. <sup>5</sup>	n.m.	n.m.
1 Gf	2	Howick	Farmhill	Yell. br. ap.	B22	30-45	10 YR 4/6-5/6	4.6	10.2	0.30	0.029	27.2	A	-	-	T	T	D	SD	A	A	4.164	0.76	2.427	18.2	0.76
				Red. ap.	B23	55-70	5 YR 5/8	4.9	11.5	0.27	0.023	29.4	A	T	T	T	T	D	SD	A	A	4.165	0.76	2.427	18.2	0.76
5M Gf	4	Wakkerstroom	Griffin	Orthic	A1	0-20	10 YR 7/6-5/8	4.3	5.6	0.39	0.069	27.5	A	-	-	T	A	D	SD	A	T	4.150	0.81	2.423	21.1	1.76
				Yell. br. ap.	B22	25-45	10 YR 5/6-5/8	4.3	6.2	0.30	0.048	26.2	A	-	-	T	A	D	SD	A	T	4.149	0.76	2.421	22.5	0.96
				Yell. br. ap. <sup>6</sup>	B22	25-45	10 YR 5/6-5/8	4.3	5.8	0.27	0.047	28.1	A	-	-	T	A	D	SD	A	T	4.144	0.68	2.418	24.7	0.96
				Red. ap.	B23	48-100	5 YR 5/8	4.1	5.6	0.27	0.048	24.1	A	T	T	T	A	D	SD	A	T	4.147	0.86	n.m. <sup>5</sup>	n.m.	n.m.
				Red. ap. <sup>6</sup>	B23	48-100	5 YR 5/8-6/8	4.1	5.7	0.28	0.049	33.5	A	T	T	T	T	D	SD	A	T	4.160	0.66	2.426	18.9	0.86
4M Gf	16	S. Springs	Ixopo	Yell. br. ap.	B21	35-65	7.5 YR 6/6	5.4	10.3	0.28	0.027	29.6	A	-	-	T	T	D	T	T	-	4.175	0.71	2.431	15.3	0.81
				Red. ap.	B22	65-140	5 YR 5/8	5.8	11.6	0.30	0.026	31.2	A	T	T	T	T	D	T	T	-	4.157	0.64	2.432	14.5	0.81
8 Gf	7	Dirkiesdorp	Appan	Orthic	A1	0-25	7.5 YR 7/8-6/8	4.4	4.2	0.37	0.088	21.6	T	-	-	T	T	D	T	T	-	4.141	0.55	2.409	31.2	0.96
				Yell. br. ap.	B22	35-60	7.5 YR 6/6	4.5	3.8	0.08	0.021	23.1	T	-	-	T	T	D	T	T	-	4.142	0.54	2.412	29.1	1.06
				Underclay		185-200	5 YR 5/8	4.4	4.6	0.04	0.009	22.3	A	T	-	T	T	D	A	T	-	4.157	0.58	2.421	22.5	0.86
Av <sup>2</sup>	2	Normandien	Normandien	Orthic	A1	0-35	10 YR 6/6	4.2	9.6	0.53	0.055	31.6	A	-	-	T	T	D	A	T	T	4.144	0.72	2.423	22.5	1.46
				Yell. br. ap.	B22	40-50	10 YR 6/8	4.3	10.1	0.07	0.007	32.5	A	-	-	T	T	D	A	T	T	4.147	0.71	n.m.	n.m.	n.m.



Table 1.9 (contd.)

Sample No. (Fig. 1.1)	Soil zone (Fig. 1)	Locality	Soil series	Diagnostic horizon <sup>2</sup>	Holozone	Depth (cm)	Munsell colour of clay fraction (powder)	pH KCl	Chemical composition				Mineralogy <sup>7</sup>							d (110) <sup>8</sup>		d (111) <sup>8</sup>				
									Fe <sub>d</sub> <sup>3</sup>	Fe <sub>d</sub> <sup>2</sup>	Fe <sub>d</sub> <sup>3+2</sup>	Fe <sub>d</sub> <sup>4</sup>	Go	He	Mh	An	Qz	Ka	Chl	Mi	Gl	%	WHR (°2θ)	%	mole % AlO <sub>3</sub> H <sub>2</sub>	WHR (°2θ)
									Σ	Σ	Σ	Σ														
98 Av	3	Windy Hill	Normandien	Yell. br. ap.	B22	55-80	10 YR 6/6	4,9	11,6	0,05	0,004	28,1	A	-	-	T	D	A	T	T	-	4,155	0,86	2,429	16,7	1,66
12M Av	7	Dirkiesdorp	Ruston	Orthic	A1	0-30	10 YR 6/6	4,2	4,5	0,27	0,060	26,1	T	-	-	T	D	A	T	-	-	4,141	0,61	2,413	28,3	1,16
				Yell. br. ap.	B22	40-90	10 YR 6/6-6/8	4,5	4,7	0,14	0,030	25,3	T	-	-	T	D	A	T	-	-	4,141	0,61	2,418	24,7	0,81
				Yell. br. ap. <sup>b</sup>	B22	40-90	10 YR 6/6-6/8	4,5	4,7	0,13	0,032	26,4	T	-	-	T	D	A	T	-	-	4,141	0,61	2,412	29,1	0,81
				S. Pl. ym	B23	110-130	7,5 YR 3/6-6/8	4,5	5,5	0,09	0,016	26,7	T	-	-	T	D	A	T	-	-	4,145	0,48	n.m. <sup>9</sup>	n.m.	n.m.
				S. Pl. Red mo	B23	110-130	5 YR 6/8-5/8	4,6	8,8	0,10	0,011	25,8	A	T	-	T	CD	CD	T	-	-	4,160	0,44	n.m. <sup>9</sup>	n.m.	n.m.
				S. Pl. Red mo <sup>b</sup>	B23	110-130	7,5 YR 3/6-6/8	4,6	5,7	0,09	0,016	24,1	A	T	-	T	CD	CD	T	-	-	4,162	0,36	n.m. <sup>9</sup>	n.m.	n.m.
267 Ha	2	Machadodorp	Doveton	Red ap.	B22	45-90	5 YR 5/8	4,7	6,5	0,07	0,011	22,6	A	T	T	T	D	T	SD	-	-	4,157	0,73	n.m. <sup>9</sup>	n.m.	n.m.
268 Ha	6	Piet Retief	Doveton	Red ap.	B22	40-75	5 YR 6/8	4,6	12,8	0,11	0,009	27,8	A	T	T	T	D	T	SD	-	-	4,144	0,61	2,421	22,5	0,66
239 Ha	5	Badplaas	Doveton	Red ap.	B22	35-60	5 YR 5/8-6/8	5,0	7,4	0,13	0,020	21,5	A	T	T	T	D	T	SD	-	-	4,160	0,76	2,429	16,7	0,96
240 Sd	5	Badplaas	Shortlands	Red str.	B22	35-45	5 YR 5/8	4,5	7,5	0,23	0,031	22,1	A	T	T	T	SD	A	SD	-	-	4,162	0,71	2,442	7,3	0,96
241 Sd	4	Albert Falia	Shortlands	Red str.	B22	40-55	5 YR 5/8	5,5	8,1	0,32	0,039	23,2	A	T	T	T	SD	A	SD	-	-	4,177	1,06	2,442	7,3	0,93
4M Sd	5	Steelpoort	Argent	Orthic	A1	0-35	2,5 YR 4/6-3/6	6,0	8,3	0,30	0,036	35,6	T	A	T	T	D	-	T	-	-	4,177	0,71	2,440	8,7	0,76
				Red str.	B22	35-120	2,5 YR 3/6	6,2	13,1	0,31	0,034	33,1	T	A	T	T	D	-	T	-	-	4,177	0,70	n.m. <sup>9</sup>	n.m.	n.m.
156 Ha	19	Unkomaas	Glansthal	Red ap.	B22	45-85	5 YR 5/8	5,3	15,4	0,65	0,042	24,6	SD	T	T	T	D	-	A	-	-	4,177	0,61	2,440	8,7	0,71
					C	210-330	5 YR 5/6	5,6	7,4	0,81	0,109	19,6	A	-	T	T	D	-	A	-	-	4,177	0,78	2,440	8,7	0,81
				Underclay		780+	5 YR 5/6	6,8	12,4	0,91	0,073	26,1	A	T	T	T	D	-	A	-	-	4,165	0,51	2,435	12,4	0,66
GLEYS																										
207 Ka	2	Dullstroom	Katapruit	Gley bn		35-45	10 YR 6/8	6,3	13,6	0,13	0,008	n.d.	SD	-	-	T	D	T	T	-	-	4,178	0,28	2,444	5,8	0,28
208 Ka	2	Dullstroom	Katapruit	Gley mo		35-45	10 YR 7/8	5,6	13,8	0,21	0,015	n.d.	A	-	-	T	D	T	T	-	-	4,165	0,38	2,437	10,9	0,46
156 Ka	2	Ivanhoe	Katapruit	Gley mo		55-70	10 YR 6/8	-	n.d.	n.d.	n.d.	n.d.	A	-	-	T	D	T	T	-	-	4,194	0,76	2,449	2,2	0,81
156 Kd	4	Tala	Volkerust	Gley cut. mo		65-80	10 YR 6/8	5,2	n.d.	n.d.	n.d.	n.d.	A	-	-	T	D	T	A	-	-	4,177	0,32	2,443	6,6	0,32
135 Kd	2	Glangarry	Volkerust	Gley cut. mo		70-85	10 YR 6/8	4,4	n.d.	n.d.	n.d.	n.d.	A	-	-	T	D	T	SD	-	-	4,180	0,51	2,444	5,8	0,51

<sup>1</sup> Samples kindly provided by Dr. M.V. Fey<sup>2</sup> Sample kindly provided by Dr. M. Farina<sup>3</sup> Yell. br. = yellow-brown; ap. = apedal; str. = structured; S. Pl. = soft plinthite; cut. = cutanic  
ym = yellow matrix; mo = mottles; bn = bands (thin)<sup>4</sup> Fine clay fraction (< 0,2 µm)<sup>5</sup> Analysis on untreated clay fractions<sup>6</sup> Analysis on samples pretreated with 5 M NaOH for 1 hour at 90°C<sup>7</sup> D, CD, SD, A, T and -; Go, He, Mh, An, Qz and Ka as Tables 1.1 - 1.2 where Ha = halloysite, Chl = chlorite (pedogenic), Mi = mica,  
Ve = vermiculite, Sm = smectite, Gl = gibbsite<sup>8</sup> as Table 1.1<sup>9</sup> Very weak reflection; n.m. = not measurable

between 4,2 and 4,9); mesotrophic red apedal/structured soils (pH ranges between 4,5 and 6,8) and gley soils (pH ranges between 4,4 and 6,3).

Several researchers, notably de Villiers and van Rooyen (1967) and Fouche and Fölscher (1975) have suggested that iron oxides in red and yellow apedal freely drained, dystrophic soils are amorphous. However, the ratio of  $Fe_O/Fe_d$  in the solums of all the soils examined, except those from the Afro-alpine zone (Fig. 1, map symbol No. 1) is low, being less than 0,10 (Table 1.9; Fitzpatrick, 1974). This suggests that there is no or little ferrihydrite (formerly referred to as "amorphous iron") and that the iron oxides are at an "advanced stage" of crystallinity (Blume and Schwertmann, 1969; Schwertmann, 1964, 1973).

The yellow-brown Afro-alpine soils with higher pH (see Table 1.9), base saturation and organic matter contents, are at a relatively lower degree of development compared with the other soils under discussion (see Appendix 1). It is significant that the Afro-alpine soils have goethite with very high XRD line broadening (i.e. low crystallinity). This tends to support the view that in these soils, goethite is poorly crystalline, which corresponds with their relatively high  $Fe_O/Fe_d$  ratios, probably due to the effect of the relatively "colder" temperate climate on the weathering and consequent release and crystallization of goethite especially in the presence of high organic matter (Schwertmann, 1966; Kodama and Schnitzer, 1977). However, the relatively low amount of oxidic iron ( $Fe_d$ ) together with the fact that chlorite, vermiculite and smectite could not be selectively dissolved by 5 M NaOH treatment (Table 1.9) made it difficult to make accurate measurements of the (110) goethite line, and it was not possible to detect the (111) and (130) lines (Table 1.9).

Fitzpatrick (1974 p.124) observed broad d(110), d(111) and d(130) spacings for goethite that shifted to higher angles for several yellow-brown and red Transvaal sesquioxidic soil clays after treatment with 5 M NaOH, indicating the presence of Al-goethite (similar to Norrish and Taylor, 1961). The magnitude of spacing shifts (and degree of line broadening) was not determined by Fitzpatrick (1974), and hence the AlOOH content of these soil goethites was not estimated. The very high amounts of Al measured in the CBD extracts (i.e.  $Al_d$ ) of chemically untreated clays from Transvaal and Natal sesquioxidic soils (Fitzpatrick, 1974 p.119; Fitzpatrick and le Roux, 1976; Fey, 1974; Fey and le Roux, 1977) often exceed the maximum substitu-



tion of approximately 33 mole % AlOOH reported for synthetic Al-goethites by Thiel (1963) and, Jonas and Solymar (1970) and do not seem to match X-ray line shifts (see Fig. 1.2). However, after pretreating a selected range of soil clays with 5 M NaOH at 90°C for 1 hour (similar to Norrish and Taylor, 1961) and determining Al and Fe in the CBD extracts, there is a fairly good correlation between line shift and Al content of natural goethites (Fig. 1.2). The AlOOH content of goethite, determined mainly by XRD line shift in soil clays varies greatly (Table 1.9), and ranges from approximately 5 mole % (high base status soils) to a maximum of approximately 31 mole % (measured for samples from Avalon and Glencoe soils) which corresponds close to that of Norrish and Taylor (1961) and the maximum reported for synthetic Al-goethites by Thiel (1963) and others.

Using Mössbauer spectroscopy, Golden (1978) recently confirmed the occurrence of finely particulate Al-goethite in the fine clay fractions of four samples (Nos. 16Y, 25 Al, 25Y and 25R)\* from two Transvaal sesquioxidic soils previously characterized by Fitzpatrick (1974) (see also Tables 1.9 and 1.10). Golden (1978) found that the Mössbauer spectra of synthetic Al-goethite showed a decrease in effective magnetic field ( $H_{\text{eff}}$ ) at the iron nucleus with increase in Al-substitution, and derived the following equation relating  $H_{\text{eff}}$  and Al-substitution (mole % AlOOH) at 77K:  $H_{\text{eff}} = 500 - 1.77 (\text{Al})$ . Using this formula and the  $H_{\text{eff}}$  values measured by Golden (1978; his Table 4.14) on the fine clay fractions of 25M Yell. br. ap. and 25M Red ap. the amount of Al-substitution was calculated (Table 1.10). Data obtained for Al-substitution in this thesis (see Tables 1.9 and 1.10) for the fine clay fractions of 25M Yell. ap. (24,7 mole % AlOOH) and 25M Red ap. (18,9 mole % AlOOH) agree quite well with the values obtained by Mössbauer spectroscopy (i.e. 27,6 and 23,7) mole % AlOOH respectively. However, the Al-substitution values calculated from Golden's Mössbauer data for the fine clay fractions (< 0,2  $\mu\text{m}$ ) of 16M Yell. br. ap. and 25M Orthic, are much higher than those determined by the writer on the whole clay fractions by XRD (see Tables 1.9 and 1.10). A possible reason for this is that the fine clays contain a higher degree of Al-substitution than the whole clays (see Tables 1.9 and 1.10) suggesting, as Norrish and Taylor (1961) found, that the smaller particle sizes contain higher Al-content.

---

\* In this thesis (see Tables 1.9 and 1.10) these samples are referred to as 16M Yell.br.ap., 25M Orthic, 25M Yell.br.ap. and 25M Red ap. respectively



Table 1.10 Comparison of XRD (this thesis) and Mössbauer (Golden, 1978) data for 2 Transvaal sesquioxidic soils

Sample No. <sup>1</sup>	Diagnostic horizon <sup>1</sup>	Fraction <sup>2</sup>	X R D			Mössbauer	
			$d(111)$ <sup>3</sup> Å	AlOOH mole % <sup>3</sup>	AlOOH mole % <sup>4</sup>	H <sub>eff</sub> at 77K kG <sup>5</sup>	AlOOH mole % <sup>6</sup>
16M Cv	Yell.br.ap.	C	2,423	21,1	27,0	n.d.	n.d.
		F/C	n.d.	n.d.	n.d.	447	29,9
25M Gf	Orthic	C	2,423	21,1	27,0	n.d.	n.d.
		F/C	n.d.	n.d.	n.d.	441	33,3
	Yell.br.ap.	C	2,421	22,5	28,8	n.d.	n.d.
		F/C	2,418	24,7	31,5	451	27,7
	Red.ap	C	n.d.	n.d.	n.d.	n.d.	n.d.
		F/C	2,426	18,9	24,3	458	23,7

<sup>1</sup> from Fitzpatrick (1974); and in Table 1.9

<sup>2</sup> where C = clay size fraction and F/C = fine clay fraction

<sup>3</sup> determined from the linear relationship between the  $d(111)$  spacing of goethite and diasporite (Fig. 1.2; Table 1.9);  $d(111) = 2,452 - 0,001377$  (Al mole %)

<sup>4</sup> determined from the equation relating Al-substitution and  $d(111)$ ;  $d(111) = 2,453 - 0,00111$  (Al mole %); from Golden (1978; his Table 4.2)

<sup>5</sup> from Golden (1978; his Table 4.14)

<sup>6</sup> determined from the equation relating Al-substitution and  $H_{eff}$ :  $H_{eff} = 500 - 1,77$  (Al mole %) (Golden, 1978)

The exceptionally high values for Al-substitution inferred by Fey and le Roux (1977) (their Table 6) for several Natal sesquioxidic soils were based solely on extracting the "chemically untreated" clay fraction (i.e. natural clay) with CBD ( $Fe_d$  and  $Al_d$ ) and subtracting the  $NH_4$ -oxalate (pH 3) extractable Fe and Al (i.e.  $Fe_o$  and  $Al_o$ ). They did not attempt to measure shift in the (111) or (130) d-spacings nor did they measure Fe and Al in the CBD extracts after treatment with 5 M NaOH as Norrish and Taylor (1961) originally did. The higher values of AlOOH determined in CBD extracts for samples not treated with 5 M NaOH ( $X_1$  in Fig. 1.2) and compared with the corresponding samples after treatment with 5 M NaOH (i) on a water bath for 1 hour ( $X_2$  in Fig. 1.2) and (ii) at 90°C for 1 hour, are probably due to solution of finely particulate gibbsite or silicate minerals. This possibly explains the high values for Al-substitution which Fey and le Roux (1977) inferred from CBD data only.



Only a limited number of topsoils and subsoils from the same profiles were examined in order to compare and evaluate the effect of higher organic matter content of the upper solum on goethite formation. The pattern for Al-substitution in the A horizons of 3 freely drained (non plinthic) dystrophic soils (Table 1.9) compared with that of the B22 and B23 horizons, indicate that there is slightly less Al-substitution and generally more poorly crystalline goethite in the A horizons. This may correspond to some extent to the dissolution of "primary Al-goethite" (see section 1.4.7) by organic matter and reprecipitation of poorly crystalline goethite in the presence of organic matter possibly with less Al-substitution.

The orthic and yellow apedal horizons\* overlying plinthite (i.e. Appam, Normandien and Ruston soils) have the highest amount of Al in the goethite structure (Table 1.9; Figs. 1.5 and 1.6). Additional evidence for this relatively high amount of Al-substitution is obtained from both chemical analysis (Fig. 1.2) and the relatively large shifts in the (110) diffraction line (Table 1.9, and Figs. 1.7 and 1.8). The reason for the high degree of Al-substitution in these soil horizons is not clear but this may be associated with a higher degree of weathering (possibly due to ferrolisis). Furthermore, the fact that goethite in the red "haematitic" mottles in the soft plinthite\* is lower in Al-substitution (i.e. from 110 line shift) and is similar to ferricretes (i.e. plots marked on Fig. 1.7 lie close to the ferricrete positions and the yellow matrix plots between ferricrete and soil clays) suggests that the mottles may in part be relict ferricrete fragments which are in the process of being weathered by ferrolisis (Brinkman, 1970) to a highly Al-substituted goethite in the yellow horizon.

Transmission electron micrographs of untreated and CBD treated soil clays from a Ruston soil (12 M Av) are shown in Plate 1.12 A, B and C respectively. In Plate 1.12 A a general view is given of the  $< 2 \mu\text{m}$  fraction of ferruginous red mottles in the soft plinthite with large electron-dense masses (almost silt size) which are clay particles strongly "cemented together" by Al-goethite and haematite. In contrast, the untreated clay sample from the overlying yellow-brown apedal horizon (Plate 1.12 B) is "more dispersed" with very fine grained Al-goethite adsorbed on the surfaces and edges of clay particles (mainly kaolinite and some halloysite). Extraction of sesquioxides (mainly Al-goethite) from the latter clay by CBD increased

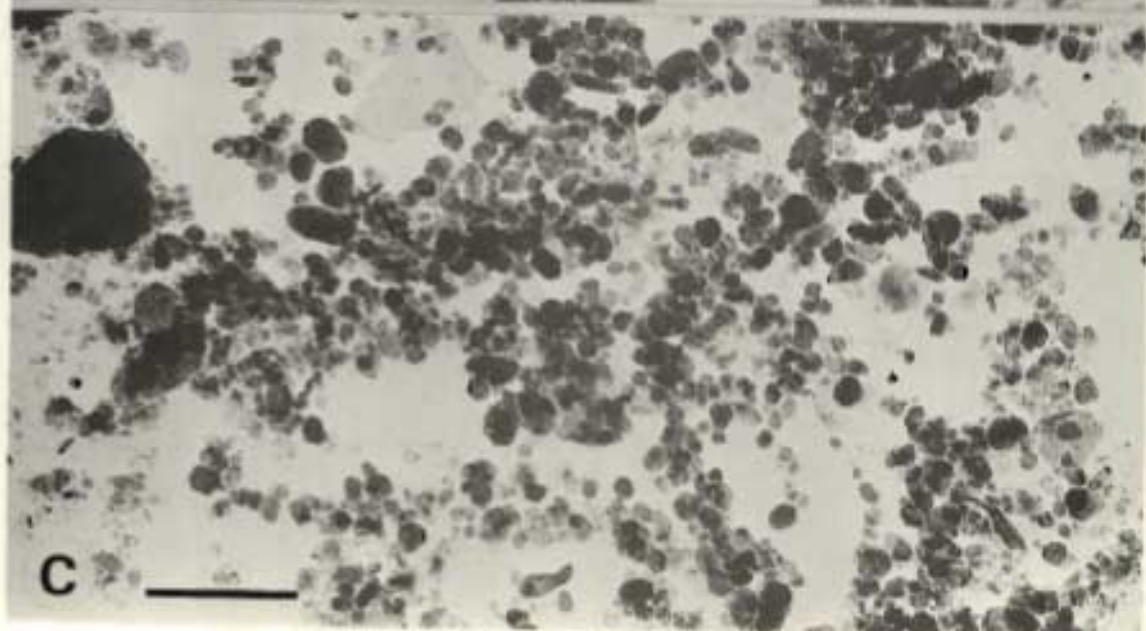
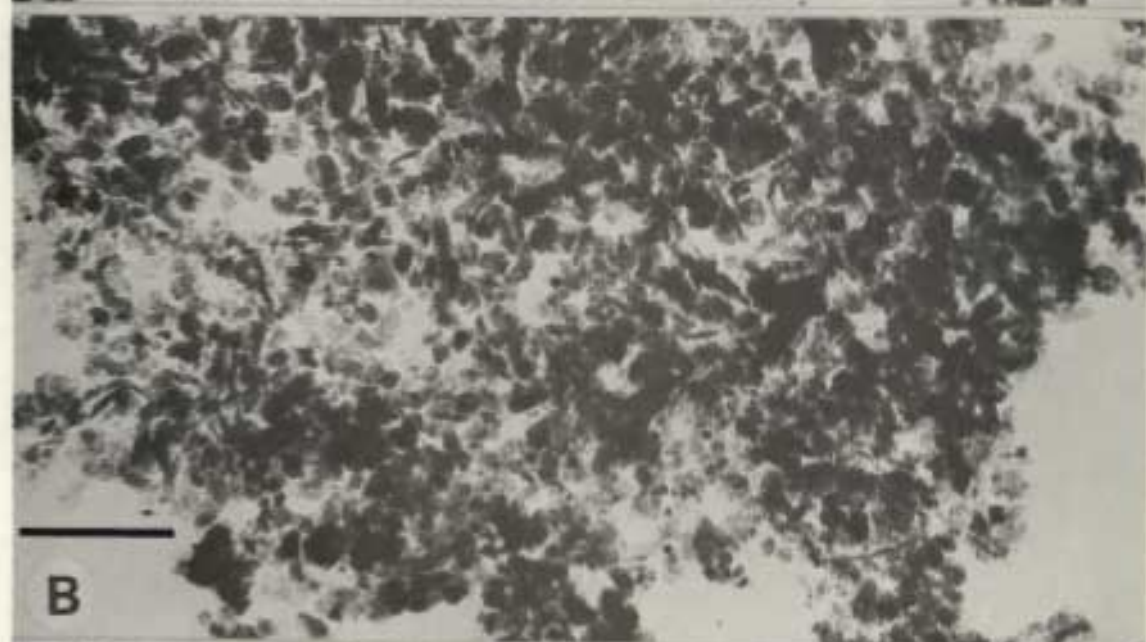
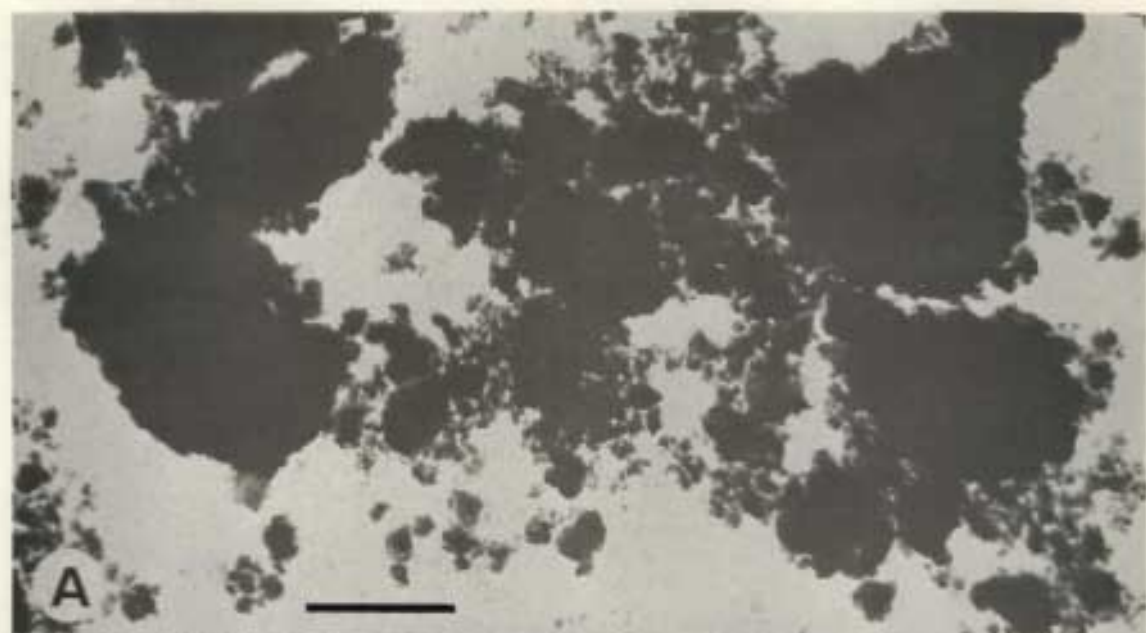
---

\* MacVicar, de Villiers, Loxton *et al.* (1977)

Plate 1.12: Transmission electron micrographs of clays from a Ruston soil (No. 12 M Av).

- A. Untreated clay from ferruginous ( $\text{Fe}_d = 8,8 \%$ ) red mottles in soft plinthite showing large electron-dense, highly flocculated clusters or masses of clay particles strongly "cemented together" by aluminous goethite (and some haematite).
- B. Untreated clay from yellow-brown apedal horizon ( $\text{Fe}_d = 4,7 \%$ ) showing smaller and more dispersed electron dense clusters than in A, with clay particles (mainly kaolinite) coated with finely grained aluminous goethite (i.e. adsorbed on surfaces and edges of clay particles).
- C. CBD treated clay from yellow-brown apedal horizon showing highly dispersed and "cleaned" kaolinite (hexagonal plates) and possibly halloysite (small thin laths). Bar is  $0,5 \mu\text{m}$ .





dispersion and "cleaned" the kaolinite and halloysite particles (Plate 1.12 C). In general agreement with Sumner (1961), Greenland, Oades and Sherwin (1968) and Jackson *et al.* (1973), this demonstrates that Fe (and Al) oxides act as a cementing agent (e.g. in mottles & plinthite) and as aggregating agent in soils with fine granular structure through the interaction (adsorption) mainly of positively charged colloidal iron and negatively charged clay minerals.

Electron optical examination together with mean crystallite dimension [as calculated from the line broadening of the (111) and (110) peaks] show that these Al-goethite particles are small ( $< 150 \text{ \AA}$ ) and this is generally supported by Mössbauer spectra (Golden, 1978).

In the light of recent findings (Fey, 1974; Fey and le Roux, 1976) that Natal strongly weathered soils generally contain small quantities of "amorphous" aluminosilicates (which have a high capacity for phosphorus retention), it is very likely that the finely particulate Al-substituted goethite is of utmost importance in anion adsorption.

The red structured and red apedal high base status soils are generally lower in Al-substitution and have a relatively high line broadening (WHH) (Table 1.9). The relatively low Al-substitution values in these soils are attributable to environmental conditions (e.g. higher pH; Table 1.9) controlling the slow release and uptake of  $\text{Al}^{3+}$ . These soils usually contain some smectite and vermiculite, no gibbsite and generally have lower amounts of kaolinitic minerals compared with the dystrophic, red and yellow soils (Table 1.9). A similar low range of Al-substitution (between 0,0 - 4,0 mole % in "lower zones"; 7,5 - 8,5 mole % in "intermediate zones"; and 10,1 - 11,0 mole % in "uppermost zones") was obtained by Zeissink (1969) in a "smectitic laterite" (SIC) profile (smectite and serpentine in the parent material decrease upward in the profile).

Goethite hand-picked from pores, veins, streaks and vugh fillings in gley materials found in hydromorphic soils in low lying (swamp areas) or other poorly drained areas are low in Al-substitution (between 2 and 10 mole %  $\text{AlOOH}$ ; Table 1.9). Some of the Al-goethite in the gleys (e.g. No. 208) may form in iron-rich saprolite (i.e. *in situ* alteration of Fe-silicate minerals) but in an environment where water movement is sluggish and leaching of silica is impeded.



Aluminous haematite (Schwertmann, Fitzpatrick and le Roux, 1977; Chapter 4) is present in all the horizons with a hue between 2,5 YR and 7,5 YR (i.e. the Al-goethite is generally masked by lesser amounts of Al-haematite) but is absent from those with a hue of 10 YR where only goethite is present (Table 1.9). Additional evidence for haematite, and in relatively small amounts compared to goethite was also obtained by Golden (1978) using Mössbauer spectroscopy at 77K in sample 25R (i.e. 25M Red ap.). Under present day weathering conditions it appears that the red soil colours (haematite) for example in Griffin soils (e.g. No. 25M) are being replaced (i.e. transformed) by yellow colours (goethite) (see Chapter 4). This goethite is possibly stabilized by incorporation of Al into its structure.

### 1.5 Overall discussion

The distribution of goethite containing materials (Fig. 1.1) described in Tables 1.1 to 1.9 in relation to the soil zones (Fig. 1) shows that they have a wide range of occurrence (i.e. soil-climate situations) and vary in morphological, chemical and mineralogical characteristics (i.e. in weathering limestone, geodes, ferricretes, concretions, crusts, pipestems, ferruginous bauxites, saprolites, soil clays and gleys).

Histograms for most of the samples analysed (Fig. 1.5) reveal a wide range in Al-substitution (between 0 and about 32 mole % AlOOH). This negates a recent statement by Nahon *et al.* (1977) that, "lower substitution rates (3 - 10%) are certainly known but they concern a type of Al-goethite little represented in nature." As shown in Fig. 1.5, the various kinds of pedogenic goethites can be roughly grouped according to amount of Al-substitution as follows: geodes < limestone weathering < pipestems and crusts < ferricretes, concretions, gleys and high base status soil clays (Sd) < saprolites and freely drained dystrophic soil clays < ferruginous bauxites < dystrophic plinthic soil clays in yellow-brown apedal (B22) horizons. This grouping is related to the different weathering and depositional environments.

In Fig. 1.6 WHH (crystallinity index) is plotted against Al-substitution [expressed in mole % AlOOH as determined from the shift in (111) spacing] and in Fig. 1.7 WHH is plotted against the shift in (110) spacing, for over 185 different goethite samples described in Tables 1.1 to 1.9 (in Figs. 1.6 and 1.7 they are indicated by symbols used in Fig. 1.1). In spite of the general scattering of the points, Fig. 1.6 shows that a broad correlation ( $r = 0,51$ ;  $p < 0,001$ ) exists between the crystallinity of the samples (as expressed by

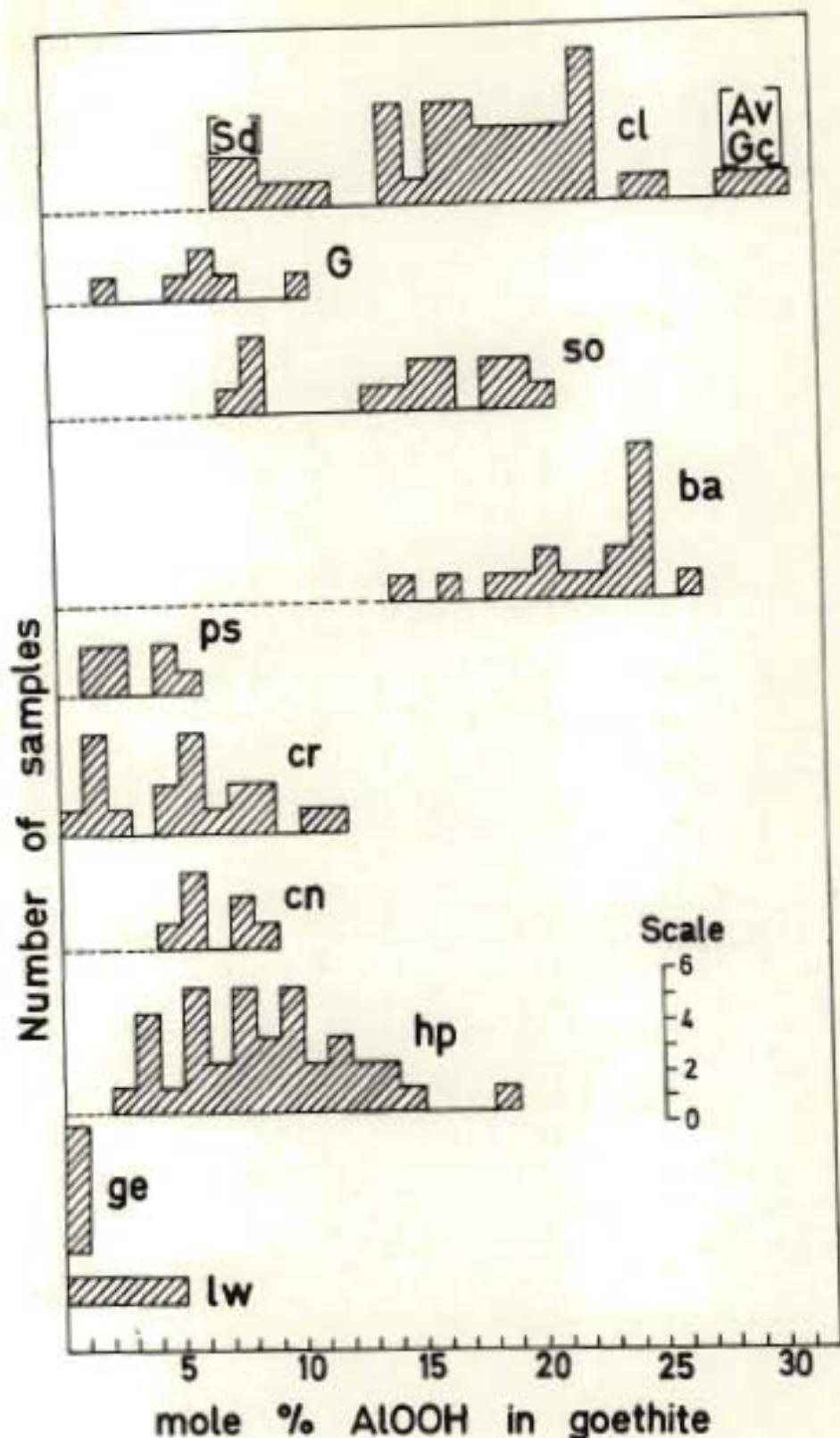


Fig. 1.5: Histogram indicating the relative proportions of Al-substitution in goethite, calculated from the  $d(111)$  line shift, for 183 samples; where: lw = limestone weathering, ge = geodes, hp = ferricretes, cn = concretions, cr = crusts, ps = pipe-stems, ba = ferruginous bauxites, so = saprolites, G = gleys, cl = soil clays, Sd = Shortlands form, Av = Avalon form (dystrophic) and Gc = Glencoe form (dystrophic)



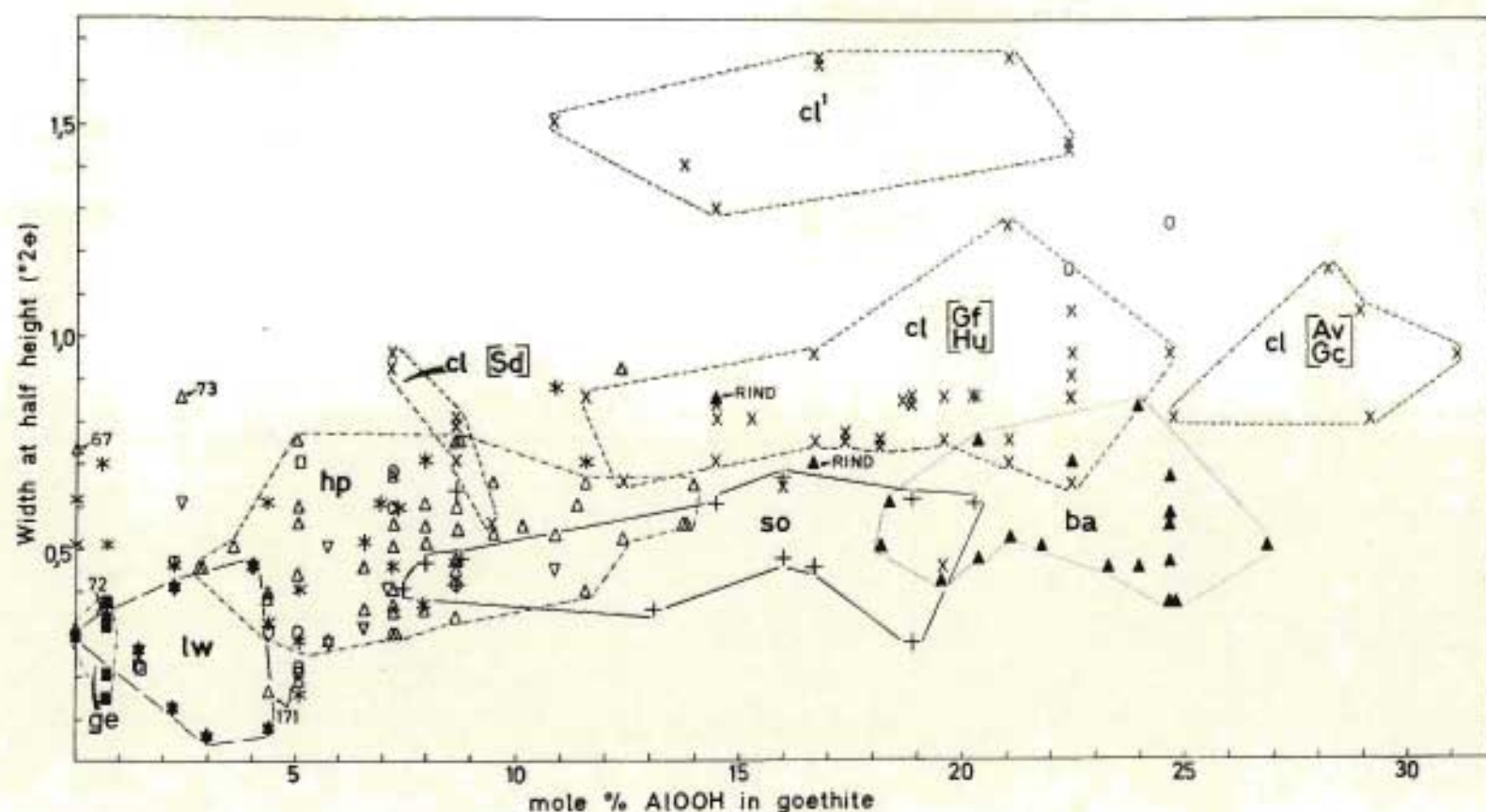


Fig. 1.6: Relationship between width at half height ( $^{\circ}2\theta$ ) and mole % AlOOH in goethite, using the d(111) line for 183 samples; where: lw = limestone weathering, hp = ferricretes, so = saprolites, ba = ferruginous bauxites, cl = soil clays, cl' = soil clays (organic-rich), Sd = Shortlands form, Gf = Griffin form (dystrophic), Hu = Hutton form (dystrophic), Av = Avalon form (dystrophic) and Gc = Glencoe form (dystrophic). Symbols as Fig. 1.1

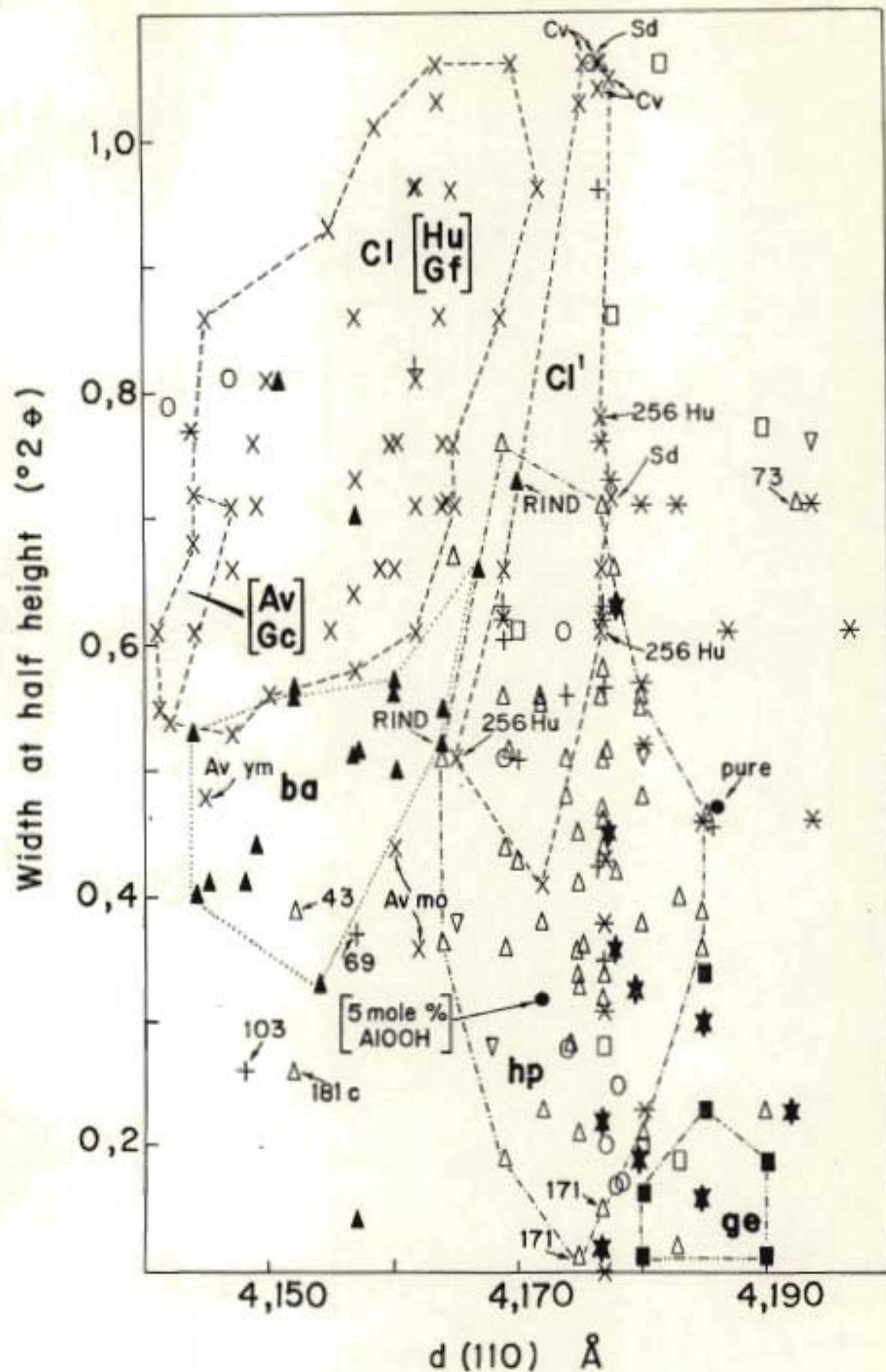


Fig. 1.7: Relationship between width at half height ( $^{\circ}2\theta$ ) and shift in the d(110) line of goethite for 200 samples. Legend as for Figs. 1.1 and 1.6; except where: Cv = Clovelly form (Afro-alpine zone), mo = mottles, ym = yellow matrix, and closed circles (●) = synthetic goethite



line broadening or WHH) and their Al content. However, within each group or kind of goethitic sample there is very little, if any significant correlation. More significant is the fact that these figures group these samples of known origin into several categories with some overlap and this can be observed more clearly by constructing trend lines for each group of goethite material through points in the appropriate area.

Goethite samples derived from the weathering of limestone are all grouped at low Al-substitution values as expected (Al free environment). However, the low  $Al_d$  content measured in some samples is not in accordance with the relatively large shift in d-spacings and in turn the excessive line broadening for certain samples (Figs. 1.6 and 1.7). Similarly, the crust samples show a very variable and erratic distribution of points, generally lying towards low Al-substitution and with very poor crystallinity. The data for these samples therefore suggest that factors other than Al-substitution may control the formation of goethite crystals with low d-spacing and poor crystallinity, especially in certain specific environments. For example, a large number of "interfering compounds" are known to exist in soils even at low concentrations (Schwertmann and Taylor, 1977), such as, Ni, Cr, Ti, Mo, V (Norris, 1975), adsorption or nucleation effects of silicates (Schellmann, 1959; Schwertmann and Taylor, 1972), phosphate (Scheffer *et al.*, 1957) and Ca and Mg (Taylor and Grayley, 1967) and some organic compounds (Schwertmann, 1969/1970).

The geodes are characterized both by a high crystallinity (low WHH) and a low AlOOH content. The ferricretes form a definite intermediate group range, with a clustering of the data from 3 to 14 mole % AlOOH substitution (Fig. 1.6). There is some evidence that goethite with higher  $Mn_d$  content is slightly less crystalline (higher WHH values) suggesting that Mn interferes with crystallization. The goethite in concretions generally fall within the same field as ferricretes, possibly due to similar mode of formation. They are both presumed to form mainly under hydromorphic conditions (i.e. impregnation of  $Fe^{2+}$  from outside under fluctuating water-table conditions).

The fields occupied by saprolites and ferruginous bauxites, which both form under conditions of free drainage, are clearly discernible in Figs. 1.6 and 1.7. Compared with soil clays they are relatively more crystalline and there is a general trend in the ferruginous bauxite field towards higher Al for Fe substitution. The analogous crystallinity may be attributed to their similar mode of formation which is associated with pseudomorphic replacement



of primary iron-silicate minerals (i.e. augites and hornblendes) by Al-goethite. This involves the transfer of Si, Mg and K away from the decomposing grain and the coprecipitation of aluminous goethite close to its source under complex interstitial Eh - pH conditions. The lower "lessivage" (i.e. relatively higher ground water-table) could account for the lower Al-substitution in the saprolites.

Although soil clays have a very wide range of Al-substitution and crystallinity, they may be zoned or split into four definite groups as shown in Figs. 1.6 and 1.7: the dystrophic yellow-brown plinthic soils (Avalon and Glencoe) with highest Al-substitution, the low base status soils (Sd) and gley material with lowest Al-substitution, and the dystrophic red and yellow freely drained soils with intermediate Al-substitution. In topsoil and B21 horizons with high organic matter contents and where "recent" weathering is superimposed on previous *in situ* weathering (e.g. bauxites and saprolites), Al-goethite still appears as the most stable Fe-oxide product but with slightly less Al-substitution and lower crystallinity (Fig. 1.6). Hence, there is the possibility of organic matter interference in goethite formation and crystallinity. Data for humic-rich Afro-alpine soils is similar and tends to cluster together in Fig. 1.7 (Cv). They are not plotted in Fig. 1.6 because the (111) line could not be measured.

Nearly all the materials described above which have formed in a waterlogged environment and/or are coupled with seasonal fluctuation in water-table level (i.e. most ferricretes, concretions, crusts, pipestems, gleys and rinds on ferruginous bauxite nodules) will tend to form "secondary goethite" lower in Al-substitution. In the case of the ferruginous bauxite nodules the rinds with lower Al-substitution (secondary Al-goethite) probably form when the nodules are exposed to an hydromorphic environment. This is due to the fact that Al and Fe are not mobilized and precipitated by the same chemical processes and as a result will tend to segregate during secondary alteration of primary Al-goethite under poorly drained conditions (e.g. Al is not effected by variations in redox potential).

Several kinds of goethitic materials with different degrees of Al-substitution may coexist side by side in one soil profile (e.g. a single highly weathered soil in the study area may contain various forms of goethite in one or more of: saprolite, the interior portion and rinds of ferruginous bauxite nodules, concretions, fragments of ferricrete, soil clays in B22 and



and Al horizons and pipestems) or even in various zones in a single fragment of ferricrete. Similarly, Nahon *et al.* (1977) have detected differences in Al-substitution (particularly in Al-haematites) in various horizons and "facies" in a ferricrete profile from Senegal. Furthermore, they suggest, with little evidence, that Al-goethite with 16 - 22 mole %  $\text{AlOOH}$  dissolves and recrystallizes into goethite and kaolinite. This is not entirely in agreement with the results presented above which indicate that generally lower amounts of Al are incorporated in secondary goethites and that Al-goethite is more the rule than the exception. Kühnel *et al.* (1975) found a general decrease in goethite crystallinity with depth in "laterites" from the Philippines and Indonesia. They mention that both profiles formed *in situ* and show that the goethite in the "altered rock" is lowest in crystallinity. Unfortunately, they do not provide detailed descriptions of these profiles, nor do they give the actual d-spacings or degree of Al-substitution, but from their XRD patterns (their Fig. 3) a shift to lower angles is clearly evident indicating possible Al-substitution with increasing line broadening. It is suggested that their "altered rock" and "uppermost horizon" resemble the saprolite and ferricrete material, respectively, described in the present investigation.

Treatment of a selected range of samples\* with 5 M NaOH on a water bath for 1 hour and at  $90^{\circ}\text{C}$  for 1 hour (c.f. 1.3.2) selectively dissolves kaolinite in soil clays very much more readily than highly crystalline gibbsite in ferruginous bauxite. In agreement with Norrish and Taylor (1961) this treatment did not appear to transform the goethite or alter its d-spacings. More severe NaOH treatment ( $90^{\circ}\text{C}$  for 3 hours and boiling for 1 hour) almost completely dissolved gibbsite in ferruginous bauxite and did not alter the goethite structure. Similarly, the highly Al-substituted goethite in the Ruston soil (12M) also strongly resists alteration and/or transformation even after boiling for 1 hour in 5 M NaOH. However, in soil clays which contain some haematite and goethite (usually with high WHH values) a proportion of goethite decreases and that of haematite increases with increasing time and temperature of NaOH digestion. This transformation from goethite to haematite therefore seems to depend to some extent on the presence and/or amount of haematite in the sample which possibly acts as a

---

\* limestone weathering (No. 262), ferricrete (No. 30), ferruginous bauxite (No. 62 b) and various soil clays (kaolinitic Nos. 25M B22 and 12M B22; haematitic Nos. 4M and 12M red mottles; smectitic No. 241)



lower nucleus for transformation. In addition, the relative resistance of the various kinds of Al-goethites to transform to haematite appears to be related to some extent with degree of crystallinity (WHH). The Al-goethite in ferruginous bauxites is generally very much more resistant to transformation than soil Al-goethite.

In several samples, especially in soil clays with 2 : 1 layer minerals and which are inherently low in oxidic Fe (e.g. Afro-alpine soils) it was not possible to observe and measure the weaker goethite lines [(111) or (130)] due to insufficient concentration of goethite and the fact that 2 : 1 layered minerals resist 5 M NaOH digestion. In certain soils therefore it was only possible to measure the strongest (110) goethite line. For this reason due to the apparent lack of information on (110) spacings in natural samples, it was considered important to investigate the magnitude of the shift (if any) and its line broadening. Although the writer is unaware of any established relationship between the (110) line shift and Al<sub>2</sub>O<sub>3</sub> content in natural or synthetic goethites there appears to be a significant correlation between (110) and (111) with:

$$d_{111} = 0.742 \quad d_{110} = 0.656 \quad (r = 0.884; n = 183; p < 0.001)$$

suggesting that Al-substitution does effect the (110) line by shifting to higher d-spacings. Furthermore, the plot of (110) vs. (111) (Fig. 1.8) shows that these samples fall into several distinct groups, (similar to Figs. 1.6 and 1.7). The ferruginous bauxite samples (Fig. 1.8) fall within an "almost" horizontal band, indicating a larger shift in the (110) spacing. This can possibly be interpreted as being due to the preferential incorporation of Al in a certain direction within the goethite crystal structure presumably due to the ionic environment in the pseudomorphous replacement of primary iron-silicates, whereas in most of the other samples Al probably substitutes for Fe uniformly throughout the goethite structure (i.e. iso-dimensional). According to Taylor and Schwertmann (1978) Al-goethite prepared from a carbonate system is more iso-dimensional than that prepared from KOH or NaOH (i.e. acicular crystals, see also Appendix 2) suggesting that different modes of formation can produce goethite crystals with different morphology. This observation is in general agreement with the morphological data (SEM, TEM and thin sections) of the various natural goethite containing materials which show a wide variation in goethite morphology and crystal size.



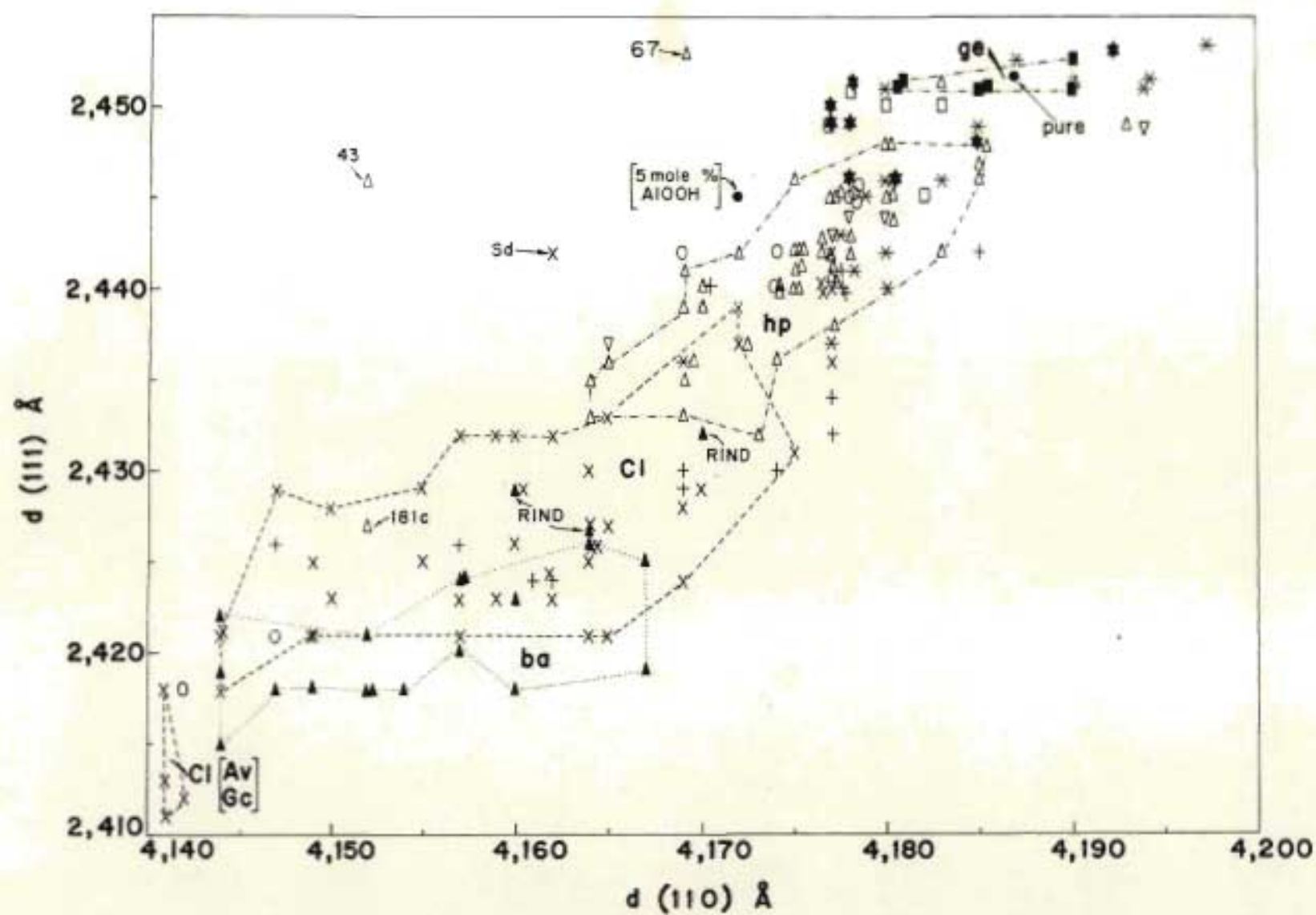


Fig. 1.8: Relationship between  $d(111)$  and  $d(110)$  of goethite for 183 samples. Legend as Figs. 1.1 and 1.6;

## 1.6 Conclusions

Several kinds of pedogenic goethitic materials (in weathering limestone, geodes, ferricretes, concretions, crusts, pipestems, ferruginous bauxites, saprolites, sesquioxidic soil clays and gleys) have been described and identified along the eastern seaboard of South Africa indicating that goethite can form and accumulate under different conditions and is widespread.

Except for soil clays from the Afro-alpine zone and some of the soft ferruginous crust samples, the ratios of  $\text{NH}_4$ -oxalate (pH 3): CBD extractable iron ( $\text{Fe}_\text{O}/\text{Fe}_\text{d}$ ) were low (generally less than 0.1). This supports the XRD data which shows that goethite is mostly present in crystalline form. The relatively high  $\text{Fe}_\text{O}/\text{Fe}_\text{d}$  values for the Afro-alpine soil clays and crusts are probably attributable to iron oxide formed mainly under relatively low weathering intensity and high organic matter conditions whereas the low ratios (i.e. crystalline oxides) can be attributed to increased weathering usually of older land surfaces.

Thin sections together with SEM and TEM show differences in morphology, size and occurrences of goethite and/or Al-goethite in a wide range of materials.

Unless kaolinite and gibbsite are removed from soil clays, ferruginous bauxites and most saprolites by 5 M NaOH digestion prior to XRD analysis there is little chance of determining the d-spacing (and hence the degree of Al-substitution) and line broadening (WHH) whereas in indurated materials (i.e. geodes, crusts, ferricretes, concretions and pipestems) chemical pre-treatment was not necessary because the iron oxides are sufficiently "naturally" concentrated.

The effect of 5 M NaOH treatment was tested using different temperatures and times on a wide range of selected materials. Although d-spacings did not alter after relatively mild treatment, transformation of goethite to haematite did occur in some samples with more drastic treatment, especially where poorly crystalline goethite was present together with some haematite. The relative resistance of Al-goethite to transform to haematite seems to be a function of crystallinity (WHH) and type of material.

The degree of Al-substitution in goethite of various samples (ranging from 0 to about 32 mole %) was determined mainly by shift in peak position



using the linear relationship between the  $d(hkl)$  spacings of pure goethite and diasporite. This relationship was used because current experimental curves tend to give widely varying values that are higher than those from the goethite-diasporite relationship. Thus, further combined XRD, Mössbauer and chemical studies should be conducted on both synthetic and natural materials in order to obtain a more precise working curve.

It is difficult to develop a completely adequate theory of the chemical and mineralogical processes involved in the formation of pure and aluminous goethites. However, knowledge of the distribution pattern of various goethite containing materials in different pedological environments provides supplementary evidence for interpreting the complex geochemical process of genesis, and allows certain conclusions to be drawn.

This study has revealed several pertinent points about the degree of Al-substitution of goethite and environmental relationships. Large differences exist between the degree of Al-substitution for acid freely drained gibbsitic (i.e. ferruginous bauxite) and kaolinitic (i.e. dystrophic sesquioxidic soils and saprolites) samples and the cemented or "hydromorphic" (i.e. ferricrete, concretions, gleys and crusts) samples. Thus, goethite formed in a freely drained acid environment has a high degree of Al-substitution (15 to about 32 mole %  $AlOOH$ ) whereas goethite formed in a hydromorphic or high pH environment has a lower degree of Al-substitution (0 to 15 mole %  $AlOOH$ ). This indicates that the degree of Al-substitution is mainly controlled by ionic environment, which in turn is strongly influenced by several pedological factors such as type of source material, efficiency of leaching and pH.

The influence of Al on goethite crystallinity is indicated by the broad linear relationship between Al-substitution and XRD line broadening ( $r = 0.54$ ;  $p < 0.001$ ). The relatively low correlation between Al-substitution and  $WHH$  suggests that factors other than Al (e.g. other cations and anions or organic matter) probably also control the formation of goethite crystals of poor crystallinity. The relationship between line broadening ( $WHH$ ) and Al-substitution grouped these samples into several categories, and this suggests that it may be useful in further distinguishing the kind of goethite in these ferruginous materials. For example primary Al-goethite in bauxites and saprolites (where Al-goethite forms by *in situ* pseudomorphic alteration of Fe-rich primary silicates under freely drained conditions) is relatively

more crystalline than what could be referred to as "secondary" Al-goethite in soil clays with the same degree of Al-substitution.

The results presented demonstrate a considerable range of properties in goethite (Al-substitution, crystallinity and morphology) from a wide range of pedogenic environments and suggest that further studies of these variations should be carried out in relation to soil genesis especially on samples from further afield. Furthermore, since goethite is the most common and stable form of Fe-oxide in soils the effect of Al-substitution on chemical and physical properties warrants still further detailed study.



## CHAPTER 2

## THE DISTRIBUTION AND NATURE OF SECONDARY MAGNETIC MINERALS

2.1 Introduction

Despite the frequent occurrence of magnetic minerals (e.g. magnetite, Ti-magnetite, maghaemite and Ti-maghaemite) in soils from Natal (Beater, 1940; Frankel and Bayliss, 1966; de Villiers and van Rooyen, 1967), the Southeastern Transvaal (Fitzpatrick, 1974; Fitzpatrick and le Roux, 1975; 1976), Australia (Frankel, 1966b; Faniran, 1970; Taylor and Schwertmann, 1974a), Canada (Pawluk, 1971; Pawluk and Dumanski, 1973), France (Chrétien, 1967), Germany (Schwertmann and Heinemann, 1959), England (Oades and Townsend, 1963), USSR (Sokolovata and Polteva, 1968), Hawaii (Matsusaka and Sherman, 1961; Matsusaka, Sherman and Swindale, 1965), Holland (van der Marel, 1951), Japan (Kojima, 1964) and Cambodia (Mitsuchi, 1976), several explanations for their formation have been offered (Oades, 1963; Mullins, 1977; Schwertmann and Taylor, 1977). There is considerable uncertainty regarding the mechanism of formation of pedogenic magnetic minerals and their composition (Taylor and Schwertmann, 1974a).

Le Borgne (1955, 1960), van der Marel (1951), and Schwertmann and Heinemann (1959) and others mentioned that burning in the presence of organic matter is one of the possible mechanisms for the formation of magnetic minerals in topsoils. However, Oades and Townsend (1963) reasoned that this mechanism could not account for the widespread occurrence of magnetic minerals in soils, and suggested that they formed pedologically (i.e. via ferrous iron in the presence of organic matter at ambient temperatures). Taylor and Schwertmann (1974b) in a study of synthetic Fe(II)-Fe(III) oxide and  $O_2$  systems at low temperature and pressure, suggested that the dominant mode of maghaemite (i.e. considered to be the major pedogenic magnetic mineral in soils) formation is via solution.

On the other hand, Bonifas and Legoux (1957), Matsusaka *et al.* (1965) and Fitzpatrick (1974) suggested that low temperature oxidation of magnetite and Ti-magnetite (i.e. topotactic oxidation) to maghaemite and Ti-maghaemite, respectively might also be a possible mechanism. De Villiers and van Rooyen (1967), and Matsusaka *et al.* (1965) postulated that maghaemite (and Ti-maghaemite) in highly weathered soils may have formed by the dehydration of lepidocrocite. Several other hypothesis



have been suggested, and the problem is not yet resolved.

Several workers (e.g. Tite and Linington, 1975) have suggested that the presence or absence of magnetic minerals in soils (determined mainly by magnetic susceptibility) can be used as indications of soil forming processes. However, Mullins (1977) is of the opinion that because of the uncertainties of the precise conditions favouring pedogenic maghaemite formation, its general use as an indicator of soil forming processes should be treated with caution. In addition, Oades and Townsend (1963) and Mullins (1977), are of the opinion that interpretations of soil forming processes using magnetic susceptibility methods suffer from certain limitations.

Magnetic minerals in soils have been reported to occur in close association with goethite and haematite but not lepidocrocite (Taylor and Schwertmann, 1974a) and in widely varying forms ranging from bulk soil material (e.g. Le Borgne, 1960), concretions (e.g. Beater, 1940; Taylor and Schwertmann, 1974a), clays (e.g. van der Marel, 1951; Oades and Townsend, 1963) and as opaque single grains (Katsura *et al.* 1962; Fitzpatrick, 1974). Furthermore, several of these forms have also been reported to occur in a wide range of climates (e.g. ranging from temperate to subtropical). Thus, one of the basic problems to resolve is that of the relationship between these various "morphological" forms of pedogenic magnetic samples (e.g. concretions, opaque single grains etc.) and their weathering environment. Hence, the identification and characterization of various forms of naturally occurring pedogenic magnetic samples from a single area, with widely varying topography and climate, such as along the eastern seaboard of South Africa (cf. Fig. 2), should provide an excellent opportunity to study the distribution and mineralochemical characteristics of magnetic minerals in different environments.

An attempt has been made by Schwertmann and Taylor (1974a) to selectively dissolve pedogenic maghaemite by boiling in oxalic acid, but the method was not quantitatively standardized. Hence, an attempt will be made, in this study, to test and standardize this method by using synthetic magnetite and maghaemite, and a wide range of natural magnetic materials.

The objective of this study is to describe the occurrence and characteristics of soil magnetic material in the study area and its association with other iron oxides [using visual magnetic attraction



in the field, X-ray diffraction (XRD), magnetic susceptibility, chemical analysis and electron microscopy] in order to elucidate the environmental and pedogeochemical conditions for the formation, transformation and preservation of soil magnetic minerals.

## 2.2 Materials

### 2.2.1 Natural samples

During the course of the land type survey several toposequence and macro-transect (i.e. climosequence) studies were made at about 2000 sites in the study area. The presence or absence of various morphological types of magnetic material was established at these sites in the field, by:

- (i) dipping a small horseshoe-magnet into the soil to attract:
  - (a) magnetic concretions<sup>+</sup> (cn)\*,
  - (b) magnetic opaque single grain particles (sg), and
  - (c) either the bulk soil and/or clay-size fraction (cl)\*, and
- (ii) testing various bands or lenses in saprolites (usually in road cuttings or quarries).

The distribution and relative amounts [expressed as absent to very few (< 1%), few (1 - 5%) or common (> 5%)] of magnetic material in soils was estimated visually in the field using a hand-magnet. Each site was plotted on 1:50 000 topocadastral sheets (i.e. land type field maps) and the amounts recorded.

More accurate estimates of the proportion of various magnetic particles (i.e. concretions and opaque single grains) in each particle size range was obtained by wet sieving, hand-picking and weighing, for a selected range of soils [cf. 2.3.1 (ii) and Table 2.1].

Sixty three ferromagnetic samples from different sites throughout the study area that best illustrated the magnetic bands in saprolites, concretions, clay-size fractions, and opaque single grains in silt- and sand-sized fractions, were carefully selected for laboratory study and are listed in Table 2.2. Locations of these samples are shown in Figs. 2.1 and 1.1

<sup>+</sup> The term "concretion" as it is used here does not necessarily imply concentric layering (similar to Taylor and Schwertmann, 1974 a and c).

\* Symbols used according to abbreviations given by MacVicar, de Villiers, Loxton *et al.* (1977) p.139-141.







Profile descriptions of representative soils used in this study are given in Appendix 1, and relevant descriptive\* and mineralochemical data of most of the clay-size fractions studied are given in Tables 1.9 and 2.2.

In addition, samples of "pure" natural magnetite were obtained from:

- (i) Wards Natural Science Est., Rochester, N.Y. (Marmora, Canada) and
- (ii) a sedimentary deposit in the Middle Ecca beds near Sheepmoor (cf. Visser *et al.*, 1947).

Two sesquioxidic soils from Gregory Falls, Australia (Krasnozems)\*\* and Ribeirão Preto, Brazil (Latosol Roxo)\*\* were also included for comparison.

#### 2.2.2 Synthetic samples

Synthetic magnetite of known composition [22,97% Fe(II) and 48,52% Fe(III)] was obtained from D. M. Farrell (Mineral Sciences Division, Canada), who prepared it by reducing "Mapico Black" (made by Columbian Carbon Company, New York, N.Y.) at 400 °C in a CO:CO<sub>2</sub> atmosphere of 10,6: 89,4 (volume %) with a flow rate of 2,0 l/min. for 3 hours (cf. Farrell, 1972, his Table 1, RMB No. 5).

Maghaemite was prepared from the magnetite (RMB No. 5) by heating in air at 315 °C for 30 minutes (similar to Farrell, 1972, his Table 2).

One g of synthetic magnetite (RMB No. 5) was preground for 15 minutes in a water slurry using an agate mortar and refluxed in 300 ml distilled water for three months in order to study some of the changes (if any) that may occur as magnetite weathers or becomes oxidized. The mineralogical changes were followed by XRD.

---

\* Colour of all samples were determined by the use of Munsell colour charts

\*\* Samples were kindly supplied by R.J. Isbell (Australia), and A.C. Moniz and P. de Souza Santos (Brazil)

## 2.3 Methods

### 2.3.1 Sample pretreatment

The relatively low concentration of magnetic minerals in some samples meant that certain physical and chemical pretreatments were necessary. Depending on the nature of the sample the following pretreatments were carried out:

- (i) Strongly magnetic bands and large fragments. The magnetic minerals (i.e. maghaemite and magnetite) in these materials are sufficiently concentrated "naturally" for XRD measurements (Appendix 3) to be made without prior chemical pretreatment. Therefore samples were finely ground by hand in an agate mortar to pass a 300 mesh sieve and used as such for study.
- (ii) Samples with ferromagnetic concretions and/or opaque single grain particles. Soils were first disaggregated ultrasonically in the presence of 0,0001M  $\text{NH}_4\text{OH}$ , and quantitatively separated by centrifugation (Jackson, 1968) and wet sieving into various particle-size fractions; > 2mm, 1-2mm (coarse sand), 0,5-1mm (medium sand), 0,062-0,5mm (fine sand), 2-62 $\mu\text{m}$  (silt), and < 2 $\mu\text{m}$  (clay).

The strongly ferromagnetic fractions from each particle size fraction were separated by ten or more successive extractions with a small horseshoe-magnet covered with plastic. The magnetic red and/or yellow-brown concretions as well as the opaque (black) single grain particles were separated from each magnetic sand fraction by hand-picking with the aid of a low-power binocular microscope and treated as in (i) for XRD analysis.

- (iii) Parent rock and surrounding weathered material. Chips of unweathered rock (dolerite and basalt) as well as the adjacent weathered isovoluminous material (biscuit-like ferruginous bauxite\* and friable saprolite) were pulverized in an agate mortar to pass a 300 mesh sieve. Samples were then soaked overnight in 0,0001M  $\text{NH}_4\text{OH}$  and treated ultrasonically for 15 minutes. The strongly ferromagnetic fraction was separated by at least ten successive extractions with a small horseshoe-mag

\*See section 1.4.7



- (iv) Soil clays. Several soils clays separated in (ii) were pretreated with 5M NaOH for one hour at 90 °C (method similar to Norrish and Taylor, 1961) in order to selectively dissolve kaolinite and gibbsite because of the generally low concentration of magnetic minerals.

### 2.3.2 Magnetic susceptibility

The magnetic susceptibilities of the soil clays and concretions\* were measured by the Gouy method (cf. Lewis and Wilkins, 1960 and others) at room temperature using, (i) pyrex tubes (2,5mm internal diameter and 100mm in length) stoppered at one end with masking tape, (ii) an electromagnet with a pole gap of 25mm and a pole diameter of 30mm with a field strength of  $10^3$  gauss, (iii) mercury (II) cobaltitetrathiocyanate  $\text{HgCo}(\text{CNS})_4$  crystals [prepared according to the method of Figgis and Nyholm (1958) as cited by Lewis and Wilkins (1960)] as a calibration standard with

$\chi_{20\text{ }^\circ\text{C}} = 16,44 \times 10^{-6}$  c.g.s. units at 25 °C. Both the magnet and the balance were encased in insulated boxes to minimize air current effects and to maintain consistent humidity.

### 2.3.3 X-ray diffraction (XRD)

XRD analysis, using a Phillips P.W. 1050/70 instrument with  $\text{CoK } \alpha$  radiation and a graphite monochromator, was conducted on samples (2.3.1) in randomly orientated form (pressing powder samples in aluminium and/or PVC holders against a filter paper surface, see Appendix 3). Patterns were run from 23° to 46° 2 $\theta$  at a scan rate of 1/4° per min. The spacing and width at half height (WHH) of the (220)\*\* magnetite/maghaemite diffraction peak was determined (see Appendix 3).

Semi-quantitative estimates for maghaemite, magnetite, haematite, goethite and other minerals were based upon relative intensities of diagnostic X-ray diffraction peaks.

### 2.3.4 Chemical extractions

Methods used for extracting samples with citrate-bicarbonate-dithionite (CBD),  $\text{NH}_4$ -oxalate (pH 3) and HCl are outlined in section 1.3.3.

\*Concretions and bands with high magnetic susceptibilities were "diluted" with quartz powder (pure quartz grains were pulverized in an agate mortar) prior to measurement.

\*\*In accordance with Taylor and Schwertmann (1974a) the (220) line was used instead of the most intense line because it was generally free from interferences.

XRD measurements were made on selected representative samples (100 to 500 mg) before and after treatment with (i) CBD (as in 1.3.3), (ii) 0,2 M  $\text{NH}_4$ -oxalate -oxalic acid (pH 3) in the dark for 2 hrs. (i.e. Schwertmann, 1964; as in 1.3.3), (iii) 0,2 M oxalic acid at 90 °C for 1 hour.

### 2.3.5 Total chemical analysis

Total Fe, Ti and Mn contents of selected samples were obtained by dissolving one hundred mg of sample in concentrated HCl and determining Fe and Mn by atomic absorption and Ti by the Tiron method (Pruden and King, 1969). Ferrous iron was determined separately using both the wet chemical technique of Pruden and King (1969), and by titrating the ferrous iron with potassium dichromate, using barium diphenylamine sulphonate as indicator.

### 2.3.6 Electron microscopy

The morphology of selected samples was investigated with the aid of a Hitachi SSM - 2 scanning electron microscope (SEM). Thin flakes from magnetic bands, concretions and ferruginous bauxite, and magnetic opaque single grain particles separated from the 0,062 - 0,5 mm fraction of C and B23 horizons of soils\*, and from pulverized dolerite, were mounted on 15 mm diameter brass stubs using either silver cement or "double-sticky" tape, and then sputter coated with a thin film of gold-palladium.

Transmission electron optical observations (TEM) using a Hitachi Hu - 11E instrument were made on selected samples. Magnetic bands and concretions were first gently crushed and dispersed ultrasonically in distilled water and the < 2µm fraction spotted on carbon coated 200 mesh per inch copper grids.

### 2.3.7 Thin sections

Optical observations were made on thin sections of coherent solid dolerite and adjacent resin-impregnated highly weathered ferruginous bauxite, and magnetic bands.

---

\*Before the magnetic opaque single grains were mounted they were cleaned of surface "debris" (i.e. coatings of fine particles in the clay-size range attached mainly by electrostatic forces) by further ultrasonication for 5 minutes (sonication periods longer than 10 minutes increasingly altered the original surface texture). The 5 minute sonication treatment removed enough of the surface "debris" to permit examination of the surface texture of these particles, but did not remove the "strongly attached" surface "overgrowth" particles.



## 2.4 Results and Discussion

### 2.4.1 Distribution and mode of occurrence

In the study area, the pedogenic magnetic samples were divided into five groups according to their morphology and origin as follows: (i) magnetic bands (bn), (ii) magnetic concretions (cn), (iii) magnetic opaque single grain particles (sg), (iv) magnetic clays (cl), and (v) magnetic bulk soil samples.

#### 2.4.1.1 Magnetic bands

Magnetic bands or lenses occur mainly in freely drained saprolites found in deep road cuttings or quarries and range in shape, thickness (4 to 50 cm), length (10 to 170 cm), colour (black to grey in the centre, and reddish-brown to yellowish-green on the edges), texture (hard, compact and cemented to loose and powdery), and magnetism (Table 2.2; Plate 2.1A). All 15 of the sites where magnetic bands were located, occur in Mistbelt regions (Figs. 2 and 2.1) and are associated with highly weathered yellow and red soils (Fig. 1, map symbol No. 2). Most of the magnetic bands examined have yellowish-brown, ferruginous crusts of varying thickness (2 - 5 cm) covering the bands. Higher proportions of goethite were identified in these crusts (Table 1.5), which tends to form a resistant coating on the bands. The goethite in these crusts which probably formed by weathering of the magnetic bands, has very high  $d(111)$  and  $d(110)$  spacings (i.e. "negative  $\Delta 100H$  values"; cf. Table 1.5), suggesting that  $Fe^{2+}$  is incorporated into the goethite structure.

These magnetic bands probably originated as "black band ore" in bogs and marshes into which streams had carried iron in solution, as colloids, in suspension, and by traction (Visser *et al.*, 1947). With subsequent dolerite intrusions, these sedimentary primary ores were probably metamorphosed together with the sediments, resulting in hard, dense magnetic bands. Subsequently, weathering of the primary magnetic ore (i.e. oxidation) and the formation of secondary goethite occurred as the ore became exposed by Tertiary and Quaternary erosion cycles. According to Visser *et al.* (1947) these sedimentary magnetic ore deposits occur at only a few localities in the Coal Measures and are not confined to any one particular horizon of the Middle Ecca beds.

#### 2.4.1.2 Magnetic concretions

In the study area, soil concretions are generally widespread, and may form substantial percentages of the whole soil profile and/or diagnostic horizon or specific particle size fractions (Table 2.1; Chapter 1)\*. Although it is common in profile descriptions or at observation sites to record the presence of concretions\*, the presence and/or abundance of magnetic concretions are not routinely recorded. However, during the course of the land type survey (while making routine field observations) many soils in the study area were found to contain large quantities of magnetic concretions ranging from fine-sand to gravel-size (Table 2.1; Fig. 2.1).

A high content of magnetic concretions are generally associated with the yellow and red freely drained dystrophic soils (Fig. 1, map symbol No. 2; Fig. 2.1) and may comprise up to about 54% of the total soil (Table 2.1). Several types of magnetic concretions (e.g. colour, shape and "magnetism") have been identified in these soils and seem to be associated with specific soil types or horizons. Low amounts of magnetic concretions (< 1%) are generally found in Vertisols (Table 2.1; Fig. 1, map symbol Nos. 9-11; Fig. 2.1) and in yellow and grey hydromorphic soils with plinthite (Table 2.1; Fig. 1, map symbol Nos. 6-8; Fig. 2.1) and in weakly developed soils (Fig. 1, map symbol Nos. 14-18; Fig. 2.1).

The distribution pattern in Fig. 2.1\*\* shows a soil-climate-terrain zonality of magnetic concretions. They are particularly prevalent in the Mistbelt and part of the Highland Montane regions, in highly weathered yellow and red soils (Fig. 1, map symbol No. 2) on crests and midslopes. In contrast, they decrease with both increasing and decreasing altitude toward the Afro-alpine region on the one hand, and Riverine and Coastal Lowland regions, respectively (Fig. 2). Although Beater (1940), and Frankel and Bayliss (1966) report the occurrence of magnetic concretions "in soils overlying Ecca shales" and in the "vicinity of Gingindlovu" respectively, they do not give any indication of the distribution and abundance.

---

\*cf. profile descriptions by: MacVicar (1962), de Villiers (1962), van der Eyk, MacVicar and de Villiers (1969), Beater (1957, 1959, 1962) and Fitzpatrick (1974).

\*\*More detailed studies may modify these patterns, which to a large extent follow the generalised soil map (Fig. 1), but from the numerous field observations (~ 2000) it should not change markedly.



Table 2.1 Amounts (mass %) of magnetic and non-magnetic concretions from 5 horizons<sup>1</sup> of four different soils

Particle size fraction	Colour	Rensburg <sup>2</sup> (No. 39) Vertic		Ruston <sup>3</sup> (No. 12M) Yell.br.ap.		Griffin <sup>4</sup> (No. 103) Yell.br.ap.		Griffin <sup>4</sup> (No. 103) Red ap.		Farningham <sup>3</sup> (No.42) Red ap.	
		Non-magnetic %	Magnetic %	Non-magnetic %	Magnetic %	Non-magnetic %	Magnetic %	Non-magnetic %	Magnetic %	Non-magnetic %	Magnetic %
> 2 mm	Reddish-brown	18,7	1,2	20,1	0,5	1,2	1,3	5,5	6,7	23,5	34,3
	Yellowish					8,2	6,2	4,3	2,4		3,2
1 - 2 mm	Reddish-brown	7,5	0,5	12,4	0,0	1,0	0,4	3,1	5,6	2,8	14,9
	Yellowish					3,4	4,1	1,0	1,2		0,6
0,5 - 1 mm	Reddish-brown and yellow	1,3	0,1	4,6	0,0	0,8	0,4	2,3	1,1	0,5	0,6
Total %		27,5	1,8	37,1	0,5	14,6	12,4	16,2	17,0	26,8	53,6

<sup>1</sup>Yell.br. = yellow-brown; ap. = apedal; <sup>2</sup>Riverine (Fig. 2); <sup>3</sup>Basin Plainland (Fig. 2);

<sup>4</sup>Mistbelt (Fig. 2)

No magnetic concretions and magnetic bands have been detected in the Afro-alpine zone (Fig. 2.1). Similarly, the relatively young soils of the Coastal Lowland and Riverine regions where soil pattern differences generally follow geological boundaries (Beater, 1957, 1959 and 1962) the amount of magnetic concretions range from absent to few (Fig. 2.1). Generally, relatively few magnetic concretions (< 5%) occur in the gently rolling Coastal Hinterland and Basin Plainland regions (Figs. 2 and 2.1). In the Afro-alpine region, the soils are mostly young (Fig. 1, map symbol No. 1) and contain high amounts of slightly altered primary magnetite and Ti-magnetite derived from basalt (e.g. single grain particles) in the sand- and silt-size fractions.

The presence of both magnetic bands and concretions in the Mistbelt and Highland Montane regions and in highly weathered, freely drained soils closely associated with basic igneous rocks indicates that they may have a similar mode of formation. Geochemically the Mistbelt and Highland Montane regions may have a slightly "reducing character" as evidenced by the continuous (i.e. throughout the year) presence of moisture in the soils or the relatively moist conditions which prevail, although the presence of goethite and haematite (cf. 1.4.9) suggests that conditions are predominantly oxidizing. Such environmental conditions could well be ideal or optimal for the formation of maghaemite. According to Taylor and Schwertmann (1974a), and Schwertmann and Taylor (1977) slow oxidation and simultaneous dehydration conditions, together with an ample supply of  $\text{Fe}^{2+}$  (i.e. from the weathering of primary ferro-magnesian silicates found in basic igneous rock) appears to favour maghaemite formation.

Large rounded magnetic fragments or nodules (cf. Plate 2.1B) coated with hard resistant goethite rinds occur mainly on the soil surface or in stonelines but may also be scattered throughout the upper parts of the solum of freely drained red and yellow soils in the Mistbelt regions. It appears from the "matrix morphology" of the interior of these rounded fragments, their rather large size, hardness and mineralogy (see below) that they are similar to the magnetic bands. It is possible that these rounded fragments are weathered fragments of the magnetic bands or layers which have become exposed by erosion, broken up and have been transported by colluviation and become rounded.

In the Mistbelt and Highland Montane regions where relatively higher amounts of magnetic concretions generally occur, lower amounts seem



to occur in soils underlying sandstone or granite compared with those overlying basic igneous rocks. In addition, the yellow-brown apedal and their topsoil horizons contain fewer red coloured magnetic concretions and larger amounts of yellow ones, whereas in the red apedal horizons higher proportions of red magnetic concretions occur (Table 2.1). Similarly in Griffin soils (i.e. yellow-brown apedal horizon overlying a red apedal horizon) lower amounts of red (and yellow) magnetic concretions occur in the upper solum, increasing in depth to the B23 but are absent in the saprolite. This suggests a transformation from the red concretions (magnetic and non-magnetic) which contain haematite and/or maghaemite to yellow ones (predominantly goethite), going up the profile.

#### 2.4.1.3 Magnetic opaque single grain particles

Magnetic opaque single grain particles generally range in size from coarse silt through to fine (mainly) and coarse sand (0,03 - 2,00 mm), have shiny, black, metallic-like colour or lustre and when powdered usually have a dark purplish hue (Table 2.2). Although these magnetic single grain particles are fairly common in soils throughout the study area, higher amounts are generally found in freely drained sesquioxidic soils derived from basic igneous rocks. Van Rooyen (1964) reports up to 81,8% (by weight) opaque magnetic minerals in the fine sand fraction (0,074 - 0,211 mm) of a Griffin soil derived from dolerite-shale colluvium in the Mistbelt region. Similarly, in petrographic studies by Verster (1964) relatively high amounts of "magnetite" were noted in fine sand fractions from highly weathered sesquioxidic soils. In addition, these particles are also often found as a black "coal, dust-like" residue in dry water channels after rains or on the beds of rivers adjacent to soils derived from basic igneous rocks.

The occurrence of similar looking metallic-like opaque grains in solid basic igneous rocks (e.g. dolerite) suggests that these grains in soils could well be primary residual weathering products (i.e. detrital) partly inherited from basic igneous rocks. Very little information is available on the weathering of natural primary magnetite and/or Ti-magnetite from igneous rocks (dolerite and basalt), especially under subtropical conditions. Therefore, an attempt was made to study the mineralogical changes associated with the chemical weathering of primary magnetic oxides, by examining the magnetic opaque single grain particles



in both the primary basic igneous rock and adjacent *in situ* weathered material (see below). In addition, a laboratory weathering experiment using synthetic magnetite (cf. 2.2.2) was carried out in order to "monitor" the natural system. Thus, maghaemite (and magnetite) has the almost unique property of being present in some form or other in both basic igneous rocks and soils derived from them. Generally, lower amounts of magnetic opaque single grains seem to occur in bottomland (i.e. hydromorphic) soils and in plinthic soils overlying sandstone (e.g. Fig. 1, map symbol Nos. 6-8). Furthermore, there is a general decrease of magnetic oxides (i.e. magnetite and maghaemite) relative to ilmenite and anatase in the more hydromorphic soils due to "goethitization" and a depletion of the magnetic oxide content as a result of reduction and dissolution.

#### 2.4.1.4 Magnetic clay-size fraction

Clay-size fractions from certain sesquioxidic red soils (i.e. Hutton and Shortlands forms) and ferruginous bauxite samples, derived from basic igneous rocks, may be ferromagnetic (i.e. may be attracted by a hand-magnet) whereas clay-size fractions from yellow-brown apedal soils are not. More quantitative information of the magnetic components in clay-size fractions was obtained from XRD and magnetic susceptibility analysis (see below).

#### 2.4.1.5 Magnetic bulk topsoil samples, attributed to heating

During field studies it was observed that bulk topsoil material (particularly near the surface, and up to a depth of only 2 to 3 cm in freely drained soils) in the Mistbelt and Highland Montane regions were relatively more strongly attracted by a hand-magnet (i.e. the whole soil, including magnetic concretions and opaque single grain particles) than from those in the Riverine regions. Le Borgne (1955, 1960) and others suggested that the increase in topsoil magnetism is possibly due mainly to the application of heat (veld fires) in the presence of organic matter. Heating soils in a reducing (or partly reducing) atmosphere (i.e. in the presence of organic matter, or under a bed of ash) forms strongly magnetic oxides (maghaemite and/or magnetite), the amount being a function of the degree (i.e. rate) and duration of heating, and the type and amount of ferruginous mineral (i.e. goethite, haematite or lepidocrocite) or organic matter present initially. Nearly all soils throughout the study area have suffered some form of repeated heating, either because of forest or veld fires and repeated clearing of land through burning off of undergrowth or of stubble. Generally, magnetic bulk topsoils were found to be



especially common where such soils were known to be heated by ground fire (e.g. in fire break zones), in contrast to areas under natural forest (i.e. on moist south facing slopes in the Mistbelt and Highland Montane regions) or in old pine plantations where ground fires have not occurred in recent times. For these reasons, the formation via heating of the ground surface appears to be a more plausible explanation than pedogenic formation (i.e. via ferrous iron in the presence of organic matter at ambient temperatures as suggested by Oades and Townsend, 1963). However, further research is required before the genesis of the magnetic minerals (probably maghaemite) in these topsoils can be fully explained.

The relatively higher proportion of "finely divided magnetic minerals" attributed to heating of surface horizons of soils in the cooler regions (Mistbelt and Highland Montane) is possibly due to the higher organic matter contents of these soils, and the relatively slower rate of burning which possibly provides ideal  $CO:CO_2$  ratios for the formation of maghaemite from finely divided goethite (cf. Chapter 1) and organic matter (i.e. by reduction). In contrast, the soils in the dry Riverine regions have relatively low organic matter contents, and veld fires in these regions tend to burn more rapidly.

The same trend described above, has also been observed frequently in soils that have suffered recent burning and which were originally covered with natural grass vegetation. It is fairly common in the Mistbelt and Highland Montane regions, for the surface layer of soils which have suffered recent veld burning (and which are highly magnetic) to have a slight "brick-red" or pinkish-red colour. This phenomenon is relatively uncommon in the Riverine regions, due mainly to the lower organic matter contents and sparse vegetation cover.

From the former discussions it can be concluded that the total magnetic moment of a bulk soil sample is made up of several components. This is particularly so in the Mistbelt and Highland Montane regions where soils may contain substantial amounts of concretions, opaque single grain particles and magnetic bands. For this reason, accurate or quantitative measurement by magnetic susceptibility methods on whole or bulk soil samples in order to estimate the "magnetism" attributable to that produced by heating suffers from certain limitations, unless the other magnetic components are selectively removed. This contention is supported, in part, by Oades and Townsend (1963).

### 2.4.2 X-ray diffraction analysis

All the selected magnetic samples were examined by XRD as a preliminary to further work. The results are shown in Table 2.2 where the  $d(220)$  spacings for maghaemite and magnetite<sup>†</sup>,  $WHH$  values for the (220) line and  $MCD$ <sup>\*</sup> are given, together with amounts of accessory minerals, sample descriptions and localities (samples are listed in groups in the following order: synthetic magnetite and maghaemite, natural magnetite, magnetic bands, magnetic concretions, magnetic opaque single grains and clay-size fractions).

The  $d(220)$  spacings obtained for pure synthetic magnetite and maghaemite are  $2,967\text{\AA}$  and  $2,951\text{\AA}$ , respectively (Table 2.2). This is in good agreement with the spacings quoted for magnetite ( $2,967\text{\AA}$ ) and maghaemite ( $2,950\text{\AA}$ ) in the 1972 ASTM data file.

The  $d(220)$  XRD spacings for the sample collection varies between  $2,931$  and  $2,971\text{\AA}$  (Table 2.2), and the unit-cell parameters ( $a_0$ ) calculated from the  $d(220)$  line, varies from  $8,293$  to  $8,407\text{\AA}$ , respectively.

This wide range in  $d(220)$  and  $a_0$  values (Table 2.2 and Fig. 2.2) may be due to several factors: (i) a continuous solid solution series between magnetite [ $d(220)=2,967\text{\AA}$ ;  $a_0=8,396\text{\AA}$ ] and maghaemite [ $d(220)=2,950\text{\AA}$ ;  $a_0=8,350\text{\AA}$ ]<sup>\*\*</sup> so that some of the higher  $d(220)$  and  $a_0$  values are possibly from cation deficient (oxidized) magnetites (or Ti-magnetites) or from maghaemites (or Ti-maghaemites<sup>††</sup>) possibly containing some magnetite (or Ti-magnetite), or (ii) isomorphous substitution of Al for Fe in the maghaemite structure to give lower  $d(220)$  or  $a_0$  values (Beneslavsky, 1957).

<sup>†</sup>The  $d(220)$  line was chosen in preference to the most intense line because it was generally free from interferences by haematite and ilmenite.

<sup>\*</sup>Mean crystallite dimension, as calculated from the (220) peak using the Scherrer formula:

$MCD = K\lambda / (B - b) \cos\theta$  in which  $K$  is constant (0.9),  $\lambda$  the wavelength of the X-radiation,  $B$  the measured width at half height ( $WHH$ ),  $b$  the instrumental line broadening (see Appendix 3) and  $\theta$  the Bragg angle of the respective line used.

<sup>\*\*</sup>Values ranging from  $8,30$  to  $8,35$  have been reported in the literature for maghaemite (cf. Lindsley, 1976; his Table L-4). This discrepancy for  $a_0$  is in line with the general disagreement and confusion regarding the structure for maghaemite.

<sup>††</sup>Oxides in which  $Ti(IV)+Fe(II)$  replaces  $2Fe(III)$  in maghaemite.



Table 2.2 Sample location, description and mineralogical composition of magnetic samples

Subsample No. (Figs. 2.1 & 1.1)	Soil zone (Fig. 1)	Locality	Subsample description <sup>1</sup>	Munsell Colour (Powder)	Mineralogy <sup>2</sup>							d(220) $\bar{A}$	VMI °2 $\theta$	MCD $\bar{A}$
					Mh	Ha	Go	Qz	Ka	Il	Mt			
-	-	-	Synthetic magnetite (cf. 2.2.2)	2,5 Y 3/0	-	-	-	-	-	-	D	2,967	0,20	1 615
-	-	-	Synthetic maghaenite (cf. 2.2.2)	2,5 YR 3/4	D <sup>8</sup>	T	-	-	-	-	-	2,951	0,20	1 615
-	-	Canada	Marmora, Ontario (Wards, cf. 2.2.1)	2,5 Y 3/0	-	-	-	-	-	T	D	2,969	0,14	> 1 $\mu$ m
721	4	Shaspmoor	Deposit, hard greyish-black zone (~ 120 cm thick)	2,5 Y 3/0	T	T	T	A	T	T	D	2,971	0,14	> 1 $\mu$ m
199 c	2	Ixopo N.	bn, friable reddish-brown zone (~ 34 cm thick) (Pl. 2.1A)	2,5 YR 3/6	D <sup>8</sup>	A	A	T	T	-	-	2,950	0,23	1 076
253 a	2	Belfast	bn, powdery brownish-black zone (~ 15 cm thick)	10 YR 3/1-3/2	D	A	A	T	T	-	T	2,935	0,17	3 229
b			bn, powdery greenish-black zone (~ 5 cm thick)	2,5 Y 3/2	D	A	SD <sup>3</sup>	T	T	-	T	2,955	0,18	2 422
187 b	2	Ixopo S.	bn, friable greenish-grey zone (~ 25 cm thick)	10 YR 3/1-3/2	D <sup>8</sup>	A	A	T	T	-	-	2,951	0,22	1 211
160 a	2	Hella-Hella	bn, friable to powdery black-grey zone (~ 5 cm thick)	10 YR 3/2-3/1	D	SD	T	T	T	-	T	2,955	0,24	969
b			bn, friable crust on edge of bn (~ 1 cm thick)	10 YR 3/2	D	SD	A	T	T	-	T	2,949	0,25	881
1030f d	2	Richmond	cn, hard dark-brown (~ 5 cm diam.) (Pl. 2.1 B) in sl of Griffin soil (~ 45-50 cm)	7,5 YR 4/4	D <sup>8</sup>	T	A	T	T	-	-	2,948	0,28	692
			-pretreatment with CBD: 1x1h; Fe <sub>d</sub> = 18,3%	5 YR 4/2-3/2	D <sup>8</sup>	T	A	T	T	-	-	2,948	0,21	1 384
e		Richmond	-pretreatment with 0,2M NH <sub>4</sub> -oxalate pH <sub>3</sub>	10 YR 5/6-4/6	D <sup>8</sup>	T	A	T	T	-	-	2,948	0,22	1 211
			cn, >2 mm fr. hard, yellow-brown at 35-45 cm, B21 hor.	2,5 YR 3/6	D <sup>8</sup>	T	A	T	T	-	-	2,945	0,26	807
f			cn, 1-2 mm fr. hard, yellow-brown at 35-45 cm, B21 hor.	5 YR 4/6-2,5 YR 3/6	D <sup>8</sup>	T	A	T	T	-	-	2,934	0,36	440
g		Richmond	cn, >2 mm fr. hard, reddish-brown at 50-70 cm, B23 hor.	2,5 YR 3/6	D	A	A	T	T	-	-	2,932	0,45	312
h			cn, 1-2 mm fr. hard, reddish-brown at 50-70 cm, B23 hor.	2,5 YR 3/6	D	A	A	T	T	-	-	2,932	0,38	404
428a a	2	Howick	cn, >2 mm fr. hard, brown-black, B22 hor.	2,5 YR 3/6	D <sup>8</sup>	SD	T	T	T	-	-	2,938	0,32	538
			-pretreated with CBD: 1x1h, Fe <sub>d</sub> = 17,5%	7,5 YR 4/4	D <sup>8</sup>	A	T	T	T	-	-	2,940	0,28	692
b			cn, >2 mm fr. hard, yellow-brown, B22 hor.	5 YR 4/6	CD	CD	A	T	T	T	-	2,936	0,40	373
d			cn, 1-2 mm fr. hard brown-black, B22 hor.	5 YR 4/6	D <sup>8</sup>	SD	T	T	T	T	-	2,939	0,33	510
			-pretreated with CBD: 1x1h, Fe <sub>d</sub> = 16,2%		D <sup>8</sup>	A	T	A	T	T	-	2,940	0,27	745
e			cn, 1-2 mm fr. hard yellow-brown, B22 hor.	5 YR 4/8	D <sup>8</sup>	SD	A	A	T	T	-	2,941	0,31	570
g			cn, 0,3-1 mm fr. hard yellow-brown, B22 hor.	5 YR 3/3	D <sup>8</sup>	A	A	A	T	T	-	2,939	0,30	605
h			cn, 0,062-0,5 mm fr. hard yellow-brown, B22 hor.	5 YR 4/4	CD	CD	A	A	T	T	-	2,938	0,35	461
238Hu	2	Belfast	cn, 0,062-2 mm fr. hard, brown, B 22 hor.	5 YR 4/4	SD	D	T	A	A	T	-	2,943	0,36	440
991a	3	Windy Hill	cn, 1-2 mm fr. hard, brown-black from Inonda soil, B21 hor.	5 YR 4/8	SD	D	T	A	A	T	-	2,940	0,35	461
172		Gingindlovu	cn, 1-2 mm fr. hard, brown-black on soil surface	5 YR 4/8	A	SD	D	T	T	-	-	2,940	0,50	269
1730f	2	Wesa	cn, >2 mm fr. in sl from Griffin soil	10 YR 5/8	CD	T	CD	T	T	-	-	2,948	0,19	1 937
62 a	2	Pietermaritzburg (cf. Plate 1.9)	eg. from dolerite core	10 YR 3/1	T	-	-	-	-	A	D	2,969	0,20	1 615
b			eg. from inner rind ba	10 YR 3/2	D	T	A	-	T	A	A	2,956	0,24	807

Subsample No. (Figs. 2.1 & 1.1)	Soil zone (Fig. 1)	Locality	Subsample description <sup>1</sup>	Munsell Colour (Powder)	Mineralogy <sup>1</sup>							d(220)	WBR	MCD
					Mh	He	Go	Qz	Ka	Il	Mt	$\lambda$	$\phi_{20}$	$\lambda$
80GF a	2	Mikes Pass-S.	sg. from basalt core	2.5 Y 3/0	CD	T	-	T	-	T	CD	2,957	0.33	510
b			sg. from spheroidal weathering basalt	10 YR 3/1	CD	T	T	T	T	T	CD	2,958	0.26	807
c			sg. 0.062-0.5 mm fr. from Farnhill soil, C hor.	5 YR 3/2	D	-	-	A	T	-	T	2,950	0.21	1 384
d			sg. - 2-62 $\mu$ m fr. (silt) Farnhill soil, C hor.	5 YR 3/2	D	-	-	A	T	-	T	2,950	0.20	1 615
			sg. 0.062-0.5 mm fr. from Farnhill soil, B22 hor.	5 YR 3/2	D	-	-	T	T	-	T	2,948	0.20	1 615
260Hu	2	Mikes Pass-N.	sg. 0.062-0.5 mm fr. from Balmoral soil, B22 hor.	5 YR 3/4	D	T	-	T	T	-	T	2,950	0.26	807
17M GF	2	Belfast	sg. 0.062-2 mm fr. Griffin soil B22 hor.	5 YR	D	A	T	-	-	A	T	2,964	0.39	387
			sg. - 2-62 $\mu$ m fr.	5 YR 3/2	D	A	T	T	T	A	T	2,954	0.45	312
246 <sup>1</sup> a	2	Ngome	sg. >0.5 mm fr. from composite ba sample	7.5 YR 3/2	CD	T	T	-	-	CD	T	2,961	0.29	646
b			sg. 0.5-0.2 mm fr. " " "	7.5 YR 4/4	CD	T	T	-	-	CD	T	2,954	0.32	538
c			sg. 0.2-0.1 mm fr. " " "	7.5 YR 4/4	D	T	T	-	T	A	T	2,953	0.38	440
d			sg. 0.1-0.062 mm fr. from composite ba sample	5 YR 3/4	CD	CD	T	T	T	T	T	2,952	0.44	323
256Hu	19	Ungahaba	sg. 0.062-0.5 mm fr. from Clanshal soil, B22 hor.	10 YR 3/2	CD	A	T	T	-	SD	CD	2,958	0.30	605
104Cv	1	Sani Pass	sg. 0.062-0.5 mm fr. from Clevelly soil, B22 hor.	5 YR 3/1	CD	-	-	-	-	T	CD	2,965	0.24	949
			sg. - 2-62 $\mu$ m fr. from Clevelly soil, B22 hor.	5 YR 3/2	D	-	-	-	-	T	A	2,959	0.34	484
238Hu	2	Belfast	sg. 0.062-0.5 mm fr., B22 hor.	5 YR 3/3	CD	A	T	T	T	SD	CD	2,966	0.21	1 384
720	3	Hillcrest	sg. from biotite in so derived from granite	5 YR 2.5/1	CD	T	SD	T	-	T	CD	2,966	0.17	3 229
172	19	Richards Bay	sg. 0.062-0.5 mm fr. from Vermood soil, A1 hor.	5 YR 2.5/1-3/1	T	A	T	T	-	SD	D	2,970	0.15	>1 $\mu$ m
12M GF	2	Fan Bult	sg. 0.062-0.5 mm from Griffin, B22 hor.	10 YR 3/1	T	T	T	T	T	D	-	-	-	-
			sg. 0.062-0.5 mm from Griffin, B22 hor.	5 YR 3/2	D	SD	T	T	T	A	T	2,947	0.25	881
23M GF	2	Wakkerstroom	sg. 0.062-0.5 mm from Griffin, B22 hor.	2.5 YR 3/0	T	T	T	T	T	D	-	-	-	-
			sg. 0.062-0.5 mm from Griffin, B22 hor.	5 YR 3/1	D	SD	T	-	T	A	T	2,944	0.40	373
4M Sd a	5	Steelpoort	sg. >2 mm fr. from Argent soil, B22 hor.	5 YR 2.5/1	A	T	-	-	-	T	D	2,970	0.17	2 422
b			sg. 1-2 mm fr. " " "	5 YR 3/1	D	A	T	-	-	T	SD	2,965	0.21	1 384
c			sg. 0.062-0.5 mm fr. from Argent soil, B22 hor.	5 YR 3/2	D	A	T	-	-	T	SD	2,963	0.25	881
d			sg. - 2-62 $\mu$ m fr. from Argent soil, B22 hor.	5 YR 3/3	CD	CD	T	-	-	T	T	2,942	0.43	334
4M Sd	5	Steelpoort	cl. <2 $\mu$ m fr. (5M NaOH treated) from Argent soil, B22 hor.	2.5 YR 3/6	SD	D	T	T	-	-	-	2,936	0.58	220
42Hu j	2	Howick	cl. <2 $\mu$ m fr. (5M NaOH treated) from Farnhill soil, B22 hor.	7.5 YR 4/4	CD	CD	SD	T	T	-	-	2,937	0.60	211
		Australia	cl. <2 $\mu$ m fr. (5M NaOH treated) from Eranosol	2.5 YR 3/6	SD	D	T	T	T	-	-	2,940	0.60	211
		Brazil	cl. <2 $\mu$ m fr. (5M NaOH treated) from Latosol Roxo	2.5 YR 4/6	CD	CU	T	T	T	-	-	2,936	0.45	312
246 e	2	Ngome	cl. <2 $\mu$ m fr. + some silt (5M NaOH treated) from composite ba sample	7.5 YR 5/6	CD	CD	T	T	T	T	-	2,943	0.65	190
246 f	2	Ngome	cl. <2 $\mu$ m (5M NaOH treated) from composite ba sample	7.5 YR 5/6	D	A	A	T	T	T	-	2,931	0.90	127
246	2	Ngome	cl. <2 $\mu$ m fr. (5M NaOH treated) from ba fragment	5 YR 4/6	D	T	T	T	T	T	T	2,936	0.85	136
246	2	Ngome	cl. <2 $\mu$ m fr. + some silt (5M NaOH treated) from ba fragment	5 YR 4/6-4/8	D	T	T	T	T	T	T	2,934	0.75	159

<sup>1</sup>Where: bn = magnetic bands, cn = magnetic concretions, sg = magnetic opaque single grains and cl = clay-size fraction, fr. = fraction, hor. = horizon, ba = ferruginous bauxite. Where: Mh = maghaemite, He = haemite, Go = goethite, Qz = quartz, Ka = kaolinite, Il = ilmenite and Mt = magnetite, D = dominant, CD = co-dominant, SD = sub-dominant.



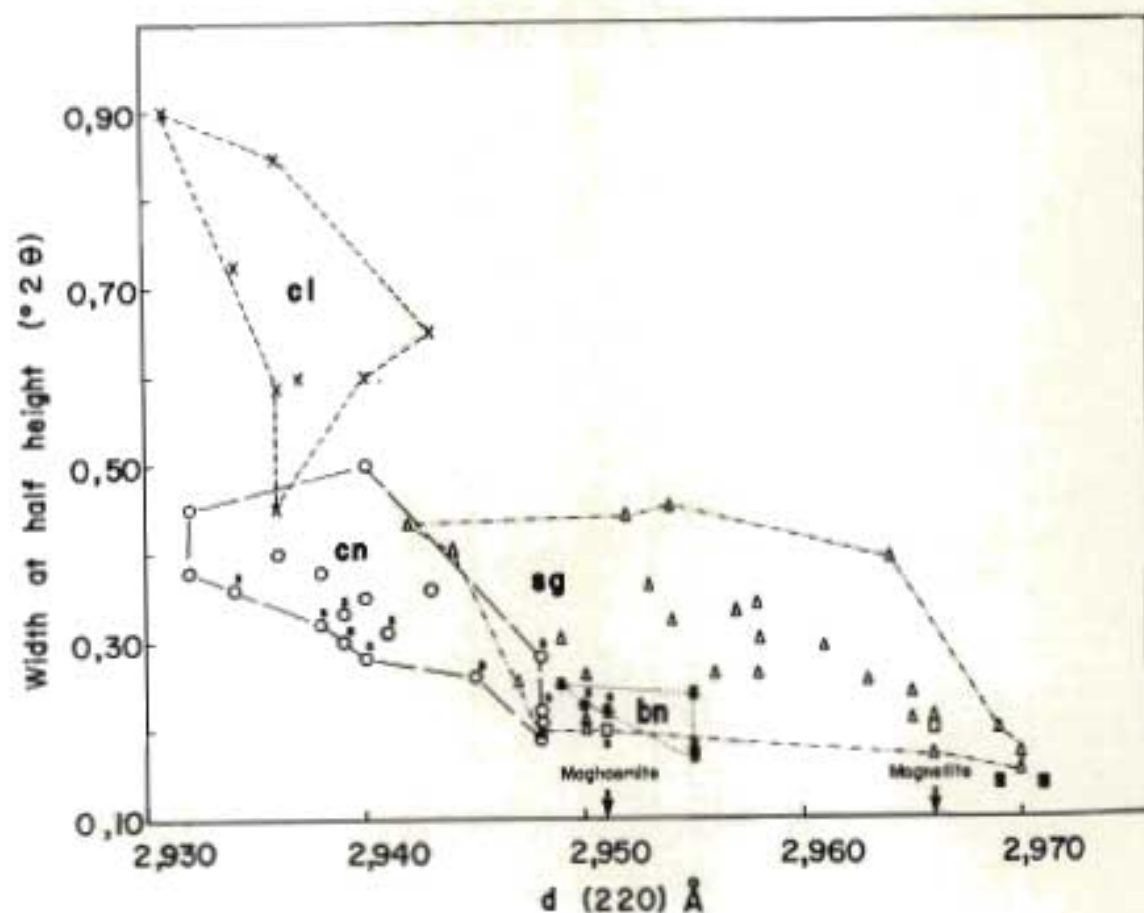


Fig. 2.2: Relationship between width at half height ( $^{\circ}2\theta$ ) and shift in the  $d(220)$  line of magnetite and maghaemite for 63 magnetic samples where : bn = bands, cn = concretions, sg = single grain, cl = clay-size fraction (symbols as in Fig. 2.1), open rectangle  $\square$  = synthetic magnetite and maghaemite as indicated, closed rectangle  $\blacksquare$  = natural magnetite deposits and s = superstructure X-ray diffraction lines

The two most outstanding characteristics of the opaque single grain particles, as compared with the other forms of magnetic materials, are their relatively higher d-spacings (Table 2.2, Fig. 2.2), and Ti(IV) and Fe(II) contents (Fig. 2.4) suggesting that they are cation deficient oxidation products of Ti-magnetite.

In contrast, the ferromagnetic clay-size fractions from soils and ferruginous bauxites have the lowest d(220) spacings ranging from 2,931 Å (i.e.  $a_0 = 8,29$  Å) to 2,943 Å and high line broadening (Table 2.2). Similarly, Beneslavsky (1957) observed a low  $a_0$  value of 8,22 Å for maghaemite in ferruginous bauxites from the USSR, and suggested that the maghaemite structure was considerably altered in size by Al substitution.

The magnetic bands have d(220) spacings (i.e. 2,941 to 2,955 Å) fairly close to that of synthetic maghaemite (2,951 Å), whereas the magnetic concretions have a wide range of values varying from 2,932 to 2,958 Å (Table 2.2, Fig. 2.2). Taylor and Schwertmann (1974a) also observed d(220) spacings for maghaemite in the lower range (between 2,938 and 2,954 Å) for Australian magnetic concretions and suggested the possibility of isomorphous substitution of Al for Fe in their samples. Similarly, Pawluk and Dumanski (1973; their Table 2) also record a relatively low d(220) spacing for maghaemite (2,94 Å) in magnetic concretions from a "poorly drained" soil of Alberta (Canada).

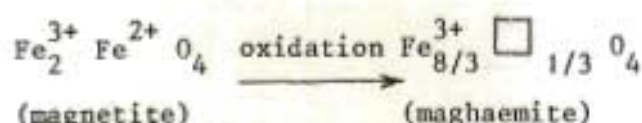
#### 2.4.2.1 Oxidation of magnetite and Ti-magnetite

In the XRD pattern of synthetic maghaemite formed by low temperature (~ 250 °C) oxidation of synthetic magnetite, it was possible to detect tetragonal lines (i.e. superstructure lines) which are forbidden in magnetite (van Oosterhout and Rooijmans, 1958; Braun, 1952). This is in agreement with findings of previous studies on maghaemite formed by low-temperature oxidation of magnetite (Feitnecht and Lehmann, 1959). The line broadening (i.e.  $\Delta 2\theta$ ) of the (220) line for the synthetic maghaemite is similar to that of the original synthetic magnetite (i.e. 0,20°; Table 2.2). In addition, small amounts of haematite were also detected in the synthetic maghaemite sample indicating that some transformation to haematite has also taken place. According to extensive work by Colombo *et al.* (1965), and Gazzarrini and Lanzavecchia (1969) magnetite oxidation can produce a mixture of magnetite, maghaemite and haematite depending on the initial haematite impurity, stacking faults in the initial magnetite and the rate of oxidation.



Moisture content may also influence the rate of transformation (Farrell, 1972; O'Reilly and Readman, 1971).

According to Stacey and Banerjee (1974) the oxidation of magnetite is achieved by a topotactic transformation\* (i.e. the anionic or oxygen cubic structure remains unchanged) and for each Fe(II) ion that diffuses out of the magnetite lattice and is converted to a Fe(III) ion, lattice vacancies are formed:



where  $\square$  represents vacancies produced from 1/3 of the original Fe(II) sites in magnetite. Maghaemite does not have an exact cubic spinel structure because these vacancies are ordered along a particular [100] axis and the repeat-distance is 3 X the cubic unit-cell parameter. Hence, the crystal structure for maghaemite is tetragonal due to its vacancy superstructure which is not present in the cubic spinel structure of magnetite.

Most significant, is the fact that several magnetic bands and concretions from soils in the Mistbelt regions display relatively strong, but somewhat broad superstructure lines (samples in Table 2.2 marked by subscript "s"). However, Taylor and Schwertmann (1974a) stated that they did not observe any superstructure lines for magnetic concretions from Australia, and consequently reasoned that the maghaemite in their samples had a random arrangement of vacant sites.

In contrast, no superstructure lines were detected in any of the magnetic opaque single grains, or clay-sized samples (Table 2.2) possibly due to a different mode of formation. The latter is partly supported by the work of Bernal *et al.* (1959) who detected 3 varieties (i.e. structures) of synthetic maghaemite depending on the process of preparation: (i) only magnetite lines are observed (true spinel structure) (ii) superstructure lines are observed which can be indexed on the assumption of a cubic primitive cell (iii) superstructure lines are observed which can be indexed with a tetragonal cell in which  $c=3Xa^{**}$  (Van Oosterhout and Rooijmans, 1958).

\* "phenomenon of mutual orientation of two or more crystals of different species resulting from solid state transformation or a chemical reaction" (Bailey, 1977).

\*\* which appears after slightly more than two thirds of the  $\text{Fe}^{2+}$  ions have been oxidized.

Hence, a variety of maghaemite structures (pure) is possible, depending on the method of formation. In addition, the incorporation of Ti and/or Al in the maghaemite structure may also produce a more random distribution of the vacancies. Furthermore, not all of the structures reported for maghaemite (i.e. ordered vacancies, primitive cubic and tetragonal) have been found for titanomaghaemites.

The XRD data presented in Table 2.3 after refluxing preground synthetic magnetite for 3 months shows only slight decreases in d-spacings (i.e. decrease in cell size) together with increases in line broadening (i.e.  $WHH$ ), suggesting weak oxidation and limited formation of cation deficient spinel (perhaps as a surface layer only). No superstructure lines were observed, possibly due to the weak development of the cation deficient spinel.

Table 2.3 Variation of XRD data for the (311) and (220) lines for magnetite after refluxing synthetic magnetite for 3 months

Sample	$d_{311}$		$d_{220}$	
	$\text{\AA}$	$\frac{WHH}{\circ 2\theta}$	$\text{\AA}$	$\frac{WHH}{\circ 2\theta}$
Synthetic magnetite <sup>1</sup>	2,532	0,22	2,966	0,20
Refluxed for 3 months, side of flask <sup>2</sup>	2,528	0,26	2,962	0,24
Refluxed for 3 months, bottom of flask <sup>3</sup>	2,529	0,26	2,964	0,24

1. After pregrinding synthetic magnetite (cf. 2.2.2) for 15 minutes in a water slurry in an agate mortar.
2. Sample material scraped off the interior walls of the flask after refluxing the preground synthetic magnetite for 3 months.
3. Bulk of sample material recovered from bottom of flask after refluxing the preground synthetic magnetite for 3 months.

Readman and O'Reilly (1970), and O'Reilly and Readman (1971) have produced non-stoichiometric or cation deficient Ti-magnetites by pregrinding titanomagnetites in a water slurry followed by oxidation in air at temperatures  $< 300^{\circ}\text{C}$ . From their kinetic oxidation data they speculated that wet ground samples could be "appreciably oxidized at room temperature over a period of  $10^6$  y", and that Ti ions have no stabilizing effect due to "vacancy concentrations".



Hence, under favourable pedogenic conditions (i.e. time for prolonged oxidation at ambient temperatures, pH, Eh and moisture status) detrital Ti-magnetite and/or magnetite could become oxidized to cation deficient Fe-Ti spinel oxides with the general formula  $\text{Fe}_a\text{Ti}_b\Box_c\text{O}_4$  (where  $a+b+c=3$  and  $\Box$  denotes a vacant lattice site). This oxidation mechanism has been partly demonstrated by comparing the XRD (Table 2.2), chemical and optical analysis (below) of magnetic grains extracted from crushed solid dolerite (No. 62a) and basalt (No. 88a) with those extracted from adjacent weathered ferruginous bauxite (No. 62b) and saprolite (No. 88). In both instances the d(220) line and hence the cell size decreased in going from the magnetic material extracted from the crushed rock to those extracted from the weathered material.

Furthermore, XRD analysis on the magnetic opaque single grains from various particle size fractions of several soils (Table 2.2) indicates that the d(220) spacing decreases continuously with decreasing particle size (i.e. from coarse to fine sand fractions, cf. Nos. 246 and 4M in Table 2.2) suggesting increasing weathering of magnetic grains according to particle size (Fitzpatrick, 1974; Fitzpatrick and le Roux, 1975; 1976).

A striking feature of the magnetic bands and concretions from the Mistbelt region (Fig. 2.1 and Fig. 2) is that their mineralogy is essentially similar (i.e. with superstructure lines). This could be attributed to similar mode of formation and, it possibly also illustrates a genetic association between them (e.g. that the concretions are derived from the bands).

According to Colombo *et al.* (1964) and others, the oxidation product of magnetite is dependent on the specific surface, crystalline perfection and amount of absorbed water in the original magnetite. Because of this, and the data presented above, two main modes of formation are possible: (i) the original magnetite produced by precipitation from aqueous solution (i.e. via green rust) oxidizes quickly (i.e. almost completely) to maghaemite frequently producing XRD superstructure lines (i.e. in magnetic bands and concretions) and (ii) the magnetite or Ti-magnetite inherited from basic igneous rocks is oxidized slowly (i.e. partly) to cation deficient spinel compounds analogous to maghaemite (i.e. in magnetic opaque single grains). The first mode of formation has been demonstrated to some extent by Taylor and Schwertmann (1974a) in synthetic studies on Fe(II) - Fe(III) oxide and  $\text{O}_2$  systems at low temperatures and pressures whereas the second



mode of formation at near ambient temperatures has been partly simulated in the laboratory by refluxing preground synthetic magnetite for 3 months in distilled water as well as in the experiments by Readman and O'Reilly (1970) on wet ground Ti-magnetite prior to oxidation in air at  $< 300^{\circ}\text{C}$ .

#### 2.4.2.2 Crystallinity

The WHH of the d(220) XRD peaks (i.e. indicator of degree of crystallinity and particle size) of various face-centred cubic minerals in 63 samples from several different localities and weathering environments in the study area demonstrate a wide-range of values between  $0,15$  and  $0,90^{\circ}2\theta$ . This range in line broadening (i.e. WHH) for these samples corresponds to a mean crystallite dimension (MCD) of between  $127\text{\AA}$  to  $>1\text{ }\mu\text{m}$  (Table 2.2) as calculated from the (220) peak using the Scherrer formula. Taylor and Schwertmann (1974a) obtained a much narrower range ( $0,35 - 0,55^{\circ}2\theta$ ) for Australian magnetic concretions.

The plot of WHH versus d(220) shows that these samples fall into four fairly distinct subgroups with very little overlap (in Fig. 2.2 the various sample types are indicated by symbols used in Fig. 2.1). Despite the sample grouping and general scattering of points in Fig. 2.2 there is a broad negative correlation ( $r=-0,64$ ,  $p < 0,001$ ) between the crystallinity of the samples (i.e. WHH) and d(220) spacing. In addition, there is better correlation ( $r=-0,81$ ,  $p < 0,001$ ,  $n=25$ ) between WHH and d(220) for the combined magnetic bands and concretions whereas the magnetic opaque single grain particles are less correlated ( $r=-0,50$ ,  $p=0,01$ ;  $n=27$ ).

In Fig. 2.2 the WHH values generally increase progressively from two origins, more or less in the regions marked maghaemite and magnetite. This can possibly be interpreted as being due to the influence of Al (i.e. in the magnetic concretions and clay-size fractions) and Ti (i.e. in the magnetic opaque single grain particles) on the crystallinity of maghaemite and cation deficient spinel oxides (i.e. Fe and Fe-Ti oxides), respectively. However, Ti-magnetites and/or Ti-maghaemites may also contain several other substituted cations such as Mn(IV), Mn(II), Mg(II), Ca(II), Cr(III), V(III) and Si(IV) but in only small amounts (Buddington and Lindsley 1964).

In the majority of the weakly- to non-magnetic clay-size fractions from red horizons in freely drained sesquioxidic soils (cf. Table 1.9), maghaemite (or magnetic minerals) is present in relatively small amounts, is very poorly crystalline or fine-grained, and accordingly it is difficult



to obtain satisfactory quantitative results using standard X-ray powder techniques. However, in some of the relatively strongly ferromagnetic clay-size fractions from red horizons in freely drained highly ferruginous soils, derived from basic igneous rocks (e.g. Table 2.2, Nos. 4Me and 42j), fairly strong but extremely broad d(220) peaks were identified (Table 2.2). Further examples of this include red soils from Australia and Brazil (Table 2.2). It is possible that in these clay-size fractions Al may substitute in the maghaemite structure, as in goethite (see chapter 1) and promote structural disorder which has the effect principally of weakening and broadening XRD reflections. This viewpoint is reinforced by the fact that no superstructure lines have been identified in the clay-size fractions suggesting that with increasing structural disorder they become weak and disappear.

Besides the possible distinction of the magnetic samples of different origin, the plot of WHH versus d(220) also suggests mode of formation, e.g. that the maghaemite and/or Al-maghaemite in the closely grouped magnetic concretions and bands formed via solution by rapid oxidation of very finely divided pure magnetite (hence superstructure lines). Furthermore, the poorly crystalline Al-maghaemite in the clay-sized fractions possibly also formed via solution (hence the incorporation of Al in the structure), whereas the maghaemite and Ti-maghaemite in the magnetic opaque single grains are formed by topotactic and epitactic alteration of detrital primary Ti-magnetite derived from igneous rocks.

#### 2.4.3 Magnetic susceptibility analysis

Magnetic susceptibility has proved to be a valuable technique in providing "quantitative information" about the presence and/or absence of magnetic compounds in soils (Le Borgne, 1955; Matsusaka and Sherman, 1961; Oades and Townsend, 1963; Tite and Linington, 1975). Applications to pedology have been reviewed by Mullins (1977) who stated that an important factor in the interpretation of magnetic susceptibility data of iron compounds in soils is the type of method used to determine magnetic susceptibility. Furthermore, Oades and Townsend (1963), and Mullins (1977) emphasized the need for care in interpretation of results in quantitative pedological studies based on magnetic susceptibility.

In this investigation the Gouy method was employed principally to determine the magnetic susceptibility of small samples generally containing low amounts of ferromagnetic minerals in the clay-size fractions



of soils. According to Mullins (1977) this method is not suitable for samples containing high amounts of ferromagnetic minerals. For this reason, only approximate magnetic susceptibility values are given for the highly ferromagnetic samples such as the magnetic opaque single grains, bands and concretions (Table 2.4). Nevertheless this method indicates that the magnetic opaque single grain particles have a very much higher magnetic susceptibility than the magnetic concretions, which in turn is relatively higher than the ferromagnetic clay-size fractions (Table 2.4).

The red soils with ferromagnetic clay-size fractions which generally give fairly strong, very **board** d(220) peaks (Table 2.2) have relatively high magnetic susceptibility values (Table 2.4). In Fig. 2.3 the magnetic susceptibility of 31 non-ferromagnetic soil clay samples are plotted against colour ( $H^* L/C$ )<sup>+</sup>. Descriptions, locations, and Munsell colours<sup>+</sup> of samples are given in Table 1.9. However, although only very weak d(220) peaks are evident in the non-ferromagnetic clay fractions (i.e. traces of maghaemite) from most red horizons from sesquioxidic freely drained soils listed in Table 1.9 (usually after 5M NaOH treatment) they are nevertheless strongly paramagnetic (Fig. 2.3). Therefore, to some extent, there is a problem in detecting small amounts of poorly crystalline maghaemite by XRD techniques. In all yellow apedal horizons no maghaemite peaks were detected in clay fractions (Table 1.9) and they are very weakly paramagnetic (Fig. 2.3).

With one exception (No. 16MY) all the non-ferromagnetic clay-size fractions from the yellow-brown apedal horizons lie in the same field (marked Y) of Fig. 2.3. Whereas the field marked R represents non-ferromagnetic clays from the red horizons from soils closely connected with or derived from basic igneous rocks. XRD analysis (Table 1.9) indicates that the latter samples contain fairly high amounts of finely divided Al-haematite which could also contribute to their relatively higher magnetic susceptibility (Mullins, 1977; Lindsley, 1976). However, the clays from the red apedal horizons of No. Gf22R and red mottles of No. Av12, derived from granite and sandstone respectively, both contain haematite, but have very low magnetic susceptibility values.

<sup>+</sup>  $H^*L/C$  = Munsell colour notations converted to a single number (Hurst, 1977; cf. Fig. 2.3)



Table 2.4 Magnetic susceptibility values of selected ferromagnetic samples after treatment with  $\text{NH}_4$ -oxalate-pH3, CBD and 0,2M oxalic acid at 90 °C for 1h

Sample No. <sup>1</sup>	Type <sup>2</sup>	Untreated $\chi \cdot 10^6$ c.g.s.	$\text{NH}_4$ -oxalate pH3 $\chi \cdot 10^6$ c.g.s.	CBD $\chi \cdot 10^6$ c.g.s.	Oxalic acid 90 °C, 1h $\chi \cdot 10^6$ c.g.s.
4Ma	sg	~ 4 500 000	nd	nd	nd
4Mc	sg	~ 2 200 000	nd	nd	nd
4Md	sg	~ 1 500 000	nd	nd	nd
88c	sg	~ 2 250 000	nd	nd	nd
199	bn	~ 3 700 000	nd	nd	nd
103d	cn	~ 2 950 000	~ 2 900 000	~ 2 700 000	150
42a	cn	~ 2 250 000	~ 2 100 000	~ 2 050 000	95
4Me	cl	650	620	12	29
42j	cl	530	470	6	15
246f	cl	490	420	5	17

1. for sample location, description and mineralogical composition cf. Table 2.2
2. where: sg, bn, cn and cl as in Table 2.2; nd = not determined

In the same way as haematite transforms to goethite (i.e. the so-called "yellowing" of red soil materials described by Schwertmann, 1971) maghaemite also appears to convert to goethite under more hydromorphic conditions (e.g. Av12) or in the presence of organic matter (e.g. Griffin soils) and possibly even more readily so, as in Av12 mo (since maghaemite is less stable than haematite, i.e.  $\Delta G_f^\circ = -163,6$  and  $-177,7$  k cal mole<sup>-1</sup>, respectively; Schwertmann and Taylor, 1977).

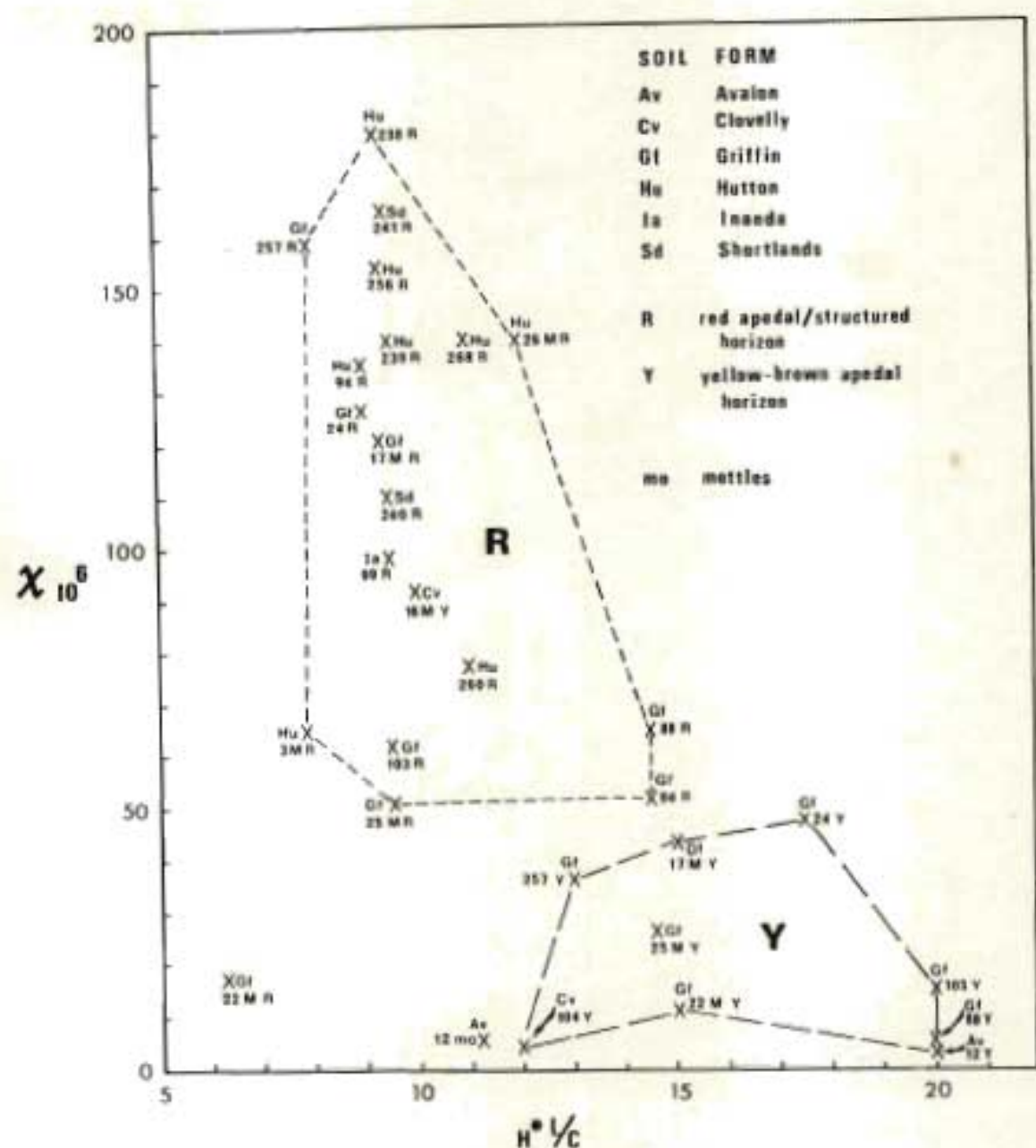


Fig. 2.3 : Relationship between magnetic susceptibility ( $\chi$ ) and colour for 31 non-ferromagnetic sesquioxidic soil clay ( $<2 \mu\text{m}$ ) samples; where:  $H^*L/C$  = Munsell colour notation converted to a single number according to Hurst (1977); H, L, and C represent hue, lightness (value), and chroma respectively, in the Munsell colour notation. The H values 2,5 YR, 5 YR, 7,5 YR and 10 YR are converted to the following equivalent  $H^*$  values 12,5, 15, 17,5 and 20 respectively



#### 2.4.4 Chemical analysis

##### 2.4.4.1 Total chemical analysis

Because monomineralic separation of titanomagnetite, titanomaghaemite and ilmenite were impossible\*, total analysis by classical wet chemical techniques (2.3.5) were necessarily made on bulk magnetic isolates. The resulting data therefore have limitations but several items of interest can nevertheless be deduced.

As expected the average Ti and Fe(II) content of the magnetic opaque single grains are much higher than in the other magnetic samples (i.e. concretions, bands, and clay-size fractions; Fig. 2.4). The higher Ti and Fe(II) contents of the magnetic opaque single grains reflect to some extent the relatively higher Fe(II) and Ti(IV) substitution in the maghaemite structure. However, it should be noted that where ilmenite is present in the sample (cf. Table 2.2) the total Fe(II) and Ti(IV) are not strictly related to the Ti-magnetite and/or Ti-maghaemite phases. Nevertheless, total chemical analysis reflects to a very large degree the differences between the magnetic opaque single grains and other magnetic forms (Fig. 2.4). A somewhat similar increase in Ti(IV) and Fe(II) content was reported by Mitsuchi (1976) for the more strongly magnetic fractions (i.e. possibly opaque single grains) separated from Cambodian Ferralsols.

The data for sample No. 4M (Fig. 2.4) also shows a progressive decrease in Ti(IV) and Fe(II) contents on going from the coarse (No.4Ma), medium (No.4Mb) and fine (No.4Mc) sand to silt (No.4Md) magnetic fraction. This is probably due to increasing oxidation of titanomagnetite [i.e. Fe(II)  $\rightarrow$  Fe(III)] and a certain amount of Ti being released from the Ti-magnetite and Ti-maghaemite structures.

---

\* Several types of textural (i.e. trellis, sandwich and composite) intergrowths or exsolution lamellae of ilmenite in Ti-magnetite and Ti-maghaemite occur in igneous rocks (Haggerty, 1976). This explains to some extent the high ilmenite contents in the magnetic opaque single grains in samples derived from dolerite and basalt associated with the Karroo system (i.e. majority of samples) but is rare in sample No. 4M derived from Ti-magnetite of the Bushveld Igneous Complex (Table 2.2). For this reason the total analysis of magnetic isolates from the latter sample could be plotted on FeO-Fe<sub>2</sub>O<sub>3</sub>-TiO<sub>2</sub> ternary diagrams (Fitzpatrick 1974; Fitzpatrick and le Roux 1975; 1976).

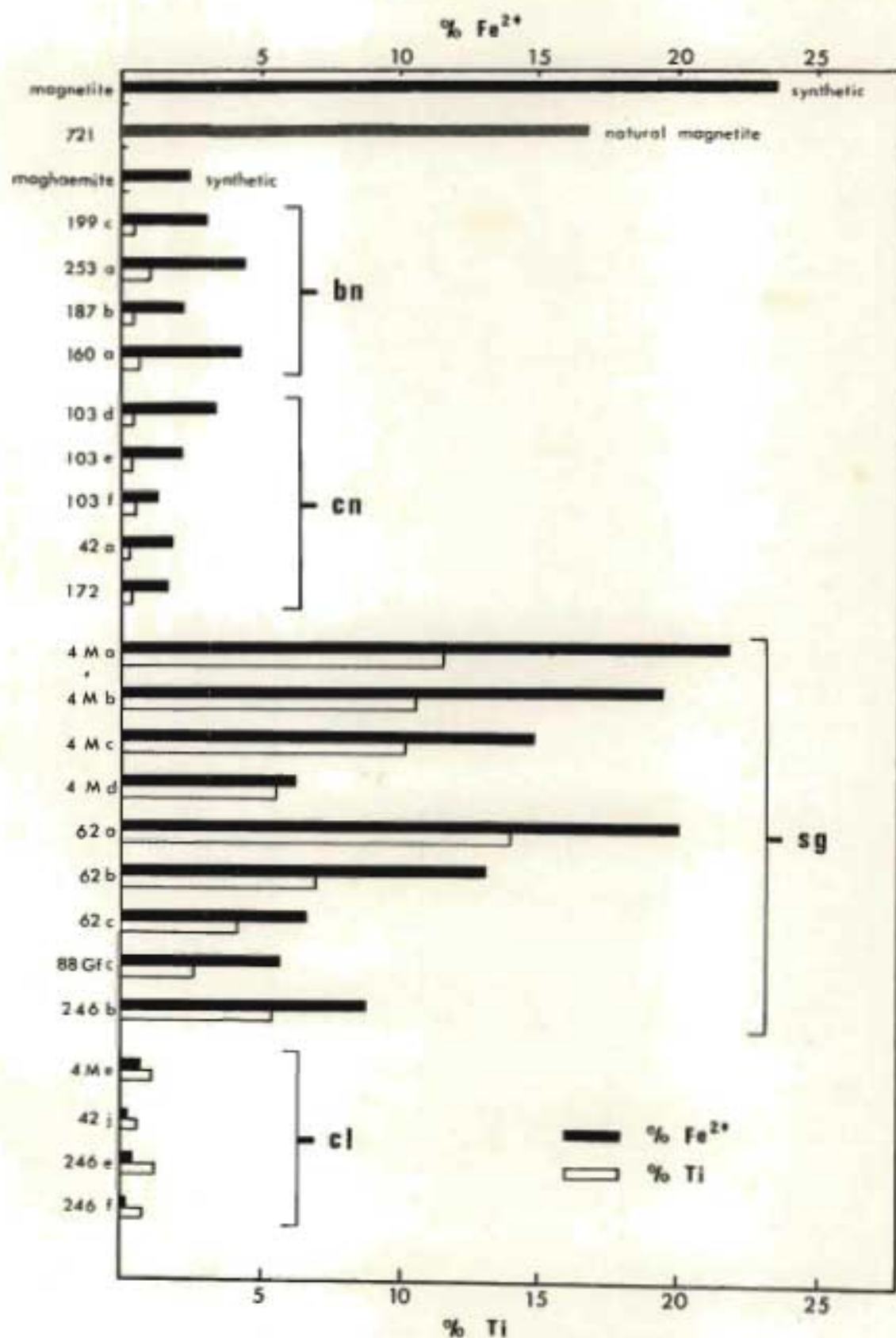


Fig. 2.4: Ferrous iron and titanium contents of synthetic and selected representative natural samples from sample collection; where: bn = bands, cn = concretions, sg = opaque single grains and cl = clay-size fractions



Even when the Fe(II) contents in Fig. 2.4 are expressed as a percentage of the total Fe they are all very much lower than 33.3% (i.e. that given for magnetite) and range from 0 to about 20% confirming the XRD data (Fig. 2.2) that the samples plot more in the maghaemite range of the maghaemite - magnetite series.

The data presented in Fig. 2.4 also tend to group the magnetic bands and concretions together on the one hand, and differentiate them from the ferromagnetic clay-size fractions with lower Fe(II) and slightly higher Ti (due mainly to anatase and rutile) contents.

There is still a lack of precise information concerning the solid solution relationships and formation (unmixing) of the various phases in the  $\text{FeO-Fe}_2\text{O}_3\text{-TiO}_2$  system involving magnetite, Ti-magnetite, maghaemite, Ti-maghaemite, ilmenite and haematite (cf. Buddington and Lindsley, 1964; Lindsley, 1976; Haggerty, 1976). For this reason, a better understanding of the composition and behaviour of these complex "primary" Fe-Ti oxides on weathering, would be of great interest not only to the petrologist but also to the pedologist, since these minerals are the principal original carriers of Fe and Ti in soils.

#### 2.4.4.2 Selective dissolution analysis

Because the main XRD peak for maghaemite (313) almost coincides with the haematite (110) and ilmenite (110) peaks it is often necessary to selectively dissolve either maghaemite or the other two oxides to concentrate the oxides or eliminate interference in order to determine their d-spacings. One of the methods tested by Taylor and Schwertmann (1974a) to dissolve maghaemite was to boil the samples in oxalic acid (no specified extraction time or concentration was given). This treatment was reported to be partly effective. They also extracted magnetic concretions with several sequential CBD treatments and treatment times.

In agreement with Taylor and Schwertmann (1974a) the magnetic concretions and bands, and in particular the magnetic opaque single grains (and synthetic maghaemite and magnetite, and natural magnetite) were generally relatively more resistant to CBD extraction than the non-magnetic goethite-rich samples (the  $\text{Fe}_d/\text{Fe}_{\text{HCl}}$  ratios in Table 2.5 are higher than those in Tables 1.3 to 1.9). The  $\text{Fe}_{\text{HCl}}/\text{Fe}_d$  ratio is between 2 to 10 times higher for the magnetic opaque single grains than for the bands and concretions (Table 2.5). This is due to the fact that the single grains contain relatively high amounts of Fe(II) (Fig. 2.4) and

Table 2.5 A comparison of Fe, Ti and Mn extracted from selected magnetic samples by 0,2M -ammonium oxalate-oxalic acid-pH 3 ( $Fe_o$  and  $Ti_o$ ) CBD ( $Fe_d$ ,  $Ti_d$  and  $Mn_d$ ), HCl ( $Fe_{HCl}$ ,  $Ti_{HCl}$  and  $Mn_{HCl}$ ) and 0,2 M oxalic acid at 90 °C for 1h

Sample No. <sup>1</sup>	Type <sup>2</sup>	$Fe_o$	$Fe_d$	$Fe_{HCl}$	$Fe_o / Fe_{HCl}$ or d*	$Ti_{HCl}$ or d*	$Mn_{HCl}$ or d*	$Ti_o$	$Fe_{HCl} / Fe_d$	0,2 M Oxalic acid 90 °C, 1h Mineralogy <sup>3</sup>				
		%	%	%		%	%	%		Fe %	Mh	He	Go	Mt
Magnetite	syn.	62,50	29,1	65,2	2,148*	-	-	n.d.	2,24	64,3	-	-	-	T
Maghaemite	syn.	0,49	25,6	58,4	0,019*	-	-	n.d.	2,28	45,2	A	-	-	-
Magnetite	nat.	5,85	4,0	54,5	1,463*	tr	tr	n.d.	13,63	38,1	-	-	-	A
199 c	bn	1,31	38,6	49,5	0,026	0,11	0,04	0,02	1,28	36,3	A	D	A	-
103 d	cn	0,09	31,8	51,3	0,002	0,13	0,08	0,01	1,61	40,2	T	A	SD	-
e	cn	1,08	41,4	42,4	0,025	0,16	0,01	0,01	1,02	37,1	T	A	SD	-
f	cn	1,13	37,1	45,2	0,025	0,22	0,01	0,02	1,22	34,5	T	A	SD	-
g	cn	0,70	33,5	48,3	0,014	0,13	0,03	n.d.	1,44	36,2	T	SD	SD	-
h	cn	0,65	43,2	50,5	0,013	0,19	0,03	n.d.	1,17	31,6	T	SD	SD	-
42 a	cn	0,36	45,0	52,2	0,007	0,23	0,05	0,03	1,16	30,1	T	D	A	-
b	cn	0,51	37,7	40,2	0,013	0,18	0,07	0,01	1,07	29,4	T	SD	A	-
d	cn	0,48	44,0	50,8	0,009	0,17	0,03	n.d.	1,15	41,5	T	SD	A	-
e	cn	0,30	39,2	45,9	0,007	0,20	0,05	n.d.	1,43	36,2	T	SD	T	-
g	cn	0,46	23,2	43,0	0,011	0,57	0,07	n.d.	1,85	31,9	T	SD	T	-
h	cn	0,36	22,1	24,7	0,015	0,72	0,05	n.d.	1,12	17,7	-	SD	T	-
62 a	sg	0,40	3,5	39,3	0,089	0,89	0,03	0,11	11,23	24,5	T	-	-	A
b	sg	0,25	10,0	26,6	0,025	0,41	0,01	0,06	2,66	21,0	T	A	A	-
c	sg	0,07	13,5	28,6	0,005	0,57	0,02	0,05	2,12	20,2	T	A	A	-
4M a	sg	3,69	4,5	45,2	0,082	3,15	0,17	0,30	10,04	35,7	T	T	-	A
b	sg	2,15	10,4	40,0	0,213	3,21	0,12	0,21	3,85	32,4	A	A	-	-
88 c	sg	1,90	8,4	51,7	0,226	2,30	0,15	0,16	6,15	42,2	T	T	-	-
4M e	cl	0,20	17,3	23,7	0,012*	1,35*	0,19*	0,01	1,37	12,5	-	SD	T	-
42 j	cl	0,41	13,9	17,8	0,029*	0,39*	0,11*	0,01	1,28	11,0	-	SD	A	-

1. for sample location, description and mineralogical composition cf. Table 2.2.

2. where: syn. = synthetic, nat. = natural, and bn, cn, sg and cl as in Table 2.2; tr = trace; n.d. = not determined

3. where: Mh, He, Go and Mt; D, CD, SD, A, T and -, as for Table 2.2



are therefore weakly soluble in CBD. Similarly, relatively low  $Fe_o/Fe_d$  or HC ratios were obtained for magnetic bands and concretions, whereas higher ratios are associated with the opaque single grains due to their higher Fe(II) contents. Baril and Bitton (1969), and McKeague, Brydon and Miles (1971), and Gamble and Daniels (1972), reported similar data for Fe extracted from magnetite. It is significant that oxalate soluble Ti follows the same pattern as Fe for the magnetic opaque single grain particles (Table 2.5)

The low ratios (i.e.  $Fe_o/Fe_d < 0.02$ ) recorded for bulk soils containing magnetic opaque single grains, suggests that the Ti-magnetite and/or Ti-maghaemite with high Fe(II) contents in these soils are coated (or protected) by resistant crystalline secondary or oxidized products of Ti-magnetite (see below). Apart from the fact that grinding increases the surface area of these magnetic opaque single grain particles which tend to concentrate mainly in the 0.026 to 0.5 mm fraction (1.4.1.3), grinding may also remove crystalline iron oxide coatings (e.g. goethite patina) and expose a core of magnetic oxide minerals with high Fe(II) contents which are more susceptible to oxalate dissolution. Furthermore, when magnetic opaque single grains from Nos. 88c and 4Mb were sequentially extracted with  $Fe_d$  before grinding (i.e. to remove oxidic Fe, mainly goethite, haematite and some maghaemite) and then subjected to 0.2M  $NH_4$ -oxalate-pH 3 treatment, higher amounts of oxalate soluble Fe were obtained (i.e. 4.21 and 3.42%  $Fe_o$  for 88c and 4Mb, respectively) again suggesting that some of these grains may have a core of relatively unoxidized Ti-magnetite or Ti-maghaemite with high Fe(II) content.

Although crystalline concretionary maghaemite is moderately resistant to both CBD (3x1/4h) and  $NH_4$ -oxalate-pH 3 extraction, it is significant that finely divided or microcrystalline maghaemite (i.e.  $MCD \leq 300\text{\AA}$ ) in concretions and clay-size fractions are selectively removed (i.e. the WHH decreases or the peak disappears even after a 1x1/4h CBD extraction, cf. Table 2.2). Oades and Townsend (1963) found that extraction of soil clays with relatively mild dithionite treatment reduced the magnetic susceptibility, possibly due to removal of poorly crystalline maghaemite. Similarly, in the ferromagnetic fractions of clay-size samples (Nos. 4M and 42) CBD removed maghaemite and reduced the magnetic susceptibility considerably, to very low values (Table 2.3).



Treatment with 0,2M oxalic acid at 90 °C for 1 h selectively removed most of the maghaemite as determined by XRD (Table 2.5) and magnetic susceptibility (Table 2.4) resulting in a relative concentration of the other Fe-oxide minerals (Table 2.5).

The magnetic concretions and bands generally contain relatively lower amounts of HCl extractable Mn and Ti than for the magnetic opaque single grains and clay-size fractions (Table 2.5) in accordance with the total Ti contents (Fig. 2.4). The low  $Mn_{HCl}$  values indicate that the concretions were probably formed in a relatively well aerated environment (i.e. similar to the bulk soils where weak reducing conditions result only occasionally in very wet seasons). The low  $Ti_{HCl}$  values could suggest that they are not derived from Ti-magnetite whereas in the magnetic opaque single grains the high HCl extractable Ti (and  $Mn^*$ ) could mean they are formed from the weathering of detrital Ti-magnetite.

#### 2.4.5. Optical examination

An attempt was made to examine each form of magnetic sample by light microscopic methods (thin sections and petrographic), and by SEM and TEM to see if any differences (or similarities) in external morphology could be observed. Except for the SEM work of Pawluk and Dumanski (1973) on ferromagnetic concretions in a poorly drained soil of Alberta (Canada), and Stieglitz and Rothwell (1972) on magnetite and other heavy minerals from lacustrine beach and dune deposits, little work has been done on the surface textures of pedogenic magnetic minerals.

##### 2.4.5.1 Morphology of magnetic bands and concretions

The thin sections of the magnetic bands (and concretions) have an overall very dark-brown appearance with numerous small holes and cracks (Plate 2.1 C), indicating to some extent a porous-like material. For the most part, the material is almost opaque especially in the very dark-brown areas, suggesting that these areas are fairly densely iron impregnated. No particular structure can be seen in the thin section except in many holes, small, round, almost opaque particles about 2 - 5  $\mu m$  in size may be seen. In several holes, the small opaque particles are scattered in the middle and increase in number toward the edges. Some of the less opaque, or less densely impregnated areas lining the walls of the holes, show small (<2  $\mu m$ ) birefringent crystals, probably

\* This could represent Mn present in the primary (Buddington and Lindsley, 1964) or highly altered (weathered) magnetic Fe-Ti oxides.



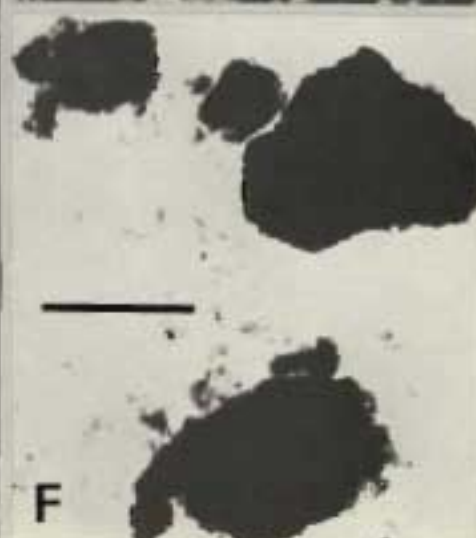
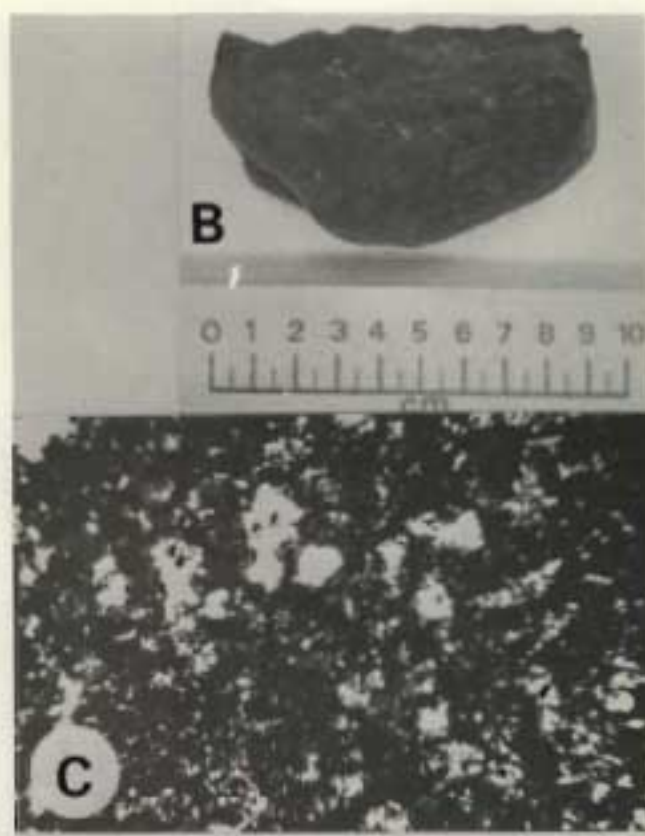
Plate 2.1: A. Photograph of a magnetic band in the C horizon of a Farningham soil in a road cutting 10km north of Ixopo (No. 199). Note hand magnet attracted to the band, immediately to the left and at the handle-join of the geological hammer.

B. Large rounded magnetic fragment or nodule from a stoneline in a Griffin soil, B22 horizon (No. 103) exposed in a road cutting 3km south of Richmond, fractured in half before photographing.

C. Thin section light micrograph of magnetic band. Ordinary light X 65.

D and E. SEM of fracture surface and cavity of magnetic band from sample No. 199 at progressively increasing magnifications, D(X 800) and E (X 1600).

F. TEM of clay-size fraction ( $<2 \mu\text{m}$ ) dispersed ultrasonically (10 min. at 20K Hz in distilled water) after gently grinding a portion of magnetic band from sample No. 199. Bar is  $0,5 \mu\text{m}$ .





goethite, suggesting more recent goethite impregnation.

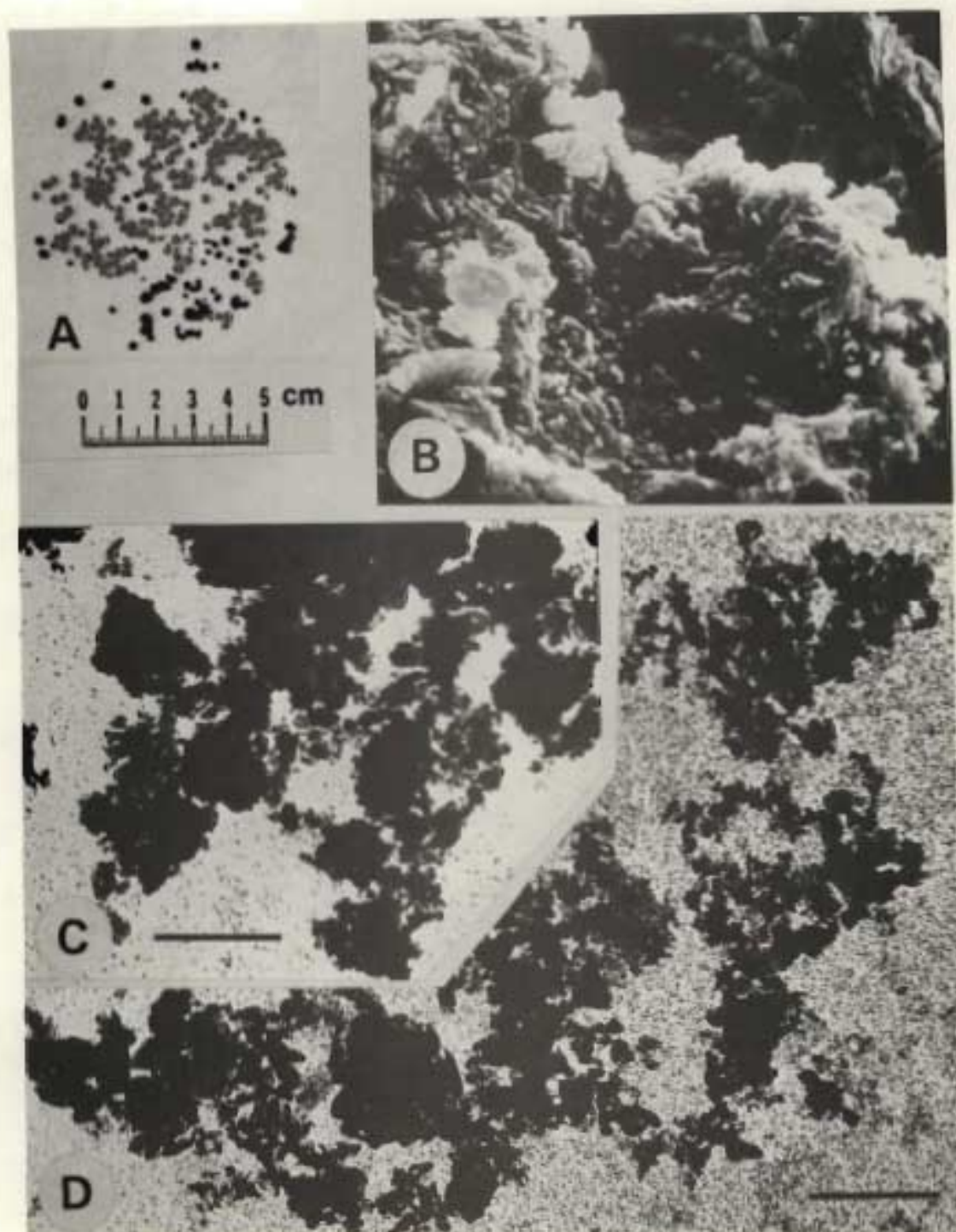
Plates 2.1 D and E, and 2.2 B are SEM photographs of the interior surfaces of a magnetic band (No. 199) and concretion (No. 42), respectively. A number of areas on these respective surfaces were examined but no features strikingly different from those shown were observed. They both seem to consist of many pores (cf. also Plate 2.1 C) surrounded by "pore infillings" with individual rods, or stubby bundles (i.e. clusters or aggregates), of the order of  $<2\ \mu\text{m}$ , closely packed or often intergrown with each other. Ferromagnetic concretions of similar micro-structure patterns were described by Pawluk and Dumanski (1973). Several spheroidal-like particles are noted in Plate 2.1 D particularly in the lower left hand corner. Although the nature and origin of these particles are not known, their shape is similar to anatase particles observed by Weaver (1976). However, crystalline maghaemite comprises the dominant mineral in these two samples with minor amounts of haematite, quartz, kaolinite, goethite and trace amounts of anatase (Table 2.2).

The similar external morphology of the fracture surfaces of the bands and concretions (and large rounded fragments) together with their similar XRD patterns (i.e. superstructure lines) again suggest that the magnetic concretions are possibly related to (i.e. possibly derived from) bands.

Plates 2.1 F and 2.2 C are TEM of representative fields of untreated magnetic particles in the clay-size fractions ( $<2\ \mu\text{m}$ ) from bands (No. 199) and concretions (No. 42a), respectively. The particles (mainly maghaemite) are highly aggregated, opaque and isodimensional, and resemble the electron micrographs of natural and synthetic maghaemite described by Schwertmann and Taylor (1977). Treatment of the clay-size fraction from the concretions (No. 42a) with a 1 x 1/4 h extraction with CBD selectively removed much of the subdominant haematite and traces of goethite in the sample, and superficial poorly crystalline maghaemite (i.e. decrease in XRD line broadening; Table 2.2) resulting in greater dispersion (Plate 2.2 D). Some of the particles in Plate 2.2 D show slight cubic-like outlines. This is to some extent in accordance with the reasonably sharp ( $\text{WHH} = 0,28^\circ 2\theta$ ) XRD lines and the fairly strong superstructure lines for maghaemite in this sample which reflects the relatively large crystal size and apparent good development of the crystals.

- Plate 2.2: A. Photograph of hard, shiny magnetic concretions from a Farningham soil, B21 horizon near Howick (No. 42).
- B. SEM of fracture surface and cavity of a concretion from sample No. 42 (X 1600).
- C. TEM of clay-size fraction ( $<2 \mu\text{m}$ ) dispersed ultrasonically (10 min. at 20 K Hz in distilled water) after gently grinding several magnetic concretions from sample No. 42a. Bar is  $0,5 \mu\text{m}$ .
- D. TEM of clay-size fraction from No. 42a (cf. C above) after 1 x 1h treatment with CBD. Bar is  $0,5 \mu\text{m}$ .





#### 2.4.5.2 Weathering of magnetic opaque single grains in ferruginous bauxites and soils derived from basic igneous rocks

As expected, the grains (i.e. mainly Ti-magnetite) observed in thin sections (Plate 2.3 A), and by SEM after being "isolated" or extracted magnetically after crushing (Plate 2.3 B) unweathered dolerite, show smooth, sharp edges and surfaces (i.e. "agate-like" fracture surfaces) with no solution pits. The small "frosted" grains observed on the surface of the magnetic grain in Plate 2.3 B have resulted from crushing. Whereas in the thin section of weathered ferruginous bauxite (No. 62b) adjacent to the dolerite (cf. Plates 1.9 and 2.3 C) the most obvious chemical alterations of the large opaque magnetic particles\* (mainly Ti-maghaemite<sup>+</sup>) are cracks, rounded edges and corners, and etched or pitted patterns on the surfaces of grains (see also Plate 2.3 D). The SEM examinations of the magnetic particle *in situ* (Plate 2.3 D-F) at progressively higher magnifications indicate several solution textures such as large and small irregular pits, and "blob-like" overgrowths which lack obvious crystal facies (Plate 2.3 F).

It is postulated that these are maghaemite or Ti-maghaemite overgrowths and form as numerous incipient crystals on detrital magnetite or titanomagnetite grains (possibly as epitactic overgrowths) by precipitation. These apparently small crystals on the surface of the titanomagnetite grain (Plate 2.3 F) could eventually develop into overgrowths with well defined crystal facies (see below) providing the physico-chemical conditions (redox, pH etc.), space and time permit.

Magnetic opaque single grain isolates from the 0,062 - 0,5 mm fraction (i.e. fine sand fraction) of a Farmhill soil, C horizon (No. 88 Gf c) derived from basalt, show mainly irregular particles with: (i) highly etched banded portions (arrowed in Plate 2.4 A) with discontinuous surfaces resulting from the splitting of primary titanomagnetite and (ii) masses of intergrown and separate crystals or particles which occur as aggregates or clusters in "pore fillings" (Plate 2.4 A - E). The latter occur above and below the banded portion

---

\* Several of these particles are visible to the naked eye.

<sup>+</sup> Following SEM studies the grain was carefully removed using tweezers under a low-power binocular microscope, powdered in an agate mortar, and examined by XRD analysis.

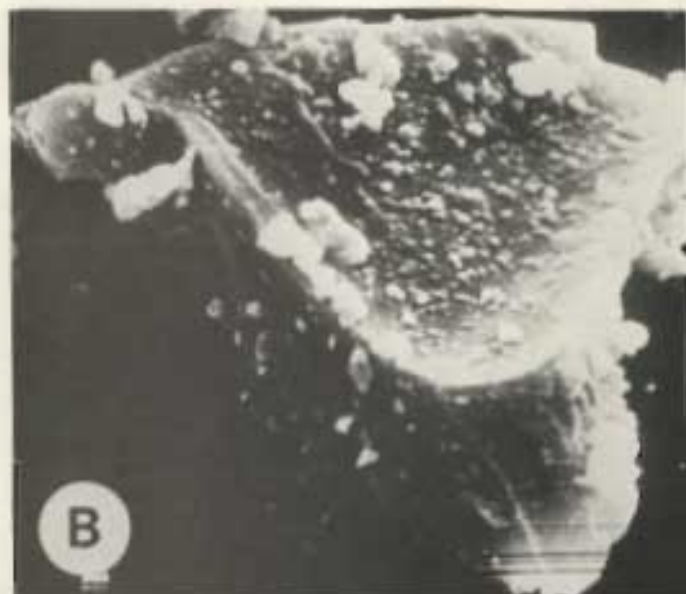


Plate 2.3: A. Thin section light micrograph of dolerite core in a ferruginous bauxite boulder-block from a Farmhill soil exposed in a railway cutting near Sweetwaters, Pietermaritzburg (No. 62a; cf. Plate 1.9) showing an opaque (black) unweathered (i.e. unetched) titanomagnetite grain. Ordinary light X 70.

B. SEM of the "fracture surface" of an unweathered opaque magnetic grain (possibly titanomagnetite) isolate from crushed dolerite from sample No. 62a. (X 224). The small loose particles on the surface of the grain are considered to be introduced during sample preparation, primarily by grinding. The lines in the lower portion of this micrograph represent electronic noise resulting from a defective scan generator.

C. Thin section light micrograph of ferruginous bauxite (No. 62b) adjacent to dolerite core (cf. Plate 1.9 D-F) showing weathered (i.e. etched) opaque single grain particles (possibly titanomaghaemite). Ordinary light X 65.

D - F. SEM of a large opaque magnetic grain (possibly titanomaghaemite) in a void in the ferruginous bauxite (No. 62b) adjacent to the dolerite core, at progressively increasing magnifications, D (X 154), E (X 770) and F (X 3080). Arrow in D shows outline of magnetic grain.





arrowed in Plate 2.4 A, and are shown at progressively higher magnifications (Plate 2.4 B - D), which appear to show features of weathering similar to that observed in the ferruginous bauxite fragment, but possibly at a more advanced weathering-stage.

Detailed SEM examination of the banded portion shows a highly cracked, etched and pitted surface with fairly large granular particles on the surface (i.e. possible epitactic crystal overgrowths) of the order of  $<2\ \mu\text{m}$ . Close examination in a void above the band (the square area marked on Plate 2.4 C), reveals that these clustered particles show some face development in the form of rough subangular platelets (Plate 2.4 E). The  $d(220)$  XRD line for maghaemite in this sample (Table 2.2) is fairly sharp ( $\text{WHH} = 0,20^\circ\ 2\theta$ ) reflecting its relatively large particle size (i.e.  $\text{MCD} = 1615\text{\AA}$ ). Despite the relatively sharp  $d(220)$  XRD peak no superstructure lines were observed, possibly due to the high amounts of Ti and  $\text{Fe}^{2+}$  in the sample (Fig. 2.4).

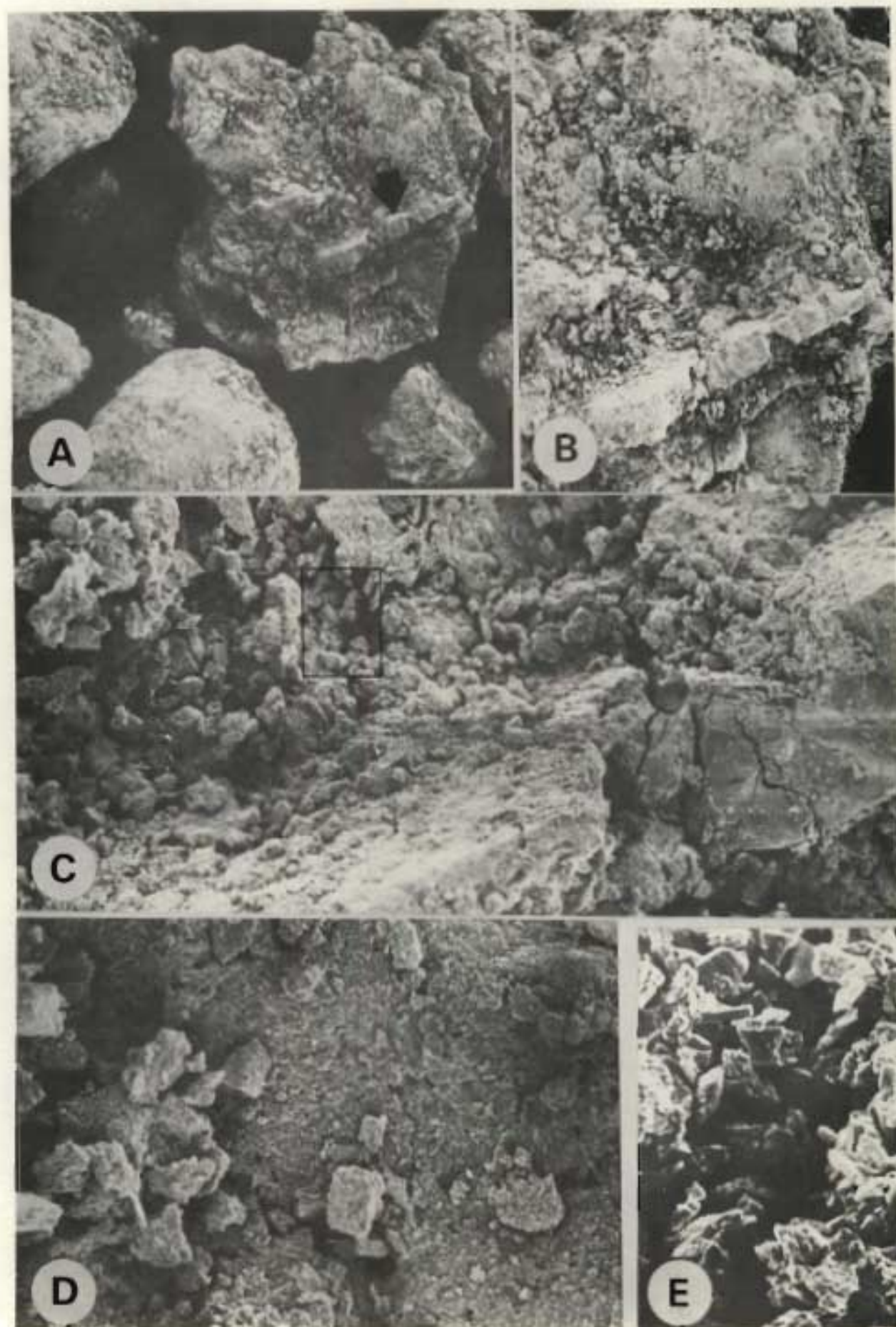
It is postulated that, with time, the primary magnetite and/or Ti-magnetite particles from basalt or dolerite parent materials weather to form soil maghaemite- and/or titanomaghaemite-rich clusters or aggregates with relatively high Fe(II) and Ti(IV) contents, mainly in the silt and fine sand fractions of freely drained soils particularly in the Mistbelt and Highland Montane regions.

These SEM and thin section observations indicate to some extent that the formation of maghaemite and/or Ti-maghaemite may occur through dissolution of magnetite or Ti-magnetite. The formation of maghaemite and/or Ti-maghaemite on the surface and in pores and cracks of weathered primary magnetite and/or Ti-magnetite particles suggests that oxidation is not attributed solely to topotactic alteration of the latter but possibly also by epitactic crystallization from solution. This will have the effect of reducing the nucleation energy for maghaemite and/or Ti-maghaemite formation considerably.

The surface texture on magnetic opaque "single grain" particles from different localities and weathering environments (i.e. ferruginous bauxite and soils) is different, and therefore may be a marker value to the pedologist of degree of weathering and "reserve" of such particles. Hence, in the same way as quartz has been used (e.g. Krinsley and Doornkamp 1973) in studying relationships between surface texture and possible environmental factors, it is suggested that magnetic opaque single grains may also be used.

Plate 2.4: A - E. SEM of magnetic opaque "single grain" isolates from the Farmhill soil (No. 88Gf), C horizon (on Mikes Pass, south aspect), of the ~62 - 500  $\mu\text{m}$  fraction (fine sand fraction) at progressively increasing magnifications A (X 77), B (X 154), C (X 770), D (X 1540) and E (X 3080; magnifications of square area in C), showing the complex microstructure of these grains.





## 2.5 Conclusions

The distribution and occurrence of several pedogenic magnetic materials in the study area were grouped according to their morphology and origin (i.e. bands, concretions, opaque single grains, clay-size fractions and bulk topsoil samples) and both field and laboratory data show a clear soil - climate - terrain zonality.

XRD analysis indicates that each of these magnetic samples broadly represent maghaemite and magnetite in an isomorphous replacement series; i.e. the magnetic bands and some of the concretions, approaching the ideal maghaemite unit cell of the type:  $\text{Fe}_{8/3}^{3+} \square_{1/3}^{*} \text{O}_4$  with superstructure lines, whilst the concretions and clay-size fractions with high WHH values progressively diverge to lower d-spacings indicating substitution of Al for Fe in the maghaemite structure; on the other hand the magnetic opaque single grain samples tend to approach the "ideal" magnetite/Ti-magnetite d-spacings but generally most of these samples have lower d-spacings indicating cation deficient Ti-magnetites with general formulae:  $\text{Fe}_a \text{Ti}_b \square_c^{*} \text{O}_4$  where  $a+b+c=3$  or substitution of  $\text{Ti(IV)} + \text{Fe(II)}$  for  $2\text{Fe(III)}$  in the maghaemite structure.

The considerable substitution of Al and Ti in the maghaemite structure presumably leads to relative disorder within the structure which possibly in turn leads to (i) a lower energy of formation and (ii) the absence of superstructure lines.

These pedogenic magnetic samples are clearly differentiated into four subgroups when the d(220) spacings are plotted against the WHH (i.e. index of crystallinity): (i) clay-sized fractions (strongly disordered and with low d-spacings), (ii) concretions (disordered to well ordered, i.e. those with superstructure lines), (iii) bands (relatively well ordered due to occurrence of superstructure lines), (iv) opaque single grain particles (wide range of order and crystallinity).

A rough distinction between the various morphological types of magnetic samples can also be made from chemical analysis; opaque single grain particles usually having higher Fe(II) and Ti(IV) contents than the clay-size fractions, bands and concretions. The bands and concretions generally have higher Fe(II) and slightly lower total Ti(IV) than the clay-size fractions.

---

$\square^{*}$  denotes a vacant lattice site.



The superstructure lines detected in several magnetic bands and concretions in soils from the Mistbelt regions suggests that the maghaemite in them is possibly formed by rapid oxidation of finely grained original magnetite which formed by precipitation from aqueous solution.

A laboratory weathering experiment carried out by refluxing wet ground synthetic magnetite for 3 months, demonstrated that magnetite can oxidize to cation deficient Fe-Ti spinel oxides at near ambient conditions. This information together with mineralogical and chemical evidence (i.e. XRD, chemical and SEM analysis) on magnetic opaque single grain particles from solid igneous rocks and adjacent weathered materials suggests that the magnetic opaque single grains are formed by topotactic and epitactic transformation of detrital magnetite and Ti-magnetite under favourable pedogenic conditions (i.e. time, Eh, pH and moisture status).

The effect of  $\text{NH}_4$ -oxalate-pH 3, CBD (1x1/4 h and 3x1/4 h) and 0,2M oxalic acid (90 °C for 1 h) treatments were tested on a wide range of selected magnetic samples. The selectivity of these methods in extracting the various oxides was largely a function of the type of material (i.e. crystallinity and composition). For example, poorly crystalline maghaemite (i.e.  $\text{MCD} \leq 300\text{\AA}$ ) was selectively removed by 1x1/4 h (and 3x1/4 h) extraction with CBD in the clay-size fractions and concretions. Oxalic acid selectively extracted higher amounts of magnetic material from the opaque single grains [high in Fe(II)] than in the concretions and bands.

Examination of opaque single grain particles by SEM revealed details and complexities not discernible with a petrographic or low-power binocular microscope. The surfaces of magnetic opaque single grain particles (examined *in situ*) in both ferruginous bauxite and the 62 to 500  $\mu\text{m}$  fractions from soil horizons are porous, and rough with ridges, knobs, furrows, and pits which are indicative of both solution and precipitation surfaces. In contrast, the outer surfaces of the magnetic concretions are generally relatively smooth, shiny and compact.

The magnetic single grain opaque particles in ferruginous bauxite and soils are presumed to contain a high proportion of oxidized or weathered detrital magnetite or Ti-magnetite from igneous sources (i.e. cation deficient Fe-Ti spinel oxides) since they are composed of loose silt-to clay-size clusters which are closely associated with the

etched and cracked surfaces of relatively large grains, and in addition have intermediate  $d(220)$  spacings between maghaemite and magnetite with high Fe(II) and Ti(IV) values.

A reasonably similar origin or mode of formation is indicated for the magnetic concretions and bands by their closely similar XRD and micro-morphology (thin section, SEM and TEM). Some of these magnetic concretions appear to be derived from the magnetic bands.

The maghaemite in the clay-sized fractions (determined mainly by magnetic susceptibility), concretions (XRD) and opaque single grains is higher in the red than in yellow-brown apedal horizons, and generally increases with depth in Griffin soils with a maximum in the red apedal horizon (decreasing in the C horizon). This suggests that maghaemite can possibly be partly dissolved in soils (i.e. depending on effective surface area which explains its relative stability in concretions and cores of magnetic opaque single grains) under the influence of organic matter (and hydromorphy) and be transformed via solution to goethite.

The exact mode of maghaemite formation is not clear from the data obtained in this investigation. However, these results imply that the maghaemite and cation deficient Fe-Ti spinel oxides detected in these soil magnetic samples can possibly form by both secondary (via solution) and topotactic formation. Finally, a third mechanism of maghaemite formation in surface horizons of soils in the Mistbelt and Highland Montane regions can be attributed mainly to heating by ground fire (i.e. influence of heat and reducing conditions in the presence of organic matter and finely divided goethite).

The distinction between secondary maghaemite (i.e. via solution formation) and oxidized magnetite and/or Ti-magnetite (i.e. topotactic formation), based on mode of origin, is to a large extent reflected in certain features of chemical composition, XRD pattern and electron optical morphology; taken together these features also illustrate that these minerals and mode of formation may grade from one form to the other but that they nevertheless can be distinguished.

The results presented demonstrate a considerable range of properties in magnetic oxides [Fe(II) and Ti(IV) contents,  $d$ -spacings, crystallinity, magnetic susceptibility, and micro-morphology] from a wide range of pedogenic environments in the study area, and suggest further avenues of research which could profitably be followed.



SOIL MINERALS IN THE  $\text{Fe}_2\text{O}_3 - \text{TiO}_2 - \text{H}_2\text{O}$  SYSTEM WITH  
SPECIAL REFERENCE TO SYNTHETIC PREPARATIONS  
AT NEAR AMBIENT CONDITIONS

### 3.1 Introduction

Regardless of parent material, titanium is invariably detected in soils. Titaniferous oxides are generally considered as inert materials in soil development and this has often been used to establish the degree of depositional uniformity in soils. However, several workers (Sherman, 1952; Sudom and St. Arnaud, 1971; Fitzpatrick and le Roux, 1976) have suggested that Ti may be mobilized in all fractions during soil weathering; recently Bain (1976) observed high amounts of X-ray amorphous and cryptocrystalline  $\text{TiO}_2$  in a peaty podzol. Further work is needed in characterizing the mobile, amorphous and poorly-crystalline fractions of Ti in soils.

In recent studies dealing with titanium in soils and clays much emphasis has been placed on the fact that Ti is commonly combined with Fe. Selective dissolution studies by Sayin and Jackson (1975) indicate that anatase in Georgia kaolinite contains small amounts of Fe. Weaver (1976) using electron probe techniques, supported this view. Moreover, several forms of secondary crystalline iron oxides containing structurally incorporated Ti (e.g. titanomagemite, titanohaematite, pseudobrookite and pseudorutile) have been detected in soils (e.g. Katsura *et al.*, 1962; Walker *et al.*, 1969; Fitzpatrick and le Roux, 1976). Their formation is thought to result mainly from the topotactic oxidation of primary minerals (e.g. titanomagnetite or ilmenite) and not to any great extent by coprecipitation and crystallization of Fe and Ti in the weathering solution.

Divergent views exist on the exact nature and genesis of these alteration products, particularly ilmenite (Palmer, 1909; Overholt *et al.*, 1950; Bailey *et al.*, 1956; Lynd, 1960; Bykov, 1964; Temple, 1966; Grey and Reid, 1975). Bailey *et al.*, 1956 and Lynd, 1960 suggested that all alteration products of ilmenite should be termed leucoxene and qualified as being either an amorphous or crystalline Fe - Ti oxide\*. However, detail X-ray

---

\* DeVilliers (1962) reports appreciable amounts of leucoxene together with ilmenite in the heavy mineral fractions of several highly weathered yellow and red soils of Natal.

studies of single grains of altered ilmenite by Temple (1966) and more recently by Grey and Reid (1974) has led to broad agreement that in nature a distinct intermediate titaniferous product referred to as pseudorutile ( $\text{Fe}_2\text{Ti}_3\text{O}_9$  - previously called arizonite) is involved in the alteration of ilmenite.

The difficulty in synthesizing pseudorutile free of other Fe and Ti oxides which coincide with some of its XRD lines, together with its poorly crystalline nature, have been major problems in characterizing this intermediate alteration product (Lynd, 1960; Karkhanavala and Momin, 1959; Grey and Reid, 1975). Little information is available on pedogeochemical conditions under which Fe and Ti may coprecipitate and crystallize from the weathering solution to form these mixed "alteration" products. Furthermore, it is not yet known what effect Ti and Fe have on the formation of iron (e.g. goethite and haematite) and titanium (e.g. anatase and rutile) oxides respectively, at ordinary pressures and temperatures.

Numerous synthesis studies have been undertaken at high temperatures and pressures to determine the stability fields of  $\text{TiO}_2$  polymorphs and Fe-Ti minerals (Buddington and Lindsley, 1964) during magmatic oxidation (i.e. in chemical petrology). Karkhanavala and Momin (1959) hydrothermally crystallized small amounts of pseudorutile at  $300^\circ\text{C}$  and 1200 lb. per sq.in. and concluded that it was "not the product of atmospheric oxidation". These results are considered to be of little value in determining the conditions and type of Fe-Ti phase which will form during the alteration of titaniferous primary minerals under earth surface conditions.

Except for the work of Weiser and Milligan (1934) on pure Ti systems, little work has been done on the precipitation and crystal growth in Ti (IV) solutions undergoing hydrolysis, particularly in the presence of other metals. Several synthetic studies have been carried out on mixed Fe-Al (e.g. Gastuche *et al.*, 1964) and Fe-Si (e.g. Herbillon and Tran Vinh An, 1969) systems *in vitro*.

The objective of this study is to examine a series of synthetic Ti and Fe-Ti oxides\* aged under different conditions, in order to obtain a better

---

\* The term oxides in this chapter includes all compounds in the system  $\text{TiO}_2\cdot\text{H}_2\text{O}$  and  $\text{Fe}_2\text{O}_3\cdot\text{H}_2\text{O}$  respectively.



understanding of possible Fe-Ti weathering products and their presence in soils.

### 3.2. Materials and methods

#### 3.2.1 Synthetic Fe-Ti oxides

Details of the method used for preparing mixed Fe-Ti oxide coprecipitates from their respective chloride salts (and aged in 0,2 M KOH) are given in Appendix 2.

Chloride contamination was avoided by employing a titanyl nitrate solution, prepared as follows: A fresh Ti oxide precipitate was obtained by adding a 10 per cent ammonia solution to 0,5 M  $\text{TiCl}_4$  (Merck, AR) until the pH of the solution was in the range 5 - 6. The resulting dense white precipitate was centrifuge-washed five times with deionised water and then dissolved in 5 M  $\text{HNO}_3$ . A fresh Ti oxide was once again precipitated with  $\text{NH}_3$  solution, centrifuge-washed with deionized water until a negative chloride test ( $\text{AgNO}_3$ ) was obtained, redissolved in 5 M  $\text{HNO}_3$ , and diluted to a concentration of 4,79 g Ti/l. The synthetic fresh titanium oxide free of chloride) was finally prepared by the addition of a 10 per cent  $\text{NH}_3$  solution to the titanyl nitrate solution until the pH was in the range 5 - 6. The white precipitate was centrifuge-washed thoroughly with deionized water and either freeze-dried immediately or aged in polyethylene bottles as follows: (i) at room temperature ( $\approx 25^\circ\text{C}$ ) for 30 and 70 days, (ii) at  $70^\circ\text{C}$  for 70 days, both at pH 5,5 and 12,0.

The synthetic fresh ferrihydrite (formerly called amorphous ferric hydroxide) was prepared by the addition of a 10 per cent  $\text{NH}_3$  solution to 0,1 M  $\text{Fe}(\text{NO}_3)_3$  solution (Merck, AR) until the pH ranged between 5 - 6. Nine mixed Ti(IV) - Fe(III) oxides of compositions 5, 10, 20, 30, 50, 70, 80, 90 and 95 mole % Ti/Ti + Fe respectively, were prepared in exactly the same manner except that titanyl nitrate replaced iron in the initial solution in different proportions (for comparison several Fe-Al and Fe-Zr coprecipitates were prepared in a similar way using nitrate salts). The freshly precipitated oxides were centrifuge-washed with deionized water until dispersion and either freeze-dried immediately or aged in polyethylene bottles as follows: at room temperature or at  $70^\circ\text{C}$  for 70 days. The pH was adjusted to 5,5 by adding  $\text{HNO}_3$  or  $\text{NH}_4\text{OH}$  every third day, and water added at intervals to compensate for evaporation. The samples were then

washed free of excess salts and freeze-dried.

Fifty mg of sample was dissolved in concentrated HCl to ascertain total Fe and Ti and duplicate samples were extracted (i) with 10 ml  $\text{NH}_4$ -oxalate (pH 3) in the dark (Schwertmann, 1964) on an end-over-end shaker for two hours and then centrifuged; and (ii) with one 15 minute treatment with citrate-bicarbonate-dithionite (CBD) (Mehra and Jackson, 1960). The extracts were analysed for Fe by atomic absorption and Ti by the Tiron method (tests for  $\text{NH}_4$ -oxalate interference in Fe and Ti determinations were negative).

X-ray powder diffraction patterns were obtained from gently pressed specimens of random orientation using a Philips PW 1050/70 instrument fitted with a graphite monochromator, and  $\text{CoK}\alpha$  radiation at a scan rate of  $1^\circ/\text{min}$ . (Appendix 3).

Infrared spectra were run in KBr pellets using a Perkin Elmer model 457.

Magnetic susceptibility was measured by the Gouy method using mercury (II) cobaltitetrathiocyanate  $\text{HgCo}(\text{CNS})_4$  as a calibration standard at  $25^\circ\text{C}$  and 2000 gauss.

Charge distribution of the oxides were determined by equilibrating 100 to 300 mg samples overnight with 10 ml 0.75 M KCl (pH adjusted to 5 or 10 with HCl or KOH) followed by a further two centrifuge-washings. The suspensions were then centrifuge-washed five times with 10 ml of 0.05 M KCl adjusted to the appropriate pH. The pH of the final washing was measured, and the tube plus contents weighed immediately after decantation. Suspensions were then centrifuge-washed five times with 10 ml 0.22 M  $(\text{NH}_4)_2\text{SO}_4$ . Potassium and Cl were analyzed in the combined extracts, made up to 50 ml with 0.22 M  $(\text{NH}_4)_2\text{SO}_4$ , by flame emission and with an Aminco-Cotlove chloride titrator, respectively. Negative and positive charges were calculated after correction for occluded salt.

### 3.2.2 Soil samples and clay analysis

Twelve soils were selected from a climatotoposequence in the study area (see Table 3.1, Appendix 1 and Fig. 1.1). Samples of the clay fraction ( $<0.2 \mu\text{m}$ ) were obtained by sonic dispersion and sedimentation,



TABLE 3.1: Sample collection and Ti and Fe extracted from subsoil clays by acid ammonium oxalate ( $Ti_o$  and  $Fe_o$ ), CBD, ( $Fe_d$ ) and total Ti ( $Ti_t$ )

SOIL TYPE	GREAT GROUP	LOCALITY (No. in Fig. 1.1)	PARENT MATERIAL	ALTITUDE (m)	$Ti_o$ %	$Ti_t$ %	$Ti_o/Ti_t$	$Fe_o$ %	$Fe_d$ %	$Fe_o/Fe_d$
Peaty podzol	Cryhumod	Ardbrecknish*	Chlorite- schists	-	1,95	5,40	0,36	6,09	8,62	0,70
Blinkklip	Cryumbrept	Lesotho (106 Ma)	Basalt	3 300	0,12	0,41	0,29	1,87	5,02	0,37
Makuya	Cryumbrept	Sani pass (235 Cv)	Basalt	3 000	0,11	0,40	0,27	1,58	6,03	0,26
Newport	Haplumbrept	Mikes pass (105 Cv)	Basalt	2 620	0,05	0,62	0,08	2,09	10,32	0,20
Ouwerf	Fragiaquult	Mikes pass (236 Pn)	Basalt	2 580	0,03	1,26	0,02	0,34	8,66	0,04
Farmhill	Umbriorthox	Richmond (103 Gf)	Shale/ Dolerite	1 050	0,03	0,71	0,04	0,39	10,37	0,04
Farmhill	Umbriorthox	Richmond (103 Gf)	Shale/ Dolerite	1 050	0,02	1,04	0,02	0,37	10,38	0,04
Vazi	Plinthaquept	Piet Retief (13 M Lo) <sup>†</sup>	Sand stone	1 370	0,04	0,81	0,08	1,50	3,60	0,41
Vazi	Plinthaquept	Windy hill (669 Lo) <sup>†</sup>	Sand stone	1 060	0,07	1,94	0,05	3,04	22,88	0,13
Clovelly	Haplorthox	Dududu	Granite	850	0,05	0,29	0,16	1,51	14,57	0,10
Shortlands	Rhodoxeralf	Albert Falls (241 Sd)	Dolerite	670	0,01	0,28	0,04	0,32	8,11	0,04
Fernwood	Quartzipsamment	Richards Bay (near 183)	Eolianite	60	0,09	1,05	0,11	3,08	7,40	0,42
Clansthal	Dystrochrept	Umkomaas (256 Hu)	Eolianite	50	0,03	0,66	0,06	0,65	15,41	0,04

\* Sample from Scotland supplied by Bain (1976)

<sup>†</sup> Bottomland soils in toposequences where 11 M Gc and 99 Ia are the upland soils respectively (see Fig. 1.1)

without pre-treatment, and freeze-dried. A Ti-rich clay sample ( $<1,4 \mu\text{m}$ ) from a peaty podzol reported on by Bain (1976) was also used. Fifty mg subsamples of clay were (i) dissolved in  $\text{H}_2\text{SO}_4$  (Pruden and King, 1969), (ii) extracted with CBD, (iii) extracted with  $\text{NH}_4$ -oxalate (pH 3); and the extracts analyzed as for the synthetic oxides. Clays (and selected synthetic oxides) were also treated with 5 M NaOH at  $90^\circ\text{C}$  for 1 hour (Norrish and Taylor, 1961).

### 3.3 Results and discussion

#### 3.3.1 Comparison of synthetic and natural Ti-oxides

The freshly prepared titanium oxide obtained by precipitating titanyl nitrate (chloride free) with  $\text{NH}_3$ , was found to be amorphous to X-rays (Fig. 3.1 h) and stayed so after aging at pH 12 for 70 days at room temperature and  $70^\circ\text{C}$ . However, at pH 5,5 and at room temperature ( $\approx 25^\circ\text{C}$ ) for 30 days it showed the strongest lines of anatase although very broad (Fig. 3.1 i). The line broadening corresponds to a mean crystallite dimension (MCD) of  $20 - 80 \text{ \AA}$ , as calculated from the (101) peak using the Scherrer formula.\* The crystallinity of the anatase improves after aging for 70 days at room temperature (Fig. 3.1 j). This observation is in general agreement with the results obtained by Weiser and Milligan (1934) after 210 days of aging. There is some evidence that traces of Cl delay the transformation of amorphous Ti-oxide to anatase and this may be the reason for the slower rate of anatase crystallization they observed.

It is difficult to accurately locate the anatase peaks at low levels of crystallinity (Figs. 3.1 h and i,  $\text{WHH} > 2,0^\circ 2\theta$  or  $\text{MCD} < 50 \text{ \AA}$ ). This is especially so when interfering clay mineral (e.g. chlorite) peaks are present, which make XRD interpretations less certain (Bain, 1976). The rate and degree of anatase crystallization increased greatly when the amorphous Ti-oxide was aged at  $70^\circ\text{C}$  for 70 days (Fig. 3.1 l).

Thus, having demonstrated that X-ray amorphous Ti and anatase with

---

\*  $\text{MCD} = \frac{K\lambda}{(B-b)\cos\theta}$  in which K is a constant (0,9),  $\lambda$  the wave length of the X-radiation, B the measured width at half height (WHH), b the instrumental line broadening (see Appendix 3) and  $\theta$  the Bragg angle of the respective line used.



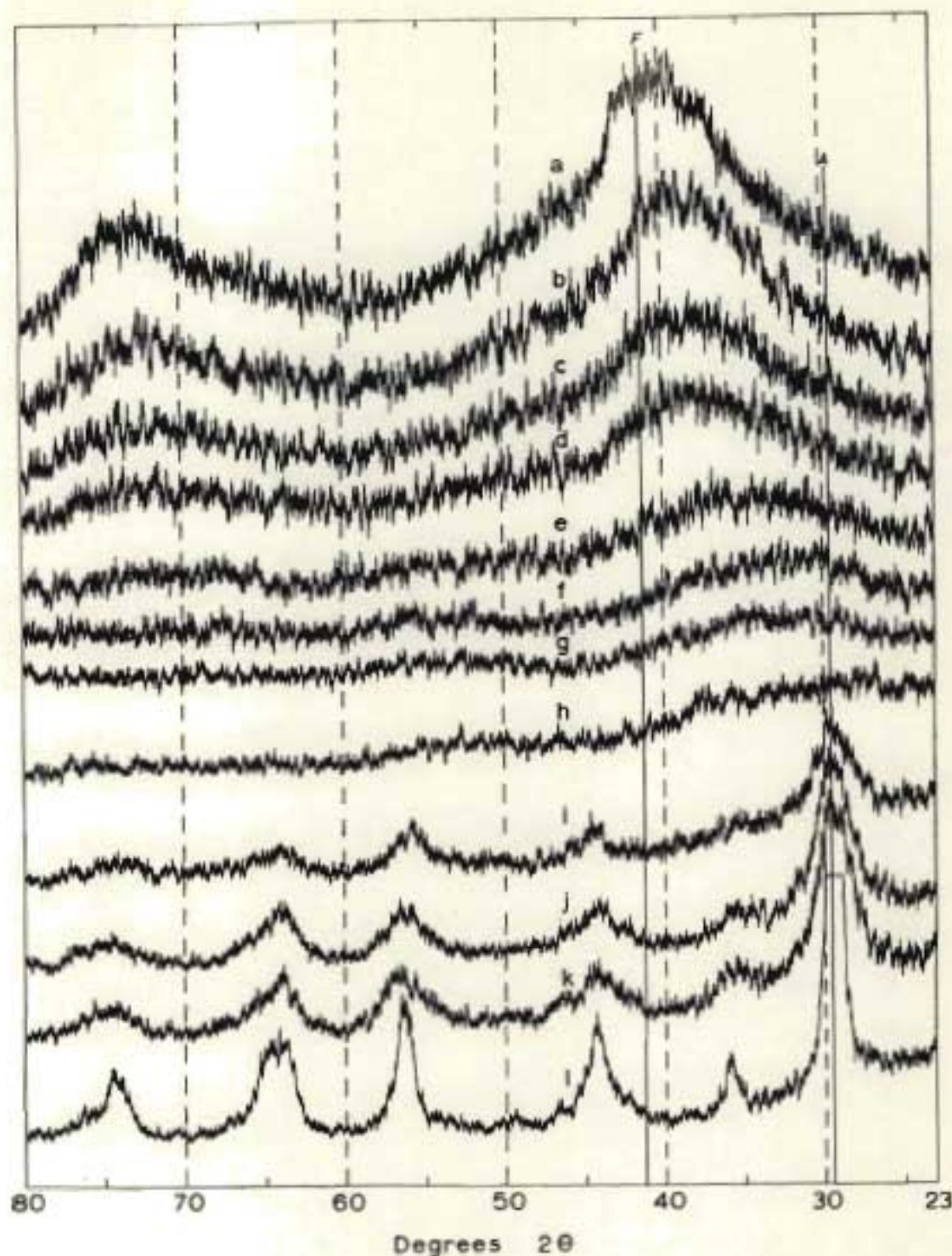


Fig. 3.1: X-ray diffraction patterns from synthetic Fe-Ti oxides. Traces a-h are for freshly precipitated oxides with: (a) 0%; (b) 10%; (c) 20%; (d) 30%; (e) 50%; (f) 70%; (g) 90%; (h) 100% in Ti/Ti+Fe respectively.

Traces i-l are for the freshly precipitated pure Ti-oxide: (i) aged at room temperature (pH 5.5) for 30 days (j) aged at room temperature (pH 5.5) for 70 days (k) as for (j) but pretreated with 5 M NaOH at 90°C for 1 hr.

(l) aged at 70°C and pH 5.5 for 70 days.

where A = anatase; F = ferrihydrite

varying MCD could be prepared, these polymorphs were used to monitor and test  $\text{NH}_4$ -oxalate (pH 3) and 1 M HCl as extraction reagents for obtaining a measure of the degree of crystallinity. The fresh, X-ray amorphous gel (Fig. 3.1 h) was found to be completely oxalate soluble ( $\text{Ti}_o/\text{Ti}_t = 1$ )\* (Figs. 3.2 and 3.3), while both the anatase aged for 70 days at  $70^\circ\text{C}$  (Fig. 3.1 l) and crystalline anatase† are insoluble ( $\text{Ti}_o/\text{Ti}_t = 0$ ) in oxalate after two hour extraction time (Fig. 3.2). The relative dissolution of extremely poorly ordered anatase in oxalate is related to the MCD of anatase [as calculated from WHH of the anatase (101) X-ray reflection‡ for crystallites  $< 50 \text{ \AA}$ , i.e.  $\text{WHH} > 2,0^\circ 2\theta$  (Fig. 3.2).] Thus, anatase with MCD  $> 50 \text{ \AA}$  or with  $\text{WHH} < 2,0^\circ 2\theta$  are resistant to oxalate dissolution (Fig. 3.2) even after successive extractions (Fig. 3.3). The X-ray amorphous Ti-oxide and the anatase with  $\text{WHH} > 2,0^\circ 2\theta$  was completely soluble in 1 N HCl, but the HCl dissolved Ti seemed to hydrolyze extremely rapidly (in some cases after standing for only 5 hours). Both these compounds are soluble in  $\text{H}_2\text{TiF}_6$  which agrees with previous work (Dolcater *et al.*, 1970; Sayin and Jackson, 1975). Therefore, acid  $\text{NH}_4$ -oxalate is the more selective extractant for X-ray amorphous  $\text{TiO}_2$  and microcrystalline anatase.

Based on these findings for synthetic materials this reagent was used to selectively extract similar material from a wide range of soil clays. The results together with  $\text{Fe}_d$ \* and  $\text{Ti}_t$  are given in Table 3.1. The ratio  $\text{Ti}_o/\text{Ti}_t$  was used because previous work on Transvaal highly weathered soils (Fitzpatrick and le Roux, 1976) using  $\text{H}_2\text{TiF}_6$ , indicated that only minor amounts of Ti are associated with kaolinite. The peaty podzol gave the highest  $\text{Ti}_o$  and  $\text{Ti}_o/\text{Ti}_t$ . Moreover, the total Ti was only partly oxalate soluble, which probably indicates that it is microcrystalline as suggested by Bain (1976). From the data in Fig. 3.2 the MCD of the anatase in the peaty podzol appears to be about  $25 \text{ \AA}$ . All the Ti in this soil clay was extracted by  $\text{H}_2\text{TiF}_6$ .

The Makuya and Blinkklip soils (formed under an afro-alpine climate) also have relatively high oxalate soluble Ti values (Table 3.1). In contrast, most of the other test soils gave low  $\text{Ti}_o/\text{Ti}_t$  and  $\text{Fe}_o/\text{Fe}_d$  values, which suggest that both the Ti and Fe oxides are crystalline. XRD data for

\*  $\text{Ti}_t$  and  $\text{Ti}_o$  represent total titanium and  $\text{NH}_4$ -oxalate (pH 3) extractable Ti respectively,  $\text{Fe}_d$  represents CBD extractable Fe.

† Obtained by courtesy from S.A. Titan Co., Rep. of South Africa.



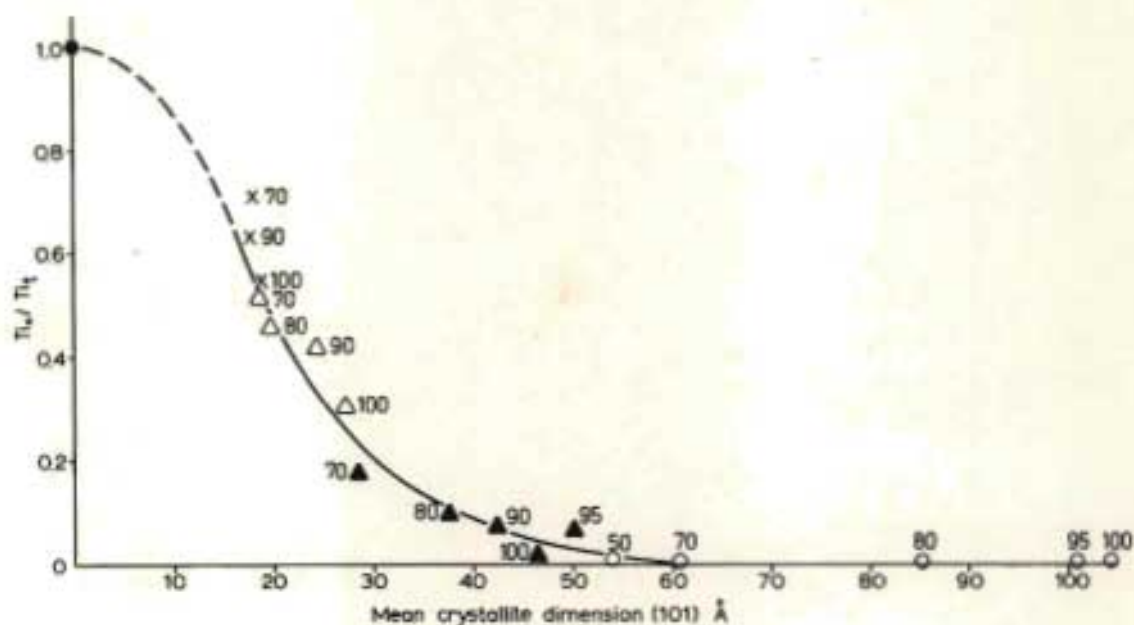


Fig. 3.2: Relationship between  $Ti_o/Ti_t$  and MCD (Å) for anatase 101 (calculated from the WHH of the anatase 101 X-ray reflection)

Symbols correspond to:

- freshly precipitated Ti and coprecipitated Fe-Ti oxides;
- X same but aged at room temperature for 10 days;
- △ same but aged at room temperature for 20 days;
- ▲ same but aged at room temperature for 30 days;
- same but aged at 70°C and pH 5,5 for 70 days.

Numbers refer to % Ti/Ti+Fe

these and several other related soil clays after 5 M NaOH treatment (see Table 1.12) indicate that the major titanium mineral present is anatase with only minor amounts of rutile (probably detrital) and pseudorutile (detected in sample at locality site No. 256 Hu; Fig 1.1). According to Sayin and Jackson (1975) NaOH treatment may dissolve or etch finer anatase particles. Since 5M NaOH pretreatment is used to concentrate the Fe-oxides in sesquioxidic clays, with high amounts of kaolinite and gibbsite, prior to XRD the effect of this pretreatment on poorly crystalline synthetic anatase was tested. The XRD patterns before and after alkali treatment remained essentially the same (Fig. 3.1 j and k) and no Ti was detected in the NaOH extract. However, the resistance of muscovite and other similar 2:1 layer silicates to alkali dissolution suggests that the  $H_2TiF_6$  dissolution method (Dolcator, *et al.*, 1970 and Sayin and Jackson, 1975) is more suitable for concentrating crystalline  $TiO_2$  in clays which are not dominated by kaolinite and/or gibbsite.

There is a significant linear correlation ( $r = 0,61$ ;  $p = 0,02$ ) between  $Ti_o/Ti_t$  and  $Fe_o/Fe_d$  (Table 3.1) suggesting that Ti follows a similar pattern to Fe in the crystallization process in soils. It is further evident that soils of cooler regions have high  $Fe_o/Fe_d$  and  $Ti_o/Ti_t$ . These observations suggest that crystallization of pedogenic iron and titanium oxides are inhibited by cool temperature conditions and possibly also by interference of organic matter (Schwertmann, 1966) and/or coprecipitation of Fe and Ti.

### 3.3.2 Freshly prepared Fe-Ti oxides

The colours of fresh and aged ~~micro-ferrihydrite~~ Fe-Ti oxides ranging in composition from  $0 < Ti/(Ti+Fe) < 1$  are given in Table 3.2, and range from brown to pale yellow to white with decreasing Fe content. Compared with these coprecipitates, physically mixing the two freshly-precipitated end members resulted in more reddish-pinkish hues suggesting that the coprecipitates are not merely physical mixtures of Ti and Fe but possibly chemical combinations of Ti and Fe. Aging of the freshly prepared oxides at pH 5,5 and 70°C also resulted in colour changes (Table 3.2).

The XRD data are shown in Fig. 3.1 a-h. The pure Fe oxide (Fig. 3.1 a) gives a pattern with two broad bands corresponding to proto-ferrihydrite (Chukhrov, *et al.*, 1972). The coprecipitates with  $0 < Ti/(Ti+Fe) < 0,30$  also resemble ferrihydrite (Fig. 3.1 b and c). However, as the Ti/(Ti+Fe) ratio



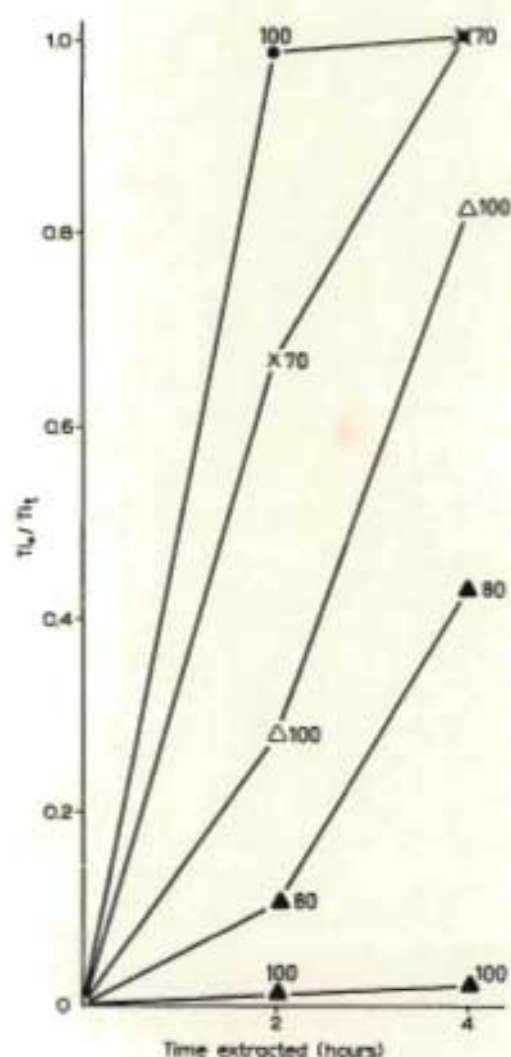


Fig. 3.3: Relationship between  $Ti_o/Ti_t$  and  $NH_4$ -oxalate extraction time (hours). Legend as for Fig 3.2

increases, the characteristic ferrihydrite pattern progressively weakens (and the two main lines gradually shift towards lower angles, suggesting Ti substitution) to give an essentially X-ray amorphous pattern with a very broad halo between  $25^\circ 2\theta$  and  $35^\circ 2\theta$  (Fig. 3.1 e - h). The net positive charge measured at pH 4,7 - 5,0 of the pure ferrihydrite and the "Ti-ferrihydrites" remained fairly constant up to a composition of  $Ti/(Ti+Fe) = 0,70$  at which point a net negative charge was measured which continued to increase sharply (Fig 3.4). A demixing of Fe or

Table 3.2: Munsell colours of freshly prepared Fe/Ti coprecipitates and after aging at 70°C (pH 5,5) for 70 days

Ti/Ti+Fe	Freshly prepared coprecipitates		Aged coprecipitates	
	Colour	Munsell notation	Colour	Munsell notation
0,00	Dusky red	10 R <sup>3</sup> / <sub>2</sub>	Dark red	10 R <sup>4</sup> / <sub>6</sub> - <sup>3</sup> / <sub>6</sub>
0,05	Dusky red	10 R <sup>3</sup> / <sub>3</sub>	Dark red - red	2,5 YR <sup>3</sup> / <sub>6</sub>
0,10	Dark reddish brown	2,5 YR <sup>3</sup> / <sub>4</sub>	Dark red - red	2,5 YR <sup>3</sup> / <sub>6</sub> - <sup>4</sup> / <sub>6</sub>
0,20	Dark red	2,5 YR <sup>3</sup> / <sub>4</sub> - <sup>3</sup> / <sub>6</sub>	Dark red	2,5 YR <sup>3</sup> / <sub>4</sub> - <sup>3</sup> / <sub>6</sub>
0,30	Dark red	2,5 YR <sup>3</sup> / <sub>6</sub>	Dark red	2,5 YR <sup>3</sup> / <sub>6</sub>
0,50	Yellowish - red	5 YR <sup>5</sup> / <sub>8</sub>	Yellowish - red	5 YR <sup>4</sup> / <sub>6</sub>
0,70	Reddish - yellow	7,5 YR <sup>6</sup> / <sub>8</sub>	Yellowish - red	5 YR <sup>5</sup> / <sub>8</sub>
0,80	Yellow	10 YR <sup>7</sup> / <sub>8</sub>	Reddish - yellow	7,5 YR <sup>6</sup> / <sub>6</sub>
0,90	Pale yellow	2,5 Y <sup>8</sup> / <sub>4</sub>	Yellow	10 YR <sup>8</sup> / <sub>8</sub>
0,95	Pale yellow	5 Y <sup>8</sup> / <sub>3</sub>	Pale yellow	2,5 Y <sup>8</sup> / <sub>4</sub>
1,00	White	5 Y <sup>8</sup> / <sub>1</sub>	White	5 Y <sup>8</sup> / <sub>2</sub>



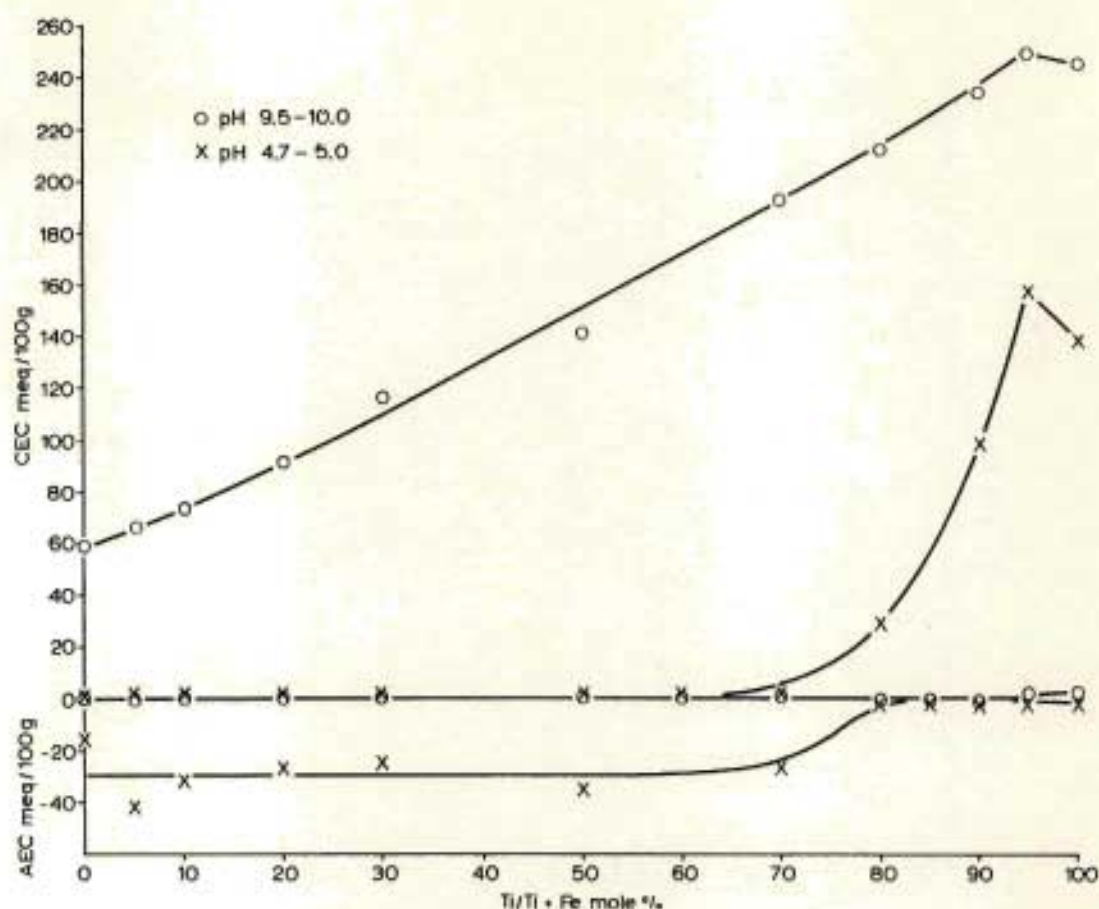


Fig. 3.4: Negative and positive charge variation with pH in relation to composition of freshly prepared Fe-Ti oxides

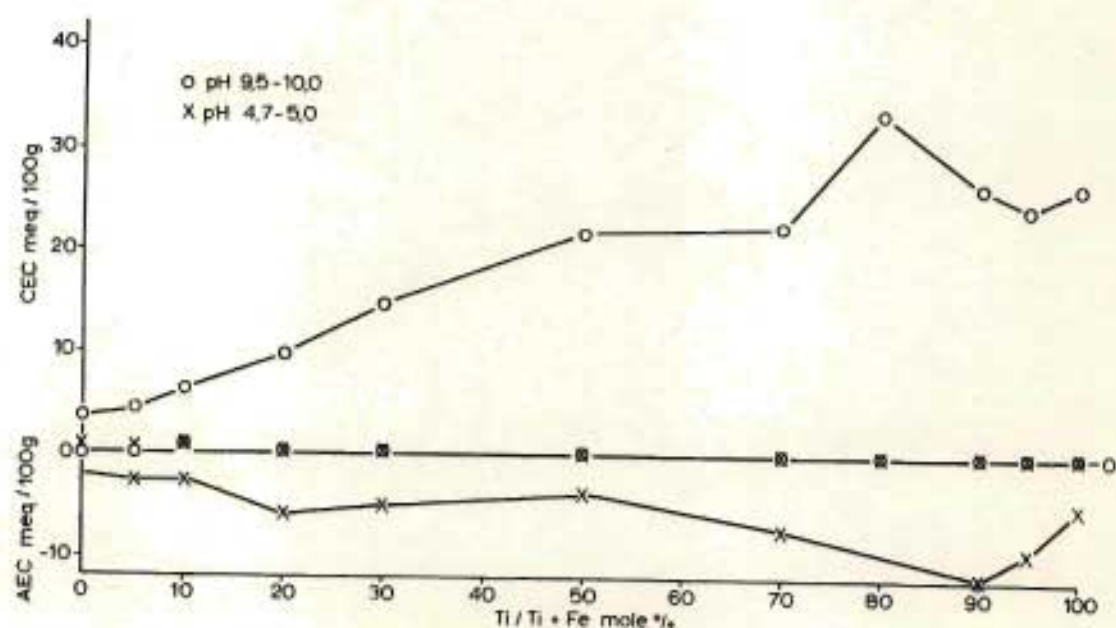


Fig. 3.5: Negative and positive charge variation with pH in relation to composition of Fe-Ti oxides aged at 70°C and pH 5.5 for 70 days

substitution of Fe in an amorphous-like titanium phase could account for both the apparent decrease in ferrihydrite (which has a high positive charge at pH 5) and the increase in net negative charge with increasing amounts of Ti. The formation of a separate negatively charged amorphous Ti-Fe phase and positively charged (pH 5) ferrihydrite phase could be analogous to that proposed for synthetic aluminosilicate (e.g. Cloos *et al.*, 1969).

The pure freshly prepared titanium member has a moderately high negative charge at pH 10 which decreases at pH 5 (Fig. 3.4). This pH dependent charge is attributed to dissociation of Ti-OH groups. The negative charge of the Ti-Fe phase could play an important role in controlling the Fe or Fe-Ti polymerization. The effect of negatively charged clay minerals in controlling Al polymerization has been discussed by several researchers.

All freshly prepared oxides are completely soluble in oxalate ( $Ti_o/Ti_t = 1$ ,  $Fe_o/Fe_t = 1$ ) which confirms the "poorly ordered" nature as shown by XRD patterns (Fig. 3.1 a - h). Furthermore, this conforms with the data of Schwertmann and Fischer (1973) for synthetic and natural ferrihydrites.

In agreement with results of Prasad and Ghildyal (1975) ferrihydrite has a high magnetic susceptibility (Fig. 3.6) which is probably due to the low degree of order resulting from weak bonding [e.g. exposed Fe (III) polymers]. There is a steady decrease in magnetic susceptibility with increasing Ti content (Fig. 3.6). The titanium which is diamagnetic, simply acts as a diluent in the freshly prepared coprecipitates as far as the magnetic susceptibility is concerned.

### 3.3.3 The effect of aging Fe-Ti oxides at room temperature

In the composition range  $0 < Ti/(Ti+Fe) < 0.3$  where ferrihydrite is present, the XRD pattern remained essentially unaltered after aging at room temperature for 70 days at pH 5.5, and the gels were also oxalate soluble. However, at Ti/(Ti+Fe) ratios  $> 0.70$  anatase was detected (Fig. 3.1). With decreasing Fe in the composition range of  $0.30 < Ti/(Ti+Fe) < 0.70$ , the (101) line of anatase becomes sharper and the product is progressively less oxalate soluble (Fig. 3.2). This is probably due to decreasing interference of Fe in the formation of anatase. Thus, in



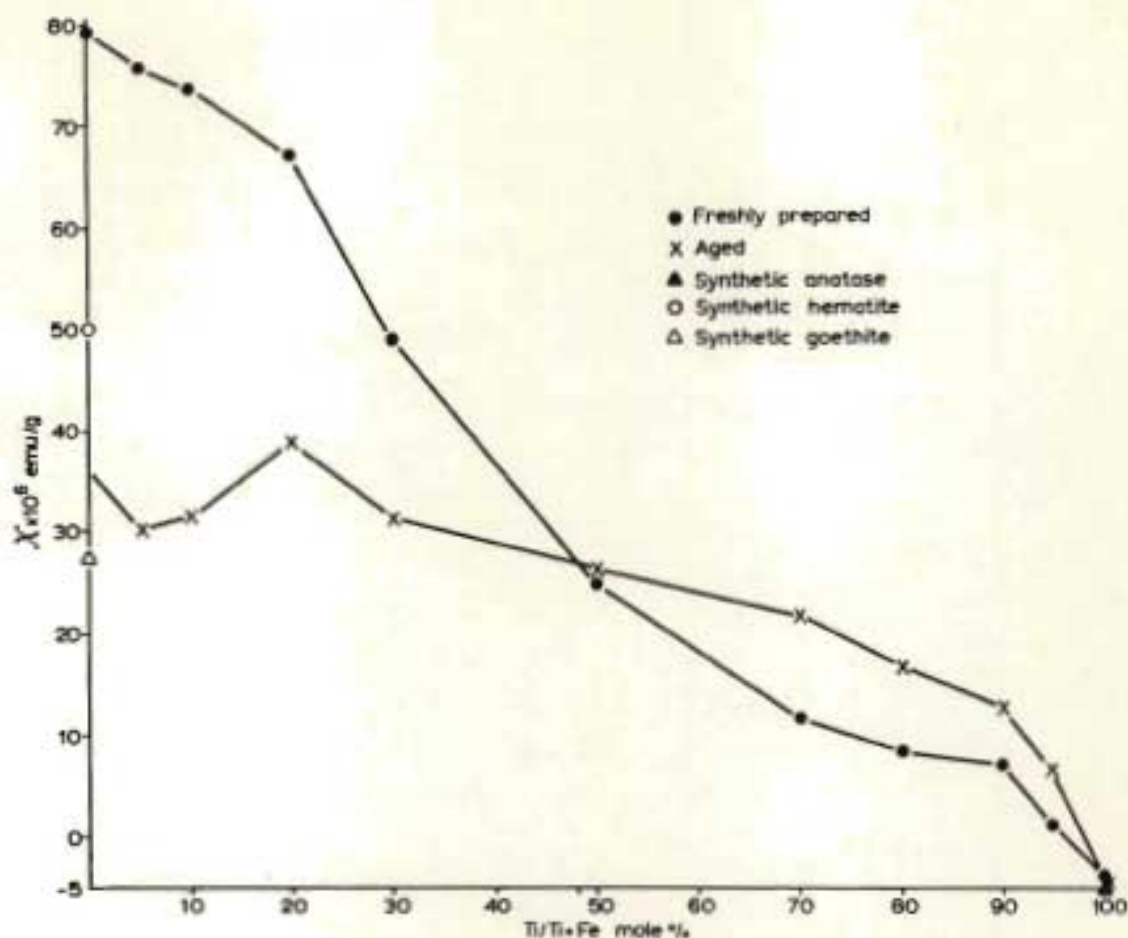


Fig. 3.6: Variation in specific magnetic susceptibility ( $\chi$ ) with the composition of freshly prepared (●) and aged (70°C at pH 5.5 for 70 days) (X) Fe-Ti oxides

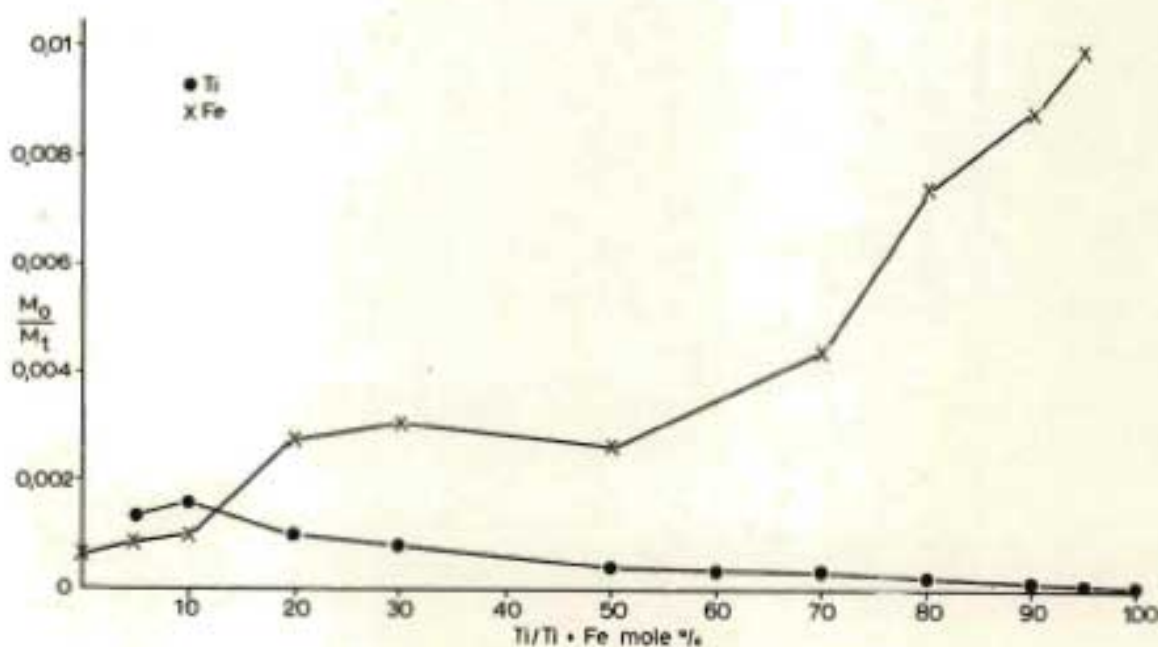


Fig. 3.7: Relationship between ammonium oxalate extractable Ti and Fe to total Ti and Fe ( $M_0/M_t$ ) and the composition of Fe-Ti oxides aged at 70°C and pH 5.5 for 70 days

the high Fe systems which are mainly ferrihydrite, crystallization proceeds slowly, while in the systems rich in Ti, crystallization takes place at a faster rate to form anatase.

#### 3.3.4 The effect of aging Fe-Ti oxides at pH 12 and 70°C for 70 days

The coprecipitates in the composition range  $0 < \text{Ti}/\text{Ti}+\text{Fe} < 0,30$  aged at pH 12 and 70°C for 70 days, contained relatively high amounts of oxalate soluble Fe and Ti (i.e. amorphous Fe-Ti) while in the oxalate residues large goethite crystals were detected by XRD (WHH of the 111 line =  $0,22^\circ 2\theta$ ) and electron microscopy. These observations are in general agreement with oxalate extraction data for oxides prepared from  $\text{FeCl}_3$  and  $\text{TiCl}_4$  and aged at pH 12 and 60°C for 30 days (Appendix 2). Because of the increased aging time, temperature and  $\text{Cl}^-$  free system employed here, the oxalate soluble values are slightly lower. The electron micrographs (Plate 3.1) show the large goethite crystals\* coated or embedded in amorphous Fe-Ti oxide.

#### 3.3.5 The effect of aging Fe-Ti oxides at pH 5,5 and 70°C for 70 days

The amounts of Fe and Ti removed by oxalate after aging the oxides at pH 5,5 and 70°C for 70 days were extremely low (Fig. 3.7) and constituted less than one per cent of the total Fe and Ti in the aged oxides (e.g.  $\text{Fe}_o/\text{Fe}_t < 0,01$ ;  $\text{Ti}_o/\text{Ti}_t < 0,002$ ). Furthermore, compared to the non-aged oxides there is a marked reduction in both charge (Figs. 3.4 and 3.5) and magnetic susceptibility (Fig. 3.6). These observations which indicate a marked degree of crystallization for the whole composition range (e.g.  $0 < \text{Ti}/\text{Ti}+\text{Fe} < 1$ ) are confirmed by both XRD (Figs. 3.1, 3.8 and 3.12) and IR (Fig. 3.9) results. Furthermore, aging at 70°C and pH 5,5 resulted in a slight increase in acidity probably as a result of the further hydrolysis.

##### 3.3.5.1 Composition range $0 < \text{Ti}/\text{Ti}+\text{Fe} < 0,20$

When the pure ferrihydrite was aged at 70°C and pH 5,5 for 70 days both goethite and haematite were detected by XRD (Figs. 3.8a and 3.12) and IR (Fig. 3.9) in agreement with previous work (Schellmann, 1959; Schwertmann, 1959). However, on increasing the Ti/Ti+Fe ratio to 0,05,

---

\* Dr. W.J. McHardy (personal communication) has carried out microanalysis on these single goethite crystals, after removing amorphous Fe-Ti with HCl, and found that Ti is incorporated in the goethite structure.



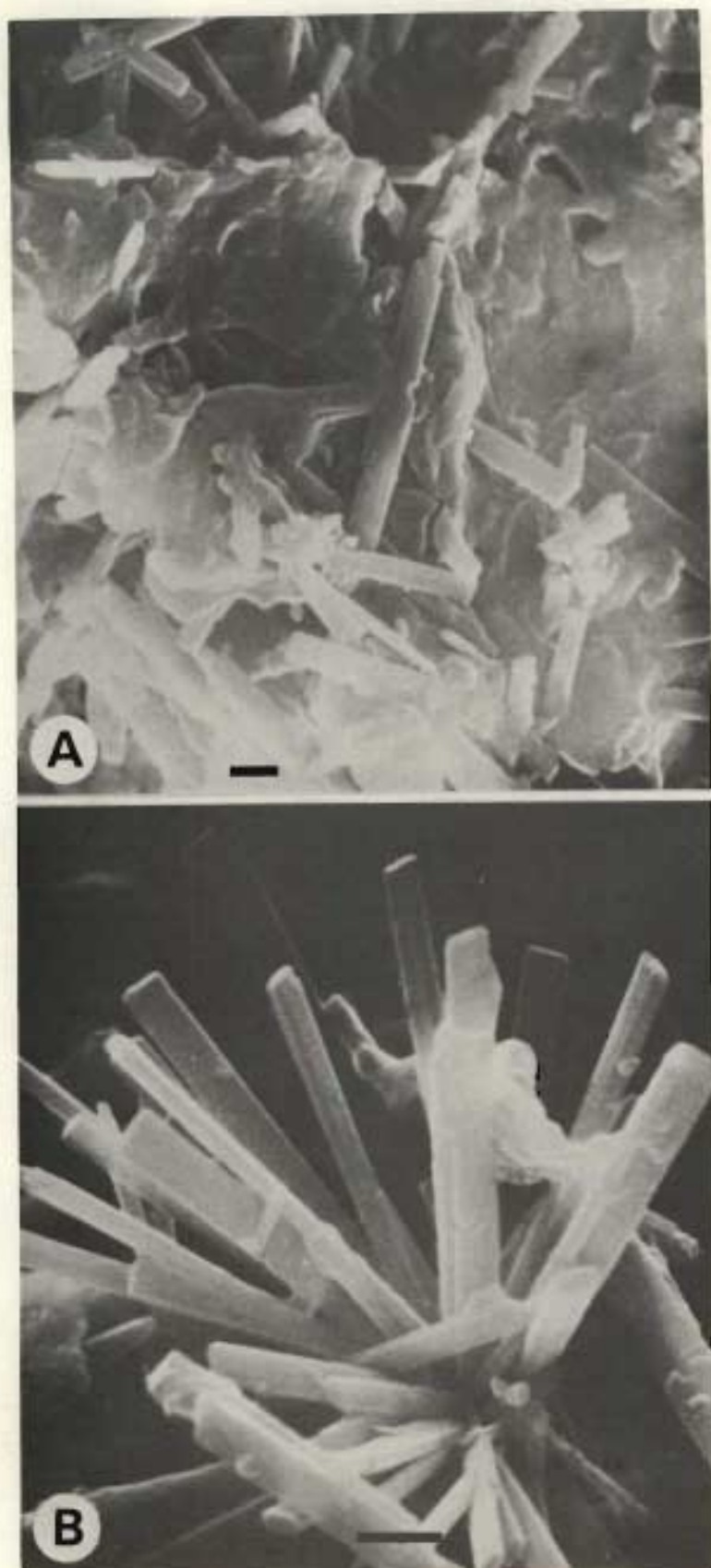


Plate 3.1: Electron micrographs of goethite prepared from Fe-Ti oxides with 30% in Ti/Ti+Fe aged at 60°C and pH 13 for 30 days and dialyzed against distilled water. Line in prints indicates 1 $\mu$ m. By courtesy of Dr. W.J. McHardy, Macaulay Inst., Aberdeen

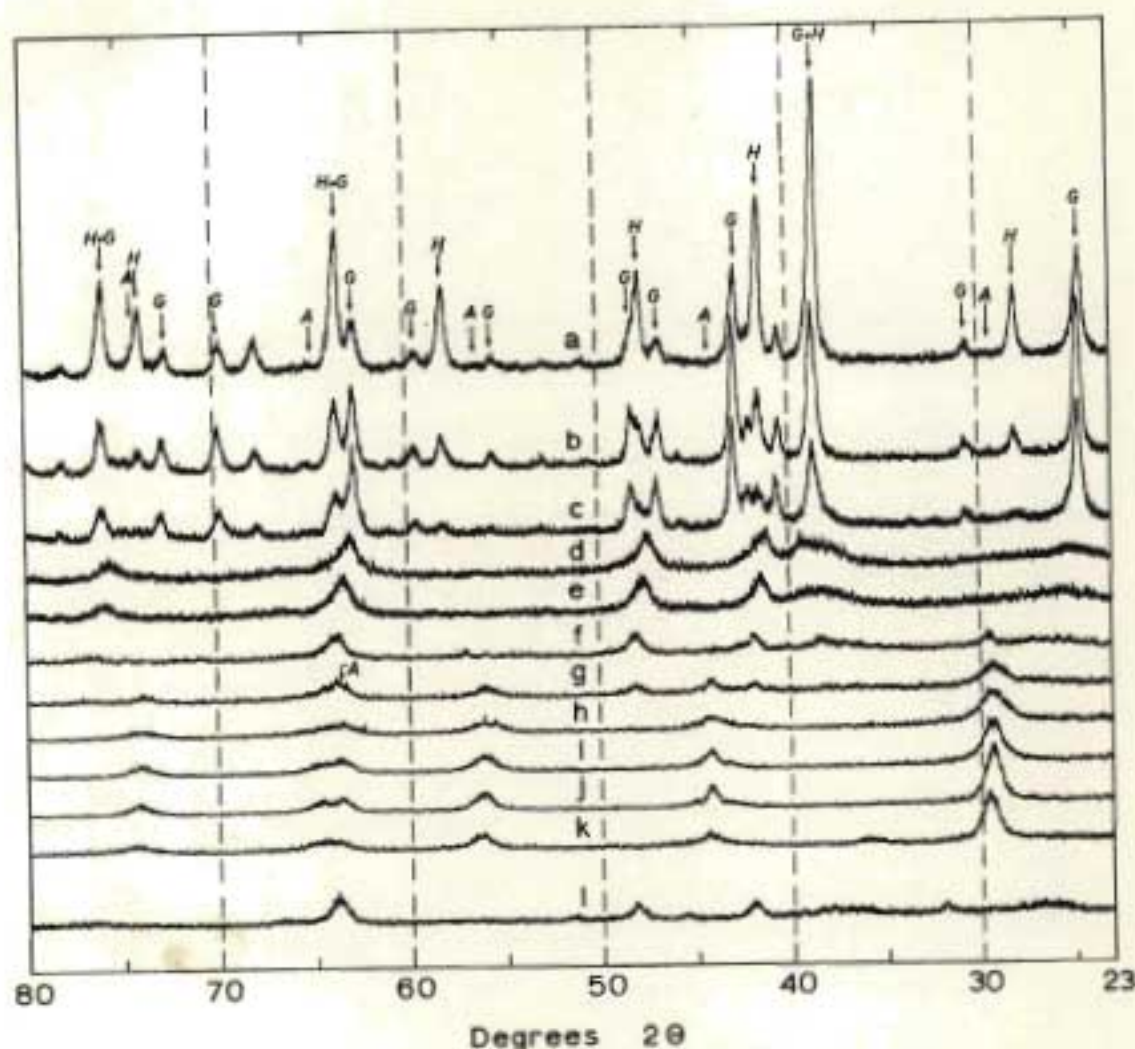


Fig. 3.8: X-ray diffraction patterns of synthetic Fe-Ti oxides aged at 70°C and pH 5,5 for 70 days with:  
 (a) 0%; (b) 5%; (c) 10%; (d) 20%; (e) 30%; (f) 50%;  
 (g) 70%; (h) 80%; (i) 90%; (j) 95%; (k) 100% in  
 Ti/Ti+Fe respectively, and (l) Indonesian pseudorutile  
 where: A = anatase; G = goethite; H = haematite

crystalline goethite is favoured, with a slightly lower X-ray line broadening while haematite is inhibited (Figs. 3.8, 3.9 and 3.12). In contrast goethite rather than haematite was suppressed in the Al-Fe coprecipitates in the composition range  $0,05 < \text{Al}/\text{Al}+\text{Fe} < 0,30$  when aged for 70 days at pH 5,5 and 70°C (Fig. 3.10; see also Schwertmann *et al.*, 1977). A possible explanation for this is that the Al-ferrihydrite structure might be less distorted than the Ti-ferrihydrite structure.



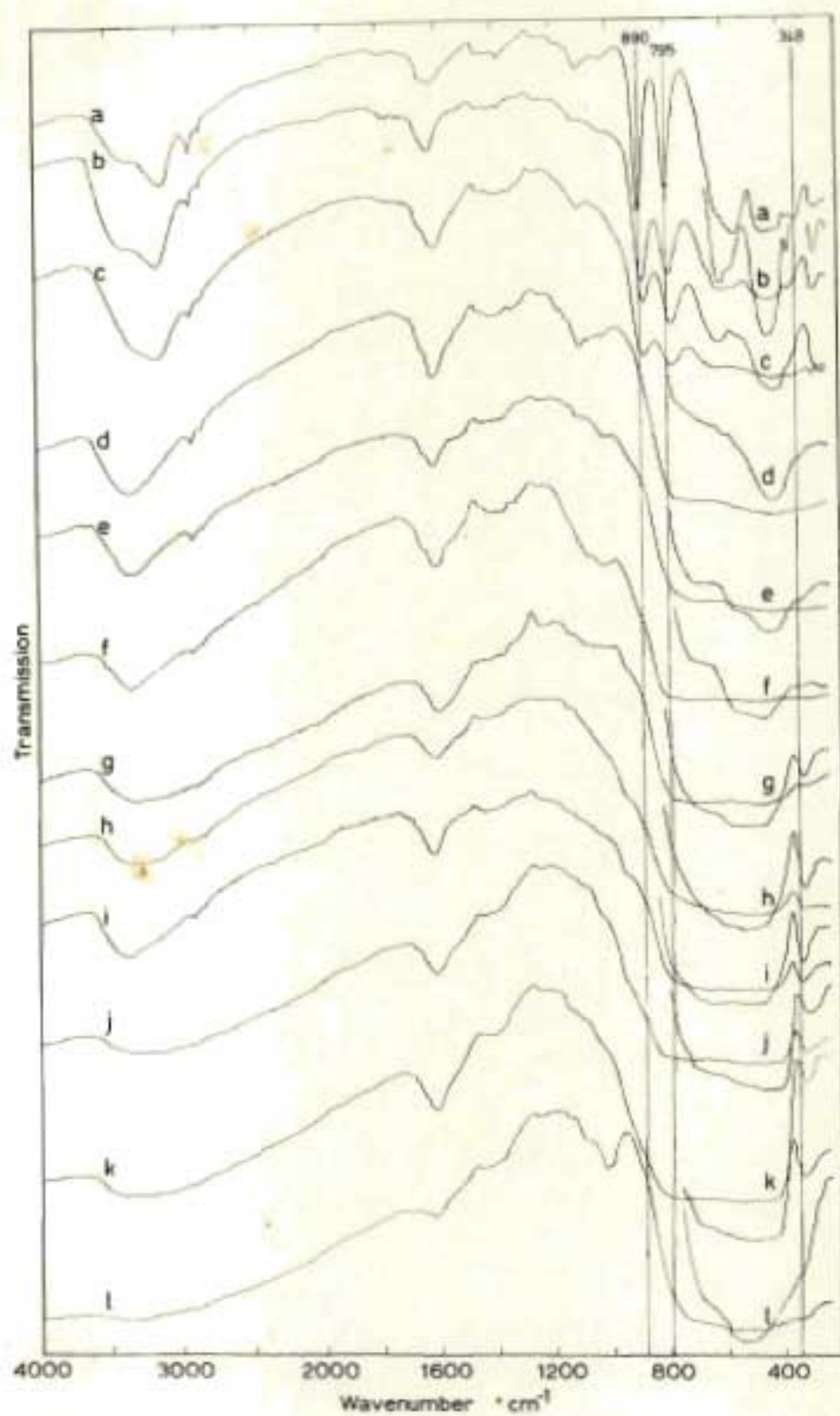


Fig. 3.9: Infrared spectra of synthetic Fe-Ti oxides aged at  $70^{\circ}\text{C}$  and pH 5,5 for 70 days. Legend as for Fig. 3.8

On increasing the Ti/Ti+Fe ratio in the composition range  $0,10 < \text{Ti}/\text{Ti}+\text{Fe} < 0,20$  the goethite peaks become progressively weaker and broader until Ti finally inhibits goethite crystallization. Herbillon and Tran Vinh An (1969) found that  $\text{SiO}_2$  inhibited the crystallization of "amorphous  $\text{Fe}_2\text{O}_3$ " to haematite.

There is a slight unexpected decrease in the d-spacing of the goethite (110) and (111) lines, together with a corresponding increase in crystallinity (determined by line broadening) as the Ti content increases, up to  $\text{Ti}/\text{Ti}+\text{Fe} = 0,10$ . The ionic size of Fe (III) ( $0,64 \text{ \AA}$ ) and Ti (IV) ( $0,68 \text{ \AA}$ ) are very similar and it is possible that small amounts of Ti ( $\sim 5$  to  $10$  mole %) may stabilize the goethite structure. A very striking feature is that the shift in d-spacing to higher angles with increasing Ti content is similar to that observed with increasing Al substitution in the goethite structure (e.g. Thiel, 1963 and others). However, much higher amounts of Al (up to 33 mole %) may be incorporated in the goethite structure, possibly because of the relatively smaller ionic radius of Al ( $0,57 \text{ \AA}$ ).

Table 3.3: X-ray diffraction and infrared absorption data for goethites in the aged synthetic Fe-Ti oxides of composition  $0 < \text{Ti}/\text{Ti}+\text{Fe} < 0,10$

Ti/Ti+Fe	$d_{110}$		$d_{111}$		IR $\text{cm}^{-1}$		
	$\text{\AA}$	$\frac{\text{WHH}}{2\theta}$	$\text{\AA}$	$\frac{\text{WHH}}{2\theta}$	890*	795*	650*
0,00	4,187	0,41	2,451	0,34	890	795	562 <sup>†</sup>
0,05	4,182	0,27	2,449	0,26	882	790	610 <sup>†</sup>
0,10	4,177	0,34	2,445	0,26	875	780	615 <sup>†</sup>

\* goethite

† haematite interference

The IR absorption maxima at 890 and  $795 \text{ cm}^{-1}$  due to O-H bending vibrations for structural hydroxyls in goethite (Marshall and Rutherford 1971) shift to lower frequencies and also broaden and decrease in intensity as the proportions of Ti in the aged oxides increases (Fig. 3.9 a - c; Table 3.3). Jonas and Solymar (1970) (see also Fig. 1.4) have observed shifts to higher frequencies in the position of the maxima of these two



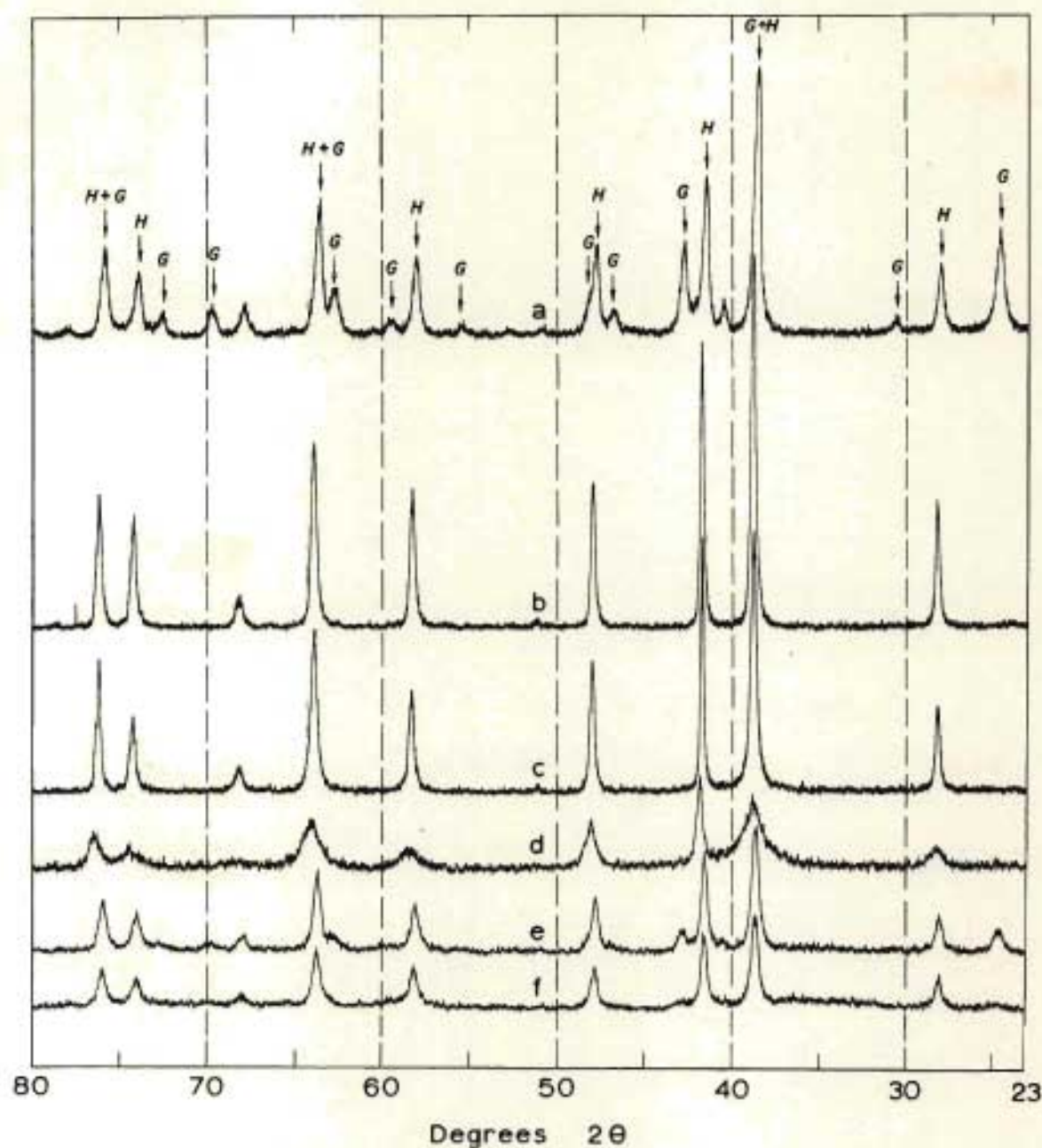


Fig. 3.10: X-ray diffraction patterns of synthetic Fe-Al oxides and Fe-Zr oxides aged at 70°C and pH 5,5 for 70 days with:  
 (a) 0%; (b) 5%; (c) 10%; (d) 20% in Al/Al+Fe  
 and (e) 5%; (f) 10% in Zr/Zr+Fe respectively  
 where: G = goethite; H = haematite

peaks with increasing Al for Fe substitution in the goethite structure.

Coprecipitates of Fe and Zr (IV) (ionic radius = 0,80 Å) in the range  $0,05 \leq \text{Zr}/(\text{Zr}+\text{Fe}) \leq 0,10$ , aged for 70 days at pH 5,5 and 70°C gave suppressed haematite reflections but the (111) goethite reflection showed a slight shift towards lower angles, suggesting isomorphous replacement of Zr for Fe in the goethite structure (Fig. 3.10 e and f). In addition, the line broadening of the (111) goethite line was larger for the aged Fe-Zr oxides than for the Fe-Ti oxides.

### 3.3.5.2 Composition range $0,20 < \text{Ti}/(\text{Ti}+\text{Fe}) \leq 0,70$

The complicated nature of the intermediate composition range (i.e. from  $0,20 < \text{Ti}/(\text{Ti}+\text{Fe}) \leq 0,70$ ) with rather broad XRD peaks (Fig. 3.8) which militate against precise peak distinction and peak height measurement (hence the hatched area in Fig. 3.12) has a pattern that resembles very closely natural Indonesian pseudorutile (Fig 3.8 l). According to Grey\* and Reid (1975) pseudorutile has only a moderate degree of crystallinity and this is confirmed by the broad X-ray diffraction lines in Fig. 3.8 and also by the relatively higher negative and positive charges (Fig. 3.5) observed for this composition range. Furthermore, the magnetic susceptibility values (Fig. 3.6) correspond closely to that for Malayan ilmenite which had undergone marked alteration to pseudorutile or "arizonite" (i.e.  $< 40 \times 10^{-6}$  c.g.s., Flinter, 1959).

The success in synthesizing pseudorutile *in vitro* by aging a Fe-Ti coprecipitate for 70 days at pH 5,5 and 70°C is probably mainly due to the role of the aqueous solution creating favourable conditions for the rearrangement of the Ti and Fe atoms which is essentially precluded for reactions at higher temperatures and pressures in the dry state (e.g. Buddington and Lindsley 1964) and is only partially successful under hydrothermal conditions (Karkhanavala, 1959; Karkhanavala and Momin, 1959). Under dry conditions and high temperatures (e.g. 1200°C) transformations are mainly topotactic. The identification of pseudorutile in these *in vitro* aging experiments suggests that pseudorutile (and anatase) can form at ambient temperatures. In addition, it demonstrates that

---

\* According to Grey (personal communication) this sample contains traces of rutile (Fig. 9 l; for comparative purposes the XRD of all the samples in Fig. 3.8 were run at the same intensity settings).



higher temperatures (e.g. magmatic or hydrothermal) are not a necessary requirement for the crystallization of pseudorutile or that it is strictly an alteration product of ilmenite, as many mineralogy text books imply.

With increasing titanium content the d-spacing shows a shift to higher angles (Table 3.4) indicating a definite decrease in the unit cell parameters as the Ti/Ti+Fe ratio increases (Fig. 3.11).

The shift in d-spacings to higher angles for both pseudorutile and goethite with increasing Ti content is not clear. A possible explanation is the incorporation of hydroxyls into the structure in order to maintain charge neutrality as a result of Ti substituting for Fe<sup>3+</sup>.

Table 3.4: Comparison between the three sharpest XRD lines for pseudorutile in the synthetic Fe-Ti oxides of composition  $0,20 < \text{Ti/Ti+Fe} < 0,70$ , Indonesian pseudorutile<sup>†</sup> and ASTM 19-635 Data reported for pseudorutile

Pseudorutile ASTM No. 19-635		Indonesian Pseudorutile <sup>†</sup> Ti:Ti+Fe = 0,69	Ti/Ti+Fe			
			0,20	0,30	0,50	0,70
			Å	Å	Å	Å
1,69	10	1,69	1,71	1,70	1,69	1,69
2,49	6	2,49	2,54	2,52	2,51	2,50
2,19	5	2,19	2,23	2,21	2,20	2,19

<sup>†</sup> Sample supplied by Grey and Reid (1975)

- \* An attempt was made to measure permanent positive charge (which could arise from the isomorphous substitution of the higher valence cation Ti<sup>4+</sup> in the Fe-oxide structures) by a method adapted from Sumner (1961) as follows: 200 to 300 mg samples were equilibrated overnight with 6 ml 0,005 M KCl (pH 10-11). The difference in chloride content between the supernatant and original solution reflects the positive or negative adsorption of chloride. However, no net positive adsorption of chloride was measured. This could possibly be due to the strong negative adsorption which is reflected by the microcrystalline nature and in turn the high surface areas of the oxides.

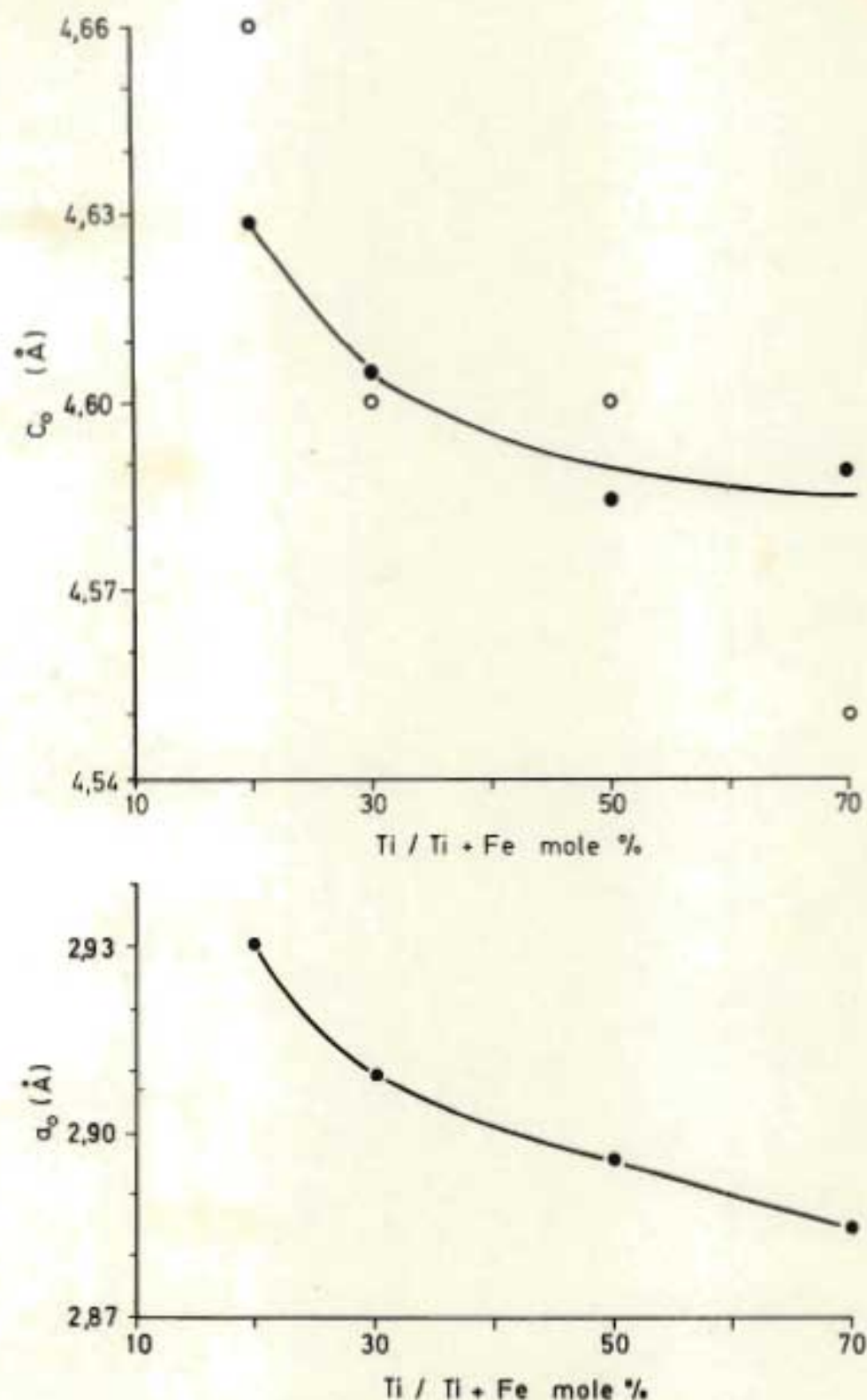


Fig. 3.11: Variation in unit cell parameters ( $a_0$  and  $c_0$ ) for pseudorutile in the composition range 0,20  $\leq$  Ti / Ti+Fe  $\leq$  0,70 (prepared from Fe-Ti oxides aged at 70°C and pH 5,5 for 70 days); where  $d_{101}$  was used to calculate the points corresponding to the open circles (o)



### 3.3.5.3 Composition range $0,70 < \text{Ti}/\text{Ti}+\text{Fe} < 1,0$

In the composition range  $0,70 < \text{Ti}/\text{Ti}+\text{Fe} < 1,0$  anatase was the main oxide detected by XRD (Figs. 3.8 and 3.12).

The IR spectra shown in Fig. 3.9 provide further evidence for the anatase phase ( $348 \text{ cm}^{-1}$ ). The low magnetic susceptibility values for the pure Ti phase compares favourably with that of synthetic anatase reported by Pankey and Senftle (1959) [i.e.  $(0,04 \pm 0,0003) \times 10^{-6}$ ]. The relatively low  $\text{Ti}_\text{O}/\text{Ti}_\text{T}$  ratio ( $< 0,01$ ; Fig. 3.7) confirmed the crystallinity of the anatase, while the low  $\text{Fe}_\text{O}/\text{Fe}_\text{T}$  ratio suggests that the Fe is incorporated in the anatase structure since no other phase was detected. The WHH of the anatase (101) line increases as the  $\text{Ti}/\text{Ti}+\text{Fe}$  ratio decreases, suggesting that higher amounts of Fe progressively inhibit anatase crystallization (Figs. 3.8 and 3.12).

Evidence for possible Fe replacement for Ti in the anatase structure was also obtained by heating the freshly prepared coprecipitates at  $250^\circ\text{C}$  for 10 days which once again resulted in smaller anatase crystals with increasing iron content as shown by the general increase in line broadening (Fig. 3.12). Thus, although anatase and ferriferous anatase show similar XRD lines they differ in WHH on heating in air or aging *in vitro* and this is related to crystallite size. Anatase formed by aging amorphous  $\text{TiO}_2$  *in vitro* at  $70^\circ\text{C}$  and pH 5,5 for 70 days has less line broadening than anatase produced by dry heating at  $250^\circ\text{C}$  for 10 days (Fig. 3.12). This suggests that the rearrangement of Ti atoms to form crystalline anatase and especially ferriferous anatase is apparently more effective in aqueous suspension than by dry heating even at high temperatures.

Coprecipitates of Zr and Ti in the composition range  $0,05 < \text{Zr}/\text{Zr}+\text{Ti} < 0,10$  aged at  $70^\circ\text{C}$  and pH 5,5 for 70 days resulted in anatase with very broad but symmetrical (101) peaks with WHH  $4,5^\circ 2\theta$ . Furthermore, a slight shift to smaller angles was observed, suggesting that Zr replaces (partly) Ti in the anatase structure. It has been suggested by Valetton (1972) that in bauxites Zr may replace Ti in the anatase structure.

CED extracts very small amounts of the total Ti ( $\text{Fe}_\text{d} = 0,90\%$ ) from the pure poorly crystalline anatase phase (e.g.  $\text{Ti}/\text{Ti}+\text{Fe} = 1$  with a WHH of 4), whereas oxalate dissolves 30% of the total Ti (Fig. 3.2). There is a fairly good relationship (Fig. 3.2) between  $\text{Ti}_\text{O}$  and the MCD of

of anatase (101) below  $50 \text{ \AA}$ ,  $\text{WHH} > 2,0^\circ 2\theta$ , regardless of composition. This relationship does not hold for CBD soluble Ti when Fe is present in the system. Thus, a fairly crystalline anatase with a WHH of  $2,8^\circ 2\theta$  and a composition of  $\text{Ti}/\text{Ti}+\text{Fe} = 0,80$  has a  $\text{Ti}_\text{O} = 4,0\%$  (Fig.3.2) and  $\text{Ti}_\text{d} = 2,1\%$ . The relatively higher amounts of CBD soluble Ti from the ferriiferous anatase phase (regardless of crystallinity) is probably due to preferential removal of Fe from the anatase structure by Fe reduction.

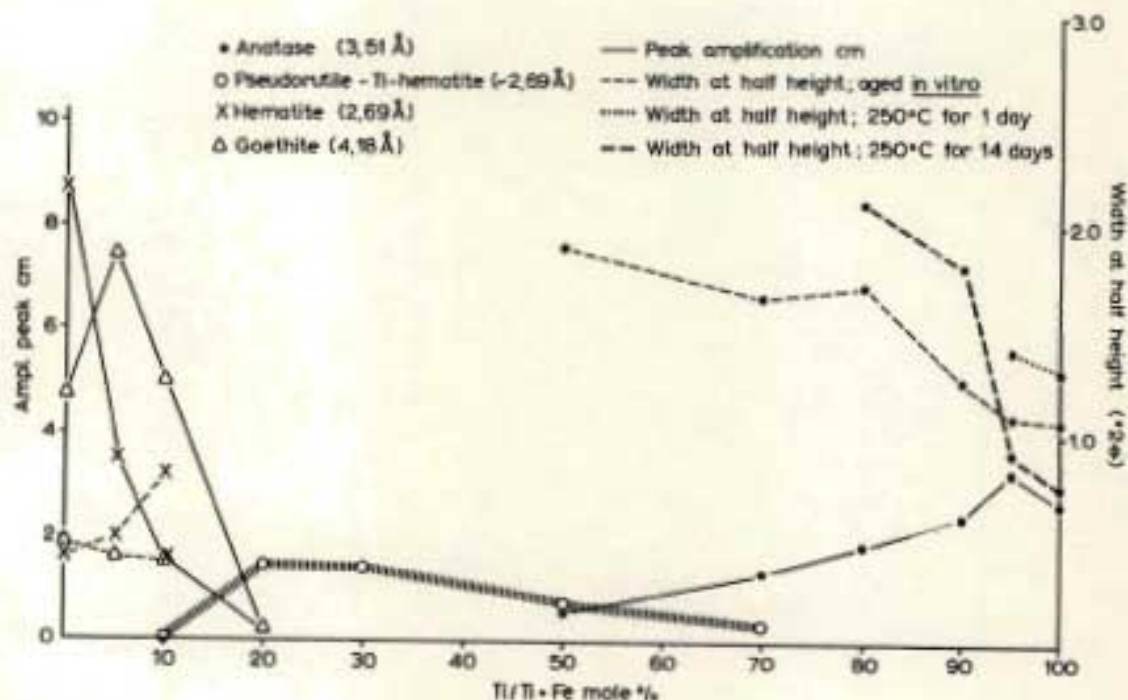


Fig. 3.12: X-ray diffraction data evaluation (cm relative intensity and width at half height) in relation to composition ( $\text{Ti}/\text{Ti}+\text{Fe} \%$ ) of the crystalline species present in the titanoferric system after aging *in vitro* for 70 days at  $70^\circ\text{C}$  (pH 5,5) and heating in air at  $250^\circ\text{C}$  for 1 day and 14 days



### 3.4 Conclusions

Titanium may occur in certain soils without being sufficiently crystalline to be detected by XRD techniques. An estimate of these poorly crystalline forms of  $\text{TiO}_2$  can however be obtained by chemical extraction technique. Extraction of a series of synthetic Ti oxides with acid ammonium oxalate (2 hours in the dark) confirmed that oxalate selectively removes X-ray amorphous  $\text{TiO}_2$  and partly dissolves micro-crystalline anatase with  $\text{MCD} < 50 \text{ \AA}$  or  $\text{WHH} \geq 2,0^\circ 2\theta$ . This method is superior to other commonly used reagents (e.g.  $\text{HCl}$  or  $\text{H}_2\text{TiF}_6$ ) and enables one to characterise more fully the nature and amounts of secondary titanium oxides ranging from X-ray amorphous  $\text{TiO}_2$  to poorly crystalline and crystalline anatase, and to relate these findings to soil development (e.g. in a soil-climate-toposequence).

The positive and negative charge of the freshly coprecipitated titanoferric oxides appear to be analogous to that proposed for synthetic amorphous aluminosilicates. Furthermore, it is suggested that the composition of the starting Fe-Ti oxide has a pronounced influence on the crystallization of the final product upon aging.

Coprecipitates of Fe and Ti aged at high pH ( $> 10$ ) and  $70^\circ\text{C}$  was found to be present primarily as an amorphous phase adsorbed on large goethite crystals (with minor Ti isomorphous substitution). Aging at lower pH (5,5) and  $70^\circ\text{C}$  for 70 days, Fe and Ti combined to form crystalline phases (e.g. goethite, haematite, pseudorutile and anatase) depending on the Ti/Ti+Fe ratio. The transformation of freshly prepared oxides to crystalline products was monitored by XRD and IR, and showed corresponding decreases in solubility in oxalate, negative and positive charges, and magnetic susceptibility.

Pseudorutile can be successfully synthesised under aqueous conditions at pH 5,5. This suggests that it may form not only from the weathering or decomposition of primary Ti-containing oxides (e.g. ilmenite) but also from the more weatherable Ti-bearing silicates (e.g. sphene, hornblende or biotite) under earth surface conditions (e.g. in bauxites and Ti-rich beach sands). This would involve removal of Fe and Ti from the primary mineral followed by precipitation and crystallization of Fe-Ti oxides rather than by topotactic oxidation of primary Ti-oxides. Thus, Fe-Ti coprecipitates ranging in composition from  $0 < \text{Ti}/\text{Ti}+\text{Fe} < 1$  may be present in the immediate

"micro-weathering zone" (e.g. cracks) of an ilmenite or sphene crystal. The composition of the weathering solution (Ti/Ti+Fe ratio) and hence the crystallization product will be dependent largely on the rate of removal of iron from the primary mineral which is controlled by the prevailing Eh-pH conditions. Under reducing conditions iron is rendered mobile in the ferrous state and is relatively more mobile than titanium. A certain amount of iron is required to form pseudorutile via solution and when the iron is removed by weathering, the titanium atoms rearrange to anatase which may contain small amounts of Fe (< 5%).

In the light of these results an appreciation of synthetic Fe-Ti oxide mixtures, precipitated and aged under conditions comparable to natural environments, is critical in studies on the genesis of weathering processes and soil formation. The application of synthetic studies of this kind to studies of secondary Fe-Ti weathering products is suggested.



## CHAPTER 4

FORMS OF PEDOGENIC IRON AND TITANIUM  
AND THEIR DISTRIBUTION IN RELATION  
TO CLIMATE AND TOPOGRAPHY

4.1 Introduction

The study area provides an excellent landscape in which to examine the distribution and genesis of pedogenic Fe and Ti. It contains many sharply divergent landforms (Fig. 2) in which a wide range of soils (Fig. 1)\* and various forms and types of Fe and Ti oxides have developed. Within 200 km the vegetative cover (Fig. 2) changes from coastal forest (Coast Lowlands), to *Acacia* savanna in the valleys (Riverine and drier Basin Plainlands), and to Afro-alpine grassland at an altitude over 3 000 m (Lesotho Plateau). The complexity of soil forming factors in the area results in a varied but repetitive pattern of a large number of different soils (Fig. 1) which conform remarkably closely with the present day bioclimate of the area (Fig. 2). However, there is some evidence that several soils in the area may also be representative of periods during which pre-weathering and colluviation of parent materials took place (de Villiers, 1962; 1965). It has therefore become apparent that the specific forms of iron and titanium compounds can only be identified after careful field observation, detailed sampling and laboratory investigation (see Chapters 1 - 3).

Samples were selected from several altitudinal sequences (i.e. climo-sequences) to encompass several soil environments. In addition, numerous toposequences and over 200 specific profiles were sampled in detail (e.g. mottles, concretions, nodules, bands, crusts, saprolites, pipestems and ferricretes etc.) during the five year reconnaissance soil survey of this area. Additional samples in the form of synthetic oxides, (pure Fe; and mixed Fe-Al and Fe-Ti oxides) and standard Fe minerals were used to provide an adequate range for comparison.

The various forms of "pedogenic" iron and titanium found in this area have been classified into 4 main categories: (i) primary, (ii) secondary layer silicate, (iii) organic, and (iv) oxidic (ferrihydrite,

---

\*To illustrate the general soil-terrain-climate relations more clearly a similar colour code was used in both the generalised sketch showing the landscape and bioclimate regions (Fig. 2) and in the generalised soil map (Fig. 1).

pseudorutile, goethite, haematite, maghaemite, lepidocrocite, anatase and rutile). The objective of this chapter is to give an overall assessment of the distribution, formation and relationships of the various pedogenic forms of Fe and Ti in the area.

## 4.2 Results and Discussion

Data presented in earlier chapters for various goethite, magnetic and titaniferous compounds as well as that for primary, secondary silicate, organic, ferrihydrite, haematite and lepidocrocite are summarized and compared in Table 4.1 for a selected range of soils covering a wide range of physiographic and bioclimatic regions (Figs. 1 and 2).

### 4.2.1 Primary Fe and Ti

The area has undergone weathering since Tertiary times (i.e. undisturbed by glaciation; de Villiers, 1962; King, 1967) and many of the soils, although depleted of primary silicate Fe (e.g. augite) contain weakly to highly oxidized detrital opaque Fe-Ti oxide grains (e.g. Ti-magnetite and ilmenite) which may provide some evidence of their parent materials and possibly the degree of weathering. Fitzpatrick and le Roux (1975; 1976) detected high concentrations of Ti-magnetite and Ti-maghaemite (up to 43 mass %) in several red structured soils. Relatively unaltered "ulvöspinel" and Ti-magnetite persist in the coarse sand fractions of these soils and with decreasing particle size become progressively altered mainly to cation deficient Ti-magnetite or Ti-maghaemite by topotactic oxidation (Fitzpatrick and le Roux, 1975; Chapter 2). The yellow-brown soils of the Afro-alpine zone contain unusually high amounts of weakly oxidized Ti-magnetite and ilmenite (Fitzpatrick, 1978). The soils in both these areas may be considered to be relatively young and have iron-rich parent materials with high contents of magnetite and/or Ti-magnetite (Table 4.1).

However, irrespective of textural class, there is a definite decrease of magnetite relative to ilmenite in successively older red and yellow soils (Oxisols) which occur in the Highland and Mistbelt areas (Table 4.1). This is due to increased weathering (i.e. oxidation and transformation to more stable oxides such as maghaemite, haematite and goethite) and depletion of the detrital magnetic opaque oxides (Fitzpatrick, 1974). The secondary weathering products may coat or protect these sand size opaque Fe-Ti oxides which eventually, with time, become concretions. Significant, is the fact that the pedogenic processes controlling these primary Fe-Ti minerals appear



Table 4.1 Relative abundance of Fe and Ti compounds in soils along the eastern seaboard of South Africa<sup>1</sup>

REGION (Fig. 2) (Location)	Soil	Soil Zone Fig. 1	Diagnostic Horizon <sup>2</sup>	Other Components <sup>3</sup>	Primary Fe and Ti <sup>4</sup>		Sec. Si, Fe	Org. Fe	Oxidic Fe and Ti <sup>6</sup>					
					Il.	Magn.			Fer.	Goethite	High Al.	Low Al.	Hem. Magh.	Lep. An.
Afro-alpine (freely drained sites)	Clovelly	1	A Orthic (sh) B Yell.-br.op.		++	++	+	++++	+++			++		
					+	+++	++	++	+++			+++		
Montane/High- lands (S-aspect; freely drained sites)	Clovelly	2	A Orthic (sh) B Yell.ap. C		++	+	tr	+++	tr	+++				tr
					++	+	tr	+		+++				tr
					+	++	tr			++				tr
Montane/High- lands (W-aspect; freely drained sites)	Hutton	2	A Orthic B Red ap. C		+	+	tr	+	tr	+++			+	tr
					+	++	tr			++++			++	tr
					+	+++	tr			++			+	tr
Montane/High- lands (S-aspect; slope gley)	Pinesburg	2	A Orthic B Yell. ap. Bg Gley cut.	bn, cr soft halo ps hard ps	++	+	tr	++	tr	+++	+			tr
					++	+	tr	+		+++	+			tr
											++			tr
										+++				tr
Highlands/Hist- belt (freely drained sites)	Griffin	2	A Orthic B2i Yell. ap. B23 Red ap. C	cn cn cn	++	+	tr	++	tr	+++	+		+	tr
				cn	tr	tr		tr	tr	+++	+++	+	+	tr
				cn	+	+	tr	tr	tr	+++	++	++	+	tr
				cn	tr	tr		tr	tr	+++	+++	+++	+++	tr
				cn	tr	tr				+++	++	+++	+++	tr
				bn	+	+++	tr			++++	+	+	++++	tr
Highveld	Arcadia	9	A1 Vertic		+		++++	++	++++					tr
Coastal Winter- land/Basin	Hutton <sup>1</sup>	4	A1 Orthic		++	+	tr	++		+++		+	+	tr
Plainlands/Highveld (Upland)		6		cn		tr					++	tr	+	tr
		7	B Red ap.	cn	++	+	tr	+		+++		+	+	tr
		8		cn		+				+++	++	++		tr
(Midslope)	Avalon <sup>2</sup>	14	A1 Orthic B22 Yell.ap. B23 Soft plinth.	cn cn Yellow mat. Red mo.	++		tr	++		+++	+		tr	+
				cn	++		tr	+		++++	+++	+	+	+
(Bottomland)	Wabank <sup>1</sup>		A1 Orthic B (hp)	cn cn	+			+++	+	++		+++		tr
				cn							+++			tr
											++++			tr
Riverine (midslope)	Shorclands	5	A1 Orthic	cn	++	++	tr			++	++	++	+	tr
		12		cn							+++	++	tr	tr
		15	B2 Red str.	cn	+	+++	+			+++	++	+++	++	tr
(Bottomland)	Rensburg		A1 Vertic	cn	+	+	+++	++	++++		+++	+		tr
Coastal Lowlands (Midslope) ("dunes")	Shorclands	19	A Orthic B Red str. A Orthic B Red ap. B Red ap.		++	++	tr	++		++	++	++	tr	tr
					+	+++	tr	tr		+++	++	+++	tr	tr
	Hutton				+++		tr	+		+	+++	+	++	++
				cn/hp/ps						+	+++	++	tr	++
										++++	+			tr

<sup>1</sup>Amounts: tr = traces; + = very small; ++ = small; +++ = medium; ++++ = large; +++++ = very large.<sup>2</sup>Slope toposquence (red-yellow-grey plinthic catena).<sup>3</sup>According to: MacVicar, de Villiers and Loxton et al. (1977) where sh = humic phase; yell. = yellow; br. = brown; ap. = apedal; cut. = cutanic; str. = structured; plinth. = plinthite.<sup>4</sup>bn = bands; cr = crusts; cn = concretions; ps = pseudomorphs; hp = ferricrete; mat = matrix; mo = mottles<sup>5</sup>Il. = ilmenite; Magn. = magnetite; <sup>6</sup>Sec. Si, Fe. = Secondary silicate Fe (Fe<sub>2</sub> - Fe<sub>3</sub>); <sup>7</sup>Org. Fe = Organic Fe (pyrophosphate extractable = Fe<sub>p</sub>); <sup>8</sup>Fer. = ferrihydrite (NH<sub>4</sub>-oxalate-pH extractable = Fe<sub>o</sub>); High Al. = high Al-substituted; Low Al. = low Al-substituted; Hem. = hematite; Magh. = maghemite; Lep. = lepidocrocite; An. = anatase.

to go on operating for a long period of time after deposition.

#### 4.2.2 Secondary layer silicate Fe and Ti

Pedogenic silicate Fe predominates in the marginalitic soils (vertic and non-vertic black clays) formed in poorly drained or "youthful" areas mainly from basic igneous rocks. Vast tracts of these marginalitic soils occur in the Transvaal Highveld (Fig. 2; Fig. 1, map symbol No. 9) and are developed under a relatively high rainfall ranging from 700 to 800 mm per annum (Fitzpatrick and le Roux, 1977; van der Merwe and Heystek, 1955). Isolated patches occur in bottomland positions in the drier regions (i.e. Riverine and Basin Plainlands, Fig. 2) throughout the region (van der Eyk, MacVicar and de Villiers, 1969; Fitzpatrick, 1974) and along the coastal lowlands (young soils derived from Fe-rich lower Ecca shales\* and dolerite;\* Beater 1957, 1959, 1962). In the Montane region, the holes and cracks of fresh to partly weathered basalt rocks in colluvial sediments, are filled with a waxy, green to red ferriferous smectitic clay.

The largest proportions of Fe (87% of the total Fe) and possibly Ti in the clay-size fractions of Transvaal Vertisols are incorporated in partly chloritized Fe-rich smectite with  $Fe > Mg + Al$  in the octahedral sheet (and interlayer positions), while in the upland non-vertic clays (Mollisol) the iron is in a more "open structured" chloritized iron-smectite (Fitzpatrick and le Roux, 1977).

The genesis of these ferriferous smectitic soils is favoured (i) primarily by a restricted internal drainage regime (i.e. controlled by topography) (ii) by an iron-rich parent rock, such as dolerite and basalt, and (iii) a limited degree of rock weathering (as suggested by the tendency of ferriferous smectite to increase with depth, especially in saprolite).

Small amounts of Fe ( $\leq 2.0\%$  Fe) may also be incorporated in the octahedral sheet of kaolinite in sesquioxidic soils. This is suggested by the incomplete Fe dissolution when clays are treated with HCl, and the

---

\*Although Beater (1959; 1970) does not report "free Fe" values (i.e.  $Fe_d$ ), the high total Fe values (8 to 21 percent  $Fe_2O_3$ ) recorded for clay-size fractions from marginalitic soils suggests that these soils derived from lower Ecca shales and dolerite contain iron-rich smectite.



Mössbauer spectroscopic data of Golden (1978) on sample Nos. 16M and 25M described by Fitzpatrick (1974).

#### 4.2.3 Organic Fe and Ti

McKeague, Brydon and Miles (1971) have shown that approximate differentiation can be made among organically complexed Fe, amorphous inorganic Fe and more or less crystalline Fe oxides by selective dissolution of soils with pyrophosphate (pH 10),  $\text{NH}_4$ -oxalate (pH 3) and citrate-bicarbonate-dithionite (CBD), respectively. These methods were also used to extract Ti (and Mn) by Fitzpatrick (1974). Throughout the study area the pyrophosphate extractable Fe ( $\text{Fe}_p$ ) and Ti ( $\text{Ti}_p$ ) decreased with depth in the profiles (Fitzpatrick, 1974; Fitzpatrick and le Roux, 1975; 1976). This may be attributed to the bonding of Fe and Ti by organic complexes in the soils. High amounts of organic Fe and Ti seem to be confined to the humic A horizons (up to 70% of the  $\text{Fe}_d$  and  $\text{Ti}_d$ ) of the Afro-alpine soils and organic-rich surface horizons of hydromorphic soils (Table 4.1). In most of the sesquioxidic freely drained soils the oxalate soluble Fe ( $\text{Fe}_o$ ) generally exceeds  $\text{Fe}_p$  especially in subsoil horizons, which in turn is generally less than 10% of  $\text{Fe}_d$  and  $\text{Ti}_d$  (Fitzpatrick, 1974).

#### 4.2.4 Oxidic Fe and Ti

##### 4.2.4.1 Protoferrihydrite and ferrihydrite

Protoferrihydrite and ferrihydrite (Chukhrov *et al.* 1972; Schwertmann and Fischer, 1973) have been observed in a number of localities throughout the study area (Fig. 4.1) mainly along drainage ditches (Plates 4.1A and 4.2 A) and water courses. Two types of occurrences were found:\* (i) brown gel-like precipitates (Plate 4.1 A) and, (ii) dark reddish-brown rusty friable crusts either "caked" on the sides of drainage ditches (Plate 4.2A) or weakly cementing unweathered gravel (Plate 4.2 D) in lithosols that have been cut by streams in the Montane region. In the gel-like samples only two "broad" XRD lines at  $\sim 2.54$  and  $\sim 1.47 \text{ \AA}$  are visible (Figs. 4.2 a and 4.3)

\*All reddish-brown gel-like samples were collected in plastic containers whereas the crust materials were scraped free of the soil surface and separated from most of surrounding soil by picking out the material with a knife. Both materials were then dispersed either by stirring or mild soniprobe treatment in distilled water and the silt and sand particles separated by sedimentation and decantation. The suspension was concentrated by centrifugation and either freeze-dried or dried on a water bath.



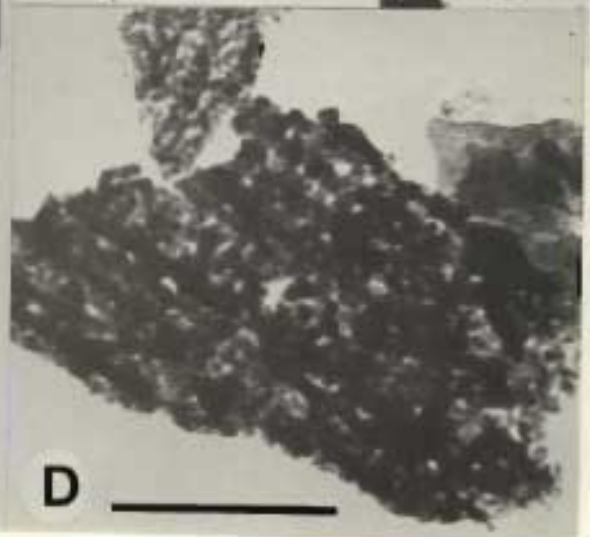




Plate 4.1: A. Photograph of drainage ditch near Cedarville (No. 13) showing a strong brown (7,5 YR 5/8) sludge-like or gel-like precipitate (i.e. "ochreous deposit") presently being deposited from spring water issuing from a crack in the side of the ditch.

B and C. TEM of ensheathed filaments of "iron-oxidizing" bacterium mainly *Sphaerotilus* encrusted with protoferrihydrite from sample No. 13, at increasing magnification. In B and C bar is 5,0  $\mu\text{m}$  and 0,5  $\mu\text{m}$  respectively.

D. TEM of protoferrihydrite from sheath structure at high magnification showing typical small spherical-like particles. Bar is 0,5  $\mu\text{m}$ .





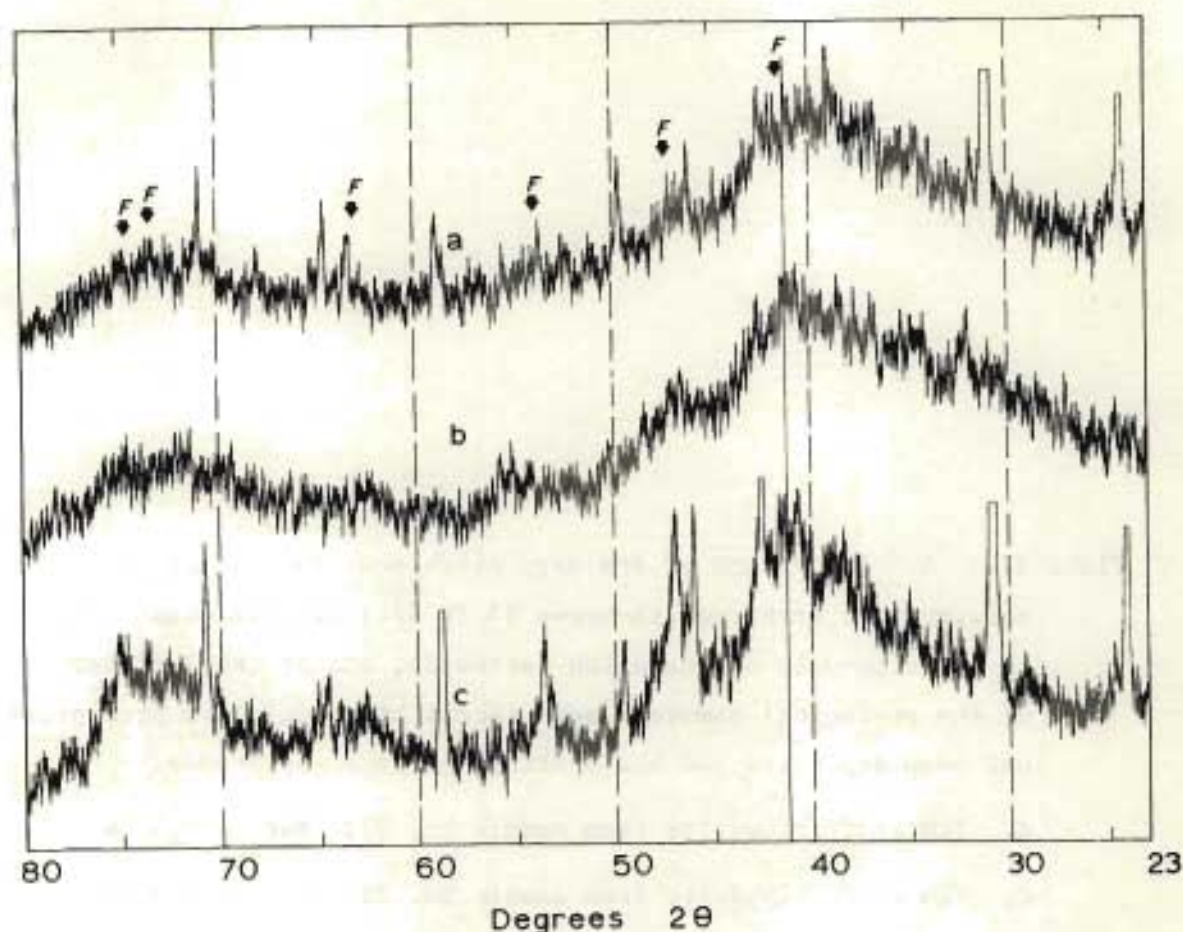


Fig.4.2: X-ray powder diffraction patterns of (a) gel-like precipitate from Cedarville, No. 13 (Plate 4.1 A), (b) crusts from Sani Pass, No. 234 (Plate 4.2 D), and (c) thin crusts from Palm Beach, No. 232 (Plate 4.2 A); where: F indicates broad XRD lines for ferrihydrite from right to left (i.e. with increasing  $2\theta$  values) at  $\sim 2.5$ ;  $\sim 2.22$ ;  $\sim 1.97$ ;  $\sim 1.71$ ;  $\sim 1.5$  and  $\sim 1.47$  Å

whereas in the crust samples the XRD lines at  $\sim 2.54$  and  $\sim 1.47$  Å are slightly sharper and the weaker lines at  $\sim 2.22$ ;  $\sim 1.97$  and  $\sim 1.71$  Å are more evident (Figs. 4.2 b and c). Furthermore, the latter samples were only 80 to 90% oxalate soluble (i.e.  $\text{Fe}_\text{O}$ ) whereas the others are completely oxalate soluble. According to Chukhrov *et al.* (1972) and Chukhrov (1973) ferrihydrite is characterized by 6 XRD lines at 2.50-2.54; 2.21-2.25; 1.96-1.98; 1.70-1.72; 1.51 and 1.47-1.48 Å whereas ferrihydrite in the initial stage of crystallization is referred to as protoferrihydrite and is characterized by only the two strongest lines at  $\sim 2.54$  and  $\sim 1.47$  Å. Hence, it is possible that the two types of occurrences identified in this




Plate 4.2: A. Photograph of drainage ditch near Palm Beach (No. 232) showing thin dark reddish-brown (5 YR 5/4) friable crusts "caked" on the side-wall of the ditch (arrowed), and on the left hand side of the geological hammer a more recent brown gel-like precipitate has been deposited and has a shiny, surface appearance.

B. TEM of ferrihydrite from sample No. 232. Bar is 0,5  $\mu$ m.

C. TEM of ferrihydrite from sample No. 234. Bar is 5,0  $\mu$ m.

D. Photograph of dark, rusty friable ferrihydrite-rich crusts weakly cementing unweathered gravel (basalt and TMS) to the surfaces of larger round basalt fragments from a lithosolic soil that has been cut by streams near the Sani Pass hotel (No. 234).





study, namely the gel-like precipitates and crusts may correspond to protoferrihydrite and ferrihydrite, respectively. Schwertmann and Fischer (1973) identified natural and synthetic samples that were also still in the protoferrihydrite stage and stated that a continuum exists between amorphous and crystalline forms, which makes any definition of poorly crystalline forms somewhat arbitrary.

TEM examination indicates that these protoferrihydrites are minute spherical particles (Plate 4.1 D) similar to those described by Schwertmann and Fischer (1973), and are embedded or encrusted in sheath structures of so-called "iron-oxidizing" bacterium (Plates 4.1 B and C, and 4.2 B and C) and comprising mainly *Sphaerotilus* (i.e. in No. 13, which was examined by Dr. J.C.G. Ottow, personnel communication). These sheaths are highly resistant to  $H_2O_2$  treatment. Several workers (Iwasa, 1965; Fischer and Ottow, 1972; Chukhrov *et al.*, 1972; Ivarson and Sojak, 1978) have described these and similar types of micro-organisms with iron encrusted filaments or sheaths.

The water issuing from the sides of drainage ditches and the mother solutions of the "presently" precipitating gel-like protoferrihydrite, have a pH range 6.0-7.0.

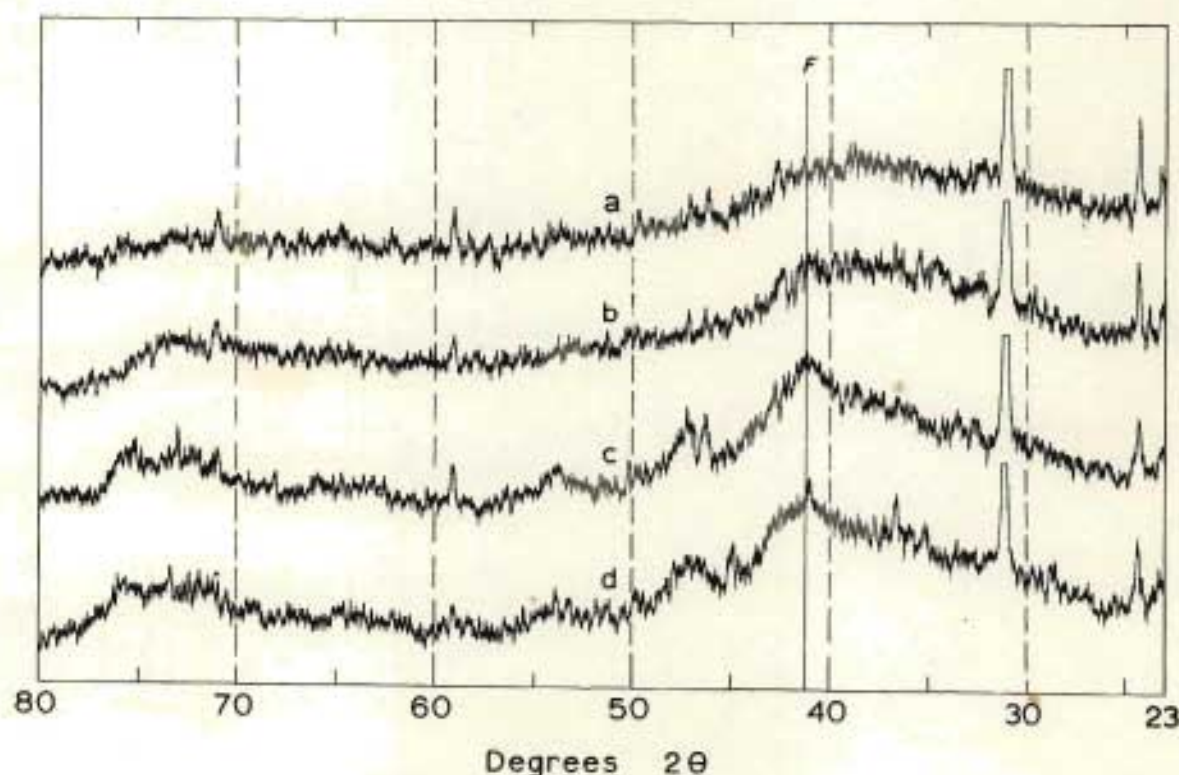


Fig. 4.3: X-ray powder diffraction patterns of natural untreated ferrihydrites from various localities: (a) Cedarville (No. 13) (b) Hella-Hella (No. 150) (c) Windy Hill (No. 54) and (d) Sani Pass (No. 234). where: F is the strongest ferrihydrite XRD line at  $2,54 \text{ \AA}$



From several aging experiments on the brown gel-like protoferrihydrite from Pietermaritzburg (aging in 0,1M KOH for 30 and 90 days at 70°C before and after  $H_2O_2$  treatment and refluxing for 30 and 90 days) it appears that its crystallization to haematite is severely delayed (Fig. 4.4 a - e) as compared with the rapid crystallization of synthetic ferrihydrite to haematite after 15 days refluxing (Fig. 4.4 f and g). In addition, after aging the natural brown gel-like protoferrihydrite in 0,1 M KOH no goethite was produced. This is in agreement with Fischer and Schwertmann (1975), and Schwertmann and Taylor (1977) that ferrihydrite is the precursor for haematite, but not for goethite formation. These experiments also demonstrate the stabilizing affect of organic matter\* (Schwertmann *et al.*, 1968; Schwertmann 1969/70) and silicic anions (e.g. Schwertmann and Thalmann, 1976) to crystallize or transform to more crystalline oxides. The data further suggest that haematite may form either very slowly or not at all from this natural ferrihydrite material. Furthermore, because goethite rather than haematite occurs at or near these sites, the ferrihydrite transforms to goethite via solution. Goethite crystallization at ambient temperatures can only occur by destructive dissolution of ferrihydrite and subsequent nucleation of goethite from solution (Schwertmann and Taylor, 1977).

High iron activity ratios,  $Fe_o/Fe_d$  [which according to Schwertmann (1964; 1973) is an indication of the amorphousness of Fe compounds] were obtained for yellow-brown humic soils in the Afro-alpine region (Tables 1.9 and 4.1) and for Vertisols in the Highveld region (Fitzpatrick, 1974; Fitzpatrick and le Roux, 1977). It can be inferred from the large proportion of  $Fe_p$  in Al horizons and because  $Fe_o/Fe_d$  ratios decrease down these profiles, that a high proportion of the oxalate extractable Fe especially in the topsoils are complexed by organic matter. However, the  $Fe_o-Fe_p/Fe_d$  in both the Al and B2 horizons (Afro-alpine soils range from 0,11 - 0,20; Vertisols range from 0,05 - 0,14) remain relatively high. In both these soils this is probably a result of the high amount of Fe which has been released from the Fe-smectite (Vertisols) or primary Fe-silicate (Afro-alpine soils) structures by weathering to form ferrihydrite, and the high silicate (and organic matter) content stabilizes the ferrihydrite and inhibits crystallization to haematite. In contrast, the "iron activity ratios" of

---

\* The % C in sample No. 13 is 9,5

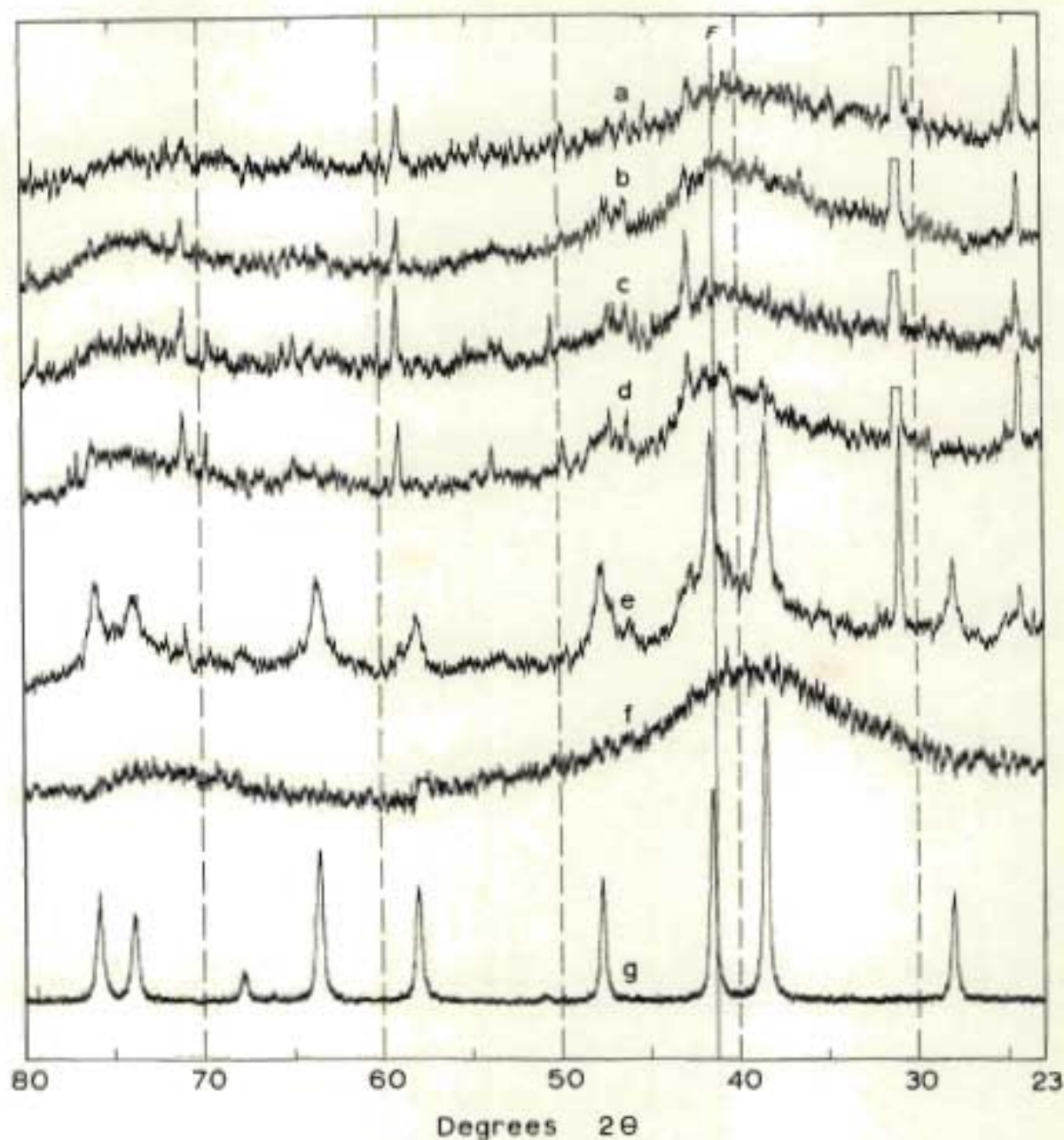


Fig. 4.4: X-ray powder diffraction patterns of natural (traces a-e, for brown gel-like precipitate, sample No. 233 from Pietermaritzburg) and synthetic (traces f and g) ferrihydrites before and after various aging treatments *in vitro*. Traces a-e are for the natural ferrihydrite: (a) untreated, (b) aged in 0.1M KOH for 30 days at 70°C, (c) as for (b) but aged for 90 days, (d) refluxed for 30 days, (e) refluxed for 90 days. Traces g and e are for synthetic ferrihydrite: (a) untreated, (b) refluxed for 15 days. where: F is main ferrihydrite XRD line at  $\sim 2.54\text{\AA}$



A and B horizons in older sesquioxidic red and yellow soils (cf. Table 1.9, and Fitzpatrick, 1974) are low ( $\leq 0.05$ ) suggesting that these highly weathered soils contain mainly crystalline forms of iron oxides (Tables 1.9 and 4.1).

#### 4.2.4.2 Pseudorutile, anatase and rutile

In the same way as ferrihydrite exhibits various degrees of order, and hence solubility in  $\text{NH}_4$  - oxalate (pH 3), this reagent was found to completely dissolve synthetic amorphous Ti and Fe-Ti oxides (i.e. XRD amorphous) and partially dissolve poorly crystalline anatase (i.e.  $\text{MCD} < 50 \text{ \AA}$ ;  $\text{WHH} > 2.0^\circ 2\theta$ ); as well as possibly poorly crystalline pseudorutile (Chapter 3). High contents of amorphous Ti (and Fe) and/or poorly crystalline anatase (or pseudorutile) were found in the Al horizons of soils from the Afro-alpine region (cf. Chapter 3, low  $\text{Ti}_o/\text{Ti}_t$ ). This is related to the cool climate and high organic content which inhibits crystallization of Ti and Fe oxides. In contrast, most of the sesquioxidic soils in the rest of the study area have low  $\text{Ti}_o/\text{Ti}_t$  and  $\text{Fe}_o/\text{Fe}_d$  (Tables 1.9 and 3.1) suggesting that the oxides are crystalline. This was also verified by detecting anatase (and goethite) and minor amounts of rutile by XRD in several soil clays after removing the dominant kaolinitic material with 5M NaOH (Table 1.9) and  $\text{H}_2\text{TiF}_6$  (Dolcater *et al.* 1970; Sayin and Jackson, 1975) digestion.

In general, titaniferous oxides are considered to be inert materials in soil development. However, in tropical and subtropical soils titanium minerals are susceptible to weathering, transformation and accumulation. Hence Sherman *et al.* (1964) proposed that Ti be included with Fe and Al oxides and hydroxides in the well known structural and energy relationship for soils: "Ionic elements  $\rightarrow$  amorphous  $\rightarrow$  mineral colloids  $\rightarrow$  crystalline minerals".

Indications of rutile (possibly ditrital) and pseudorutile were observed by XRD (very broad peaks) and light microscopy (opaque ilmenite and Ti-magnetite grains with complex brownish - grey, poorly crystalline replacement textures) in the silt and fine sand fractions of highly weathered soils. Too few samples were examined for definite conclusions

to be drawn regarding the distribution of rutile and pseudorutile in these soils. It would appear though from the petrographic studies (grain counts) undertaken by de Villiers (1962), van Rooyen (1964), Verster (1964) and Verster (personal communication) that relatively higher amounts of "leucoxene"\* and "altered" opaque minerals\* are present in the highly weathered soils than in those of the Riverine region.

Generally chemical weathering results in a decrease in magnetite/Ti-magnetite and then ilmenite, with a relative increase in "pseudorutile" and  $\text{TiO}_2$  (anatase and rutile). Thus in the Afro-alpine soils high amounts of magnetite/Ti-magnetite, ilmenite and amorphous Ti (oxalate extractable) are present, whereas in the Highland Montane and Mistbelt regions, and in the red coastal dunes, ilmenite, rutile and "pseudorutile" dominate. Although pseudorutile has been identified qualitatively in some soils by light microscopy, XRD data is still lacking.

From synthetic studies conducted at near ambient conditions (Chapter 3) it has been established that Ti may enter the goethite structure, and that a "partial" solid solution of goethite-pseudorutile-anatase exists. It could well be possible that, in nature such a solid solution prevails. The co-existence of goethite, anatase and pseudorutile (leucoxene) in these soils suggests that this is perhaps possible. It is possible therefore, that much of the "pseudorutile" in the finer particle sizes occurs as a poorly crystalline secondary deposition product formed via solution from the weathering of Ti-silicates, while in the coarse silt in fine sand fractions, pseudorutile occurs largely as an altered primary ilmenite (similar to alteration of Ti-magnetite to Ti-maghaemite). To what extent, Ti-magnetite and ilmenite are involved in the formation of secondary oxidic Fe and Ti as compared with silicate Fe and Ti (e.g. hornblende and sphene) is not yet known.

---

\* According to Hutton (1977) leucoxene is a nonspecific name for fine-grained Ti-minerals and recommends that this term should not be used. Lynd (1960) suggested that all alteration products of ilmenite should be termed leucoxene, qualified as being crystalline or non-crystalline, and that chemical analysis should give  $\text{TiO}_2$ , FeO and  $\text{Fe}_2\text{O}_3$ ; Golding (1961) added  $\text{SiO}_2$ . Detailed XRD studies of this material in single grains of altered ilmenite by Temple (1966), and Grey and Reid (1975) indicated that this Fe-Ti alteration product is poorly crystalline pseudorutile ( $\text{Fe}_2\text{Ti}_3\text{O}_9$ ).



#### 4.2.4.3 Goethite

Goethite is the most widespread and abundant of the Fe oxides and is considered the most stable form in the area (Chapter 1 and Table 4.1). The reason for this high stability possibly arises from the fact that in most of the highly weathered saprolites and soils the goethite structure is "stabilized" by isomorphously substituted Al (10 to 25 mole %). From the examination of over 200 goethitic materials from various environments the degree of Al-substitution (as measured mainly by XRD line shift) appears to be controlled by its mode of formation. Thus goethite formed under conditions of free drainage where Fe precipitates close to its source are highly Al-substituted and range from 15 to 30 mole % Al (combined thin sections and XRD studies on dolerite saprolites indicate that primary Fe-silicate minerals are totally replaced *in situ* by finely divided Al-goethite) whereas under conditions where there is a definite migration of Fe due to strongly acid or reducing conditions or by organic matter complexation the degree of Al-substitution is lower (e.g. in lowland ferricretes, crusts, pipestems and certain topsoil horizons). There is some evidence that the finely divided Al-goethite in the saprolite ("primary" goethite) may transform via solution to a less Al-substituted "secondary" goethite.

Soils or materials which contain goethite only have colours ranging between 7.5 and 10 YR but often these yellow colours are masked by the presence of organic matter or finely divided hematite which tends to give colours that are redder than 7.5 YR (Schwertmann and Taylor, 1977).

#### 4.2.4.4 Haematite, and its transformation to goethite

Differentially disordered Al-haematite (i.e. differential line broadening and shift to higher angles of their XRD lines) was identified in a red freely drained soil clay (No. 4M) and in various synthetic preparations by Schwertmann, Fitzpatrick and le Roux (1977) and Schwertmann, *et al.* (1978). As seen in Table 4.2 and Fig. 4.5, similar XRD patterns for haematites are obtained for a wide range of different kinds of pedogenic materials in the study area (i.e. several soil clays, saprolites, geodes, bands, concretions and ferricretes) and synthetic preparations (cf. Section 3.2.1. and Appendix 2). Al-substituted haematites (i.e. shift towards

In this connection, Francombe and Rooksby (1959) observed and explained differential line broadening of haematite formed from pure goethite by heating at high temperatures (i.e.  $> 320^{\circ}\text{C}$ ).

The so-called "yellowing" of red soil materials (i.e. the transformation from haematite to goethite; Schwertmann, 1971) may be viewed in this region, from a variety of aspects with increasing detail: (i) increasing altitude, (ii) from north to south aspect, (iii) with decreasing profile depth, (iv) down toposquences to wetter areas, and (v) in mottles and concretions. The dominant soils in the Afro-alpine region are yellow-brown (10 YR 6/6) soils, which besides organic Fe and some ferrihydrite contain predominantly finely divided goethite. The high organic matter content, which decomposes slowly in this humid-temperate climate, influences the Fe-balance to provide slow hydrolysis of Fe (III) compounds for goethite synthesis (Schwertmann, 1966a). MacVicar (1978) has observed a similar "yellowing" trend in humic soils derived from Table Mountain sediments on Early Tertiary plateaux (cf. Fig. 4.2; Fig. 1, map Symbols 3 and 14) in moving south of Port Edward.

In the relatively warmer and more humid Highland Montane and Mistbelt regions (where weathering is stronger and has been active for very long periods) three main types of freely drained soils occur; uniform red (Hutton form), yellow (Clovelly form) and yellow-red (Griffin form) (Table 4.1, Appendix 1). Generally, the red Hutton soils occur on the warmer drier northern aspects while the Clovelly and Griffin soils occur on the cooler moister southern aspects (Fig. 2). The Highland Montane, Mistbelt and Coastal Hinterland plateau regions (older surfaces) are dissected by drier younger valleys which generally contain red high base status soils (e.g. Shortlands form) on freely drained sites (Fig. 2; Table 4.1). Similar soils are found along the coast lowlands. Taylor and Graley (1967) and Isbell *et al.* (1976) have also shown that with increased leaching (i.e. with increasing rainfall in a climosequence) there is an increase in proportion of yellow soils relative to red soils. Transformation from red to yellow-brown also seems to take place on a more localized scale in yellowing of red mottles in plinthite (which invariably occurs in a red-yellow-grey soil toposquence), and small concretions (red haematite cores surrounded by goethite-rich rinds). Somewhat similar patterns



were observed by Fölster, Kalk and Moshrefi (1970) in "ferrallitic savanna" soils in south Sudan.

In accordance with Schwertmann and Taylor (1977) goethite dominates in cooler (e.g. Afro-alpine region and southern aspects of the Highland Montane and Mistbelt regions) wetter (plinthic soils) areas where haematite formation is inhibited through higher concentrations of organic compounds which either prevents the formation of ferrihydrite (a necessary precursor for haematite formation) or inhibits its transformation to haematite. Haematitic soils are formed where there is either a more rapid decomposition of organic matter (i.e. in warmer or more arid\* areas) or absence of organic matter (subsoil horizons). Furthermore haematite formation is promoted when there is a rapid release of Fe from Fe-bearing silicates\* and/or primary detrital opaque oxides\*\* (i.e. generally in soils derived from Fe-rich parent materials\*\*\*). Thus in the Mistbelt and Highland Montane regions yellow horizons are generally poorer in "weatherable" Fe minerals (i.e. derived from parent materials which are inherently low in Fe or where the Fe has been depleted due to stronger weathering).

Different hypotheses exist concerning the genesis (and origin of soil colour) of soils with yellow B horizons overlying either a red (Griffin form) or mottled (Avalon form) horizon. De Villiers (1962, 1964, 1965) suggested that these profiles consist of two (or more) depositional layers which may include "preweathered" or buried soils (i.e. polygenesis). Furthermore, de Villiers (1962, 1964), MacVicar (1962), van Rooyen (1964) and Easton (1970) regard the subsoil red colouration in Griffin soils as evidence of a certain amount of podzolization. However, field and mineralo-chemical evidence presented here and by Fitzpatrick (1974) indicates that organic matter and reducing conditions are the main factors controlling the mineralogical transformation of the red materials (haematite containing) to yellow (goethite) via a dissolution-reprecipitation reaction (see also

---

\*Thin sections and electron microprobe studies by Walker (1967) and Walker and Ribbe (1967) of immature, calcareous Red Desert soils (Baja California) concluded that iron bearing silicates (e.g. hornblende, biotite and Fe-rich smectite) were pseudomorphically replaced by haematite.

\*\*Polished surface studies by van Houten (1968) on detrital opaque oxide grains (e.g. magnetite and ilmenite grains) revealed haematite either coating the grains or in thin lamellae.

\*\*\*Other factors which may favour the formation of haematite are the adsorption of Ca and Mg in the clay fraction (Taylor and Grayley, 1967) and adsorption of oxalate ions by ferrihydrite (Schwertmann 1969/70).



Schwertmann 1971; Schwertmann and Taylor, 1977). In this regard, it is significant that Darby (1954) observed yellow-brown subsurface horizons which appeared to have developed a greater thickness and higher intensity of yellow colour under long established wattle plantations in the Mistbelt and Coastal Hinterland regions.

#### 4.2.4.5 Maghaemite, and its transformation to goethite

In the study area 5 types of magnetic materials (maghaemite-rich) were identified according to their morphology, origin, mineralogy and composition (cf. Chapter 2). Indications are that all five types occur in freely drained red and yellow soils in the Mistbelt and Highland Montane regions and may be identified in the field by means of a hand magnet. However, with increasing altitude towards the cool Afro-alpine region and with decreasing altitude to dry river valleys, the maghaemite content gradually decreases (Table 4.1; Fig. 2.1). Furthermore, in the Mistbelt and Highland Montane regions the magnetic material is generally more abundant in the red than in the yellow horizons and also increases with depth, suggesting dissolution by reduction and/or complexation and transformation to goethite (Table 4.1).

#### 4.2.4.6 Lepidocrocite

Ferruginous mottles, bands (Plate 4.3 A), crusts (Plate 4.3 A and B) and pipestems (Plate 1.8 C and D) containing lepidocrocite are optimally developed in slope gleys (i.e. Ouerf soils)\* mainly on the cooler south and south west facing mid- and foot- slopes of the Highland Montane region (Table 4.1; Figs. 2 and 4.7). This region is characterized by a mean annual temperature range of 13 - 17 °C and a mean annual rainfall range of 850 - 1100 mm (Phillips, 1973). In contrast, these lepidocrocite containing materials have not been located in gleyed soils of the drier and warmer Riverine, Coastal Lowland, and Basin Plainland regions (Fig. 2). In the Highland Montane region lepidocrocite seldom occurs in the very lowest catenary positions with permanent or prolonged ground water conditions although Reerink (1961) identified lepidocrocite in a Katspruit soil (i.e. bottomland gley soil). There is resemblance between major aspects of the Ouerf soil (Appendix 1) and "pseudogleyed" soils reported from other regions. Its presence (and distribution) in the field is easily recognized by the orange colour 7.5 YR 6-7/4-8.

\*cf. Appendix 1 and Schwertmann and Fitzpatrick (1977, their Fig. 1) for descriptions of these soils (i.e. Pinedene ouerf)





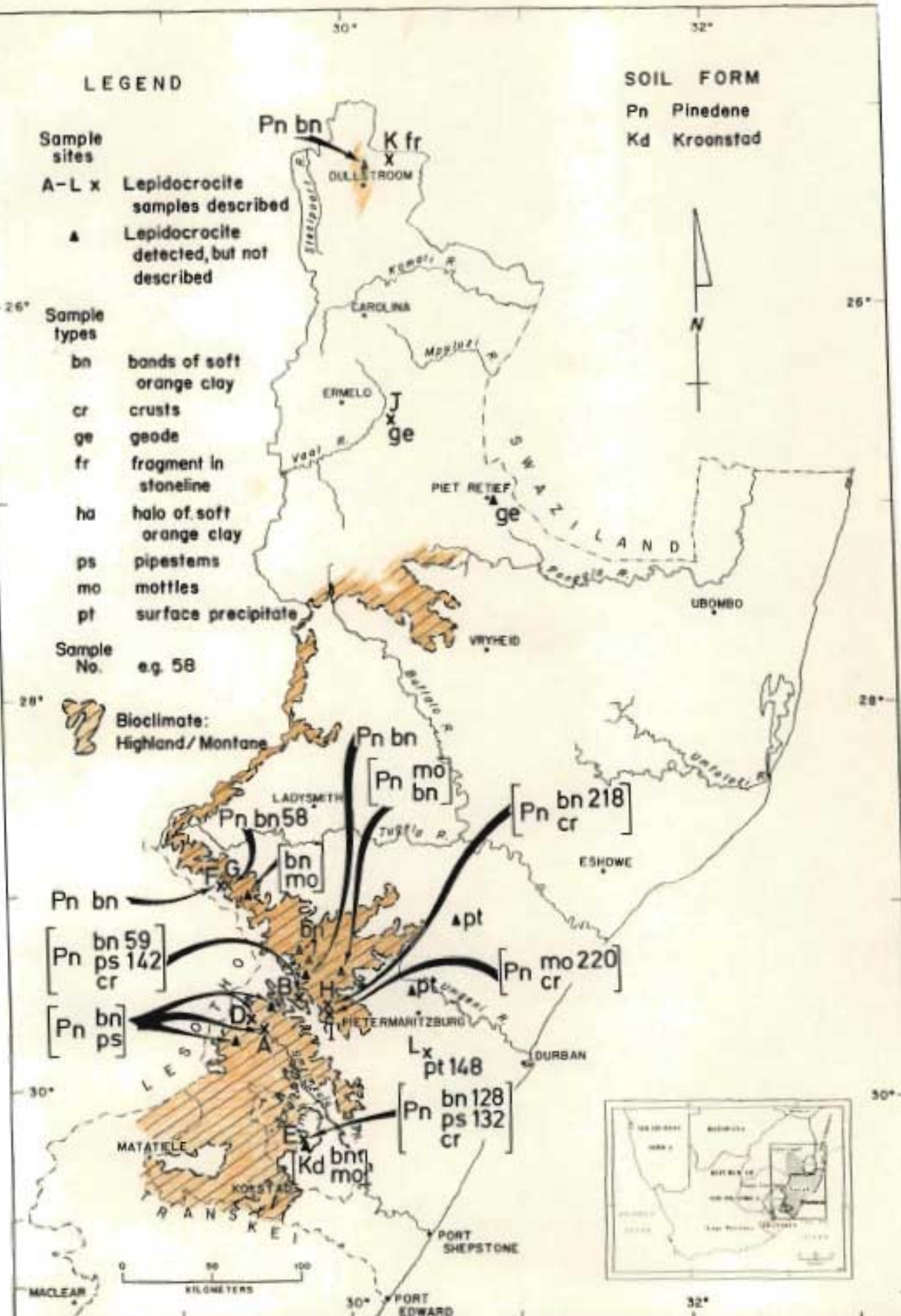


fig. 4.7: Map showing sampling sites of various lepidocrocite containing materials, a distribution of the Highland Montane region where high amounts of lepidocrocite are found in "slope clay".



The lower soil temperature, lower evaporation and slower water movement at these sites cause hydromorphic conditions which allow Fe to occur in the ferrous and ferric state and form both lepidocrocite and goethite. The orange clay bands (bn) contain highest amounts of lepidocrocite with relatively low line broadening (Fig. 4.8 Nos. 59, 218, 128 and 58) and  $Fe_o/Fe_d$  ratios (Schwertmann and Fitzpatrick, 1977). However, the crystallinity of the lepidocrocite (as measured by XRD line broadening, cf. Fig. 4.8 Nos. 36, 132 and 142) decreases when approaching root channels (Plate 1.8 C and D) due to a high  $PCO_2$  content which results in higher amounts of goethite (Schwertmann and Fitzpatrick, 1977).

The type of thin ferruginous crust that is formed in Ouerf soils near Impendla (Plate 4.3 A and B) has remarkably similar morphological (Plate 4.3 B) and mineralogical (i.e. lepidocrocite-rich covering and goethite-rich matrix with similar  $d_{110}$ -spacing and WHH cf. Table 1.5) features resembling that of a thin iron-pan from a Stagnopodzol near High Force (North of England). This together with the relatively similar, cooler (i.e. temperate-like) climates and soil type suggests a similar mode of formation, with Fe being reduced under anaerobic conditions (i.e. retarded drainage due to impermeability of underlying gleys) and lepidocrocite and goethite forming on re-oxidation (i.e. in better aerated zones such as more sandy layers adjacent to clayey layers).

De Villiers and van Rooyen (1967) suggested the occurrence of poorly crystalline lepidocrocite (XRD amorphous) in a yellow-brown apedal horizon of a freely drained Griffin soil in the Mistbelt/Highland Montane region, the identification being based on an increase in "magnetic attraction" after heating. In agreement with these authors no lepidocrocite was detected by XRD in yellow and red freely drained soils (Table 1.9). Pretreatment of clays extracted from these soils with  $H_2O_2$  (i.e. to oxidize organic matter) significantly reduced the large increase (i.e. measured before  $H_2O_2$  treatment) in magnetic susceptibility after heating (cf. Fitzpatrick, 1974). This suggests that de Villiers and van Rooyen (1967) probably formed maghaemite by the ignition of goethite in the presence of organic matter. Furthermore, Schwertmann and Fitzpatrick (1977) found that poorly crystalline lepidocrocite from "slope gley" soils is partly  $NH_4$ -oxalate (pH3) soluble, suggesting that if poorly crystalline lepidocrocite were present in freely drained soils relatively higher  $Fe_o/Fe_d$  ratios would be expected, which is not the case (see Table 1.9).

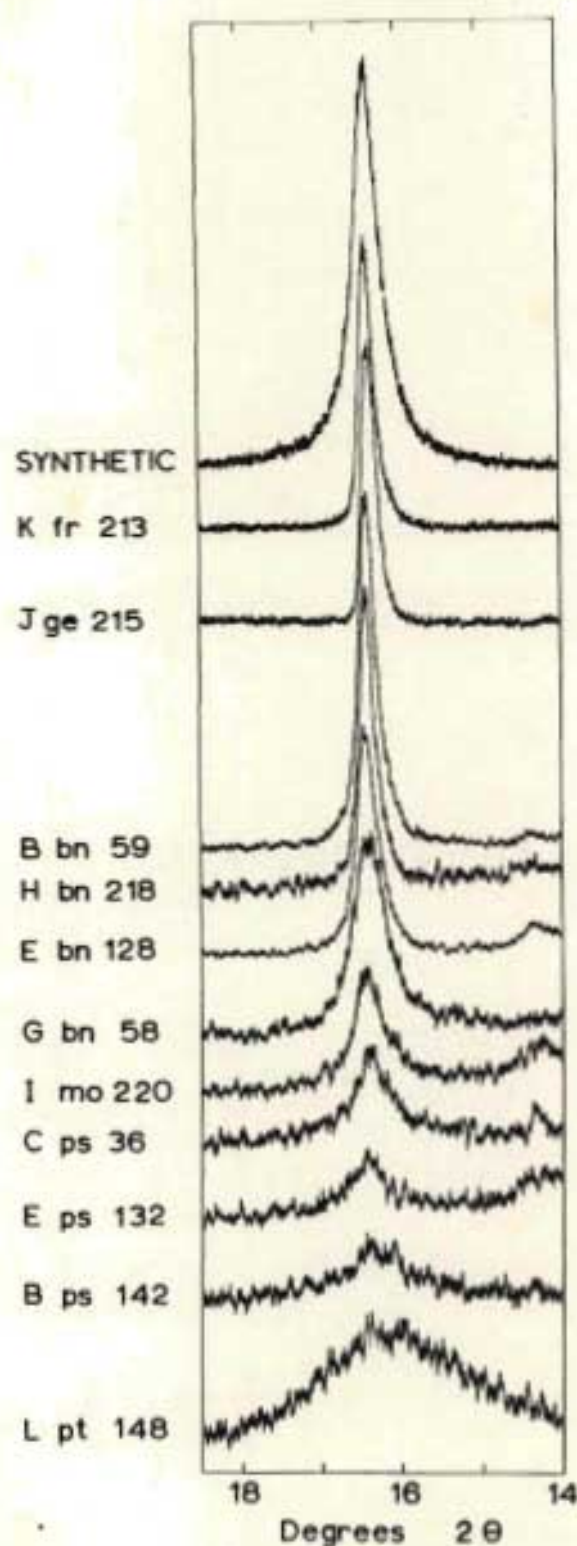


Fig. 4.8: X-ray powder diffraction patterns of the (020) reflections for synthetic (prepared by oxidation of  $\text{FeCl}_2$  solution) and various types of lepidocrocite containing materials; where: A-L, fr-pt and 213-148 represent the sample site, type and number respectively, as indicated in Fig. 4.7



Extremely poorly crystalline lepidocrocite [half width of the (020) line ranges from  $1,4 - 1,6^{\circ}2\theta$ ;  $Fe_o/Fe_{HCl} = 0,85$ ] with (020) reflections shifted to higher d-spacings (Fig. 4,8, No. 148) has been found at several sites in the region in yellowish-brown precipitates derived from surface waters (Fig. 4,7). Schwertmann and Fitzpatrick (1977) found that after  $H_2O_2$  treatment (removal of organic carbon) the lepidocrocite converted to goethite slowly at room temperature whereas a coarser crystalline lepidocrocite does not (Schwertmann and Taylor, 1972). Schwertmann (personal communication) has carried out high resolution electron microscope studies on these samples (No. 148) confirming XRD data (i.e. broad peaks) that the crystals are very small, and that they do not lie on their basal planes (i.e. 010) but on the b-axis, and explaining the fact that the basal (020) spacing is suppressed relative to the (120) spacing.

In contrast, two "geode samples" shown in Plate 4.3 C and D from the Transvaal (Fig. 4.7, Sites K and J) were found to have a thin surface coating of very crystalline ( $WHH = 0,10^{\circ}2\theta$ ) lepidocrocite (Fig. 4.8 Nos. 215 and 213) and under the TEM showed very large elongated plates with serrated "cubic-like" crystals (Plate 4.3 E). The cubic morphology of No. 213 indicates that lepidocrocite may have formed by pseudomorphous replacement of pyrite.

#### 4.3 Conclusion

Various Fe and Ti compounds (primary, secondary layer silicate, organic and oxidic i.e. ferrihydrite, pseudorutile, anatase, rutile, goethite, haematite, maghaemite and lepidocrocite) were found in several materials occurring in a wide-range of pedogenic environments by both field (distribution, occurrence and morphology) and laboratory (mineralogy and composition) methods. The presence of these pedogenic Fe and Ti minerals and/or materials is a feature common to the whole study area. There seems little doubt that in this area, these various forms and types of pedogenic Fe and Ti compounds are related to factors such as climate, topography, hydromorphy and parent material. Organic matter seems to strongly control the formation, stability and transformation of these compounds and influence their relationship with climate and topography. Several of these forms and their relationships are easily recognized in the field by colour and morphology. Further important differences include

degree of Al and Ti substitution, and crystallinity. A fundamental aspect about the pedochemistry and genesis of Fe and Ti compounds is that it may be considered to represent the intersection between the fairly divergent disciplines, pedology and crystallography.



## APPENDIX 1

PROFILE DESCRIPTIONS AND SAMPLE INFORMATION  
OF SELECTED SOIL SERIES

## AND

## FERRUGINOUS BAUXITE

Soil form and series<sup>1</sup> : Clovelly blinkklip (humic phase)  
Great group<sup>2</sup> : Cryumbrept  
Site No. (Fig. 1.1) : 106 Cv/Ma  
Soil zone (Fig. 1) : 1  
Region (Fig. 2) : Afro-alpine; Lesotho Plateau  
Elevation : 3 050 m  
Terrain morphology : Midslope

Horizon	Description
Orthic A1	0-30cm; black (10 YR 2,5/1 moist) gritty silt loam; weak, very fine subangular blocky to weak; very fine granular to porous; very friable when moist; abundant roots and humic material; many gravelly fragments of basalt; clear wavy transition (similar to Plate App. 1.1 C).
Yell. br. ap. 11 B21	30-50cm; dark brown (7,5 YR 3/2, moist) gritty silt loam; massive with occasional weak, coarse platy structure; porous; friable when moist; few roots; abundant (50-70%) medium and small fragments of basalt; clear wavy transition.
Yell. br. ap. 111 B22	50-65cm; dark brown (7,5 YR 4/4, moist) gritty silt loam; weak, medium platy structure; friable when moist; weakly compacted; many medium and small fragments of basalt; roots rare; diffuse wavy transition.
Yell. br. ap. 111 B23	65-110cm; as above, but slightly more compacted in places; gradual diffuse transition.
Yell. br. ap. 111 B3	110-125+ cm; dark brown (7,5 YR 4/4, moist) gritty silt loam; moderate, coarse platy structure; porous with discontinuous vesicular pores; very compact in places; usually friable when removed; friable when moist; many medium and small basalt fragments with coatings of fine sand and silt on upper surfaces; stone orientation following shape of soil surface; roots rare (cf. Plate App. 1.1 B and D).

<sup>1</sup>According to the system in use in South Africa: MacVicar, de Villiers, Loxton *et al.* (1977); where: yell.=yellow, br.=brown, ap.=apedal, str. structured.

<sup>2</sup>According to the system in use in U.S.D.A. : Soil Survey Staff (1975) The cryic temperature regime is based on unpublished calculated temperatures for this region, obtained from Dr. R.E. Schulze (manuscript in preparation).

Plate App. 1.1: A. Mass-movement terraces (terraces) in the Afro-alpine region near Sani Pass, formed partly by present-day freeze-thaw cycles.

B. Compact layer at depth of 110-125cm in Blinkklip (humic phase) soil (No. 106) above Sani Flats in Lesotho showing lenticular or platy structure (with discontinuous vesicular pores). Length of knife is approximately 15 cm.

C. Profile of Milford soil (No. 266) near Naudesnek showing the sharp line of demarcation between the humic surface soil and compact subsoil horizons. Numerous fragments of unweathered basalt occur throughout the profile.

D. Fragment of basalt from Milford soil B23 horizon (No. 266) showing a capping of fine sand and silt on the upper surface with a "nest" of tightly packed stones beneath it.





(i) Note on the evolution of these soils<sup>\*</sup>

The compact horizons in these soils are most strongly developed at depths of 70 to 130cm, are usually shallower and tend to occur less frequently on the warmer north facing slopes, whereas on the cooler south facing slopes they appear to be much thicker and deeper. In addition, these compact "layers" occur mostly above elevations of approximately 2 280m and in areas having an Afro-alpine climate. Furthermore, they are usually extremely hard and resist digging with hand tools, but crumble easily between thumb and forefinger. Air-dry clods from these horizons slake fairly easily when immersed in water, soften when allowed to take up water slowly and therefore may meet the criteria of a fragipan horizon according to Soil Survey Staff (1975).

The compacted horizons could have been perennially frozen during part of the Pleistocene period and underwent gradual freezing and thawing to give the characteristic lenticular (platy) or massive structure shown in Plate App. 1.1 B (forms as the soil freezes layer by layer, as a result of the redistribution of moisture), capping of fine material shown in Plate App. 1.1 D (filling the space created by the gradual disappearance of ice around stones) and compaction (stone orientation and tight packing due to ice expansion and contraction from repeated slow freeze-thaw cycles). The presence or combination of the above features is used by many workers (FitzPatrick, 1956) to indicate previous permafrost formation. Another criterion frequently used is the presence of well formed "frost wedges", but this has not to date been observed by the author.

Under the present day climatic conditions in this region freezing does not extend to the depth at which these compact horizons were observed. This together with the above morphological features and the great thickness of this horizon in places, indicates that these layers are related to a permafrost condition (and are now considered as fossilized permafrost layers).

Although permafrost is absent in the profiles today, contemporary frost processes (i.e. periglacial) play an important role in the formation of these soils. This is seen especially in the surface characteristics of the landscape, such as in the formation of stone stripes (Harper, 1969; Hastenrath and Wilkenson, 1972) and terracettes (Plate App. 1.1 A).

---

\* More detailed discussion and analytical data of these soils are given by Fitzpatrick (1978).



Soil form and series <sup>1</sup>	: Clovelly clovelly
Great group <sup>2</sup>	: Haplorthox
Site No. (Fig. 1.1)	: 16M Cv
Soil zone (Fig. 1)	: 2
Region (Fig. 2)	: Highveld (high rainfall zone: 800-900 mm)
Elevation	: 2 150 m
Terrain morphology	: Midslope

Horizon	Description
Orthic A1	0-10cm; moist; 95% very dark greyish-brown (10 YR 3/2 when moist); sandy loam; weak to moderate crumb; loose when moist or wet; soft when dry; clear smooth transition to:
Yell. br. ap. B22	10-25cm; moist; 90% yellow-brown (7.5 YR 6/6 -5/5 when moist); sandy loam; massive; loose when moist or wet; soft when dry; few medium sized quartz fragments; gradual undulating transition to:
C	25-100cm; wet; variegated pink, yellowish-brown and greyish weathered shale with stratified geo-structure silty clay.

Soil form and series <sup>1</sup>	: Pinedene ouwerf
Great group <sup>2</sup>	: Fragiaquilt
Site No. (Fig. 4.7)	: B (Pn; bn59, ps142)
Soil zone (Fig. 1)	: 2
Region (Fig. 2)	: Montane, Highland Montane
Elevation	: 1 750 m
Terrain morphology	: Midslope

Horizon	Description
Orthic A1	0-35cm; black (10 YR 3/2 moist); sandy clay loam; weak fine subangular blocky to weak; porous; friable when moist; slightly hard when dry; very few medium quartz fragments; gradual undulating boundary.
Yell. br. ap. B22	35-95cm; Yellowish-brown (10 YR 5/6-4/4 moist); sandy clay loam; massive; friable when moist; slightly hard when dry; very few indurated medium ferruginous pipestems; few medium quartz fragments; clear undulating boundary.
Gley cutanic B23	95-180cm; moist; grey to light grey (10 YR 6/1-7/1); clay with common, medium, prominent orange (7.5 YR 6/8) mottles; friable and plastic when moist; hard when dry; very few indurated medium ferruginous pipestems; few medium quartz fragments; clear undulating boundary.
C	180-200cm; moist; grey to light grey (10 YR 6/1-7/1); clay with many, coarse (2 to 6cm thick) orange (7.5 YR 6/8) bands; friable and plastic when moist; hard when dry, very few medium quartz fragments.

---

1 and 2. *Loc. cit.*

Soil form and series<sup>1</sup> : Hutton farningham  
 Great group<sup>2</sup> : Umbriorthox  
 Site No. (Fig. 1.1) : 92 Hu  
 Soil zone (Fig. 1) : 2  
 Region (Fig. 2) : Uplands, Mistbelt  
 Elevation : 990 m  
 Terrain morphology : Midslope

Horizon	Description
Orthic A1	0-40cm; moist; moist 100% dark reddish brown (5 YR 3/2); clay loam; fine weak subangular blocky; friable when moist; slightly hard when dry; few fine hard iron-manganese concretions; gradual smooth boundary.
Red ap. B1	40-75cm; moist; moist 95% dark reddish brown (5 YR 3/4); clay; structureless (apedal); very friable when moist; very friable when dry; very few fine hard iron-manganese concretions; diffuse smooth boundary.
Red ap. B21	75-110cm; moist; moist 95% red (2,5 YR 4/6); clay; structureless (apedal); very friable when dry; very few fine hard iron-manganese concretions; gradual smooth boundary.
Red ap. B22	110-145+cm; moist; moist 90% red (10 R 4/8); clay; structureless (apedal); very friable when dry; very few fine hard iron-manganese concretions; few large yellowish ferruginous bauxite boulders.

Description and analytical data of ferruginous bauxite underlying a Farningham soil near Pietermaritzburg

Site No. (Fig. 1.1) : 62 ba  
 Soil zone (Fig. 1) : 2  
 Region (Fig. 2) : Uplands, Mistbelt  
 Elevation : 970 m  
 Terrain morphology : Midslope

Morphology and appearance: Brittle to moderately hard. Massive, medium-grained, porous, uniform yellowish-brown.

Parent rock: Dolerite

Weathering: Partly preserved joint planes and original dolerite rock structure indicative of residual weathering

Mineral constituents: (from X-ray diffraction analysis)

Gibbsite and goethite (dominant); quartz, magnetite/Ti-magnetite/maghaemite, ilmenite (accessory); kaolinite, halloysite, anatase (traces 0-5%).

Chemical composition:

31,5%	Al <sub>2</sub> O <sub>3</sub>
32,7%	Fe <sub>2</sub> O <sub>3</sub>
10,9%	SiO <sub>2</sub> (6,4% Quartz; 4,5% Reactive SiO <sub>2</sub> ).
16,4%	Loss on ignition
5,3%	TiO <sub>2</sub>
0,6%	MnO
97,4	Total



Soil form and series<sup>1</sup> : Griffin farmhill  
 Great group<sup>2</sup> : Umbriorthox  
 Site No. (Fig. 1.1) : 103 Gf  
 Soil zone (Fig. 1) : 2  
 Region : Uplands, Mistbelt  
 Elevation : 905 m  
 Terrain morphology : Midslope

Horizon	Description
Orthic A1	0-40cm; moist; dark brown (7,5 YR 3/2 when moist); sandy clay; very weak subangular blocky; loose when moist or wet; firm when dry; few fine to medium hard ferruginous concretions; gradual clear boundary.
Yell. br. ap. B21	40-55cm; moist; dark brown (7,5 YR 4/4 when moist); sandy clay; massive (apedal); loose when moist or wet, soft when dry; few to common fine to medium hard ferruginous concretions; gradual diffuse boundary.
Yell. br. ap. B22	55-65cm; as above but strong brown (7,5 YR 5/6 when moist); gradual clear boundary.
Red ap. B23	65-80cm; moist; red (2,5 YR 3/6 when moist); clay; massive (apedal); very fine weak yellow streaks; loose when moist or wet; soft when dry; common fine to medium hard ferruginous concretions; undulating clear boundary.
C	80+cm; moist; yellow (7,5 YR 7/8 when moist); variegated red channels in stratified shale geo-structure friable when moist and hard when dry.

Soil form and series<sup>1</sup> : Inanda inanda  
 Great group<sup>2</sup> : Haplohumox  
 Site No. (Fig. 1.1) : 99 Ia  
 Soil zone (Fig. 1) : 3  
 Region (Fig. 2) : Coastal Hinterland  
 Elevation : 1 040 m  
 Terrain morphology : Midslope

Horizon	Description
Humic A1	0-85cm; moist; moist 100% black (10 YR 2,5/1); sandy clay; weak to moderate fine angular blocky; friable when moist; slightly hard when dry; few fine hard iron-manganese concretions; diffuse smooth boundary.
Red ap. B21	85-135cm; moist; moist 100% dark red (2,5 YR 3/6); clay loam; massive apedal; very friable when moist, slightly hard when dry; few firm medium insect casts; few fine hard iron-manganese concretions.

Soil form and series<sup>1</sup> : Avalon ruston  
 Great group<sup>2</sup> : Plinthaquox or (Plinthic) Haploorthox  
 Site No. (Fig. 1.1) : 12M Av  
 Soil zone (Fig. 1) : 7  
 Region (Fig. 2) : Basin Plainlands; Upland-moist  
 Elevation : 1 300 m  
 Terrain morphology : Midslope

Horizon	Description
Orthic A1	0-34cm; moist; 95% very dark greyish-brown (10 YR 3/2 when moist); sandy loam; weak crumb; loose when moist, soft when dry; abundant roots; few fine to medium indurated iron-manganese nodules; gradual smooth transition to:
Yell. br. ap. B21	34-95cm; moist; 90% yellowish-brown (10 YR 5/6-4/4 when moist); sandy loam; massive; loose when moist; soft when dry; few fine indurated iron-manganese nodules; gradual undulating transition to:
Soft plinthic	95-130cm; moist; 40-50% red (2,5 YR 5/8 - 4/8 when moist); prominent mottles in a yellowish matrix; sandy loam; common indurated iron-manganese nodules; gradual smooth transition to:  130-150cm; moist; light grey matrix and pink to pale red mottles with some fine speckles of red (red becomes yellow/pink and yellow becomes grey with depth); few fine iron-manganese concretions; gradual transition to:
C	150+cm; wet; gleyed weathered sandstone.

Soil form and series<sup>1</sup> : Wasbank wasbank  
 Great group<sup>2</sup> : Psammaquent (on hard plinthite)  
 Site No. (Fig. 1.1) : 35 Wa  
 Soil zone (Fig. 1) : 7  
 Region : Basin Plainlands, Upland - moist  
 Elevation : 1 300 m  
 Terrain morphology : Bottomland

Horizon	Description
Orthic A1	0-15cm; moist; 90% very dark grey (7,5 YR 4/0 when dry); 95% black (7,5 YR 2,5/0 when moist); loamy sand; weak crumb; loose when moist or dry; abundant organic matter; clear smooth transition to:
E-horizon	15-35cm; moist; 90% grey to dark grey (5 YR 4/4 when moist); very faint circular yellowish mottles; loamy sand; single grain; ; very loose when moist or wet; few medium Fe-Mn concretions; gradual transition to:
Hard plinthic	35+cm; ferricrete (pisolitic) with many Fe-Mn concretions cemented together; grey sandy loam.

Soil form and series<sup>1</sup> : Glencoe appam  
 Great group<sup>2</sup> : Haplorthox (on hard plinthite)  
 Site No. (Fig. 1.1) : 11M Gc (32)  
 Soil zone (Fig. 1) : 7  
 Region (Fig. 2) : Basin Plainlands; Upland - moist  
 Elevation : 1 300 m  
 Terrain morphology : Crest

Horizon	Description
Orthic A1	0-30cm; dry; 95% brown (7,5 YR 4/2 when moist); sandy loam; weak crumb; loose when moist, soft when dry; abundant roots; common medium indurated iron-manganese nodules; gradual smooth transition to:



Horizon	Description
Yell. br. B21	30-70cm; moist; 90% brown (7,5 YR 4/4 when moist); sandy loam; massive; loose when moist, soft when dry; few roots; very common medium indurated iron-manganese nodules; gradual smooth transition to:
Hard plinthic	70-180cm; ferricrete (pisolitic to visicular) comprising abundant iron-manganese concretions of varying colour (red-purple to yellow); common nodules ranging in size from 4 to 70mm, oval shaped with shiny surface; yellow sandy loam fills vesicular pores; crust is slightly porous.
C	180+cm; moist; 85% red (2,5 YR 4/6 - 3/6 when moist); sandy clay loam; massive; slightly sticky and soft when wet; soft when dry; common medium indurated iron-manganese nodules.

Soil form and series<sup>1</sup> : Shortlands shortlands  
 Great group<sup>2</sup> : Rhodoxeralf  
 Site No. (Fig. 1.1) : 241 Sd  
 Soil zone (Fig. 1) : 4  
 Region (Fig. 2) : Riverine  
 Elevation : 780 m  
 Terrain morphology : Midslope

Horizon	Description
Orthic A1	0-35cm; dry; moist 100% dusky red (2,5 YR 3/2); clay; moderate to strong medium subangular blocky; very few black faint clayskins on ped faces; firm when moist; hard when dry; very few fine hard iron-manganese concretions; gradual smooth boundary.
Red str. B22	35-90cm; dry; moist 95% dark reddish brown (2,5 YR 3/4); clay; moderate to strong coarse to medium subangular blocky; few brown faint clayskins on ped faces; firm when moist; hard when dry; very few fine hard iron-manganese concretions; clear wavy boundary with tongues.
C	90-105cm; moist; yellowish crumbly weathered dolerite with few fine tongues of B22 material.

Soil form and series<sup>1</sup> : Rensburg reensburg  
 Great group<sup>2</sup> : Pelludert  
 Site NO. (Fig. 1.1) : 39 Rg  
 Soil zone (Fig. 1) : 4  
 Region : Riverine  
 Elevation : 770 m  
 Terrain morphology : Midslope

Horizon	Description
Vertic A1	0-105cm; moist; moist 100% black (7,5 YR 2,5/0); clay; strong coarse angular blocky and wedge; many very wide vertical cracks; very sticky and very plastic when wet; very firm when moist; very hard when dry; common prominent black clayskins on ped surfaces and shiny grooved pressure faces (slickensides) especially at lower depths; few fine to medium hard iron-manganese concretions; very few small dolerite and angular ferruginized shale fragments; gradual

Horizon	Description
Firm Gley G	105-130cm; wet; wet 80% olive (5 Y 4/3); common medium distinct yellow olive elongated streaks; clay; strong coarse angular blocky and wedge; very sticky and very plastic when wet; very firm when moist; very hard when dry; many prominent olive grey shiny grooved pressure faces (slickensides); few fine to medium hard iron-manganese concretions; common white medium to large hard lime nodules; very few small dolerite and angular ferruginized shale fragments.

Soil form and series<sup>1</sup> : Katspruit katspruit  
 Great group<sup>2</sup> : Haplaquept  
 Site No. (Fig. 1.1) : 208 Ka  
 Soil zone (Fig. 1) : 2  
 Region (Fig. 2) : Highveld (high rainfall zone: 800 -900 mm)  
 Elevation : 2 100 m  
 Terrain morphology : Bottomland

Horizon	Description
Orthic A1	0-15cm; moist; very dark grey (10 YR 3/1 when moist); clay; strong fine subangular blocky, fine distinct reddish-orange streaks along root channels, moderately porous; friable when moist; hard when dry; few small hard ferruginous concretions; clear smooth transition.
Firm gley G1	15-25cm; moist to wet; dark grey (10 YR 4/1 when moist); clay; coarse angular blocky to prismatic when dry; massive when wet; common faint yellowish-orange mottles; friable when moist; very hard when dry; diffuse undulating transition.
G2	25-70+cm; wet; dark grey (2,5 Y 5/2 when moist); gleyed and with increasing depth blocks become lighter coloured with greenish hues (5 GY 5/1); clay; massive when wet; few diffuse fine yellowish brown mottles; friable when moist; very plastic when wet; hard when dry.

---

1 and 2. *Loc. cit*



## APPENDIX 2

## PREPARATION AND CHARACTERIZATION OF SYNTHETIC OXIDES

- (i) Goethite and mixed Fe-Ti and Fe-Al oxides prepared from chloride salts aged at pH 13

Freshly precipitated ferrihydrite (formerly referred to as amorphous ferric hydroxide) was prepared by adding dropwise over 3 hours at room temperature an equivalent amount of ferric chloride (AR) to 250 ml of 2 M KOH, while stirring rapidly (method similar to Landa and Gast, 1973). Mixed Fe-Ti and Fe-Al coprecipitates were prepared in exactly the same manner, except that (i) 5, 10 and 20 %  $\text{TiCl}_4$  (AR); (ii) 5 and 10 %  $\text{TiCl}_3$  (AR); (iii) 5 and 10 %  $\text{AlCl}_3$  (AR) replaced iron in the initial solution.

The freshly precipitated gels were either used immediately after being washed with deionized water until dispersion, or aged in 0.2 M KOH (pH 13) at  $60^\circ\text{C}$  in polyethylene bottles for 30 hours and 30 days respectively, then dialyzed exhaustively against distilled water. The dialyzed gels were then concentrated in a Sorvall ultracentrifuge at  $20\,000 \times g$ . A small sample was taken for electron optical study (with a Hitachi HU - 11E instrument; dilute aqueous suspensions were dried on collodion coated 200 mesh per inch copper grids) and the remainder freeze dried for later use in XRD, IR and chemical analysis.

A 100 mg sample was dissolved in concentrated HCl to ascertain the total Fe, Ti and Al and a duplicate sample extracted with a 100 ml  $\text{NH}_4^+$  oxalate (pH 3).

When the freshly prepared ferrihydrite is aged at pH 13 and  $60^\circ\text{C}$  relatively crystalline acicular goethite crystals become evident after 30 hours (Plate App. 2.1 A). Further aging for 30 days results in goethite crystals with a more pronounced (smooth) surface and less striated or "splintered" appearance (Plate App. 2.1 C). The presence of crystalline goethite was confirmed by XRD (Fig. 1.3) and IR (Fig. 1.4) measurements. The low  $\text{Fe}_{\text{ox}} / \text{Fe}_{\text{HCl}}$  ratios (Fig. App. 1.1) also confirm the crystalline nature of the material, in general agreement with Landa and Gast (1973). Furthermore, the colours change from red-brown in unaged Fe and Fe-Al oxides to bright yellow in the corresponding aged oxides. However, aged Fe-Ti oxides become increasingly red in colour

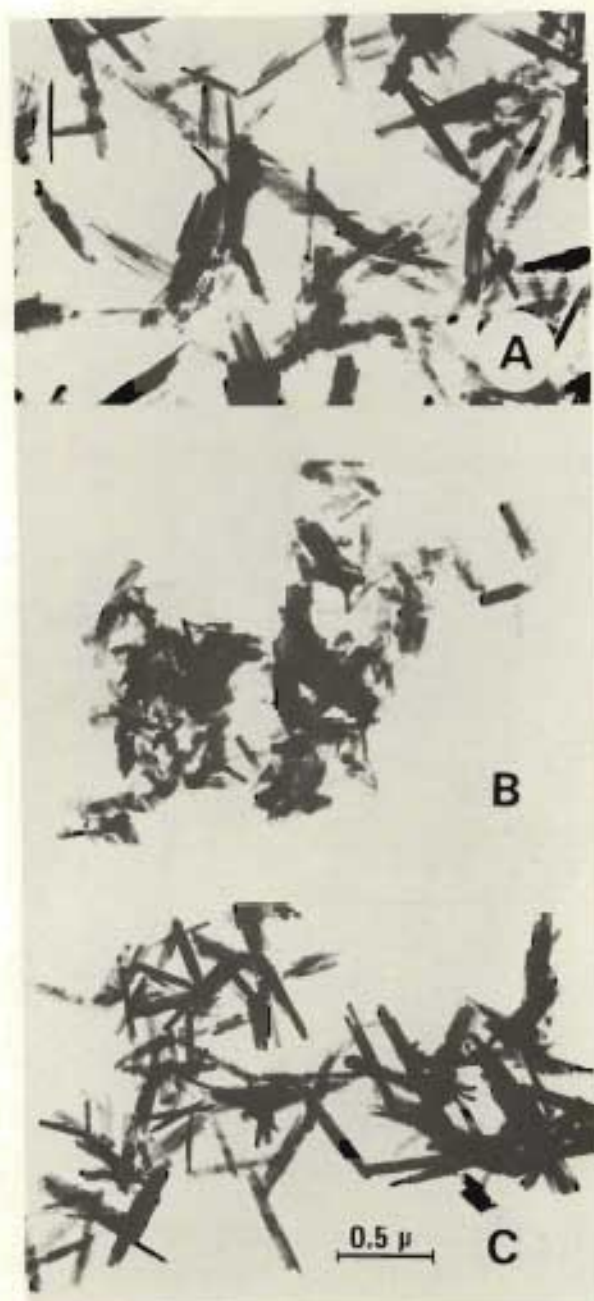


Plate App. 2.1: Electron micrographs of goethite prepared from:  
A. precipitated ferric oxide gel, pH 13, aged for 30 hours;  
B. coprecipitated alumino-ferric oxide gel (5% in Al/Al + Fe)  
pH 13, aged for 30 hours; C. precipitated ferric oxide gel,  
pH 13, aged for 30 days. The scale applies to all figures



with increasing Ti content, suggesting possible higher amounts of "amorphous" Fe compounds\*.

Electron microscopy demonstrates that goethite crystals formed from the pure system have "elongated" acicular crystals (Plate App. 2.1 C) whereas goethite formed in the presence of Al resulted in much shorter, stubby crystals (Plate App. 2.1 B, i.e. crystal growth is retarded along the  $[001]$  axis) This is in agreement with Thiel (1963) and Norrish and Taylor (1961) that substitution of Al in the goethite structure changes crystal structure (shifted d-spacings; Fig. 1.3) and decreases crystal size. However, goethite crystals formed in the presence of Ti (Plate App. 2.2) are decidedly larger than those in the pure iron and Fe-Al systems (Plate App. 2.1). Electron micrographs of the Fe-Ti system invariably showed the goethite crystals to be either embedded in an "amorphous like" mass or strongly coated by such material (Plate App. 2.2, A,C and E). In addition, there appeared to be an increase in the incidence of various types of twinned goethite crystals. In spite of this admixture of "amorphous material" very sharp XRD peaks were obtained for goethite in the 5% ( $WHH=0,51^\circ 2\theta$ ), 10% ( $WHH=0,30^\circ 2\theta$ ) and 20% ( $WHH=0,22^\circ 2\theta$ ) Ti/Ti+Fe samples. However, the  $d(111)$  line showed a slight but consistent decrease in d-spacing with increasing Ti content. Although an explanation for this cannot be given yet, the possible incorporation of hydroxyl ions into the goethite structure could be involved (see Chapter 3).

In Fig. App. 2.1, the relative amounts of total Fe, Ti and Al extracted by oxalate (e.g.  $Fe_{ox}/Fe_{HCl}$ ) as a function of aging time, are given. The amount of iron extracted by oxalate from the pure iron system is less than that for the mixed systems (Fig. App. 2.1). The Fe-Ti system shows almost a linear increase of Ti retained by goethite with time, and approaches between 2-4% at 30 days aging. In addition relatively more oxalate soluble Fe and Ti (i.e. "amorphous" Fe-Ti) is extracted as the Ti/Ti+Fe ratio increases. Also the amount of Ti extracted by oxalate from the aged Fe-Ti oxides is greater than the amount of Al extracted in corresponding Fe-Al oxides, suggesting that Al(III) ions enter the goethite structure more easily (and in larger amounts) than Ti(IV) ions, probably because of the smaller ionic radius of the Al(III) ion.

---

\* During the aging of precipitates obtained from  $TiCl_3$ , the suspension turned from black to dark reddish brown (within 8 hrs) possibly due to oxidation of Ti(III) to Ti(IV).

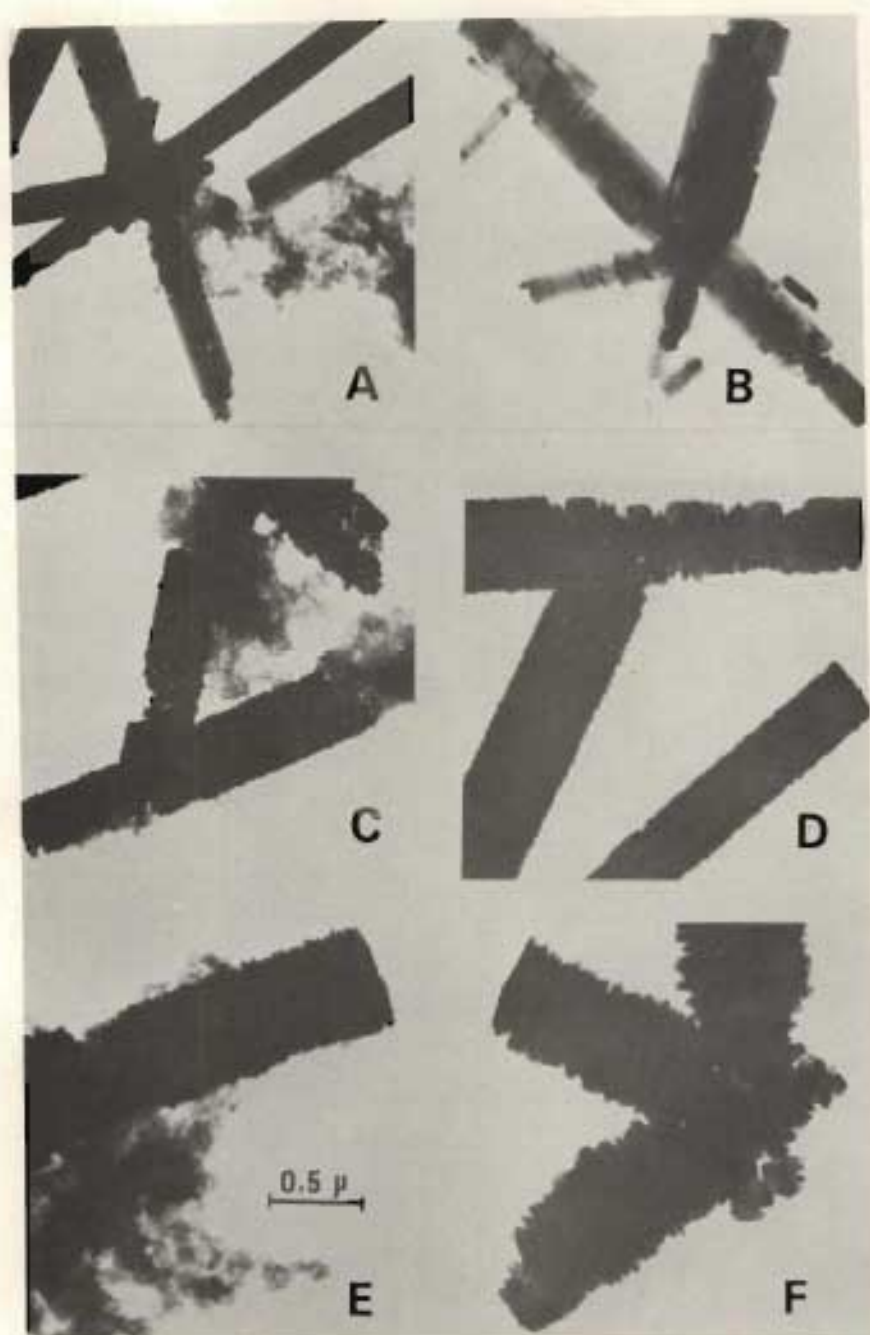


Plate App. 2.2: Electron micrographs of goethite prepared from Fe-Ti oxide gels, pH 13, aged for 30 days ( $60^{\circ}\text{C}$ ) and dialyzed against distilled water with: A. 5% in Ti/Ti+Fe; B. 5% in Ti/Ti+Fe and oxalate treated; C. 10% in Ti/Ti+Fe; D. 10% in Ti/Ti+Fe and oxalate treated; E. 20% in Ti/Ti+Fe; F. 20% in Ti/Ti+Fe and oxalate treated. The scale applies to all figures



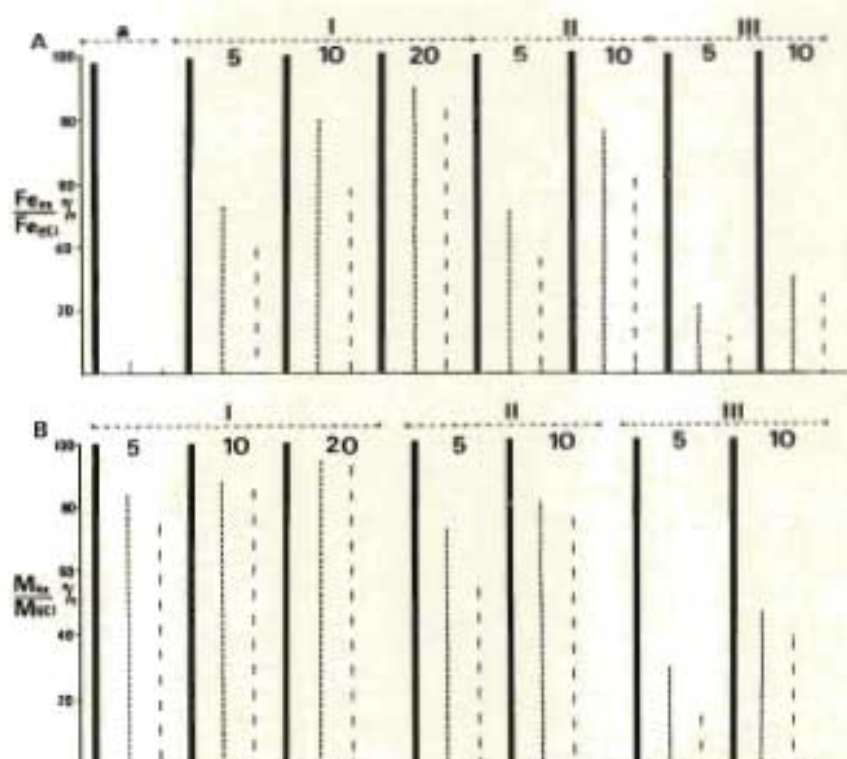


Fig. App. 2.1:  $NH_4$ -oxalate- $pH_3$ , extractable (ox) Fe or M(Ti and Al) expressed as a percentage of the total (HCl) Fe or M present in synthetic gels. A. Fe extracted from ferric and mixed gels. B. Ti and Al extracted from mixed gels. Where: (a) Pure ferric gel: (i) prepared using  $TiCl_4$  (5, 10 and 20% in Ti/Ti+Fe); (ii) prepared using  $TiCl_3$  (5 and 10% in Ti/Ti+Fe); (iii) prepared using  $AlCl_3$  (5 and 10% in Al/Al+Fe).  
 — freshly precipitated gel;  
 ..... aged for 30 hours;  
 ----- aged for 30 days.

The surface of these large chunky twin goethite crystals becomes deeply pitted during oxalate treatment (Plate App. 2.2 B,D and F). This pitting was not observed during treatment of pure synthetic goethite or aluminous goethite. It appears, therefore, that a strongly chemisorbed phase (easily removed by oxalate treatment) "coats" goethite crystals formed in the Fe-Ti oxide gels. This chemisorbed phase is, in many respects, similar to that reported by Herbillon and Tran Vinh An (1969) for silico-ferric gels.

(ii) Haematite prepared by refluxing ferric nitrate

One litre of solution containing 160 g  $\text{Fe}(\text{NO}_3)_3 \cdot 9\text{H}_2\text{O}$  was refluxed ( $100^\circ\text{C}$ ) for 10 days (method similar to Breeuwsma, 1973). A dense red precipitate was then obtained by adding 5 M KOH dropwise over 3 hours until a pH of 7 was reached. The resulting red precipitate was then centrifuge-washed five times with deionized water. The pH was adjusted to 5 by adding dilute  $\text{HNO}_3$  and refluxed for a further 15 days. The precipitated oxide was then finally centrifuged-washed with deionized water until dispersion and freeze-dried.

The X-ray diffractogram only shows diffraction peaks for haematite (see Fig. 4.4).



## APPENDIX 3

## X-RAY DIFFRACTION ANALYSIS

## (i) Apparatus

X-ray diffraction was carried out on a Philips unit with a P.W. 1130/90 generator, P.W. 1050/70 goniometer, A.M.R. E3-202/GVW E202-225 graphite monochromator, using  $\text{CoK } \alpha$  radiation,  $1.0^\circ$  divergence slit and  $0.1^\circ$  receiving slit and proportional counter.

Standard experimental conditions were 35 kV, 20 mA, scanning speed of  $1^\circ 2\theta$  per min. for all samples except for ferrihydrite samples ( $1.0^\circ 2\theta$  per min.), paper speed 10 mm per min., and variable ratemeter settings. Scanning for all samples occurred over the range from  $20-45^\circ 2\theta$ , except for ferrihydrite and synthetic samples which were run from  $10 - 85^\circ 2\theta$ .

## (ii) Sample preparation

Powdered samples (freeze dried or crushed) were packed into either rectangular aluminium (Klug and Alexander, 1954) or PVC\* (for small amounts of sample) holders (Plate App. 3.1) by compressing the samples against a filter paper surface to minimize preferred orientation (Norrish and Taylor, 1962) using the device\*\* shown in Plate App. 3.1. In order to prevent sample material from adhering or sticking to the surface of the plunger, the plunger surface was finely ground, lapped and then polished.

The reference sample used to determine instrumental line broadening (b) was prepared from  $\alpha$ -quartz which had been ground in an agate mortar and treated with 5M HCl. The  $\alpha$ -quartz (101) line ( $d=3.34 \text{ \AA}$ ) gave a width at half height (WHH) value of  $0.14^\circ 2\theta$  (i.e. b). Strong line broadening in many samples reduces the accuracy of d-spacing measurement. It should also be noted that the quartz (100) and (110) peaks interfere with the goethite (110) and (111) peaks respectively, so that for samples containing more than about 10% quartz (i.e. given as accessory amounts or higher in Tables 1.1 to 1.9), the accuracy of both the line position and WHH measurements is limited. This problem was alleviated, as far as possible by repeated soniprobe and sedimentation treatments in water or  $0.001 \text{ M NH}_4\text{OH}$ .

\* "Darvic" PVC sheeting made by AE & CI

\*\* The writer gratefully acknowledges Mr. C.R. Morewood, of the Faculty of Science Workshop, University of Natal, who constructed this device.

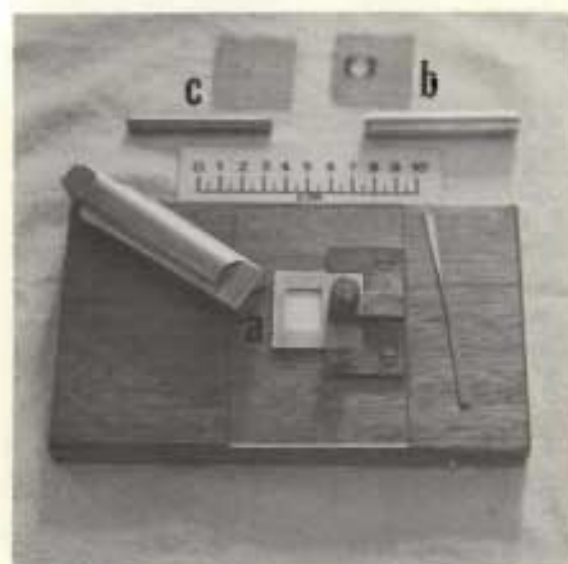


Plate. App. 3.1: Device used for preparing disorientated powdered samples for X-ray diffraction measurement. Samples were packed into either (a) rectangular aluminium holders (20mm by 15mm) or round holders made from "Darvic" PVC sheeting (diameter of b and c is 11 and 8mm respectively) and compressed against a filter paper surface to minimize preferred orientation



## REFERENCES

- ACOCKS, J.P.H. 1953. Veld types of South Africa. Botanical Survey Memoir No. 28 Dept. Agric. Union S. Afr., Govt. Printer, Pretoria.
- ALEXANDER, L.T. and J.G. CADY. 1962. Genesis and hardening of Laterite in soils. Tech. Bull. No. 1282. Soil Conservation Service, USDA Washington, D.C.
- ATKINSON, R.J., A.M. POSNER and J.P. QUIRK. 1968. Crystal nucleation in Fe (III) solutions and hydroxide gels. J. Inorg. Nucl. Chem. 30: 2371-2381.
- BAIN, D.C. 1976. A titanium-rich soil clay. J. Soil Sci. 17: 68-70.
- BAILEY, S.W. 1977. Report of the I.M.A.- I.V.Gr. Joint Committee on Nomenclature. Amer. Mineral. 62: 411-415.
- BAILEY, S.W., E.N. CAMERON, H.R. SPEDDON and R.J. WEDGE. 1962. The alteration of ilmenite in beach sands. Econ. Geol. 51: 263-279.
- BARIL, R. and G. BITTON. 1969. Teneurs elevees de fer libre et l'identification taxonomique de certains sols du Quebec contenant de la magnetite. Can. J. Soil Sci. 59: 1-9.
- BEATER, B.E. 1940. Concretions and refractory deposits in some Natal coastal soils. Soil Sci. 50: 313-329.
- 1957. Soils of the Sugar Belt : Part 1 - Natal North Coast, Natal Regn. Surv. Rept. 3, Oxford.
- 1959. Soils of the Sugar Belt : Part 2 - Natal South Coast, Natal Regn. Surv. Rept. 4, Oxford.
- 1962. Soils of the Sugar Belt : Part 3 - Zululand, Natal Regn. Surv. Rept. 5, Oxford.
- 1970. Soil series of the Natal Sugar Belt. S. Afr. Sugar Ass., Durban.
- BENESLAVSKY, S.I. 1957. New aluminium-bearing minerals in bauxites. Dokl. Akad. Nauk. S.S.S.R. 113: 367-369.
- BERNAL, J.D., D.R. DASGUPTA and A.L. MACKAY. 1959. The oxides and hydroxides of iron and their structural interrelationships. Clay Mineral. Bull. 4: 15-30.
- BLUME, H.P. and U. SCHWERTMANN. 1969. Genetic evaluation of profile distribution of aluminium, iron and manganese oxides. Soil Sci. Soc. Amer. Proc. 33: 438-444.
- BONIFAS, M. and P. LEGOUX. 1957. The presence of massive maghaemite in lateritic weathering products (in French). Bull. Serv. Carte geol. Alsace-Lorraine: 10(2).

- BRAUN, P. 1952. A superstructure in spinels. *Nature* (London) 170: 1123.
- BREEUWSMA, A. 1973. Adsorption of ions on hematite ( $\alpha - \text{Fe}_2\text{O}_3$ ). *Med. Landbouwhogeschool, Wageningen* 73-1. p.9.
- BREWER, R. and J.R. SLEEMAN. 1963. Pedotubules: their definition, classification, and interpretation. *J. Soil Sci.* 14: 156-166.
- BRINKMAN, R. 1970. Ferrollysis, a hydromorphic soil forming process. *Geoderma*. 3: 199-206.
- BYKOV, A.D. 1964. Proarizonite as a secondary mineral due to supergene alteration of ilmenite. *Dokl. Akad. Nauk. S.S.S.R.* 156: 567-570.
- BUDDINGTON, A.F. and D.H. LINDSLEY. 1964. Iron-titanium oxide minerals and synthetic equivalents. *J. of Petrology*. 5: 310-357.
- CHRETIEN, J. 1967. A study of concretions and ferruginous materials in a red soil in a temperate climate. *Annls. Agron.* 18: 339-60.
- CHUKHROV, F.V. 1973. Mineralogical and geochemical criteria in the genesis of red beds. *Chemical Geology*. 12: 67-75.
- CHUKHROV, F.V., B.B. ZVYAGIN, L.P. ERMILOVA and A.I. GORSHKOV. 1972. New data on iron oxides in the weathering zone. *Proc. Int. Clay Conf., 1972 (Madrid)* 1: 397-404.
- CLOOS, P., A.J. LEONARD, J.P. MOREAU, A. HERBILLON and J.J. FRIPIAT. 1969. Structural organization in amorphous silico-aluminas. *Clays and Clay Mineral.* 17: 279-287.
- COLOMBO, U., F. GAZZARRINI, G. LANZAVICCHIA and G. SIRONI. 1965. Magnetic oxidation: a proposed mechanism. *Science*. 147: 1033.
- CORNELL, R.M., A.M. POSNER and J.P. QUIRK. 1974. Crystal morphology and the dissolution of goethite. *J. Inorg. Nucl. Chem.* 36: 1937-1946.
- CORRENS, C.W. and W. VON ENGELHARDT. 1941. Röntgenographische Untersuchungen über den Mineralbestand sedimentärer Eisenerze. *Nachr. Akad. Wiss. Göttingen Math.-Phys. Klasse.* 213: 131-137.
- DARBY, G.D. 1954. The characteristics of South African wattle soils. Ph.D. dissertation, University of Natal.
- DAVEY, B.G., J.D. RUSSELL and H.J. WILSON. 1975. Iron oxide and clay minerals and their relation to colours of red and yellow podzolic soils near Sydney, Australia. *Geoderma*. 14: 125-138.
- DE VILLIERS, J.M. 1962. A study of soil formation in Natal. Ph.D. dissertation, University of Natal.
- \_\_\_\_\_ 1964. The genesis of some Natal soils. 1. Clovelly, Kranskop and Balmoral series. *S.Afr.J.Agric.Sci.* 7: 417-438.
- \_\_\_\_\_ 1965. Present soil-forming factors and processes in tropical regions. *Soil Sci.* 99: 50-57.



- DE VILLIERS, J.M. and M.L. JACKSON. 1967. Aluminous chlorite origin of pH-dependent cation exchange capacity variations. *Soil Sci. Soc. Amer. Proc.* 31: 614-619.
- DE VILLIERS, J.M. and T.H. VAN ROOYEN. 1967. Solid solution formation of lepidocrocite-boemite and its occurrence in soil. *Clay Mineral.* 7: 229-235.
- DOLCATER, D.L., J.K. SYERS and M.L. JACKSON. 1970. Titanium as free oxide and substituted forms in kaolinites and other soil minerals. *Clays and Clay Mineral.* 18: 71-79.
- DUDAL, R. 1968. Definitions of soil units for the soil map of the world. *World Soil Resources Report No. 33.* Rome : World Soil Resources Office, F.A.O.
- DU TOIT, A.L. 1954. The geology of South Africa. 3rd ed., Oliver and Boyd, Edinburgh.
- EASTON, J.S. 1970. Phosphorus-silicon relationships in sesquioxenic soil and colloidal systems. M.Sc. Agric. dissertation, University of Natal.
- EDWARDS, D. 1967. Plant Ecology Survey of the Tugela Basin. Town and Regional Planning Commission, Natal. Vol. 36.
- ESWARAN, H. 1971. Electron scanning studies of the fabric of fracture surfaces. *Soil Sci. Soc. Amer. Proc.* 35: 787-790.
- ESWARAN, H. and F. DE CONINCK. 1971. Clay mineral formations and transformations in basaltic soils in tropical environments. *Pedologie (Ghent).* 21: 181-210.
- FANIRAN, A. 1970. Maghemite in the Sydney duricrusts. *Am. Miner.* 55: 925-933.
- FARRELL, D.M. 1972. A study of the infra-red absorption in the oxidation of magnetite to maghaemite and hematite. *Mines Branch Invest. Rep. IR. 72-18.* Dept. of Energy, Mines and Resources, Canada.
- FEITKNECHT, W. and H.W. LEHMANN. 1959. Über die oxidation von Magnetit zu  $\alpha - \text{Fe}_2\text{O}_3$ . *Helv. chim. Acta.* 42: 2035-2039.
- FEY, M.V. 1974. Characteristics of sesquioxenic soils. Ph.D. dissertation, University of Natal.
- FEY, M.V. and J. LE ROUX. 1976. Quantitative determination of allophane in soil clays. p.451-463. In S.W. Bailey (Ed.) *Proc. Int. Clay Conf. 1975 (Mexico City).* Applied Publishing, Ltd., Wilmette, Ill.
1977. Properties and quantitative estimation of poorly crystalline components in sesquioxenic soil clays. *Clays and Clay Mineral.* 25: 285-294.
- FISCHER, W.R. and J.C.G. OTTOW. 1972. Abbau von Eisen (III) - citrat in durchlüfteter wässriger Lösung durch Bodenbakterien. *Z. Pflanzenernähr. Bodenk.* 131: 243-253.

- FISCHER, W.R. and U. SCHWERTMANN. 1975. The formation of hematite from amorphous iron (III) hydroxide. *Clays and Clay Mineral.* 23: 33-37.
- FITZPATRICK, E.A. 1956. An indurated soil horizon formed by permafrost. *J. Soil Sci.* 7: 248-254.
- FITZPATRICK, R.W. 1974. Mineralo-chemical studies on soils and related material from pedosystems in the Southeastern Transvaal. M.Sc. Agric. dissertation, University of Natal.
- 1978. Periglacial soils with fossil permafrost horizons in southern Africa. *Proc. 4th S. Afr. Soc. Quat. Res.* 1977. *Ann. Natal Museum.* 23(2): 475-484.
- FITZPATRICK, R.W. and J. LE ROUX. 1975. Mineralo-chemical studies on titaniferous red soils of varying base status and structure. *Proc. Soil Sci. Soc. S. Afr. (Blyde River)* : 344-375.
- 1976. Pedogenic and solid solution studies on iron-titanium minerals. In S.W. Bailey (Ed.) *Proc. Int. Clay Conf. 1975 (Mexico City).* Applied Publishing, Ltd., Wilmette. Ill.: 585-599.
- 1977. Mineralogy and chemistry of a Transvaal black clay toposequence. *J. Soil Sci.* 28: 165-179.
- FLINTER, B.H. 1959. The alteration of Malayan ilmenite grains and the question of "arizonite". *Econ. Geol.* 54: 720-729.
- FÜLSTER, H., E. KALK and N. MOSHREFI. 1970. Complex pedogenesis of ferrallitic savanna soils in South Sudan. *Geoderma.* 6: 135-149.
- FOUCHE, P.S. and W.J. FÜLSCHER. 1975. Anorganiese amorfemateriaal in sekwiksiedryke suurgrond van Transvaal. *Proc. Soc. Soil Science S. Afr. (Blyde River)* 395-413.
- FRANCOMBE, M.H. and H.P. ROOKSBY. 1959. Structure transformations effected by the dehydration of diaspor, goethite and delta ferric oxide. *Clay Mineral. Bull.* 4: 1-14.
- FRANKEL, J.J. 1966a. The basal rocks of the Tertiary at Uloa, Zululand, South Africa. *Geol. Mag.* 103: 214-230.
- 1966b. Some mineralogical observations on Australian lateritic rocks. *Aust. Jour. Sci.* 29: 115-117.
- FRANKEL, J.J. and P. BAYLISS. 1966. Ferruginized surface deposits from Natal and Zululand, South Africa. *J. Sed. Petrol.* 36: 193-201.
- GAMBLE, E.E. and R.B. DANIELS. 1972. Iron and silica in water, acid ammonium oxalate, and dithionite extracts in some North Carolina Coastal soils. *Soil Sci. Soc. Amer. Proc.* 36: 939-943.
- GASTUCHE, M.C., T. BRUGGENWERT and M.M. MORTLAND. 1964. Crystallization of mixed iron and aluminium gels. *Soil Sci.* 98: 281-289.
- GAZZARRINI, F. and C. LANZAVECCHIA. 1969. Role of crystal structure, defects and cationic diffusion on the oxidation and reduction processes of iron oxides at low temperatures. In: J.W. Mitchell et al. (Editors), Reactivity of Solids. Wiley, New York, N.Y. p. 57.



- GOLDEN, D.C., J.M. BIGHAM and S.B. WEED. 1977. Surface charge and phosphate adsorption on Al-substituted goethite. *Agron. Abstr. Div. S-9*: p.188.
- GOLDEN, D.C. 1978. Physical and chemical properties of aluminium-substituted goethite. Unpublished Ph.D. dissertation, Dept. of Soil Science, N.C. State Univ. at Raleigh.
- GOLDING, H.G. 1961. Leucoxene terminology and genesis. (Discussion). *Econ. Geol.* 56(6): 1138-1149.
- GREENLAND, D.J., J.M. OADES and T.W. SHERWIN. 1968. Electron microscope observations of iron oxides in some red soils. *J. Soil Sci.* 19: 123-126.
- GREY, I.E. and A.F. REID. 1975. The structure of pseudorutile and its role in the natural alteration of ilmenite. *Am. Mineral.* 60: 898-906.
- HAGGERTY, S.E. 1976. Oxidation of opaque mineral oxides in basalts. In: D. Rumble (Ed.) Oxide Minerals : Mineralogical Society of America. Short course notes. Vol. 3.
- HARPER, G. 1969. Periglacial evidence in southern Africa during the Pleistocene epoch. *Palaeoecology of Africa*. Edited by E.M. van Zinderen Bakker. 4: 71-101.
- HASTENRATH, S. and J. WILKINSON. 1972. A contribution to the periglacial morphology of Lesotho, Southern Africa. *Biuletyn Periglacialny*. 22: 157-167.
- HAUGHTON, S.H. 1969. Geological history of Southern Africa. Geological Soc. of S. Afr., Cape Town.
- HERBILLON, A.J. and J. TRAN VINH AN. 1969. Heterogeneity in silicon-iron mixed hydroxides. *J. Soil Sci.* 20: 223-235.
- HORNUNG, M. 1977. Notes on the sites visited during the field excursion. Meeting at High Force 1975 - The Soils of Upper Teesdale. North of England Soils Discussion Group Proceedings 12, 1975. p. 19
- HURST, V.J. 1977. Visual estimation of iron in saprolite. *Geol. Soc. Am. Bull.* 88: 174-176.
- HUTTON, J.T. 1977. Titanium and zirconium minerals, In: J.B. Dixon and S.B. Weed (Ed.) Minerals in soil environments. Agron. Soc. Amer. Publ.
- ISELL, R.F., P.J. STEPHENSON, G.C. MURTHA and G.P. GILLMANN. 1976. Red basaltic soils in north Queensland. 1. Environment, morphology, particle size characteristics and clay mineralogy. CSIRO Div. of Soils Tech. paper No. 28: 1-28.
- IVARSON, K.C. and M. SOJAK. 1978. Microorganisms and ochre deposits in field drains of Ontario. *Can. J. Soil Sci.* 58: 1-17.
- IWASA, J. 1965. Mineralogical studies of iron from minerals in soils. *Bull. Nat. Inst. Agric. Sci. B*, 15: 187-236.

- JACKSON, M.L. 1968. Soil chemical analysis - advanced course, published by the author, Dept. of Soil Science, Univ. of Wisconsin, Madison, Wisconsin.
- JACKSON, M.L., S.Y. LEE, J.L. BROWN, I.B. SACHS and J.K. SYERS. 1973. Scanning electron microscopy of hydrous metal oxide crusts intercalated in naturally weathered micaceous vermiculite. *Soil Sci. Soc. Amer. Proc.* 37: 127-131.
- JONAS, K. and K. SOLYMAR. 1970. Preparation, X-ray derivatographic and infrared study of aluminium substituted goethites. *Acta Chim. Acad. Sci. Hung.* 66: 383-394.
- KARKHANAVALA, M.D. 1959. The nature of arizonite. *Econ. Geol.* 54: 1302-1308.
- KAEKHANAVALA, M.D. and A.C. MOMIN. 1959. Subsolidus reactions in the system  $Fe_2O_3 - TiO_2$ . *J. Am. Ceramic Soc.* 42: 399-402.
- KATSURA, T., I. KUSHIRO, S. AKIMOTO, J.L. WALKER and G.D. SHERMAN. 1962. Titanomagnetite and titanomaghemite in a Hawaiian soil. *J. Sediment. Petrol.* 32: 299-308.
- KELLER, W.D. 1964. The origin of high-alumina clay minerals - a review. *Clays and Clay Mineral.* 19: 129-151.
- KING, L.C. 1953. A Miocene marine fauna from Zululand. *Trans. Geol. Soc. S. Afr.* 56: 59-91.
- 1967. South African Scenery. (3rd ed. revised). Oliver and Boyd, Edinburgh.
- 1970. Uloa Revisited. *Trans. Geol. Soc. S. Afr.* 73: 151-157.
- KLUG, H.P. and L.E. ALEXANDER. 1954. X-ray Diffraction Procedures for Polycrystalline and Amorphous Materials, Wiley, New York.
- KODAMA, H. and M. SCHNITZER. 1977. Effect of fulvic acid on the crystallization of Fe(III) oxides. *Geoderma*. 19: 279-291.
- KOJIMA, M. 1964. The free iron minerals contained in Kanto loam. *J. Sci. Soil Tokyo*. 35: 174-170.
- KRINSLEY, D.H. and J.C. DOORNKAMP. 1973. Atlas of quartz sand surface textures. Cambridge Univ. Press. London.
- KÜHNEL, R.A., H.J. ROORDA and J.J. STEENSMA. 1975. The crystallinity of minerals - a new variable in pedogenic processes: A study of goethite and associated silicates in laterites. *Clays and Clay Mineral.* 23: 349-354.
- LANDA, E.R. and R.G. GAST. 1972. Evaluation of crystallinity in hydrated ferric oxides. *Clays and Clay Mineral.* 21: 121-130.
- LE BORGNE, E. 1955. Abnormal magnetic susceptibility of the top soil. *Annls. Geophys.* 11: 399-419.
- 1960. The influence of fire on the magnetic properties of soil, schist and granite. *Annls. Geophys.* 16: 159-196.
- LE ROUX, J. 1973. Quantitative clay mineralogical analysis of Natal Oxisols. *Soil Sci.* 115: 137-144.



- LEWIS, J. and I. WILKINS. 1960. Modern Co-ordination chemistry. Inter Sci. pubs. N.Y. p.400.
- LINDSLEY, D.H. 1976. The crystal chemistry and structure of oxide minerals as exemplified by the Fe-Ti oxides: In D. Rumble (Ed.) Oxide Minerals: Mineralogical Society of America Short course notes. Vol. 3.
- LOXTON, R.F. and O.J. VAN STRATEN. 1973. Erosion cycles in relation to genesis and classification of soils. Paper presented at Soc. Soil Sci. S. Afr. Cong. (Salisbury).
- LYND, L.E. 1960. Alteration of ilmenite. *Econ. Geol.* 55: 1064-1068.
- MACVICAR, C.N. 1962. Soil studies in the Tugela Basin. Ph.D. dissertation, University of Natal.
- 1978. Advances in soil classification and genesis in southern Africa. Paper read at the 8th Congress of the Soil Science Society of Southern Africa, Pietermaritzburg.
- MACVICAR, C.N., J.M. DE VILLIERS, R.F. LOXTON, E. VERSTER, J.J.N. LAMBRECHTS, F.R. MERRYWEATHER, J. LE ROUX, T.H. VAN ROOYEN and H.J. VON M. HARTSE. 1977. Soil Classification. A binomial system for South Africa. Sci. Bull. 390. Soil and Irrigation Research Institute. Dept. Agricultural Technical Services, Pretoria.
- MARSHALL, P.R. and D. RUTHERFORD. 1971. Physical investigations on colloidal iron-dextran complexes: *J. Colloid Interface Sci.* 37: 390-402.
- MATSUSAKA, Y. and G.D. SHERMAN. 1961. Magnetism of iron oxide in Hawaiian soils. *Soil Sci.* 91: 239-245.
- MATSUSAKA, Y., G.D. SHERMAN and L.D. SWINDALE. 1965. Nature of magnetic minerals in Hawaiian soils. *Soil Sci.* 100: 192-199.
- MAUD, R.R. 1965. Laterite and lateritic soil in coastal Natal, South Africa. *J. Soil Sci.* 16: 60-72.
- 1968a. Quaternary geomorphology and soil formation in coastal Natal. *Z. Geomorph. Supplementhand* 7: 155-199.
- 1968b. Further observations on the laterites of coastal Natal. *Trans. 9th Int. Congr. Soil Sci. Adelaide* 4: 151-158.
- MCKEAGUE, J.A., J.E. BRYDON and N.M. MILES. 1971. Differentiation of forms of extractable iron and aluminium in soils. *Soil Sci. Soc. Amer. Proc.* 35: 33-38.
- MEHRA, O.P. and M.L. JACKSON. 1960. Iron oxide removal from soils and clays by a dithionite-citrate system buffered with sodium bicarbonate. *Clays and Clay Mineral.* 7: 317-327.
- MILLOT, G. 1970. Geology of Clays. Chapman and Hall, London.
- MITSUCHI, M. 1976. Characteristics and genesis of nodules and concretions occurring in soils of the R. Chinit area, Kompong Thom Province, Cambodia. *Soil Sci. Plant Nutr.* 22: 409-421.

- MULLINS, C.E. 1977. Magnetic susceptibility of the soil and its significance in soil science - A review. *J. Soil Sci.* 28: 223-246.
- NAHON, D., C. JANOT, A.M. KARPOFF, H. PAQUET and Y. TARDY. 1977. Mineralogy, petrography and structures of iron crusts (ferricretes) developed on sandstones in the western part of Senegal. *Geoderma*. 19: 263-277.
- NORRISH, K. 1975. Geochemistry and mineralogy of trace elements. In A.R. Egan and D.J.O. Nicholas (Ed.) *Proc. Waite Inst. Symposium on trace elements in Soil-Plant-Animal Systems (Adelaide, 1974)*. Academic Press.
- NORRISH, K. and R.M. TAYLOR. 1961. The isomorphous replacement of iron by aluminium in soil goethites. *J. Soil Sci.* 12: 294-306.
- \_\_\_\_\_. 1962. Quantitative analysis by X-ray diffraction. *Clay Mineral. Bull.* 5, 28: 98-109.
- OADES, J.M. 1963. The nature and distribution of iron compounds in soils. *Soils Fertil.* 26: 69-80.
- OADES, J.M. and W.N. TOWNSEND. 1963. The detection of ferro-magnetic minerals in soils and clays. *J. Soil Sci.* 14: 179-187.
- O'REILLY, W. and P.W. READMAN. 1971. The preparation and unmixing of cation deficient titanomagnetites. *Z. Geophys.* 37: 321-327.
- OVERHOLT, J.L., G. VAUX and J.L. RODDA. 1950. The nature of "arizonite". *Am. Mineral.* 35: 117-119.
- PALMER, C. 1909. Arizonite, ferric metatitanate. *Am. J. Sci.* 28: 353-356.
- PANKEY, T. and SENFTLE, F. 1959. Magnetic susceptibility of natural rutile, anatase, and brookite. *Am. Mineral.* 44: 1307-1309.
- PAWLUK, S. 1971. Characteristics of Fers Eluviated Gleysols developed from acid shales in Northwestern Alberta. *Can. J. Soil Sci.* 51: 113-124.
- PAWLUK, S. and J. DUMANSKI. 1973. Ferruginous concretions in a poorly drained soil of Alberta. *Soil Sci. Soc. Amer. Proc.* 37: 124-127.
- PERINET, G. and R. LAFONT. 1972a. Sur la presence d'hematite alumineuse disordonnée dans des bauxites du Var. *Compt. rend. Acad. Sci. Paris.* 274: 272-274.
- \_\_\_\_\_. 1972b. Sur les paramètres cristallographiques des hematites alumineuses. *Compt. rend Acad. Sci. Paris.* 275: 1021-1024.
- PHILLIPS, J. 1973. The agricultural and related development of the Tugela Basin and its influent surrounds. *Natal Town and Regional Planning Rep.* vol. 19.
- PRASAD, B. and B.P. GHILDYAL. 1975. Magnetic susceptibility of lateritic soils and clays. *Soil Sci.* 120: 219-229.
- PRUDEN, G. and H.G.C. KING. 1969. A scheme of semi-micro analysis for the major elements in clay minerals, based on modifications to conventional methods of silicate analysis. *Clay Mineral.* 8: 1-13.



- READMAN, P.W. and W.O'REILLY. 1970. The synthesis and inversion of non-stoichiometric titano - magnetites. *Phys. Earth planet. Interiors*. 4: 121-128.
- REERINK, F.O. 1961. Clay mineralogical studies in the Tugela Basin. M.Sc.Agric. dissertation, University of Natal.
- ROORDA, H.J. and P.E. QUENEAU. 1973. Recovery of nickel and cobalt from limonites by aqueous chlorination in sea water. *Trans. Inst. Mining Met.* C82: 79-87.
- SAYIN, M. and M.L. JACKSON. 1975. Anatase and rutile determination in kaolinite deposits. *Clays and Clay Mineral.* 23: 437-443.
- SCHEFFER, F., B. MEYER and U. BABEL. 1959. Magnetic measurements as aids in the determination of iron oxide in the soil. *Beitr. Miner. Petrogr.* 6: 371-387.
- SCHEFFER, F., E. WELTE and F. LUDWIEG. 1957. Zur Frage der Eisenoxidhydrate in Boden. *Chem. Erde*. 19: 51-64.
- SCHHELLMAN, W. 1959. Experimentella undersökningar över die sedimentaire bildning von goethite und hematit. *Chemie Erde*. 20: 104-135.
- SCHWERTMANN, U. 1959. Über die Synthese definierter eisenoxyde unter verschiedenen Bedingungen. *Z. Anorg. Allg. Chem.* 298: 337-348.
- 1964. Differenzierung der eisenoxide des bodens durch extraktion mit ammoniumoxalat-lösung. *Z. Pfl. Ernähr. Düng. Bodenk.* 105: 194-202.
- 1966. Inhibitory effect of soil organic matter on the crystallization of amorphous ferric hydroxide. *Nature*. 212: 645-646.
- 1966a. Die Bildung von Goethite und Hämatit in Böden und Sedimenten. *Proc. Int. Clay Conf. (Jerusalem)* 1: 159-165.
- 1969/1970. Der Einfluss — organischer Anionen auf die Bildung von Goethit und Hämatit aus amorphem Fe(III)-hydroxid. *Geoderma*. 3: 207-214.
- 1971. Transformation of hematite to goethite in soils. *Nature*. 232: 624-625.
- 1973. Use of oxalate for Fe extraction from soils. *Can. J. Soil Sci.* 53: 244-246.
- 1973a. Electron micrographs of soil lepidocrocites. *Clay Mineral.* 10: 59-63.
- SCHWERTMANN, U. and W.R. FISCHER. 1973. Natural "amorphous" ferric hydroxide. *Geoderma*. 10: 237-247.
- SCHWERTMANN, U., W.R. FISCHER and H. PAPENDORF. 1968. The influence of organic compounds on the formation of iron oxides. *Trans. 9th Intern. Congr. Soil Sci. (Adelaide)*. 1: 645-655.

- SCHWERTMANN, U., W.R. FISCHER and R.M. TAYLOR. 1974. New aspects of iron oxide formation in soils. Trans. 11th Int. Congr. Soil Sci. (Moscow): 237-247.
- SCHWERTMANN, U. and R.W. FITZPATRICK. 1977. Occurrence of lepidocrocite and its association with goethite in Natal soils. Soil Sci. Soc. Am. J. 41: 1013-1018.
- SCHWERTMANN, U., R.W. FITZPATRICK and J. LE ROUX. 1977. Al substitution and differential disorder in soil hematites. Clays and Clay Mineral. 25: 373-374.
- SCHWERTMANN, U., R.W. FITZPATRICK, R.M. TAYLOR and D.G. LEWIS. 1978. The influence of aluminium on iron oxides. Part II. Preparation and properties of Al substituted hematites. Clays and Clay Mineral. (in press).
- SCHWERTMANN, U. and HEINEMANN, B. 1959. The occurrence and formation of maghemite in soils of N.W. Germany. Neues Jb. Miner. Mh. 8: 174-181.
- SCHWERTMANN, U. and R.M. TAYLOR. 1972. Transformation of lepidocrocite to goethite. Proc. Int. Clay Conf., 1972 (Madrid): 343-350.
- 
1977. Iron oxides, In J.B. Dixon and S.B. Weed (Ed.) Minerals in soil environments. Agron. Soc. Amer. Publ.
- SCHWERTMANN, U. and H. THALMANN. 1976. The influence of  $[Fe(II)]$ ,  $[Si]$  and pH on the formation of lepidocrocite and ferrihydrite during oxidation of aqueous  $FeCl_2$  solution. Clay Mineral. 14: 189-200.
- SHERMAN, G.D. 1952. The titanium content of Hawaiian soils and its significance. Soil Sci. Amer. Proc. 16: 15-18.
- SHERMAN, G.D., Y. MATSUSAKA, H. IKAWA and G. UEHARA. 1964. The role of the amorphous fraction in the properties of tropical soils. Agrochimica VIII, 2: 146-163.
- SOIL SURVEY STAFF. 1975. Soil taxonomy : A basic system of soil classification for making and interpreting soil surveys. USDA Handb. 436. U.S. Govt. Printing Office, Washington, D.C.
- SOKOLOVATA, T.A. and R.N. POLTEVA. 1968. The study of iron-manganese concretions from a strongly podzolic soil profile. Trans. 9th Int. Congr. Soil Sci. IV: 459-66.
- SPENCER, W.G. 1973. The effect of aluminous goethite on the evaluation of bauxite deposits. Proc. Aust. I.M.M. Conf., West. Aust.: 565-571.
- STACEY, F.D. and S.K. BANERJEE. 1974. The physical principles of rock magnetism. Amsterdam: Elsevier.
- STEPHENS, C.G. 1971. Laterite and silcrete in Australia. A study on the genetic relationships of laterite and silcrete and their companion materials, and their collective significance in the formation of the weathered mantle, soils, relief and drainage of the Australian continent. Geoderma. 5: 5-52.



- STIEGLITZ, R.D. and B. ROTHWELL. 1972. Scanning electron microscopy of Lake Michigan beach and dune sands from Terry Andrae-Kohler State Park, Wisconsin : Geol. Soc. Amer. Abs. with Programs, p. 350.
- SUDOM, M.D. and R.J. ST. ARNAUD. 1971. Use of quartz, zirconium and titanium as indices in pedological studies. Can. J. Soil Sci. 51: 385-396.
- SUMNER, M.E. 1961. The influence of precipitated iron oxides on the surface properties of clays and soils. Ph.D. dissertation, University of Oxford.
- TAYLOR, R.M. and J.B. GILES. 1970. The association of vanadium and molybdenum with iron oxides in soils. J. Soil Sci. 21: 203-215.
- TAYLOR, R.M. and A.M. GRALEY. 1967. The influence of ionic environment on the nature of iron oxides in soils. J. Soil Sci. 18: 341-348.
- TAYLOR, R.M. and R.M. MCKENZIE. 1966. The association of trace elements with manganese minerals in Australian soils. Aust. J. Soil Res. 4: 29-39.
- TAYLOR, R.M. and U. SCHWERTMANN. 1974a. Maghemite in soils and its origin. I. Properties and observations on soil maghemites. Clay Mineral. 10: 289-298.
- \_\_\_\_\_ 1974b. Maghemite in soils and its origin. II. Maghemite synthesis at ambient temperature and pH 7. Clay Mineral. 10: 299-310.
- \_\_\_\_\_ 1974c. The association of P with iron in ferruginous soil concretions. Aust. J. Soil Res. 12: 133-145.
- \_\_\_\_\_ 1978. The influence of aluminium on iron oxides Part 1. The influence of Al on Fe oxide formation from the Fe(II) system. Clays and Clay Mineral. (in press).
- TEMPLE, A.K. 1966. Alteration of ilmenite. Econ. Geol. 61: 695-714.
- THIEL, R. 1963. Zum System  $\alpha\text{FeOOH}$ - $\alpha\text{AlOOH}$ . Z. Anorg. Allg. Chem. 326: 70-78.
- TITE, M.S. and R.E. LININGTON. 1975. Effect of climate on the magnetic susceptibility of soils. Nature. 256: 565-566.
- TORRENT, J. and J. BENAYAS. 1977. Origin of gibbsite in a weathering profile from granite in west-central Spain. Geoderma. 19: 37-49.
- TURNER, J.L. 1973. Description of the physiographic regions of Natal and Zululand. p.250-259: In: The agricultural and related development of the Tugela Basin and its influent surrounds, by Phillips, J., Town and Regional Planning Rep. vol. 19.
- VAN DER EYK, J.J., C.N. MACVICAR and J.M. DE VILLIERS. 1969. Soils of the Tugela Basin. Natal Town and Regional Planning Rep. vol. 15.
- VAN DER MAREL, H.W. 1951. Gamma ferric oxide in sediments. J. Sedim. Petrol. 21: 12-21.
- VAN HOUTEN, F.B. 1968. Formation of red beds in \_\_\_\_\_ Geol. Soc. Amer. Bull. 78: 353-368.

- VAN DER MERWE, C.R. and H. HEYSTEK. 1955. Clay minerals of South African soil groups. 11 Subtropical black clays and related soils. *Soil Sci.* 79: 147-158.
- VAN OOSTERHOUT, G.W. and C.J.M. ROOLJMAN. 1958. A new superstructure in gamma-ferric oxide. *Nature*. 181: 44.
- VAN REEUWIJK, L.P. and J.M. DE VILLIERS. 1970. A modal system for allophane. *Agrochemophysica*. 2: 77-82.
- VAN ROOYEN, T.H. 1964. Pedogenese van die Kranskop en Clovelly series in Natal. M.Sc.Agric. dissertation, University of Natal.
- VALETON, I. 1972. Developments in soil science, 1. Bauxites. Elsevier Publ. Comp., Amsterdam. p.194.
- VERSTER, E. 1964. 'n Mineralogiese ondersoek van sekere Natalse rooigronde. M.Sc.Agric. dissertation, University of Natal.
- VISSER, H.N., L.J. KRIGE and F.C. TRUTER. 1947. The geology of the country south of Ermelo. Expl. Sheet 64, geol. Surv. S. Afr., Govt. Printer, Pretoria.
- WALKER, T.R. 1967. Formation of red beds in modern and ancient deserts. *Geol. Soc. Amer. Bull.* 78: 353-368.
- WALKER, T.R. and P.H. RIBBE. 1967. Formation of iron-rich authigenic clay by intrastratal alteration of hornblende in an arid climate: a contribution to the origin of hematite-stained matrix in red beds. *Geol. Soc. Amer. Spec. Pap.*, 101 Abstr, 1966: 233
- WALKER, J.L., G.D. SHERMAN and T. KATSURA. 1969. The iron and titanium minerals in the titaniferous ferruginous latosols of Hawaii. *Pac. Sci.* 23(3): 291-304.
- WEAVER, C.E. 1976. The nature of  $TiO_2$  in kaolinite. *Clays and Clay Mineral.* 24: 215-218.
- WEISER, H.B. and W.O. MILLIGAN. 1934. X-ray studies on the hydrous oxides. iv. Titanium Dioxide. *J. Phys. Chem.* 38: 513-519.
- ZEISSINK, H.E. 1969. The mineralogy and geochemistry of a nickeliferous laterite profile (Greenvale, Queensland, Australia). *Mineral. Deposita*. vol. 4: 132-152.



